EFFECT OF ALLOYING ADDITIONS ON THE MICROSTRUCTURE AND MECHANICAL PROPERTIES OF Fe-Al BASED LIGHTWEIGHT STEEL

A dissertation work

submitted in partial fulfillment of the requirements

for the award of the degree of

DOCTOR OF PHILOSOPHY

in

METALLURGICAL AND MATERIALS ENGINEERING

by

SHIVKUMAR KHAPLE

(Roll No.714143)

Under the guidance of

Dr. G. Brahma Raju

Assit. Professor, MMED, NIT Warangal

&

Dr. V.V. Satya Prasad

Scientist H, DMRL, Hyderabad

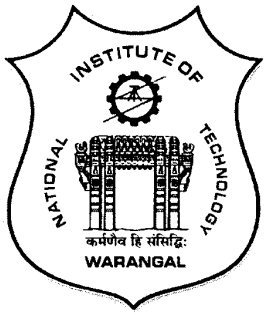

DEPARTMENT OF METALLURGICAL AND MATERIALS ENGINEERING

NATIONAL INSTITUTE OF TECHNOLOGY

WARANGAL-506 021 (T.S) INDIA

JANUARY - 2021

DEPARTMENT OF METALLURGICAL AND MATERIALS ENGINEERING
NATIONAL INSTITUTE OF TECHNOLOGY
WARANGAL-506021 (T.S) INDIA

CERTIFICATE

This is to certify that the work presented in the thesis entitled **"Effect of alloying additions on the microstructure and mechanical properties of Fe-Al based lightweight steel"** which is being submitted by **Mr. Shivkumar Khaple (Roll No.714143),** is a bonafide work submitted to National Institute of Technology, Warangal in partial fulfilment of the requirements for the award of the degree of **Doctor of Philosophy** in **Metallurgical and Materials Engineering.**

To the best of our knowledge, the work incorporated in this thesis has not been submitted to any other university or institute for the award of any other degree or diploma.

Dr. G. Brahma Raju

Asst. Professor and Thesis Supervisor

Department of Metallurgical and Materials Engineering
National Institute of Technology
Warangal-506021

Dr. V.V. Satya Prasad

Scientist 'H' and Co-supervisor

Defence Metallurgical Research Laboratory
Kanchanbagh
Hyderabad-500058

Thesis Approval for Ph.D

The thesis entitled **"Effect of alloying additions on the microstructure and mechanical properties of Fe-Al based lightweight steel"** which is submitted by **Mr. Shivkumar Khaple (Roll No.714143),** is approved for the degree of **Doctor of Philosophy** in Metallurgical and Materials Engineering.

Examiner

_____

Supervisors

VVS. Prasad

_____

_____

Chairman

Amit Kr. Khanna 11/01/2021

_____

Date: 11-01-2021

DECLARATION

I, Shivkumar Khaple, hereby declare that this dissertation work entitled **"Effect Effect of alloying additions on the microstructure and mechanical properties of Fe-Al based lightweight steel"** submitted in partial fulfillment for the award of degree of **Doctor of Philosophy (in Metallurgical and Materials Engineering)** to the Department of Metallurgical and Materials Engineering, National Institute of Technology, Warangal is a bonafide work which was carried out by me under the supervision of **Dr. Brahma Raju Golla** and **Dr. V.V. Satya Prasad**. I also declare that the content of this thesis has not been submitted previously in part or full in any University or Institute for the award of any degree or diploma.

Shivkumar Khaple
Roll No. 714143
Department of Metallurgical and
Materials Engineering

ACKNOWLEDGEMENTS

I express my gratitude and sincere thanks to my respected research supervisors Dr. G. Brahma Raju, Assit. Professor, Department of Metallurgical and Materials Engineering, National Institute of Technology, Warangal and Dr. V.V. Satya Prasad, Scientist 'H', Defence Metallurgical Research Laboratory (DMRL), Hyderabad for constructive ideas, invaluable guidance, discussions, suggestions and constant encouragement and support at various phases of the experimental and thesis work. Without their untiring mentorship, constant inspiration, valuable discussions and suggestions, this thesis wouldn't have been possible. I appreciate them for critically going through the draft of my thesis and research papers.

I sincerely thank Dr. G. Madhusudhan Reddy, Director, DMRL, Dr. Vikas Kumar, Dr. S.V. Kamat, former Director, DMRL for their kind support and help during the period of this study. I gratefully acknowledge Defence Research and Development Organization (DRDO), India for providing facilities for carrying out this work.

I am thankful to Shri. B. GopalaKrishna, Group Head, Advanced Melting Technologies Group for his very kind and generous help. I take this opportunity to thank Dr. Asit Kumar Khanra, Associate Professor and Head of the Department, Metallurgical and Materials Engineering, National Institute of Technology, Warangal for his support. I owe my immense debt of gratitude and reverence to members of the Doctoral Scrutiny Committee Dr. Joseph Davidson, Mechanical Engineering Department, Prof. G. V. S. Nageswara Rao and Dr. T. Mahesh Kumar, Department of Metallurgical and Materials Engineering for their constructive criticism, useful suggestions, and periodical reviews of my progress during the course of Ph.D work. I would like to thank technical and supporting staff of Department of Metallurgical and Materials Engineering, National Institute of Technology, Warangal for their technical and administrative support.

It is my privilege to express sense of gratitude to DMRL Scientists Dr.D.V. V SatyaNarayana, Dr.Ujwal Prakash, Dr. R.G. Baligidad for their support and technical help. I wish to express my gratitude to my colleagues of Electro-slag Refining Group Dr. M. Sankar, Shri Shishir and Ms. Geetha Shree. Special thanks to Dr. U. Ravikiran, Dr. Prem Kumar, Shri Venkat, Dr. A. Sambasiva Rao, Dr. Zafir Alam, Dr. S. S. Kalyan Kamal for their valuable help on varied occasions.

It is great pleasure to acknowledge the members of ElectroSlag Refining Group, Analytical Chemistry, Structure and Failure Analysis, Electron Microscopy, Mechanical Engineering, Metal Working Group, Mechanical Behaviour Groups of DMRL for several helps. Special thanks to Shri M. Chandrashekar, Shri Satish Reddy, Shri K. Lakshnmana Rao, Shri K. Srisailam, Shri Nageshwara Rao, Shri Gandharav Singh, Shri Basuki Dey, Shri N.U. Vaidya, Shri Rajesh Sharma, Shri T. Venugopal, Shri. S. Kumar, Shri S. Venkat, Shri Deepak, Shri Vikram, Shri Tapan Kumar for their kind help. I would like to thank HRD, TCG, TIC and Establishment groups of DMRL for administrative support.

Thanks to co-research scholars at National Institute of Technology, Warangal, Shri S. Siva Kumar, Shri K. Venkatesh Reddy, Shri T. Saravan Kumar, Dr. M. Ali, Dr. P. Prakash, Shri V. Raju and Sri Shiva Bejugama for their support and help during my PhD.

I express gratitude to my parents and family members who have been patient, supportive, and caring throughout of this research work. I thank almighty from depth of my heart for his constant shower of blessings at all the times of my life.

K.Shivkumar

(SHIVKUMAR KHAPLE)

LIST OF ABBREVIATIONS AND SYMBOLS

UTS	Ultimate tensile strength
TE	Total elongation
YS	Yield strength
EPMA	Electron probe micro Analysis
SEM	Scanning electron microscopy
BSE	Back scattered electron
SE	Secondary electron
XRD	X-Ray diffraction
EDS	Energy dispersive spectroscopy
HV	Vickers Hardness
kg	Kilogram
AIM	Air induction melting
VIM	Vacuum induction melting
VAR	Vacuum arc melting
AIMFC	Air induction melting with flux cover
ESR	Electro Slag Refining
n	Strain hardening exponent
MPa	Mega Pascal
s	Second
mbar	Milli bar
ppm	Parts per million
K	Strength coefficient

hcp	Hexagonal close packed
fcc	Face centered cubic
bcc	Body centered cubic
Nb	Niobium
Ti	Titanium
Fe	Iron
Al	Aluminium
C	Carbon
W	Tungsten
Mn	Manganese
Li	Lithium
Mg	Magnesium
Cr	Chromium
TRIP	Transformation induced Plasticity
TWIP	twinning-induced plasticity

LIST OF FIGURES

LIST OF TABLES

ABSTRACT

In the present investigation, the effect of alloying additions on the microstructure and mechanical behaviour of ferritic Fe-Al lightweight steels has been studied. An attempt has been made to correlate between the microstructure and mechanical properties (such as hardness, tensile strength and ductility). In particular, reduction of grain size and subsequent improvement in the mechanical properties of single phase ferritic Fe-7Al alloy was achieved with the addition of inoculants such as diborides (ZrB_2 and TiB_2) and strength improvement with the addition of carbon. Further, efforts were made to study the effect of strong carbide formers such as Nb and Ti on the properties of Fe-7Al-0.35C based steel as it was measured with better strength and moderate ductility. All the raw materials such as iron, aluminium, carbon and other alloying additions were melted in induction melting or arc-melting processes to get cast ingot/pan cake. The cast alloy was hot worked to 80% reduction and then subjected to annealing heat treatment. Detailed characterization of these alloys was carried out using chemical analysis, density measurement and microstructural characterisation (optical and scanning electron microscope (SEM)). Phase analysis was made by X-ray diffraction (XRD), electron probe micro analysis (EPMA). The observed microstructural phases were well correlated with the TheromoCalc predictions. Mechanical properties such as hardness (micro and bulk) and tensile properties of all the developed steels were carried out as per the ASTM standards. The present research revealed that the addition of diborides to disordered Fe-7Al base alloy aids in the grain refinement (from 632 μm to 66 μm). Nonetheless, it resulted marginal improvement in strength, however, ductility was measured significantly high (varied between 19% and 38%). On the other hand, addition of carbon (0.2 to 2.2%) to Fe-7Al base alloy resulted in significant improvement in strength, but at the cost of ductility. However, the ductility of Fe-7Al-0.35C steel in hot-rolled and annealed condition was observed to be more than 12% which is the minimum requirement for the formability operation of the steels in automobile applications. Further, the addition of niobium (0.2 to 1%) lead to Fe-7Al-0.35C steel lead to in-situ formation of niobium carbide and κ-carbide precipitates which caused grain refinement from 320 μm to 80 μm. All the alloys demonstrated good (20% or more) tensile elongation. Also, about 80% increase in the yield strength (430 to 732 MPa) was witnessed with the Nb

addition. Similarly, addition of titanium (0.2 to 1 %) to Fe-7Al-0.35C steel resulted in-situ formation of titanium carbide along with κ-carbide precipitates which lead grain refinement from 162 μm to 48 μm. All these alloys also exhibited a significant enhancement in tensile elongation (18% or more). The yield strength of steel increased moderately from 408 to 568 MPa with the Ti addition from 0.2 to 1.0. These low-density steels with all the above alloying additions show a reduction in density of ~ 10% compared to the conventional steel (7874 kg/m^3).

Keywords**:** Lightweight steels, disordered Fe-7Al, borides, carbon, Nb, Ti, melting, hot and cold rolling, microstructure, grain refinement, precipitates, hardness, tensile properties, fractography, structure-property correlation

CONTENTS

Chapter 1

INTRODUCTION

1.1 Introduction

Steels are an important class of engineering materials that are produced in large tonnages. In view of their attractive properties such as high strength, good formability, recycling and economical aspects, they are suitable for various engineering applications including automobile, aerospace, rail, marine, structural, heavy duty industrial equipment and machinery and energy sectors etc. **(Frommeyer et al. 2000, Herrmann et al. 2003)**. Despite the evolution of lightweight materials (such as Al and Mg alloys, and various polymer, ceramic and composite materials) and their heavy competition with ferrous materials, yet the steels have been in growing demand because of their excellent combination of properties. Nevertheless, the high density of steels and its poor corrosion and oxidation behaviour restricted some of its widespread applications. Therefore, there is a need and urgent pressure on the steel producers to innovate new grades of steels with lower density and without compromising on its desirable properties.

Requirement for lightweighting of steel for structural application has ever increased, particularly for automobile and transportation applications. This is due to the increasing demand to improve fuel efficiency, reduce the CO_2 (thus contribute in controlling the global warming), enhance strength to weight ratio, make material suitable for environmental conditions emission and cater to the increased safety of the passenger. Focus is mainly to reduce the density of the structure without affecting other properties. This can be achieved by down-gauging of the conventional steel by the steel with higher strength and stiffness and finding newer steel compositions as per the requirements. However, the down-gauging of the steel sheet is limited by dent resistance and stiffness that it offers. So, the novel idea is to reduce the density of the steel itself. The density of the steel can be reduced by alloying with the addition of light weight elements like Li, Mg, Al, Si etc. or lighter materials (such as ceramics) as alloying or reinforcement agent.

Considering its strong effect on the density reduction and improvement in strength as well as other engineering aspects such as alloy making and workability, Al has emerged as the single most important alloying element in the development of low-density bulk steels **(Br¨ux et al. 2002).**

1.2 Motivation for the work

Disordered Fe-Al alloys are an emerging class of low-density/lightweight steels containing 6–9wt.% of aluminium in steel. These Fe–Al alloys have raised considerable interest due to their low-density, high ductility, cost-effectiveness and feasibility for bulk production. These low-density and high strength materials are envisaged in the development of an advanced lightweight ground transportation system, huge structures like bridges, tunnels and also being deemed for certain defence applications like troop's carrier and armour, etc. Alternatively, they are also considered as potential candidates for steam turbines in thermal power plants **(Frommeyer et al. 2000, Heo et al. 2012, Kartikasari 2014, Pramanik et al. 2018).**

The Fe-Al ferritic steels received relatively less attention in the early steel literature, probably because of their unappealing combination of strength and ductility **(Frommeyer et al. 2000, Herrmann et al. 2003).** In the recent past, the present authors and various research groups investigated Fe–7wt.%Al lightweight steels (which is single phase ferritic steel among the group of Fe-Al steels) in terms of alloy making(air induction melting with flux cover (AIMFC) etc.), adopting hot/cold rolling and other mechanical working methods to produce steels with better properties **(Khaple et al. 2010, Sikka et al. 1993).** Nevertheless, these alloys depict large grain size (about 1 mm) in cast condition. They exhibited about 18% tensile elongation and yield strength of 300 MPa at room temperature in the hot-rolled condition. However, the strength and ductility values are still low as compared to other competitive structural materials **(Frommeyer et al. 2000, Rana et al. 2013).** Hence, there is a need to further improve the room temperature tensile properties and formability of these lightweight steels. In fact, in view of these observations, the present PhD work has been carried to bridge the gaps in the development of Fe-Al lightweight steels.

1.3 Objectives of the present study

The main objective of present project work is to improve the mechanical properties of single phase ferritic Fe-7Al lightweight steel by controlling microstructure with the addition of inoculants (such as diborides: ZrB_2 and TiB_2) and carbon (in the wide range: 0.012 to 2.2wt.%). Based on these results, further the effect of strong carbide formers such as Nb and Ti on the structure and properties of Fe-7Al-0.35C based steels was systematically studied. Following are the major objectives of the proposed research work:

1) Identify the research gaps in the development of light weight steels based on the literature (Sir, should we remove his point or should we shift at the end of chapter 2, as section 2.13.)
2) Reduce the grain size of Fe-7wt.%Al steel with the addition of inoculants (ZrB_2 and TiB_2) and carbon (from 0.012 to 2.2wt.%)
3) Investigate the effect of inoculants (ZrB_2 and TiB_2) and carbon on the microstructure and mechanical properties of Fe-7wt.%Al steel
4) Study the effect of Nb addition (0.2, 0.4, 0.7 and 1wt.%) on the microstructure, hardness and tensile properties of Fe-7wt.%Al-0.35wt.%C steel
5) Understand the influence of Ti (0.2, 0.5, 0.75 and 1 wt.%.) on the grain refinement, hardness and strength of Fe-7wt.%Al-0.35wt.%C steel
6) Correlate structure-property of the developed light weight steels and asses its potential for different applications by comparing its properties with the literature

1.4 Organisation of the proposed thesis

The present thesis has been organised in to eight chapters and a brief description of the chapters is given below:

Chapter 1: As described above, a brief introduction followed by possible gaps that exist in the field of ferritic lightweight steels along with the objectives of the current PhD work **is** illustrated.

Chapter 2: This chapter reviews thoroughly the previous existing studies on ferritic lightweight steels. The advancements that are taking place in the areas of alloy design, melting approach, thermo-mechanical processing, heat treatments, effect of microstructural modification etc. are presented. Initially, the lightweighting approach was introduced along with phase diagram of the alloy system. This is accompanied by highlights on use of recent advancements to improve mechanical properties.

Chapter 3: It describes the raw material, alloy selection and experimental procedures such as melting, thermo-mechanical processing and cast alloy preliminary characterisation using chemical analysis, radiography and density measurements. Further detailed microstructural characterisation of steel samples includes study of the microstructure by optical microscope, its microstructural characterization and X-ray diffraction (XRD), scanning electron microscope (SEM) and electron-probe micro analysis (EPMA). Micro-chemical analysis of the phases is carried out by wavelength dispersive spectroscopy (WDS) and energy dispersive spectroscopy (EDS). This is followed by the evaluation of hardness and the tensile properties of the alloys along with the fractography.

Chapter 4: In this chapter, the effect of inoculants (ZrB_2 and TiB_2) additions on the grain refinement aspects is studied. Its influence on the microstructural features such as grain size, in the as cast, hot-rolled and annealed condition is investigated and micro-chemical analysis of the various phases is characterised. These microstructural findings were correlated with the mechanical properties for the alloy.

Chapter 5: This chapter reports the microstructural evolution in the wide range of carbon (0.012 to 2.2wt.%). The improvements in the strength of the lightweight steels by the various morphology of the carbides are described. The mechanisms of the correlation between microstructure and mechanical properties are discussed. The results are compared with the carbon containing lightweight Fe-Al ferritic steels reported in the literature.

Chapter 6 describes the understanding of the role of Nb on the in-situ formation of carbides and its effect on the microstructure and mechanical properties of Fe-7Al-0.35C alloy. Four alloys with Nb content in the range of (0.2 to 1 wt.%) were prepared, hot-

rolled and characterised. Thermo-Calc software is used to predict the phases present in the alloys which are validated by experimental work.

Chapter 7: In this chapter, the effect of Ti on the in-situ formation of carbides, the microstructure and mechanical properties of Fe-7Al-0.35C lightweight steel is reported. Here the morphology, micro-chemical analysis, volume fraction of the various precipitates formed are characterised. The microstructural features and the mechanical properties are compared with the other ferritic lightweight steels from the literature.

Chapter 8: This chapter summarizes the conclusions and the scope for future work that emerge out from the thesis: The main findings of the microstructural features, hardness and tensile properties of each of the alloy system are concluded. This chapter also lists out the possible areas of future research that can take up in the development of Fe-Al based lightweight steels.

Chapter 2

LITERATURE SURVEY

Chapter 2: This chapter reviews thoroughly the advancements that are taking place in the lightweight steels. This is accompanied by highlights on the use of recent advancements to improve mechanical properties.

2.1 Introduction

This chapter reviews thoroughly the previous work done on ferritic lightweight steels. It also reviews the developments that are taking place in the lightweight steels. Initially, the general considerations of lightweight steels, and the concepts involved in lightweightening/lowering the density of steel structures will be introduced. This will be followed by a comprehensive review of Fe-Al system, the phases and different types of low-density or lightweight steels. The advancements that are taking place in the areas of alloy design, melting approach, thermo-mechanical processing, heat treatments, effect of microstructural modification etc. are presented. This is accompanied by highlights on use of recent advancements to improve mechanical properties. Finally, the conclusions will bring forth significance of lightweight steels and throw light on future direction in the development of Fe-Al based lightweight steels.

2.2 General considerations of lightweight steels

Steels are engineering materials that are produced in very large quantities. They find application in various engineering sectors such as automotive, marine, aerospace, construction of buildings, machinery and heavy equipment and etc. **(Rana et al. 2014;**

Frommeyer et al. 2000). Despite the evolution of lightweight materials such as Al and Mg alloys, plastics, and various competing composite materials, the steels still have been in great demand and extensively used for countless applications because of their excellent combination of strength, formability, affordability, and recyclability (**Frommeyer et al. 2006, Br¨ux et al. 2002).** However, density of steel is much higher as compared to the light materials as mentioned above. Therefore, there is a need and urgent demand on the steel producers to innovate new grades of steels with lightweight/lower density and higher strength. The low-density and high strength steels are envisaged in the development of advanced lightweight ground transportation system, huge structures like bridges, tunnels and also being deemed for certain defence application like troops carrier, armour etc. Alternatively, they are also considered as potential candidates for steam turbines in thermal power plants (**Khaple et al. 2010, Herrmann et al. 2003, Khaple et al. 2015, Jimenez and Frommeryer 2011).**

2.3 Importance of lightweightening/lowering the density of steel structures

Requirement for lightweightening of steel for structural applications has increased, particularly for automobile applications. This is due to the ever increasing demand to improve fuel efficiency, reduce the CO_2 emission and cater to the increased safety of the passenger. It is reckoned that about 10% reduction in weight of the vehicle can improve the fuel efficiency by 7 %. This also implies that there is a reduction of 20 kg of CO_2 emission for every kilogram reduction in the weight of the vehicle **(Lee et. al. 2010)**. Hence, focus is mainly to reduce the density of the structure without adversely affecting other properties. **Fig. 2.1** explains the concepts used for reducing the weight of the steel part. This can be achieved by down-gauging of the conventional steel by using the steel with higher strength and stiffness **(Fig. 2.1a).** However, the down-gauging of the steel sheet is limited by dent resistance and stiffness that the steel offers. Another novel idea is to reduce the density of the steel itself for the given thickness **(Fig. 2.1b).**

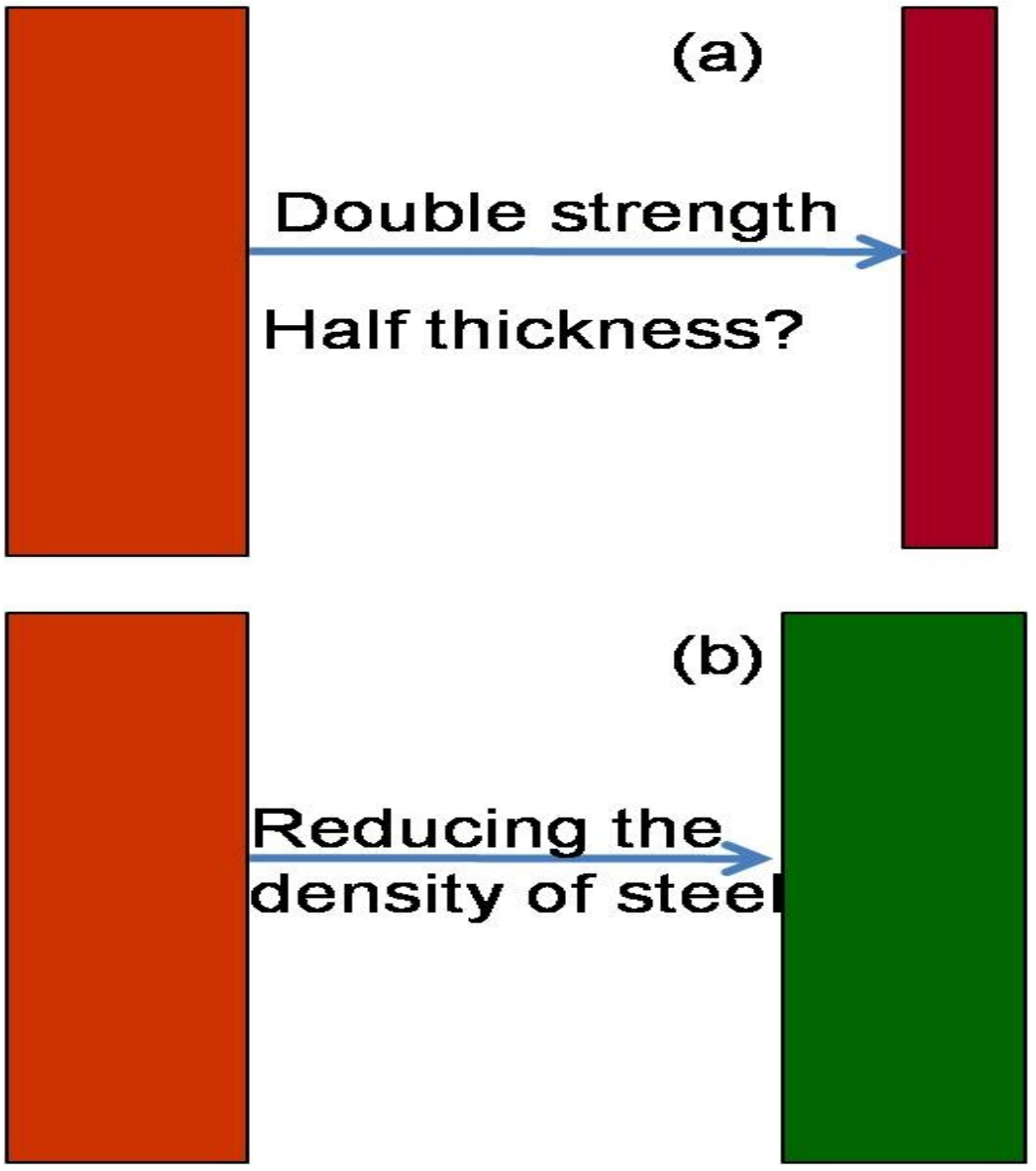

Fig. 2.1 The concepts of lightweightening (a) down-gauging of steel with higher strength steel and (b) reducing the density of the steel itself for given thickness.

2.3.1 Lightweightening and improving strength of steels

In the last three decades, automobile industry witnessed the development of various grades of steel primarily focusing on the improvement of strength and formability, so that the down-gauging of the same steel parts can be made. Steels developed in automobile industry based on their strength can be classified as (a) Low-strength steels such as mild steel and interstitial free (IF) steel, (b) Conventional high-strength steels (HSS) such as bake hardening (BH), carbon-manganese (C-Mn) and high strength low alloy (HSLA) steel and (c) Advanced high-strength steels (AHSS) such as dual phase (DP), complex phase (CP), transformation-induced plasticity (TRIP), twinning-induced plasticity (TWIP) and martensitic steels (**Soleimani et al. 2020,** https://www.worldautosteel.org/). **Fig. 2.2** shows the famous banana curve of various steels .

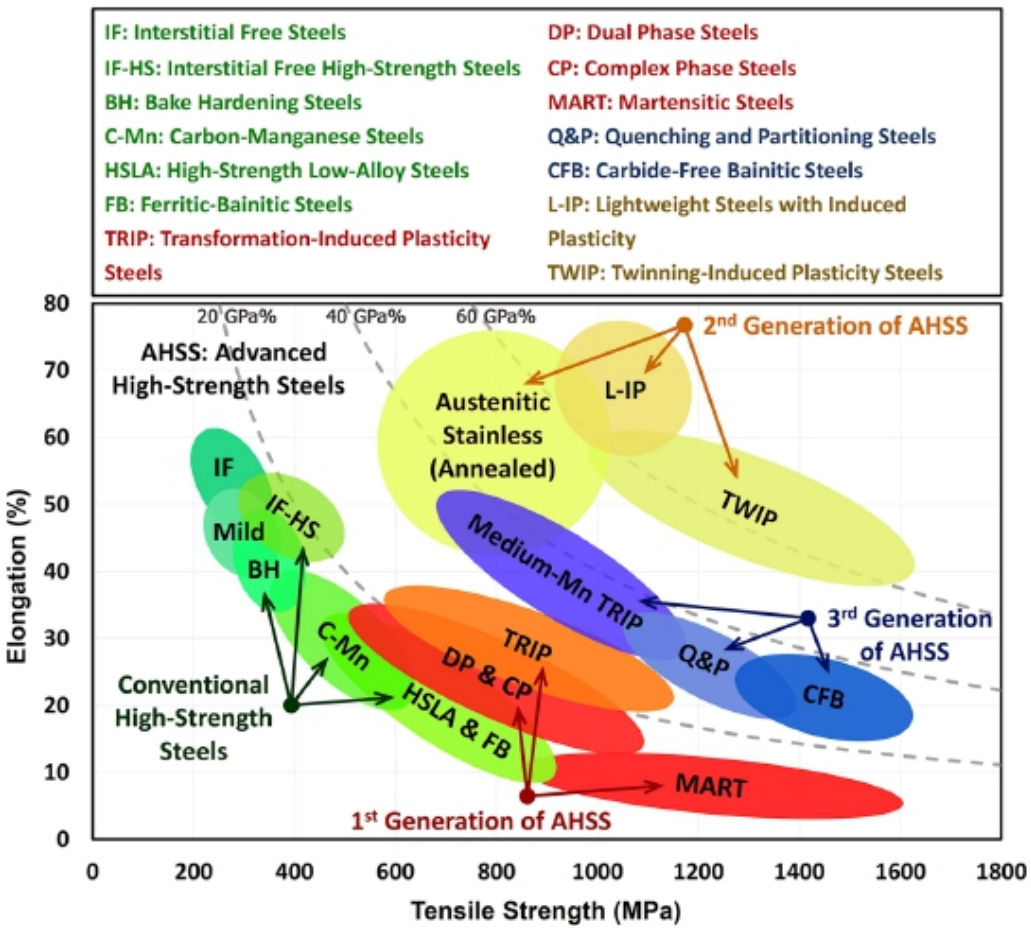

Fig. 2.2 The famous banana curve of various steels used in automobile industry **(Soleimani et al. 2020).**

2.3.2 Lightweightening by reducing the density of the steel itself

Lightweightening of the steel or reduction in density of the steel can be achieved by alloying the steel with low density alloying elements such as Li (0.534 g/cm^3), Mg (1.738 g/cm^3), C (2.26 g/cm^3), Si (2.33 g/cm^3), Al (2.70 g/cm^3), Mn (7.21 g/cm^3), Cr (7.19 g/cm^3) and etc. These elements are expected to contribute to the reduction in density of the steels by affecting the lattice parameter of the steel and also due to their lower atomic masses. However, there is no solubility of lighter elements like Li and Mg in Fe. These elements are highly reactive and flammable. **Fig. 2.3** illustrates the density reduction in steel by alloying with lighter elements than iron. For example, addition of 12wt.% Al to Fe reduces the density by 17%, of which 10% is caused by lattice dilatation and 7% is contributed by reduction in atomic mass **(Chu et al. 1994, Lehnhoff et al. 2014)**. Each wt.% of Al gives the reduction in density of about 1.3%. For the alloying elements such as C, Si, Al and Mn, a linear decrease in the density of the steel was reported. Above 2% of carbon, graphite phase starts formation, which reduces the strength. Addition of more than 7% of Al in steel tends to form short range ordering, where the ductility starts degrading because of the ordering effect. The effect of Si is similar to Al but almost at half the quantity, which means that, at above 3.5wt.% of Si in steel, ordered phase would form to hinder the ductility. The contribution to the density reduction by the addition of Mn and Cr is comparatively less, but these elements offer to increase the strength of the steel by solid solution strengthening in the matrix.

Considering its strong effect on density reduction and improvement in strength as well as other engineering aspects such as alloy making and workability, Al emerged as the single most important alloying element in the development of lightweight bulk steels. In all the low density/light weight steels, Al is the main element employed for reducing the density. In some cases, Si is also added along with Al. Although Al can be added in low-density ferritic steels upto 11 wt.% **(Lilly et al. 1998, Vyas et al. 1992, Rana et al. 2013, Pramanik and Suwas 2014),** it has been suggested that the Al content should be restricted to less than about 6.5 wt.% **(Frommeyer et al. 2006, Vyas et al. 1992)** due to the propensity for short-range ordering at higher Al contents, which increases brittleness and adversely affects formability **(Frommeyer et al. 2006, Vyas et al. 1992, Rana et al. 2013, Pramanik and Suwas 2014, Frommeyer 1997, Herrmann et al. 2013, Rana 2014, Rana and Liu 2013).** Carbon and manganese are austenite stabilizers which are

added in Fe-Al alloys to get the austenitic phase which is very important in the phase transformation (heat treatment) of steels. Concurrent addition of C and Mn to Fe-Al alloy leads to the stabilization of austenite phase at low temperature. Addition of carbon in Fe-Al leads to the formation of κ-carbide which is an intermetallic phase though it improves strength but leads to reduction in ductility. The addition of Mn to Fe-Al-C leads to the drastic improvement in strength due to solid solution strengthening but reduces ductility due to the formation of bulky κ-carbides. These steels are prone to cracking due to the bulky κ-carbides during hot and cold working **(Sohn et al. 2014, Han et al. 2010, Shin et al. 2010).**

2.4 Types of low-density or lightweight steels

Based on the temperature and the relative amount of the alloying additions (Al, C and Mn), the matrix phase of the steel can be ferritic, austenitic or a mixture of both these phases (**Chen et al. 2017)**. Hence based on the microstructural features the low density steels are categorised into four types namely ferritic steels, austenitic steels, ferritic based duplex steel and austenitic based duplex steels **(Herrmann et al. 2003, Khaple et al. 2010, Morris et al. 2007, Rana et al. 2013, Satya Prasad et al. 2014, Castan et al. 2013, Falat et al. 2005, Zargaran et al. 2014, Brüx et al. 2012)**. **Table 2.1** shows the composition range and broad tensile properties of the four types of low density steels. The ferritic steels are high in Al whereas the austenitic steels are high in carbon and manganese. In comparison to ferritic steels, low density steels with higher Mn and Al content have a more diverse microstructure and superior mechanical properties.

Deleted[khaple H]: The lightweight steels with Al and Mn content display a variety of microstructural features which enhances the mechanical properties compared to the conventional structural steels.

(i) Ferritic low-density/lightweight steels have high amount of Al (upto 12%), Mn upto 4 % and low carbon. These steels generally exhibit elongated ferritic microstructure at the hot working temperature. At room temperature, based on the Al and C content, these steels show generally ferritic structure along with minor amount of κ carbide precipitates.

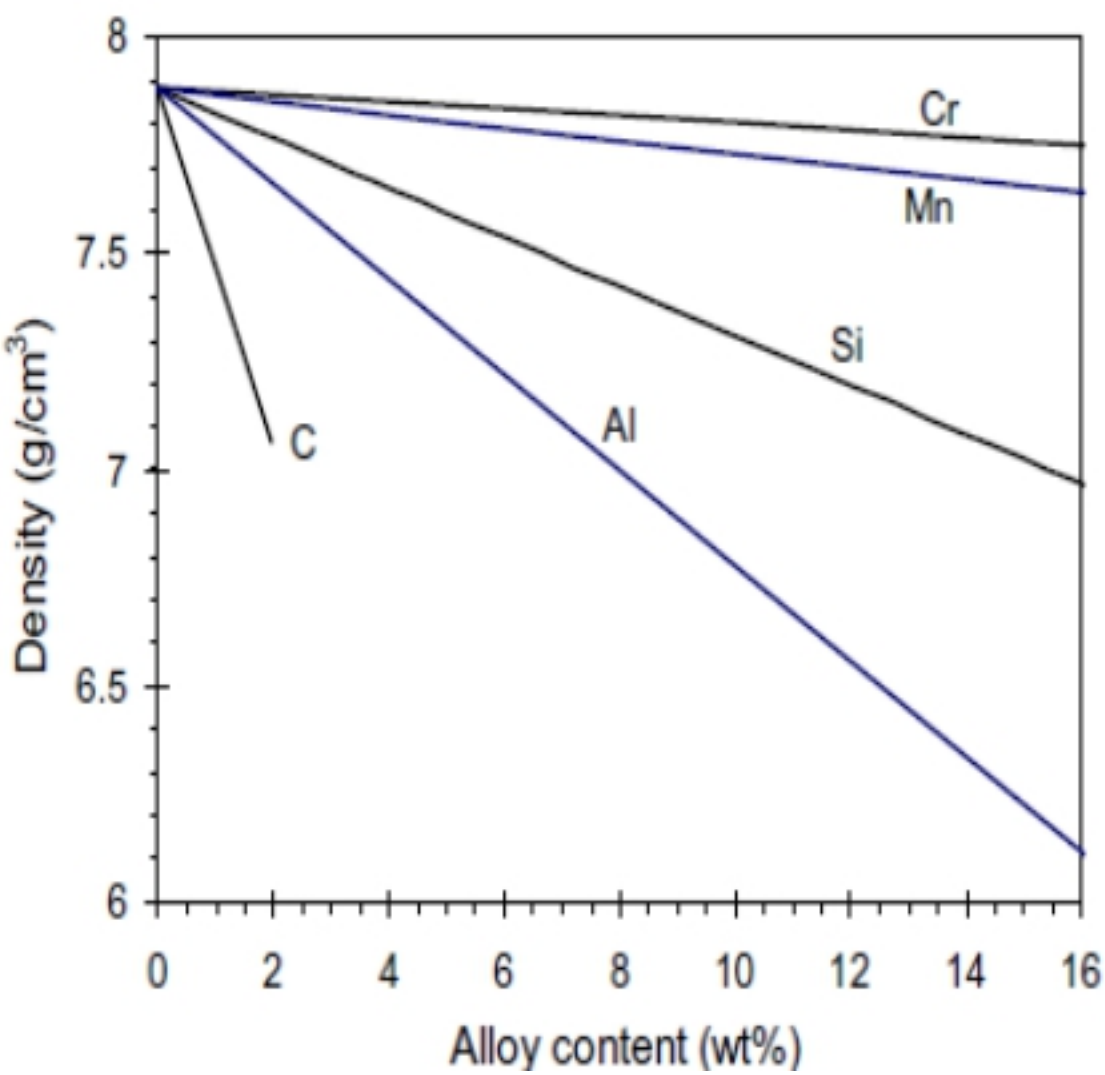

Fig. 2.3 The density reduction in steel by alloying with lighter elements **(Chu et al. 1994, Lehnhoff et al. 2014, Bohnenkamp and Sandström 2000)**

Among all the low-density steels, ferritic steels are comparatively easy to work with the conventional process of hot working and cold working and basically cold worked sheets can be produced of these steels. The ferritic steels have tensile properties similar to that of conventional high-strength low-alloy steels (HSLA) and with an added advantage of density reduction. These steels are also recognised as the first generation of advanced high-strength steel **(Herrmann et al. 2003, Khaple et al. 2010, Morris et al. 2007, Rana et al. 2013, Satya Prasad et al. 2014, Castan et al. 2013, Brüx et al. 2012)**.

(ii) Austenitic low-density/lightweight steels have high amount of Mn (12 to 30%) and carbon (upto 2%). It can also accommodate high amount of Al (upto 12%) **(Frommeyer et al. 2003, Lai and Wan 1989, Springer and Raabe 2012, Gutierrez-Urrutia and Raabe 2013)**. These steels show single austenitic phase at the hot working temperature. These steels have mainly austenitic phase with traces of ferrite, κ-carbide and β-Mn phase. In the cast condition, these steels show dendritic microstructure comprising a mixture of austenite and ferrite because of the large amount of segregation caused by the significant quantity of alloying elements. The homogenisation is generally carried out at a reheating temperature of 1100-1250^{0}C for adequate time. The recrystalised microstructure contains equiaxed austenitic grains with annealing twins **(Jung et al. 2015, Park et al. 2010, Yoo and Park 2008, Choi et al. 2007, Lin et al. 2014)**. The slow cooling of these steels results in the formation of κ-carbides as well as ferritic phases which most likely appear along the austenitic grain boundaries and also inside the matrix of austenite. These κ-carbides are about 3 to 6 times bigger in size compared to those resulting from solutionising, quenching and aging process which reduces the ductility and toughness. Hence these steels are generally water quenched from solution temperature (900–1100^{0}C) to avoid the precipitation of coarse κ-carbide. Aging of austenitic Fe-Mn-Al-C steels, in a temperature range of 500 to 900^{0}C, two types of κ-carbides are formed, namely intergranular and intragranular κ-carbides. The morphology of these carbides drastically affects the properties of the steel.

The fine κ-carbide precipitate which forms during ageing process enhances the yield strength considerably (**Howell and Van Aken 2009, Woo and Kim 2013, Bausch et al. 2009; Frommeyer and Brüx 2006, Kim et al. 2013**) whereas the intergranular κ-carbide is very coarse and drastically reduces the ductility. In general, these steels exhibit good combination of strength (600-1700 MPa) and ductility (upto 85%) **(Chen et al. 2017).**

(iii) Ferritic based duplex low-density/lightweight steels contain Mn upto 12 % and Al upto 7%. They exhibit higher volume fraction of ferrite (greater than 50%) with very small amount of austenite at the hot working temperature **(Rana et al. 2014, Han et al. 2010, Sohn et al. 2014, Sohn et al. 2013, Shin et al. 2010, Seo et al. 2012, Sohn et al. 2014, Lee et al. 2015, Jeong et al. 2013)** The austenite phase is less stable since the alloying elements are less. Based on the processing condition and also the large variation in C and Mn content, these steels can exhibit a variety of complex transformation at ambient temperature. These steels are cold rolled and then annealed at an intercritical temperature from 700 to 900^0C, followed by austempering. These dual phase steels with plastic deformation of ferrite and retained austenite exhibit superior strength and plasticity compared to the ferritic and HSLA steels **(Park et al. 2013, Rigaut et al. 2007, Cai et al. 2014, Han et al. 2012, Seol et al. 2013, Sohn et al. 2015.)**

(iv) Austenitic based duplex low-density/lightweight steels contain lower amount of Mn and carbon compared to austenitic low-density steels **(Etienne et al. 2013, Zhao et al. 2016, Yang et al. 2016, Wu et al. 2013, Ha et al. 2016)**. At hot working temperature, these steels exhibit substantial amount of austenite which is a continuous phase with lesser amount of ferrite phase. Due to the higher alloying elements the austenite phase is quite stable. At room temperature, these steels may have stable austenite phase along with κ-carbide precipitates and a small quantity of ferrite phase and is also known as triplex steels owing to the three phases. The tensile properties are much better than ferritic and ferritic based low density steels **(Yang et al. 2015, Zhang et al. 2015, Zhang et al. 2015, Rana et al. 2012, Hwang et al. 2011).**

2.5 Phase diagram of Fe-Al alloy

The ferritic Fe-Al steel system is primarily based on Fe-Al binary phase diagram, which is shown in **Fig. 2.4 (Kubaschewski, 1982, Frommeyer and Brüx 2006).** Al is a strong ferrite stabilizer, which reduces the austenitic loop significantly while zooming the ferritic phase field. This results in a fully ferritic microstructure at room temperature. The solubility of Al in BCC iron is very high.The solidus temperature for pure iron is 1538^{o}C, which can be brought down by increasing the Al content. At 34wt.% of Al, the solidus temperature is about 1220^{o}C. The solubility of Al in austenite is very limited (0.65 wt.%). It is clear from the Fe-Al phase diagram that above 1wt.% of Al, the hardenability transformation which occurs from austenite to martensite is ruled out.

Based on the Al content the main phases observed at room temperature are disordered α A2 (Fe-Al), ordered (DO_3) Fe_3Al and ordered (B2) FeAl. The α ferrite solid solution occurs in Fe-Al system upto 10wt.% of Al. It is BCC solid solution with disordered A2 lattice. The position of the Fe and Al atoms are distributed statistically as shown in **Fig. 2.5a**. At higher Al content, the A2 (Fe-Al) lattice gets ordered. Ordered super lattice of Fe_3Al occurs with about 12 to 22 wt.% Al content. This structure has 12 Fe atoms and 4 Al atoms, with a total of 16 atoms per unit cell which is as given in **Fig. 2.5b.** At temperature above 552^{0}C, the first order transformation from Fe_3Al to ordered (B2) FeAl occurs. Here the corner positions are occupied by Fe atoms and centre positions are occupied by Al atoms or vice versa **(Fig. 2.5c).** At still higher temperature, (B2) FeAl transforms to disordered α ferrite A2 (Fe-Al) as described in the above phase diagram. Fe_3Al occurs by the second order transformation from FeAl through ordering of α ferrite A2 (Fe-Al) phase below 552^{0}C **(Frommeyer and Brüx 2006, Kubaschewski 1982).**

Table 2.1 showing the different types of lightweight/low-density steels **(Chen et al. 2017)**

Types of steels	Characteristic Features		
	Microstructure of hot-rolled steel	Typical range of composition (wt.%)	Tensile Properties
Ferritic steels	Fe-Al α phase	Al : 2-12%, Mn : 0- 4% C : 0.05-0.5%	UTS : 250-600 MPa TE : 10-30%
Austentic steels	γ phase	Al : 5-12%, Mn : 12- 30% C : 0.6-2.0%	UTS : 800-1700 MPa TE : 30-85%
Ferritic based duplex steels	γ in Fe-Al α phase	Al : 3-7%, Mn : 2- 12% C : 0.05-0.5%	UTS : 400-900 MPa TE : 10-40%
Austenitic based duplex steels	α in γ phase	Al : 2-9%, Mn : 5- 30% C : 0.5-0.8%	UTS : 800-1300 MPa TE : 20-50%

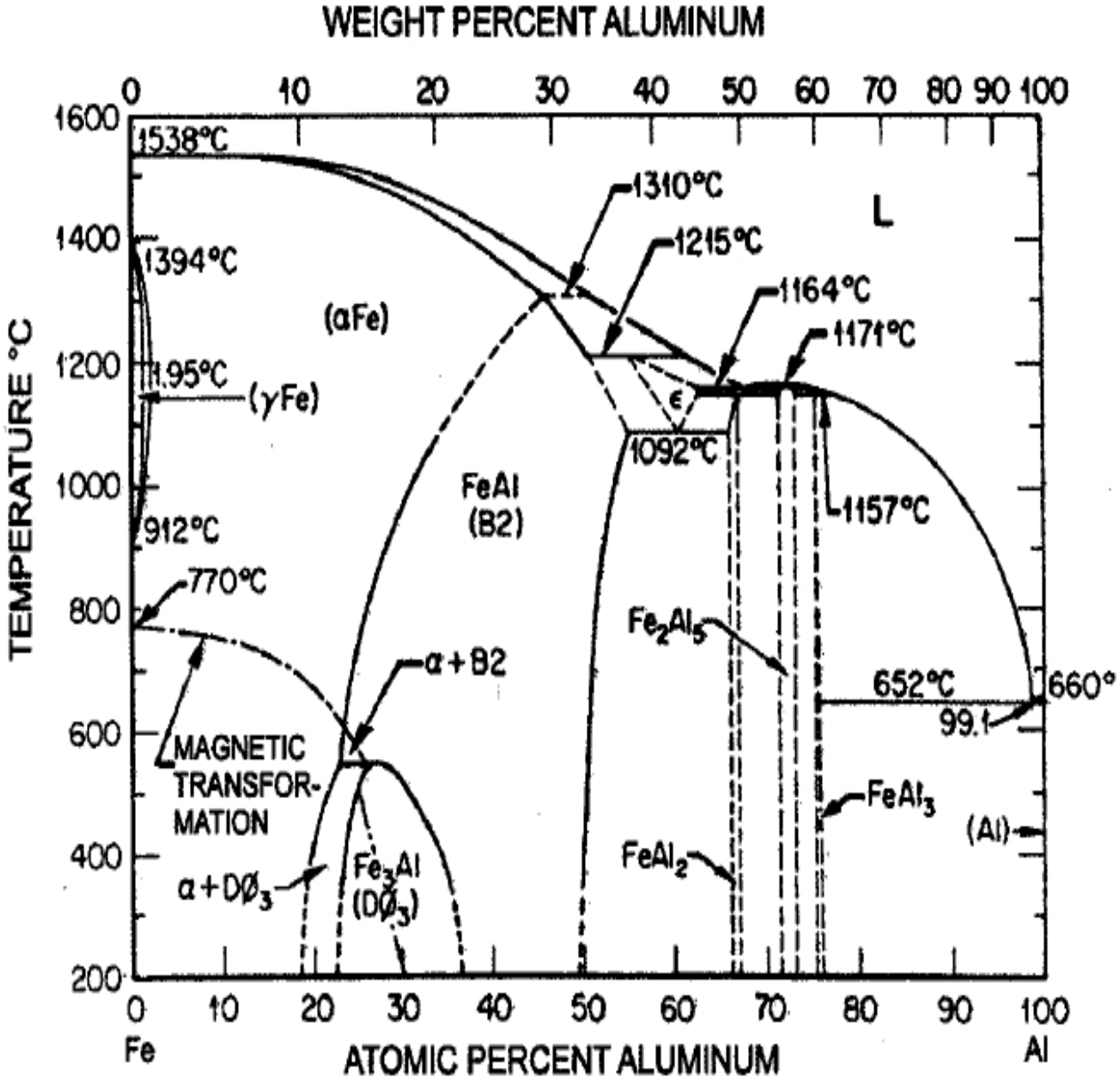

Fig. 2.4 The Phase diagram of Fe-Al with variation of Al (**Frommeyer and Brüx 2006, Kubaschewski, 1982**).

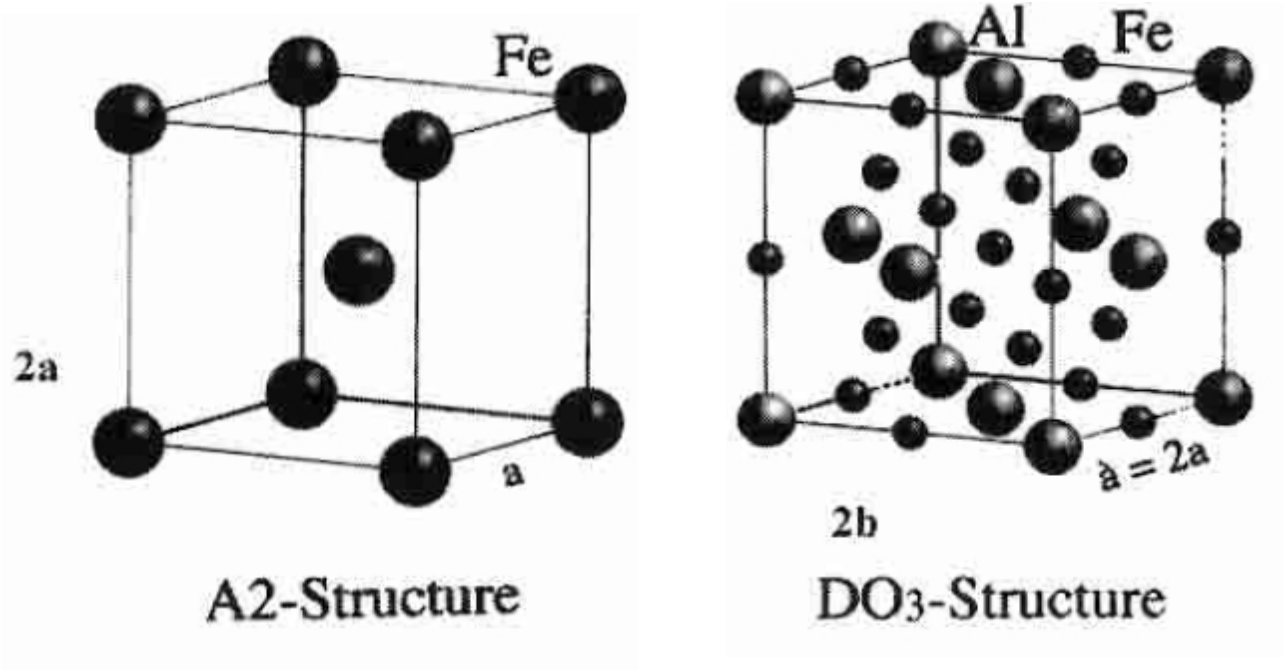

Fig. 2.5 BCC lattice structures by adding Al to Fe. (a) Dis-ordered A2, (b) Ordered DO_3 and (c) Ordered B2 (**Frommeyer and Brüx 2006).**

There are two more areas, which are denoted by K1 and K2 and are known as K-state in the Fe rich part of Fe-Al phase diagram as shown in **Fig. 2.6 (Kubaschewski 1982, Davies 1963, Marceau et al. 2015).** This K-state is an intermediate stage which is caused by the complex short-range ordering reactions which is still not clear. It was observed that short-range ordering occurs with 6.2 to 9.6 wt.% of Al while cooling below 400^0C **(Marcinkowski and Taylor, 1975)**. It was noticed that at about 250^0C, degree of short-range ordering was highest. The disordering to ordering transformation affects tensile properties of the alloy such as ductility and strength. Among all the phases described above, the alloys with disordered α A2 (Fe-Al) show good ductility. The alloys with ordered DO_3, B2 and complex K-state show poor ductility and exhibit brittle fracture behaviour at room temperature **(Stoloff 1998).**

In Fe-Al system, α(Fe-Al), Fe_3Al and FeAl are the important phases from structural application point of view. Fe_3Al and FeAl alloys are intermetallic in nature and are well-known as iron aluminide. It was witnessed that alloys based on single phase α(Fe-Al) exhibited good ductility but very poor high temperature strength, whereas iron aluminides offered good tensile and creep properties at intermediate temperature. Fairly low cost of the material and good corrosion resistance at high temperature are the key properties of Fe-Al alloys. Some physical properties of Fe-Al based alloys are given in **Table 2.2.**

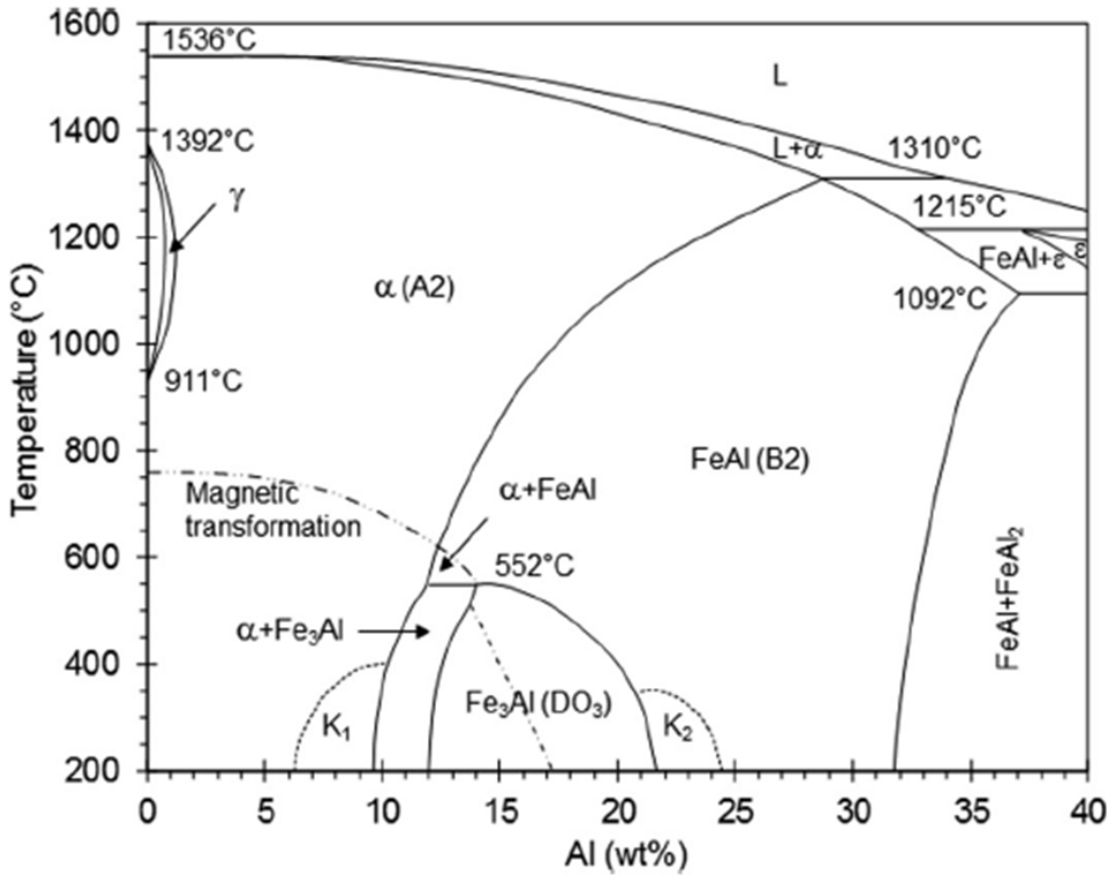

Fig. 2.6 The Fe-Al phase diagram, where intermediate regions are marked as K1 and K2 **(Kubaschewski 1982, Davies 1963, Marceau et al. 2015).**

Table 2.2 Typical physical properties of alloys based on Fe-Al BCC lattices. (**Stoloff 1998)**

Phases	Crystal structure	Critical ordering temperature (^{0}C)	Melting point (^{0}C)	Density (gm/cm^3)
Fe-Al (at 7wt.% Al)	Disordered BCC α (Fe-Al)	200 (at 10wt.%Al)	1530	7.2
Fe_3Al	DO3 (bcc) B2 (bcc)	552 760	1520 1540	6.72 -
FeAl	B2 (bcc)	1250	1250	5.56

2.5.2 Disordered *α*-(Fe-Al) ferritic based lightweight/low-density steels

As discussed above, the earlier research on Fe-Al alloy was focused on the development of iron aluminides for high temperature applications, and very limited study on the alloys containing disordered *α*-phase was reported. Demand for reducing weight of steel for structural applications has increased. This is more particularly for automobile applications in the wake of an ever increasing demand to improve the fuel efficiency, reduce CO_2 emission and increase safety of passenger. Recently renowned interest is generated in these alloys because of the excellent properties they offer such as reduction in density, lower raw material cost, good ductility and reasonable strength. The corrosion resistance is improved by the presence of Al in the steel. These alloys offer good soft magnetic properties as well (**Syahrila and Rawlings 2002**). They have tremendous potential for automobile application because of the lightweightening of the steels (offered by the reduction in the density of the steel itself).

Disordered Fe-Al alloys are an emerging class of low-density/lightweight steels containing aluminium in the range of 6–9wt.% in steel (All compositions are in wt.%). These Fe–Al alloys have raised considerable interest due to their low-density, high ductility, cost-effectiveness and feasibility for bulk production. These low-density and high strength materials are envisaged in the development of an advanced lightweight ground transportation system, huge structures like bridges, tunnels and also being deemed for certain defence applications like troop's carrier, armour, etc. Alternatively, they are also considered as potential candidates for steam turbines in thermal power plants **(Frommeyer et al. 2000, Heo et al. 2012, Kartikasari 2014, Pramanik et al. 2018).**

As discussed earlier, addition of Al which being a ferrite stabilizer in iron/steel, reduces the austenitic loop significantly while zooming the ferritic phase field (**Fig. 2.4**). This results in a fully ferritic microstructure at room temperature. The solid solubility of Al in bcc iron is upto 10wt.% and it's solubility in FCC iron is limited to 0.65wt.%. About 1.wt.% Al is sufficient to avoid the occurrence of γ phase **(Prescott and Graham, 1992).** Addition of 34% of Al to pure Fe reduces the solidus temperature from 1538^{o}C to 1215^{o}C. The Fe-Al ferritic steels received comparatively less attention in early steel literature. It was probably because of their unappealing high temperature properties such as creep and tensile. During that time research was mainly focused to develop materials for high temperature applications.

The density of the ferritic lightweight steel was examined by various techniques namely levitation, pycnometric and X-ray diffraction technique (theoretical density and lattice constants) for different Al content. The plot of density measurements for several Al content is shown in **Fig. 2.7.** As the Al content increases there is a reduction in the density of the steel. The density of the steel reduced from 7.8 to 7.25 g/cm^3 (at about 6 wt.%Al), further the steel density approached to 7g/cm^3 (at 8.5wt.%Al). Hence, more than 10 % decrease in density is achieved **(Frommeyer et al. 2000).**

The elastic modulus of the steel is affected by the addition of Al. As the Al content increased in the steel, a down-ward trend in the elastic modulus was observed. The effect of Al content on elastic modulus is shown in **Fig. 2.8**. This is primarily due to the reduction in the lattice energy of Fe-Al solid solution. It is also caused by the longer distance between Fe and Al atoms in the lattice **(Frommeyer et al. 2000).**

Although Al can be added in low-density ferritic steels upto 11 wt.% **(Lilly et al. 1998, Vyas et al. 1992, Rana et al. 2013, Pramanik and Suwas 2014)** it has been suggested that the Al content should be restricted to less than about 6.5 wt.% **(Frommeyer and Br¨ux 2006, Vyas et al. 1992)** due to the propensity for short-range ordering at higher Al contents >11%, and at above 12% completely ordered (DO_3) Fe_3Al aluminde is formed which increases brittleness and adversely affects formability, particularly the room temperature ductility is less than 5%

2.6 Microstructure and mechanical properties of Fe-Al based lightweight steels

Since aluminium content of Fe-Al based ferritic steel is high (6-9wt.%) and it has traces of carbon (<0.03%) the phase transformation of ferrite to austenite is ruled out at all the range of the temperature. Therefore, for these steels the hot-working process is generally carried out in the single ferrite region. Since the addition of Al to steel stabilizes the ferrite region upto the melting point of these steels, over and above it increases the temperature of recrystallisation of ferrite matrix. For this reason, the adequate grain refinement cannot be achieved by dynamic/static recrystallisation. This results in more of elongated grains of the ferrite matrix in the direction of rolling. Generally, a columnar single phase ferrite microstructure is observed in the as-cast steels. Depending on the cooling rate from the hot working condition, κ-carbides are formed in the ferrite grain boundries **(Rana et al. 2013, Brüx et al. 2013).** These κ-carbides are generally elongated, thick and shape is of rod-type. Moreover, they are semi coherent with the α Fe-Al matrix **(Seol et al. 2013).**

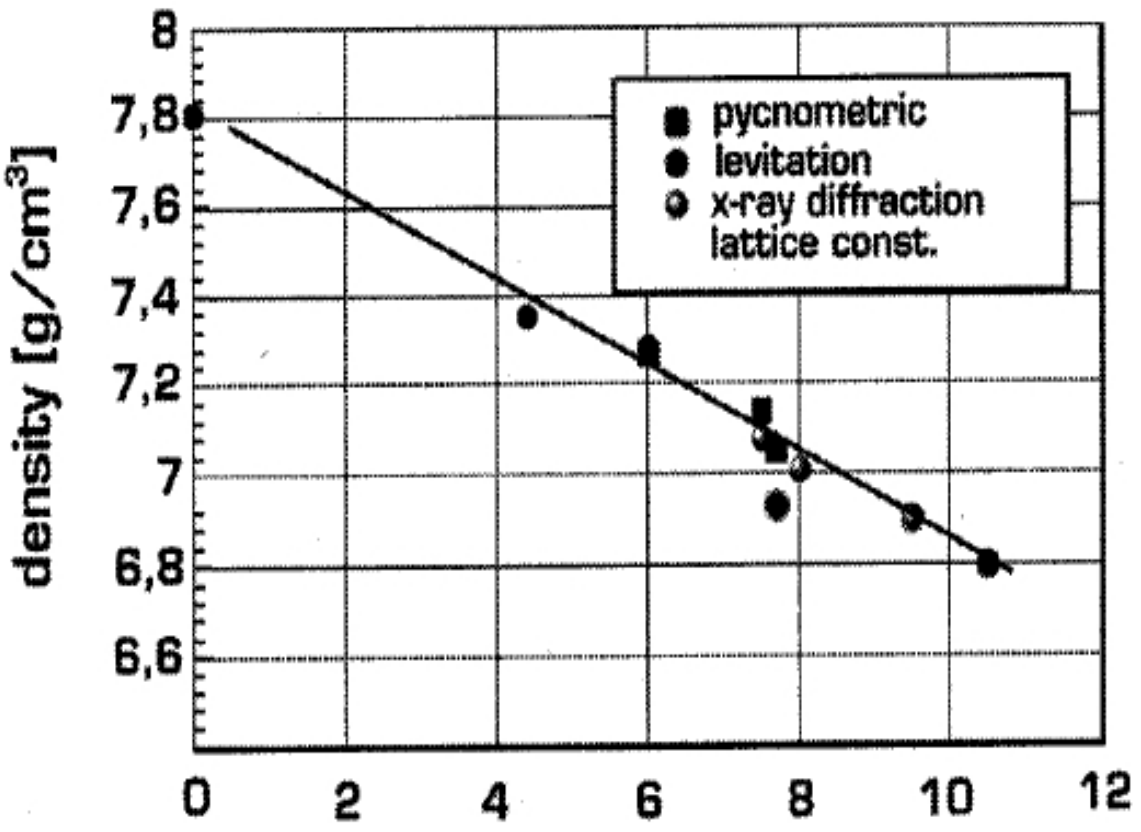

Fig. 2.7 The effect of Al content on density of steel measured using different techniques **(Frommeyer et al. 2000).**

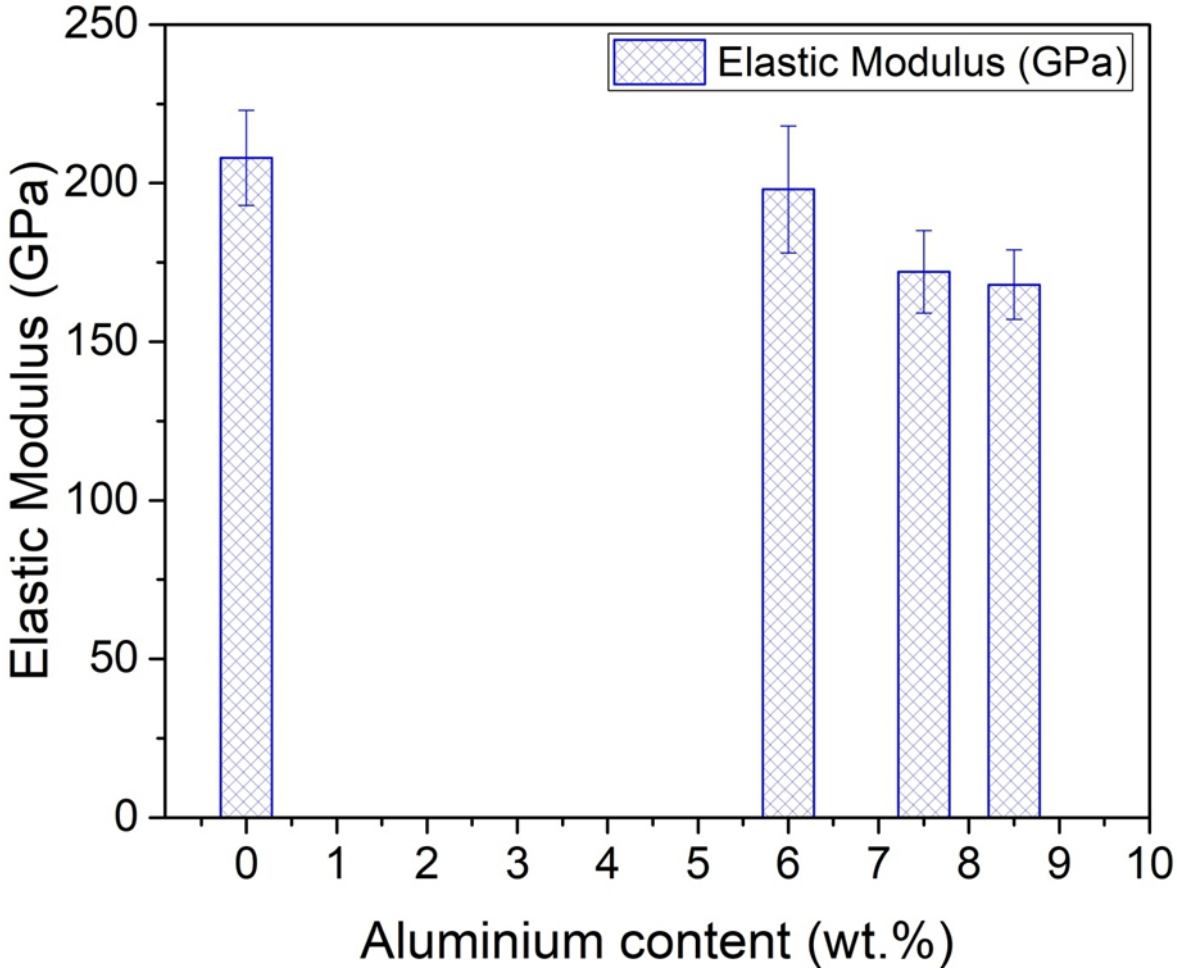

Fig. 2.8 Variation of elastic modulus of steel with Al content **(Frommeyer et al. 2000)**.

The tensile properties of Fe-Al solid solution are moreover affected by even minute quantity of carbon as it leads to the generation of harmful κ-carbide precipitates along the grain boundaries. In binary Fe-C and ternary Fe-Al-C alloy system, the solubility of carbon (below 500°C) in αFe and α(Fe-Al) is less than 13 and 50 ppm, respectively. Carbon content more than that mentioned above leads to the formation of κ-carbide precipitates. These are basically carbon stabilised ordered solid solution and exist over a range of composition in the form of $Fe_{4-y}Al_yC_x$ where x is $0 \leq x \leq 1$ and y is $0.8 \leq y \leq 1.2$. They are of perovskite structure related to L12' type. The size of the κ-carbide precipitates increases with increase in the carbon content. Hence, the work on Fe-Al (ordered or disordered alloys) system was carried out with high purity raw materials with negligible carbon **(Mendiratta et al. 1987, Morris et al. 2007, Herrmann et al. 2003, Rana et al. 2013).**

Herrmann et al. 2003 studied the mechanical behaviour of the as-cast samples with the Al content in the range of 2-9.6wt.%. All the alloys showed a single phase with very coarse grain (approx. 1mm) microstructure **(Herrmann et al. 2003).** It was observed that long duration heat treatments (14 days/320^{0}C) resulted in the formation of κ-carbides (thin to thick rod/plate type) on the grain boundaries. The mechanical properties are shown in **Fig. 2.9**. It is noticed that the strength and ductility of these steels are dictated mainly by solid solution strengthening of Al. Though the contribution from the short-range ordering is only minor but it is also depends on the quenched in excess vacancies resulting from heat treatments. It was observed that quenching from high temperature results in excess vacancies which add on to hardening. Post annealing treatment to soften the material by eliminating the excess vacancies is very slow process. It has also been observed that as the Al content increases in the solid solution range (disordered-A2 Fe-Al) upto about 13wt.%, the yield strength also increases due to solid solution strengthening according to Suzuki's theory of solid solution strengthening. Further increase in the amount of Al lead to the formation of ordered intermetallics, namely Fe_3Al (DO_3) and FeAl (B2) causing drastic decrease in strength as well as ductility.

The strength of the ferritic iron-aluminium steels can be increased by work hardening during deformation. The rate of work hardening for Fe-Al alloys estimated with respect to different Al content is shown in **Fig. 2.10**. In case of α(Fe-Al) alloys with Al upto 7wt.%,

the work hardening rate is very low. With further increase in Al to 16%, there is a steep rise of the work hardening rate due to the change from the disordered to K1 state to ordered state and drops to a reasonable rate above 20%. In Fe-Al steels, the deformation is mainly due to generation of dislocation and slips within the grains. For a complete disordered state (6wt.%Al), dislocation glide bands were noticed besides dislocation tangles among them. For K1 state (8wt.%Al), straight segments of paired dislocation with narrow mechanical antiphase boundaries were observed at low strain rate. At high strain rate, dense dislocation bundles were seen in the ferrite. In addition some undeformed B2 regions were observed signifying that the deformation of matrix is not uniform. It is proposed that strain hardening of the steel is primarily governed by shearing of the ordered phases through super-dislocation. The deformed structure at room temperature was observed for different Al content. It was reported the dislocation structure exhibited an evolution from a single bowed dislocation to paired super-dislocations with a strong inclination to form straight screw segments when the phases changes from disordered to complete ordered phase. Due to the inadequate dislocation mobility, deformation twinning takes place more easily at higher Al content and lower temperature **(Herrmann et al. 2003).**

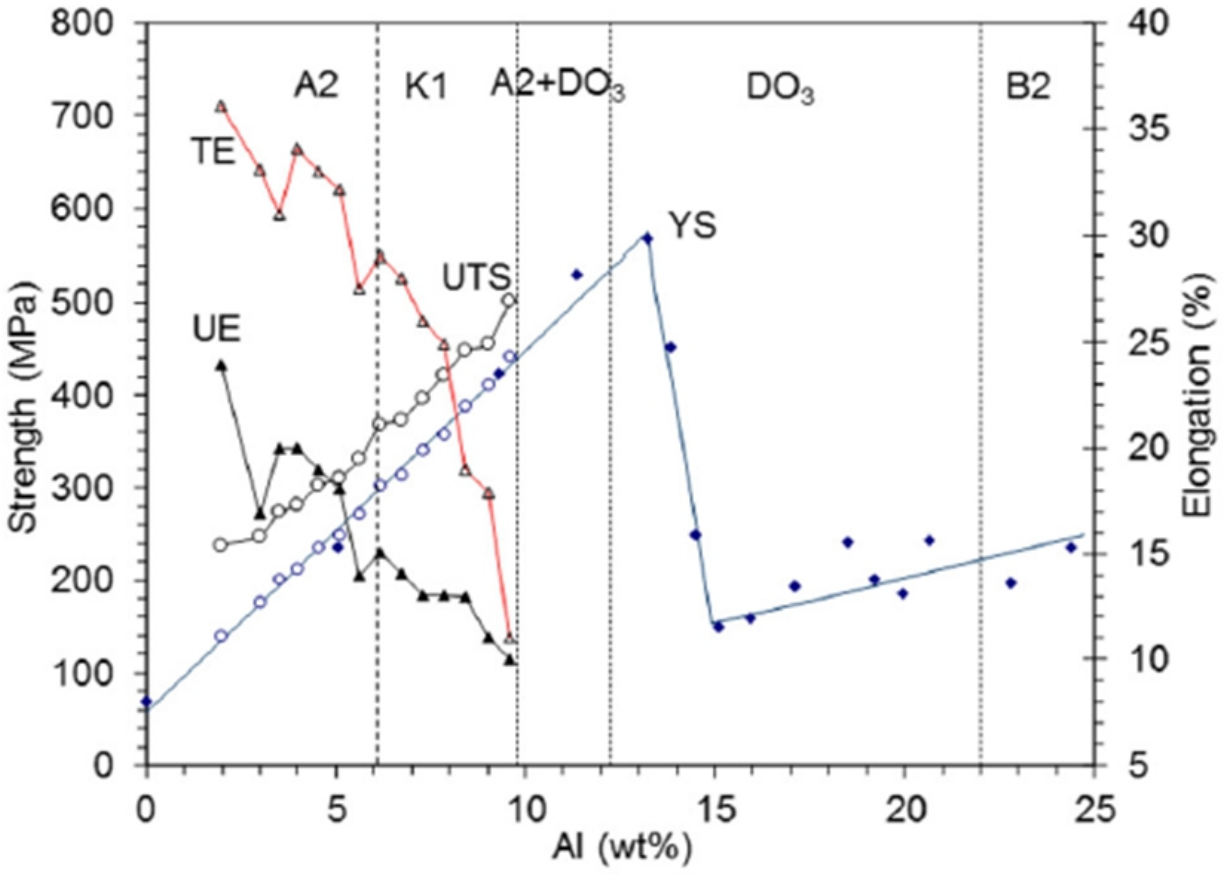

Fig. 2.9 Variation of tensile properties of Fe-Al alloy with different Al content. Lattice structure and strengthening caused due to solid solution is indicated**.** TE-total elongation, UE-Uniform elongation **(Frommeyer et al. 2000, Herrmann et al. 2003).**

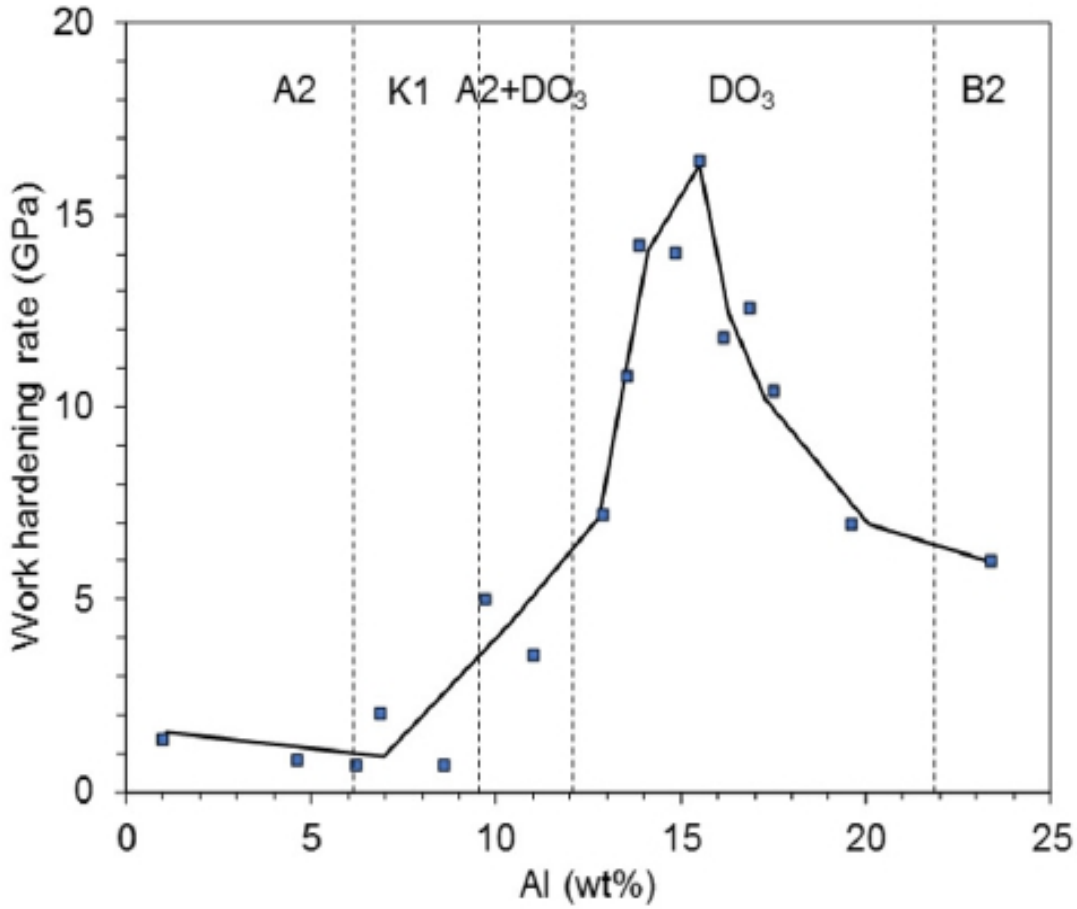

Fig. 2.10 The plot of rate of work hardening with Al content. The influence on lattice structure is also indicated **(Frommeyer et al. 2000, Herrmann et al. 2003)**

Hot torsion process was used to understand the role of various deformation parameters (such as strain, strain rate and temperature) on Fe-8wt% Al low density steel. The test was carried out at three temperature namely (900 to 1100^0C), with a stain rate of 0.1 to 10/s. In this alloy, the dynamic recrystallisation observed has been of two types. Continuous dynamic recrystallisation (CDRX) is noticed at low strain rate and low temperature and on the other hand discontinuous dynamic recrystallisation (DDRX) is noticed at high strain rate and high temperature which is shown in **Fig. 2.11.** In DDRX, the orientation of the newly recrystalised grains is random. Whereas in CDRX, since the original grains are elongated in the direction of the shear, subgrains start nucleating inside the grains, favourably near the previous grain boundaries. This microstructure exhibits strong intensity of cube texture, which comparatively has a low formability. There is a condition in which the deformation changes from CDRX region in the plot to DDRX region based on the strain rate and the temperature at which the deformation is carried out. Hence formability of these ferritic steels can be increased by carrying out deformation of the steel basically hot working at very high temperature and high stain rate which preferably may produce random orientated recrystallised grains. These orientated recrystallised grains may aid to combat with surface defects such as roping **(Castan et al. 2013).**

Rana et al. 2013, have studied the Fe-Al solid solution steels at Al content of 6.8, 8.1 and 9.7wt.%. To avoid the detrimental effect caused by the presence of κ carbide, high purity interstitial free raw materials were used. The damaging effect of addition or the presence of small amount of carbon is avoided. All the melts were taken by vacuum induction melting and hot worked to 3 mm sheets after 85% reduction. Steel with 6.8%Al could be successfully cold worked to 1 mm whereas the steel with 8.1 and 9.7wt.%Al cracked during cold rolling. Hence, these steels were subjected to warm rolling to get 1mm sheets. All these steels were annealed and properties were evaluated. It has been observed that as the Al content increased from 6.8 to 9.7wt.% the decrease in density from 7.21 to 6.802 g/cm^3 is observed. The average grain size was large (70 to 90 μm) for alloys with 6.8 and 8.1 wt.%Al when compared to Fe-9.7w.%Al (smaller grain size 17.5 μm).

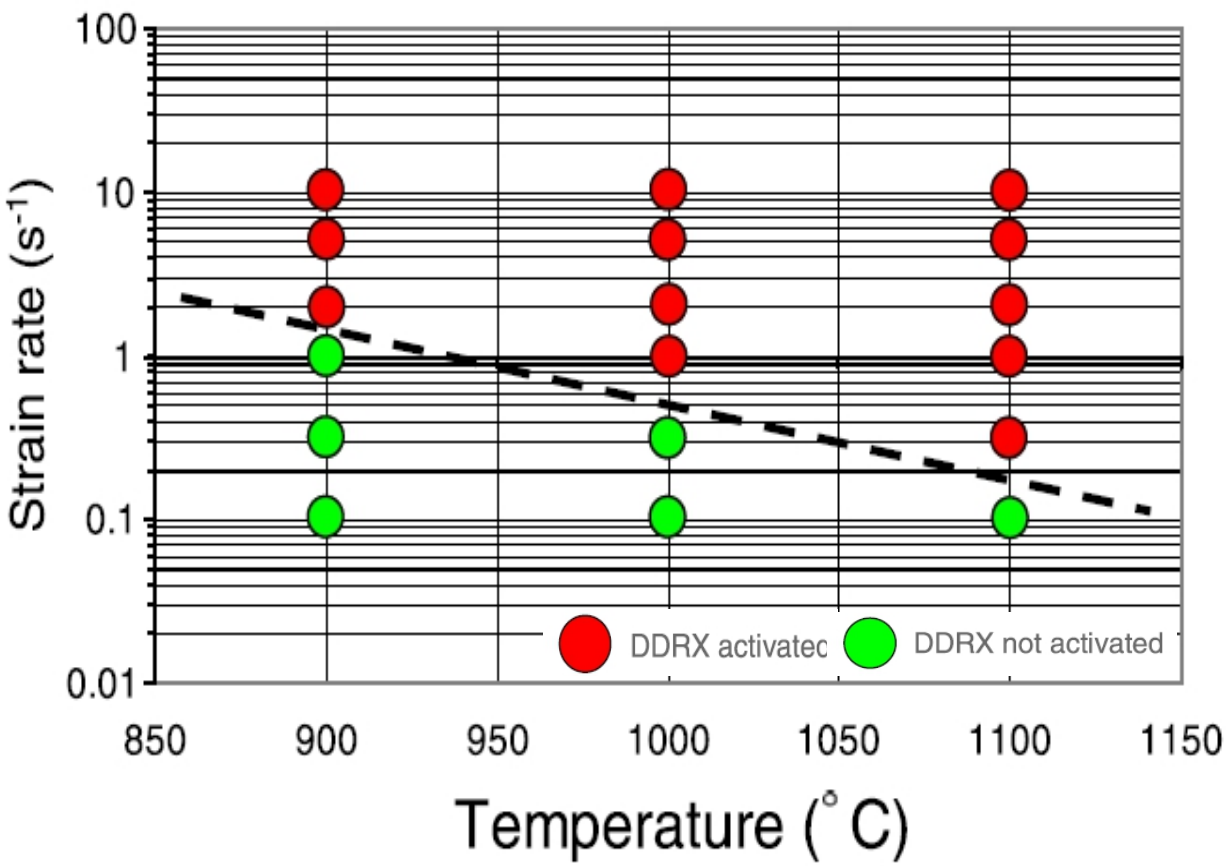

Fig. 2.11 A map of strain rate vs. temperature showing the areas of mechanisms in Fe-8wt.%Al ferritic steel **(Castan et al. 2013).**

The tensile properties of Fe-6.8wt.%Al (YS 342 MPa and %El 31.1) are similar to the properties reported by **Brüx et al 2002**. On the other hand, the tensile properties particularly; ductility is much better compared to the similar composition reported by **Baligidad et al. 2007** with small amount of carbon in Fe-Al alloys. Light weight steels with 6.8 and 8.1wt.%Al have shown better tensile properties compared to the corresponding dual phase steels, DP450 and DP500, respectively. Here, 450 and 500 indicates the strength values of these steels respectively. In terms of weight savings and performance improvement also these steels have exhibited noticeable improvement compared to interstitial free steel and dual phase (DP450 and DP500) steels for automobile applications.

Pramanik and Suwas 2014 have investigated the Fe-Al lightweight steels with Al ranging from 5 to 9wt.%. As the Al content increased about 10% reduction in density was observed for these steels. Further, the increase in the strength in this composition range of lightweight steels was primarily attributed to solid solution strengthening. Detailed analysis of the different mechanisms involved in strengthening of low-density Fe-6.8wt.%Al steels was studied by **Pramanik et al. in 2018**. The fine scale tools such as Mössbauer spectroscopy, X-ray line profile analysis, small angle X-ray scattering (SAXS), and transmission electron microscopy (TEM) were used for the analysis. In this alloy the contribution to the increase in strength is ascribed to various mechanisms. The mechanisms which are considered are based on the grain size, dislocations arising during deformation, formation of ordered phase, lattice frictional stress and the solid solution from Al atoms. The yield strength of alloy in the cold rolled condition has resulted in 1800 MPa which reduces drastically upon subsequent annealing to 265 MPa. The extent of strengthening contribution from each mechanism for Fe-6.8wt.%Al steel under different processing condition is plotted as in **Fig. 2.12.** It is clear that the contribution by solid solution strengthening, lattice frictional stress and the formation of ordered phase is constant across all deformation condition indicating that heat treatment has least effect on the strengthening by these mechanisms. It can be noticed that in cold rolled sample, the contribution for increase in the strength is predominantly by gain size and dislocations. However, with the increase in the annealing period the contribution from these mechanisms to strengthening of the alloy reduces drastically (**Fig. 2.12).**

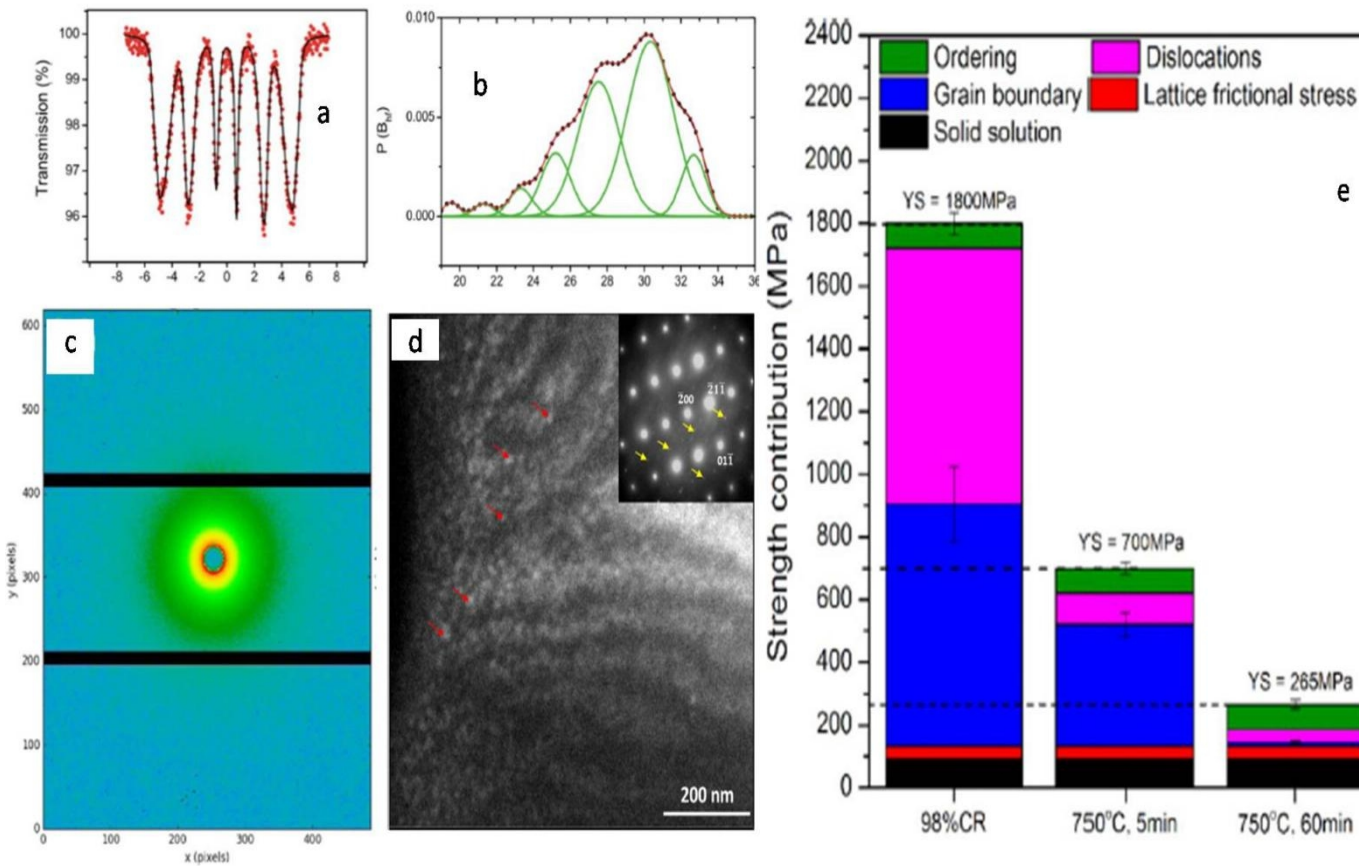

Fig. 2.12 Advanced technologies used to characterise Fe-6.8Al steel. (a) Mossbauer spectra, (b) B_{hf} distribution, (c) 2D-SAXS profile, (d) Dark field TEM micrograph and (e) Plot showing the cumulative contribution of different mechanisms in strengthening of Fe-6.8wt.%Al low density steel **(Pramanik et al. 2018).**

One of the major intrinsic problems of totally ferritic Fe-Al lightweight steel is about their large grain size. These steels cannot be refined by phase transformation as they are stable upto their melting point without γ phase formation. Hence, recrystallisation is the only process to get fine grains. However, it has been discovered that as the Al concentration of the steel increases, the recrystallisation stop temperature rises, reducing the number of rolling passes that enhance grain refinement via recrystallisation Hence, the properties of α(Fe-Al) steels are seriously relying on as-cast microstructure. Therefore, greater focus is required to reduce the as-cast grain size. **Slater et al. in 2019** evaluated the effect of alloying elements (Si, Al, Mn) on the solidification parameters particularly liquidus temperature, mushy zone width and segregation in the steels. Al has been varied in the range of 2.9 to 10.7wt.% whereas Si varied in between 2.5 to 6.2 wt.%. One melt with 6.1Si-0.3P and two melts were cast with 7Al-0.5Mn and 7Al-0.5Mn-1.5Si. The average gain size obtained for various composition of steel is shown in **Table 2.3.** The steel with all levels of Al (2.9-10.7wt.%) have shown larger average grain size compared to the steels with Si addition. Addition of 0.35wt.%P to Fe-6.1wt.%Si alloy resulted in the minimum average grain size (260 μm) among all the alloys studied. The average grain size of less than 500μm could be achieved by the addition of small amount of Si and C to Fe-7Al-0.5Mn alloy.

Deleted[khaple H]: Nevertheless, it is revealed that as the Al content increases in the steel, the recrystallisation stop temperature also increases which decreases the number of rolling passes that promote refinement of grains by recrystallisation.

Khaple et al. 2010 have investigated the effect of melting process (VIM,-vacuum induction melting, AIMFC-Air induction melting with flux cover) and different Al (7, 9 and 16 wt.%) amounts. The effect of these parameters on microstructure and mechanical properties was analysed. Alloys made by AIMFC process have shown lower in sulphur and higher in hydrogen content at each level of Al. It was reported that as Al content increased the hardness of the alloys increased irrespective of the melting process. A schematic diagram of the melting process (AIMFC/VIM) is as shown in **Fig. 2.13**. The melting process of all alloys made by both the process (AIMFC/VIM) showed single phase microstructure. Higher the Al content, more is the hydrogen content found in the alloys. This hydrogen in the alloys leads to hydrogen embrittlement. The hydrogen pick-up by Al was not only during melting but also during processing (to make plates/sheets from ingot) and fabrication process (such as cutting and machining). In Fe-Al alloys, the Al of the alloy reacts with the hydrogen present in the moisture even at room temperature and leads to hydrogen embrittlement.

Table 2.3 The average grain size obtained for various low-density steels **(Slater et al. 2019).**

Steel Sample	Composition in wt.%	Grain Size in (μm)
1	Fe-(2.9Al to 10.7)Al	672 to 750
2	Fe-2.5Si	575
3	Fe-(4.2 to 6.2) Si	245 to 223
4	Fe-7Al -0.5Mn	784
5	Fe-0.3P-6.1Si	260
6	Fe-7Al -1.5Si -0.5Mn	620
7	Fe-7Al -0.1C -0.5Mn-	484±49

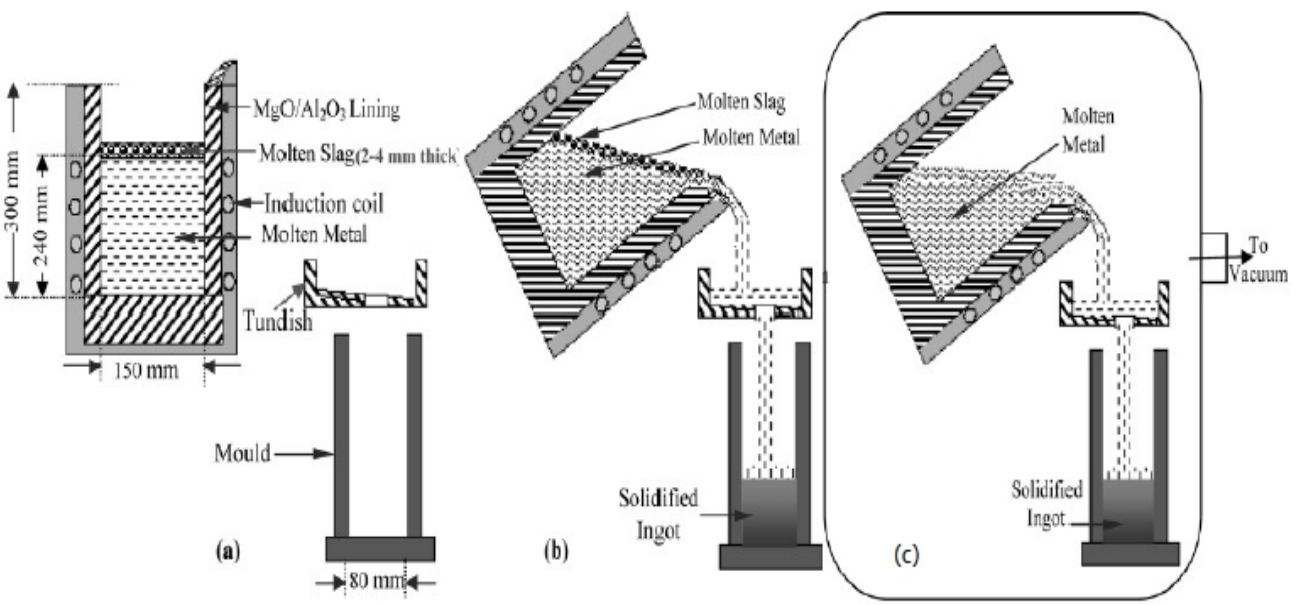

Fig. 2.13 A schematic diagram showing the induction melting in air (a) set up, (b) melting process with flux cover (c) melting process in vacuum **(Khaple et al. 2010, Satya Prasad et al. 2014).**

In case of Fe-16wt.%Al alloy made by AIMFC process, tensile samples could not be prepared as samples cracked during fabrication itself. However, alloy made by VIM process for the same composition could be fabricated, but failed during tensile testing at very low stress indicating very low ductility. For 9wt.%Al alloy, the samples could be fabricated successfully for the alloys made by both the process. On the other hand the Fe-9wt.%Al samples made by AIMFC process fractured at low stress showing low ductility. Nevertheless, at 7wt.% Al alloys made by AIMFC and VIM process have shown similar properties with reasonable ductility. It is attributed to the reason that at 7wt.%Al, the hydrogen embrittlement is not affected, whereas above 7wt.%Al i.e. higher (9 and 16)Al content, the hydrogen embrittlement is more severe. It affects not only during melting, solidification, fabrication but also during tensile testing **(Khaple et al. 2010, Satya Prasad et al. 2014).**

2.7 Addition of carbon to lightweight steels

Alloys based on Fe-Al system with excellent high strength to weight ratio, oxidation resistance, low density and inexpensive raw material costs are expectant to cater for many structural applications. From the literature on Fe-Al alloys, it is clear that these alloys have lower ductility and toughness at room temperature. The vulnerability of Fe-Al to hydrogen embrittlement is the foremost reason for these poor properties. Addition of carbon to iron-aluminium alloys is observed to be appropriate for decreasing the hydrogen embrittlement. The numerous benefits of alloying carbon to steel along with high Al is given in **Table 2.4.** It also leads to the improved strength because of the carbide formation. Among all the Fe-Al alloys, FeAl based B2 alloys have been studied initially because of its surpassing properties such as low density, excellent corrosion and oxidation resistance. But in these alloys, addition of carbon leads to formation of graphite, which reduces its performance as high temperature structural material.

Table 2.4 Benefits of carbon alloying to steel containing Al in the melt

Parameters	Benefits /advantages
Raw material cost	Reduces material cost in the form of cheap raw material such as and commercial Al and scrap of steel.
Cost of Melting process	Melting cost can be less because of conventional melting process such as air induction melting
Hardness and strength	Strengthening by having carbon in interstitial and also as carbides.
Hydrogen embrittlement	Reduces hydrogen embrittlement by trapping the hydrogen along with Al.
Sliding wear	Lower wear rate due to the formation of hard and complex carbides of Al, Fe with carbon.

2.7.1 Lightweight steels based on Fe-Al-C system

In case of Fe-Al alloy, it is recently conceived that addition of carbon is more favourable. Based on the Al content, addition of carbon generates different kind of microstructures. It becomes significant to examine the effect of carbon and unravel the mechanisms which results in the strength improvement of the alloy. It is manifested that the Fe-Al alloy properties depend on the type of carbide, amount of volume fraction, distribution of the carbides and their formation process.

Carbon addition to Fe-Al low density steel is more advantageous. It results in the reduction of the cost of raw materials as steel scrap can be used which is the cheapest among different supplies of iron. Conventionally available low cost melting processes such as induction/arc melting can be used. Hence use of steel scrap and commercial

purity Al reduces the production cost of these alloys compared to the presently available automobile steels such as dual phase, complex and advance high strength (AHSS) steels.

The addition of carbon leads to considerable improvement in machinibility by decreasing the hydrogen mobility. As the solubility is less than 0.045wt.%C in these alloys, carbon precipitates out as perovskite type $Fe_3AlC_{0.5}$ phase known as κ-phase. The isothermal section of Fe-Al-C system at room temperature is shown in **Fig. 2.14 (Palm and Inden 1995).** The schematic diagram of $Fe_3AlC_{0.5}$ carbide (κ-phase) with the arrangement of the atoms is shown in **Fig. 2.15**. Homogenous distribution of these carbides operates as traps for hydrogen which is the reason for machinability improvement. Additionally, these fine carbides aid in obstructing grain growth during hot working. This is contrary to the very poor machinability because of surface cracking noticed in case of Fe-Al alloys containing low carbon.

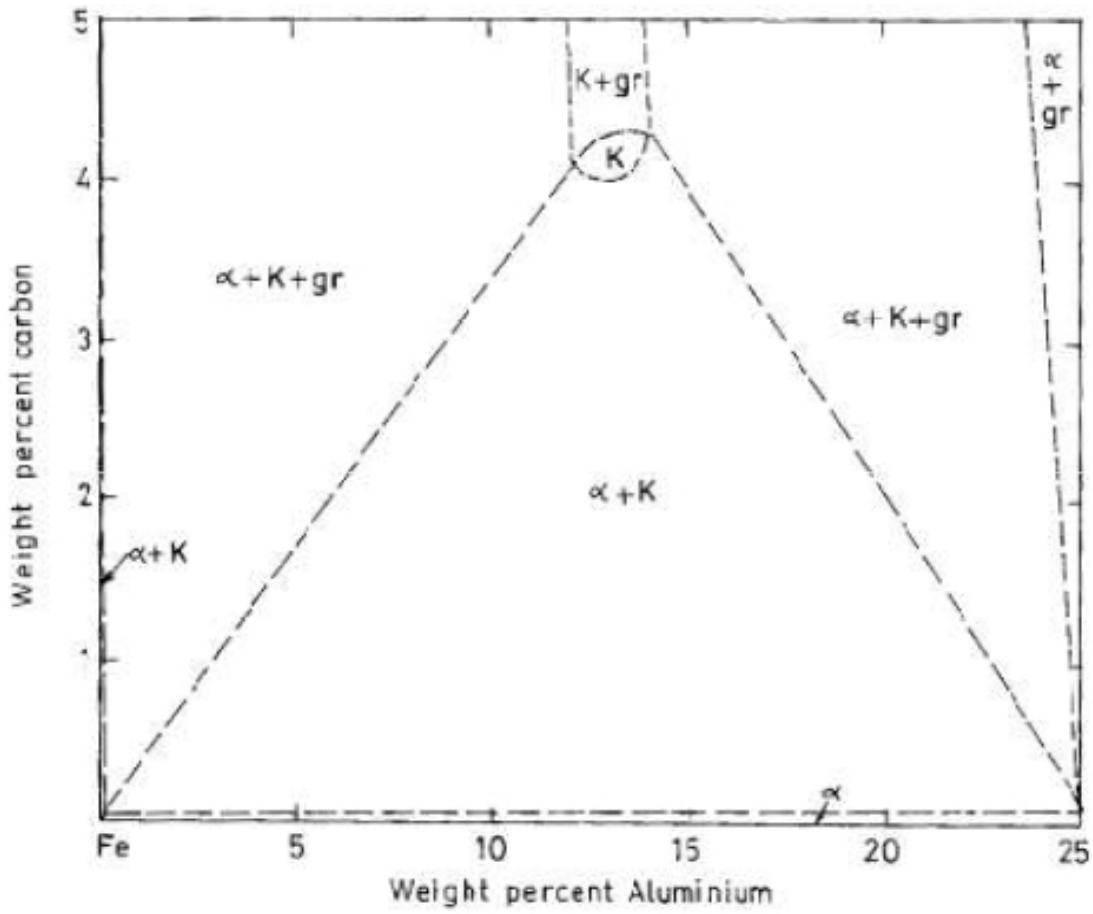

Fig. 2.14 The isothermal section of Fe-Al-C system at temperature **(Palm and Inden 1995).**

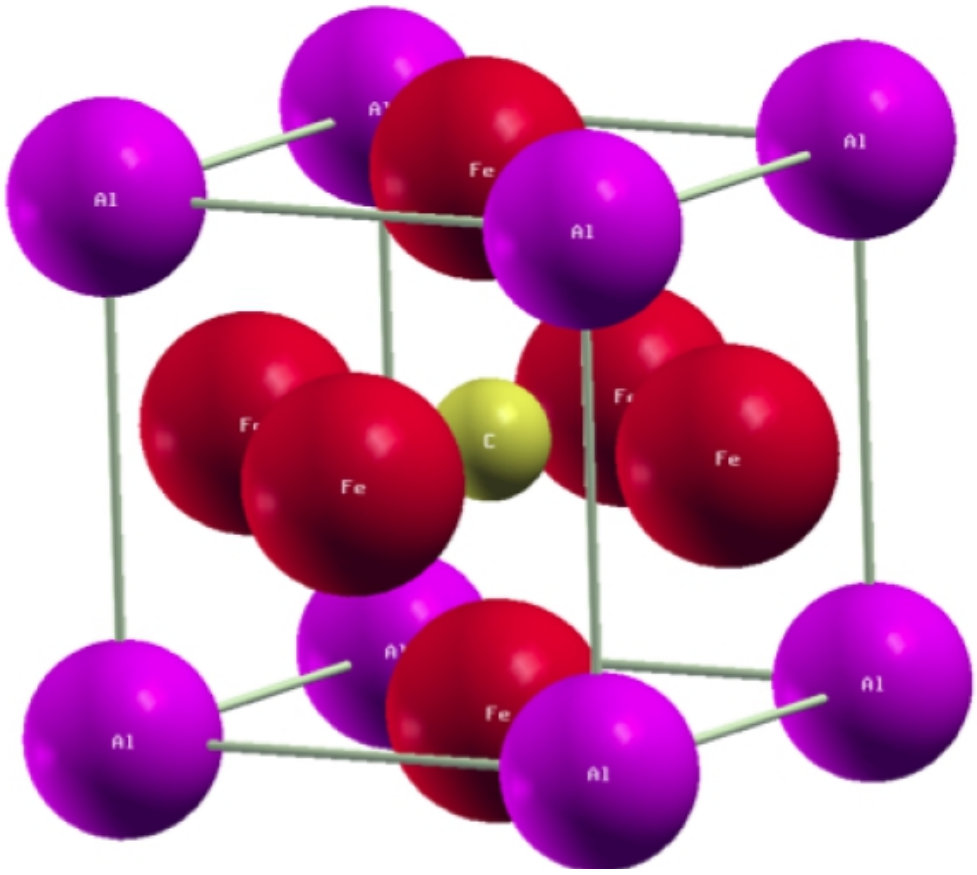

Fig. 2.15 A schematic diagram of κ-carbide unit cell. Al is at the corner position, Fe occupies the face centered position and carbon atom sits at the centre, which is also an octahedral site of Fe and Al atoms **(Seung-Woo Seo 2010).**

2.7.2 Low-density/Lightweight Ferritic steels based on Fe-Mn-Al-C system

To get austenite in Fe-Al alloys, high amount of Mn and carbon are added which are austenite stabilizers. By the addition of Mn to Fe-C system, there is a gradual shift of the high temperature peritectic reaction to lesser carbon content as Mn content is increased. Further with Mn greater than 13% **(Chen et al. 2017),** the peritectic reaction fades away completely. Al being ferrite stabilizer, addition of it to Fe-Mn-C system expands the ferrite region and reduces the single phase region of austenite. A typical equilibrium phase diagram of Fe-Mn-Al-C system at fixed level of carbon (0.85%), aluminium (7wt.%) with varying Manganese is as shown in **Fig. 2.16.** The quaternary Fe-Mn-Al-C alloy phase equilibrium have been examined by many authors **(Ishida et al. 1990,**

Goretskii and Gorev 1990 Cheng et al. 2008, Buckholz et al. 2013). Mainly austenite, ferrite, cementite and κ-carbide are the four phases which are found in these alloys at hot working temperatures. The other phases that are reported in these alloys are M_3C, $M_{23}C6$, M_7C_3 carbides and β-Mn. The stability of the phases depends on the alloy composition and the temperature. κ-carbide forms in these steels below 950^0C and its stability reduces as the carbon content decreases. With the increase in the Mn content, the single phase region of the austenite is stretched towards lower temperature, the solvus line of κ -carbide is also reduced and β-Mn phase appears. It is reported that the β-Mn phase observed with Mn higher than 20%. The stability of β-Mn phase is more with the higher Mn content (**Kim and Kang, 2015, Connétable et al. 1990)**. Even 2%Al is adequate to form κ-carbides in Fe-Al-C system whereas at least 5%Al is required in Fe-Al-Mn-C system to form κ-carbide with 2% Mn content. This implies that Al restricts the formation of M_3C, $M_{23}C6$, M_7C_3 type of carbides whereas Mn restricts the formation of κ-phase. It is also reported that disorder-order (BCC_A2 (α) to BCC_B2) transformation happens at higher than 2% Al. As the content of Al and Mn is increased the transition temperature of disordered to order increases. Whereas with the increase in carbon content this transition temperature decreases. This suggests that increasing the concentrations of Al and Mn enriches the formation of ordered phases within the ferrite, on the other hand the ordered phase formation is restricted by increasing the carbon content. The thermodynamic calculation and the experimental results revealed that the austenite single phase region is somewhat narrowed as the temperature is dropped from 1200 to 900^0C.

The isothermal section of the phase diagrams at 900^0C has considerable importance in the alloy design as this is generally the hot working temperature practised during industrial production of the components. In this system, austenite is not a stable phase at lower temperature but numerous heat treatment processes can be adopted to obtain different phases with various morphologies to get better combination of properties. Aluminium addition to Fe-Mn-C steel leads to the generation of short-range ordering (SRO), κ-carbide precipitate and also increases the stacking fault energy (SFE). Fe-Al-Mn-C steels having high SFE containing SRO the plastic deformation is largely influenced by planar glide. Deformation mechanisms such as twinning-induced plasticity (TWIP) and Transformation-induced plasticity (TRIP) are used to correlate the microstructure with properties of Fe-Al-Mn-C steels. The advanced deformation mechanisms are operating in high Mn austenitic Fe-Al-Mn-C steels. The essential criteria for the alloy design can be

hot working in the absence of κ-carbide, forbid the formation of coarse of κ-carbide on the grain boundaries and avoiding the formation of $M_{23}C6$, M_3C, M_7C_3 type of carbides at lower temperatures.

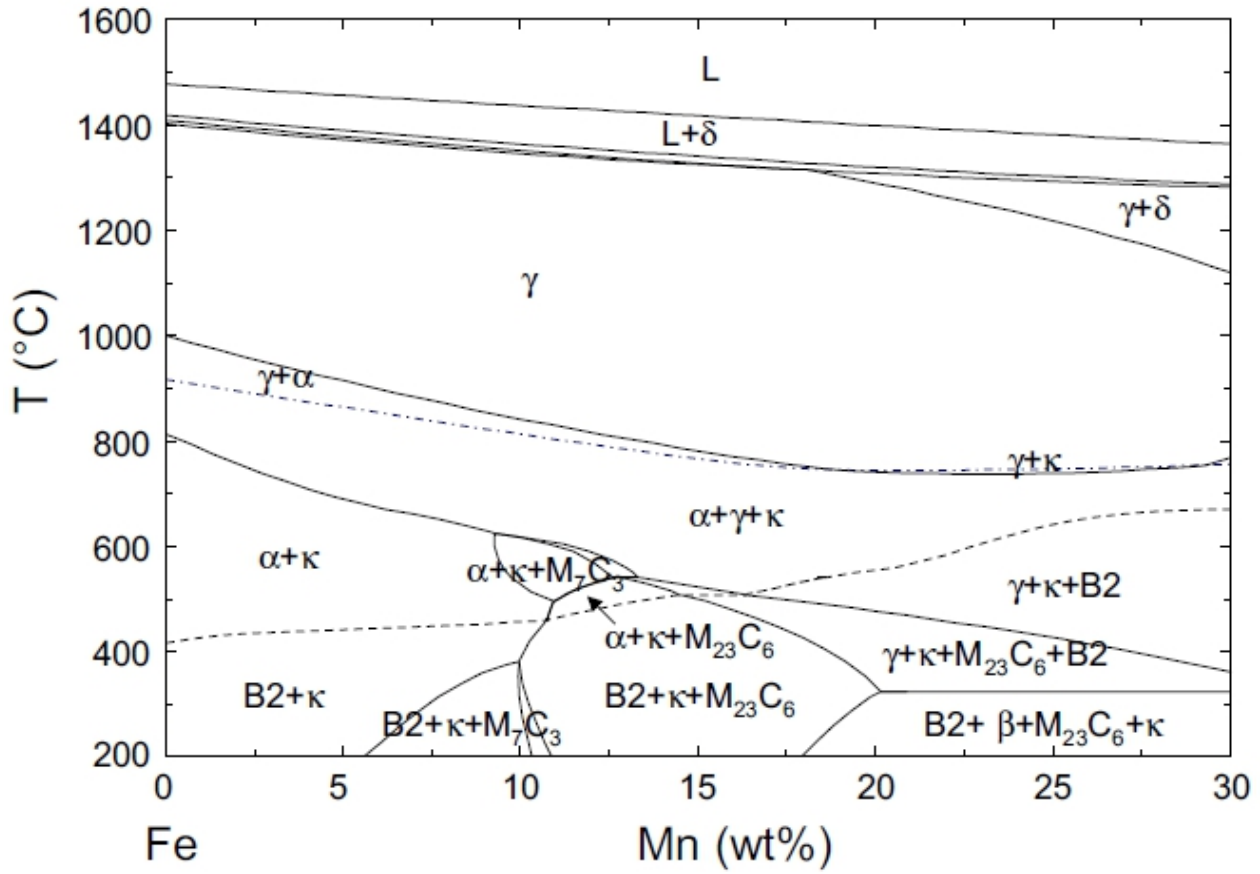

Fig. 2.16 A typical equilibrium phase diagram of Fe-Mn-Al-C system at fixed level of carbon (0.85%), aluminium (7wt.%) with varying manganese **(Ishida et al. 1990, Goretskii and Gorev 1990, Cheng et al. 2008, Buckholz et al. 2013).**

2.8 Effect of carbon on microstructure and mechanical properties of lightweight steels

Very limited work has been reported in case of Fe-Al alloys with lower Al content. Since the Al content is comparatively low, the oxidation resistance offered is less and its high temperature properties are not so good compared to the iron aluminides and other heat resistant steels. The distinct advantage of these low Al containing Fe-Al alloys is that these alloys are less prone to hydrogen embrittlement. Therefore, these alloys are easy to make and process. Additionally, these alloys exhibit better tensile ductility compared to other iron aluminides. In the recent trend for lightweightening of structural materials, particularly with respect to automobile application, these alloys have gained more prominence. The reduction in density offered by these alloys with about 7wt.% Al is about 10%, which is the desirable requirement with reasonable strength. In majority of the research for Fe-Al ferritic steels, the high purity iron is used where carbon content is less than 0.05wt.% **(Rana et al. 2013, Herrmann et al. 2012, Supdita et al. 2014).** This was basically to avoid the formation of κ-carbide (perovskite carbide, $Fe_3AlC_{0.5}$) which is a brittle phase which affects the ductility. However, recent research on Fe-Al alloys by few authors **(Baligidad 1998, Baligidad and Satya Prasad 2007, Sanders and Sauthoff 1997)** have shown that carbon addition to Fe-Al alloys have more beneficial effects. Uniform distribution of the κ-carbide improves the ductility by reducing the hydrogen embrittlement effect. It increases machinability, additionally; the cost of the raw material can be reduced. Moreover, this alloy can be made by the conventional melting processes such as air induction melting.

Very few authors have reported the effect of carbon on Fe-Al alloy with Al in the disordered range **(Baligidad 1998, 2004, Jiménez and Frommeryer 2011, Khaple et al. 2010).** Baligidad et al. in 1998 have studied Fe-Al alloys in the range of 8.5 to 16wt.% with carbon in the range of 0.1 to 1wt.%. The room temperature ductility in tensile condition is plotted for different Al and carbon content and is shown in **Fig. 2.17**. Higher the Al content in Fe-Al alloys, lower is the ductility with similar level of carbon content. However, the creep, tensile strength at high temperature as well as the room temperature ductility of the Fe-Al-C alloys are better than corresponding binary Fe-Al alloys. **Jiménez and Frommeryer 2011** have studied the effect of 1wt.% carbon on Fe-Al alloys with Al

varying in the range of 2 to 6wt.%. In case of Fe-6wt.%Al, the carbon content was varied from 1 to 1.8wt.%. Here the objective was to examine different carbides formed in the system. It was observed that ferrite, ferrite + Fe_3C pearlite, κ-carbides and $M_{23}C_6$ phases were present in the alloys. It was also reported that as the Al content increases the formation of carbides (Fe_3C and $(Fe, Al)_{23}C_6$) is reduced. Further, it is noticed that graphite formation has been reported with higher carbon (C>1.2wt.%) in Fe-6wt.%Al alloy. However, the effect of these phases on the mechanical properties is not reported.

Most of the research carried by Baligidad on Fe-Al alloys was made by air induction melting process followed by electroslag refining (ESR) process. Fe-Al-C alloys made by ESR process resulted in better properties because of uniform distribution of κ-carbide precipitates in the alloys. However, these alloys were prone to decarburisation as they exhibit poor oxidation at higher temperature. Nevertheless, decarburisation seems to be problematic only at temperature higher than 800^0C. The microstructure which consists of α (Fe-Al) ferrite and κ-carbide is stable upto 600^0C. By having fine κ-carbides and homogenously distributing these carbides in low Al containing Fe-Al-C ferritic steels can be one of the candidate materials for lightweightening of various components particularly in automobile industries.

2.9 Effect of alloying elements on microstructure and mechanical properties of lightweight steel

Even small quantity of κ-carbides affects the mechanical properties of the steel particularly the ductility. In order to avoid the detrimental effect of κ-carbides formation, microalloying elements such as Ti, Nb and B are used to lock the free interstitial free elements including carbon. **Brux et al. 2002** studied the effect of microalloying elements on the microstructure and mechanical properties of Fe-6Al ferritic steel. They found that addition of microalloying elements (Ti, Nb and B) refined the ferritic grains upto an average grain size of 40μm. They have reported that the optimum combination of the microalloying elements have displayed better tensile properties which is due to grain refinement of the ferritic grains.

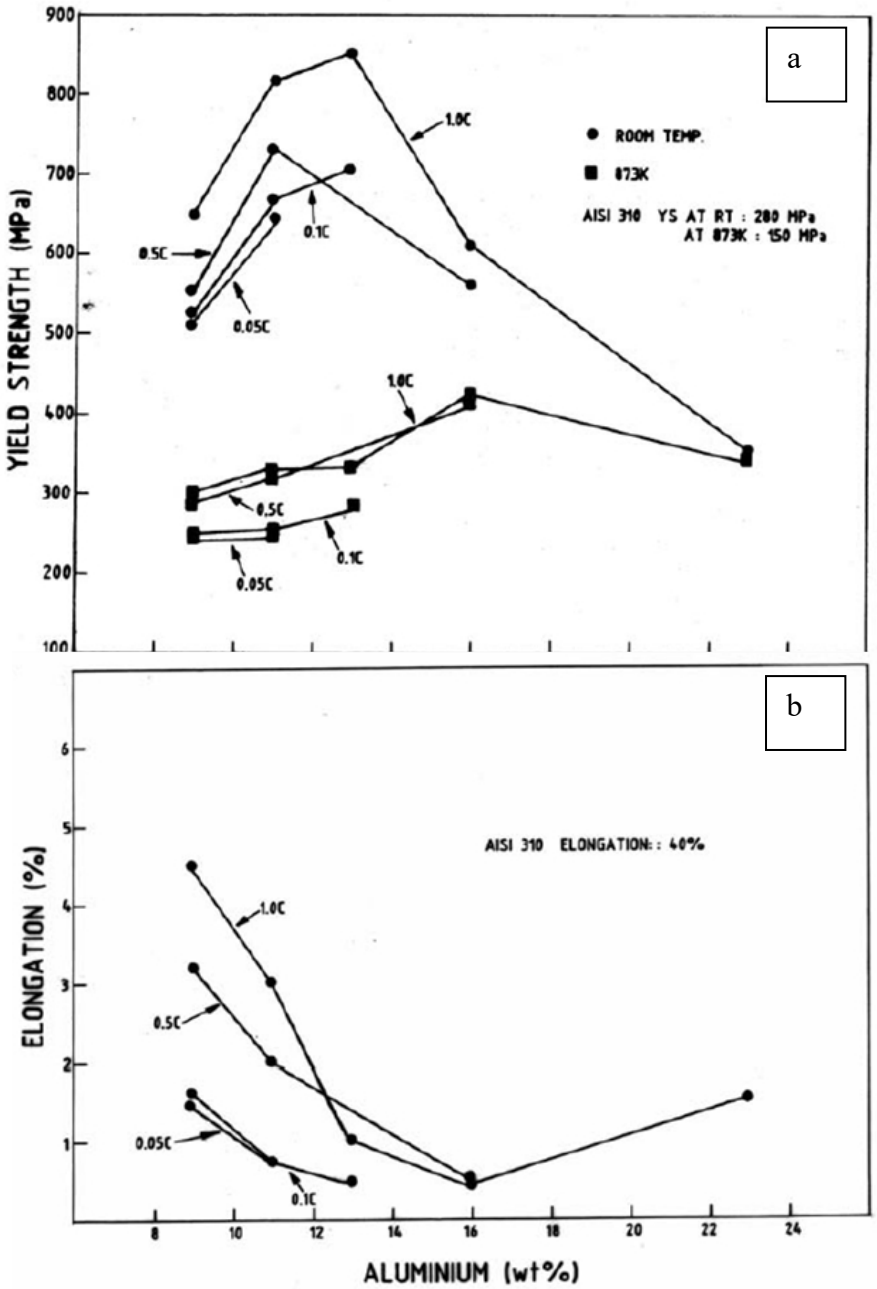

Fig. 2.17 The plot of tensile properties (a) strength and (b) ductility with variation in Al and carbon content in steel **(Baligidad and Satya Prasad 2007).**

Researchers from Pohang University, Pohang Iron and Steel Company (POSCO), South Korea have done extensive study on Mn containing ferritic low-density steels. Addition of Mn to Fe-Al based steel stabilizes the austenite phase as Mn is an austenite stabilizer. It also opened up the window of heat treatment as different phases can be obtained by following various schedules of heat treatment. There is solubility of Mn in the matrix of Fe-Al and also in the precipitate of κ-carbide $(Fe,Mn)_3AlC_{0.5}$ as well. This increases the strength and hardness of the matrix and the precipitate in Fe-Mn-Al-C steels compared to Fe-Al-C steels. Addition of Mn to Fe-Al-C ferritic steel enhanced the mechanical properties considerably. However, the workability of Fe-Mn-Al-C steels is poor compared to similar composition of Fe-Al-C ferritic steels as these Mn-containing steels were prone to cracking in both the hot and cold rolled condition **(Shin et al. 2010, Han et al. 2011, Sohn et al. 2013).** The researchers from South Korea focused on examining the size, shape and distribution of κ-carbides in the ferritic steels to derive the maximum benefits.

Lee et al. 2013 studied the effect of variation of alloying elements (Al, Mn and C) on the microstructure evolution in Fe-Mn-Al-C ferritic low density steel. They attempted to relate the microstructure evolution of these steels with the prediction of the phases and their volume fractions obtained by calculation based on thermodynamics. The microstructure of each alloy composition is systematically analysed experimentally after the thermo-mechanical processing from ingot to sheet. They ascertained that the thermodynamic calculation based on thermodynamic data can be used to predict the microstructure evolution. This will help the researchers in designing new steels with the required microstructure.

Shin et al. **2010** reported cracking in the Mn containing Fe-Al-C ferritic steel during hot rolling. Steel with higher than 6% Mn and 7.5% Al displayed cracking behaviour compared to the steel with lower 3-4% Mn and 5.5-6.5% Al. They observed that ferrite bands or the densely populated coarse κ-carbides in the secondary bands did not play crucial role in the formation of cracks. They found that steel containing higher Mn and Al content cracked during hot rolling because of the formation of higher volume fraction of continuous thin κ-carbide film. The main reason for the cracking of these steels is due to the crack initiation in continuously formed film type κ-carbide precipitates between the ferrite and secondary phase bands. Cracks formed and propagated (in a cleavage manner) by combining with many voids at the interfaces between the bands. Some of the

guidelines suggested to address the cracking problem are (i) Improvement in the solidified structure by controlling the casting process, (ii) Increasing the homogenisation time, (iii) increasing the hot rolling temperature, (iv) Reducing the alloying elements added to the steel such that the combined Al+Mn content should be less than 10%.

Research on cracking phenomena taking place in Mn containing ferritic steel during cold rolling has been extensively studied. **Han et al. 2011** studied the cracking phenomenon taking place during cold rolling of Mn containing ferritic low density steels with different carbon content. The carbon content varied from 0.1 to 0.3%. They found that Fe-5±1Mn-7±1Al steel with 0.1% carbon cracked whereas steel with 0.3% C did not crack during cold rolling. Only some of the steel with 0.2%C cracked. They observed that the cracks initiated at continuously formed coarse κ-carbides along the band boundaries and also noted the abrupt propagation of the cracks in the ferrites in a cleavage manner in steel with lower carbon content (0.1%). The secondary bands densely populated with discontinuous κ-carbides in the form of fine lamellar (which is mostly present in steel with higher carbon content) did not play significant role in the cracking process. Effect of Al (4 to 6%) content on the cracking behaviour of Fe-(0.3±0.1)C-(3±1)Mn steel is reported by **Sohn et al. 2014** Al being the ferrite stabilizer affects the morphology, particularly the size and the volume fraction of the κ-carbides formed in the steel. Both the centre and the edge cracks occurred in steel with higher (6wt.%) Al content. The tendency of cracking in lower Al (4wt.%) content steel was very less. Cracking in steel with higher Al content was caused by continuously formed κ-carbides which were long and lamellar, whereas in lower Al (4wt.%) steel the k-carbides were thin, short and discontinuous which prevented from cracking.

In ferritc (Fe-Al-C) low-density Mn containing steel, with 6-8wt.% of Al, cracking phenomena is observed due to the formation of κ-carbides. With an aim to eliminate κ-carbide formation and maintain the density of the steel, Al content was reduced to 5wt.% and effect of Si study was studied by **Heo et al. 2012.** The Fe-5Al-8Mn-0.2C lightweight steel with Si (1 and 2wt.%) was processed and characterised. They found that the base alloy with 5wt% Al does not show any κ-carbide precipitates instead very complex cementite comprising Fe, Mn and C was reported. The ductility of the base alloy is reasonably good (15%) whereas addition of Si to the base alloy drastically decreases the ductility to less than 5%. Si in the Fe-5Al-8Mn-0.2C lightweight steel form undesirable

complex hard and brittle carbides. Hence, density reduction by the alloying with Si to Fe-Al-Mn-C based steels is not recommended.

Pramanik and Suwas 2020 studied the effect of Cr and Mn addition on the microstructure and mechanical properties of Fe-Al ferritic steels. Addition of 6.3 wt.% of Cr to Fe-6.5wt.%Al and addition of 3.1wt.% of Mn to Fe-3.7wt.%Al lead to the decrease in the density of 7 and 7.5 gm/cm^3, respectively compared to density of pure iron (7.8 gm/cm^3).

The elastic modulus of Fe-6.5Al-6.3Cr steel is 186 GPa, whereas Fe-6.5Al-3.1Mn steel is 178 GPa. The steel with Cr and Mn alloying additions displayed higher elastic modulus than the elastic modulus (175GPa) of the base (Fe-6.5Al) alloy. It is also reported that addition of Cr to Fe-6.8Al improved tensile properties marginally (YS-529 and %El-27%) when compared to tensile properties (YS-494 and %El-25%) of Mn added Fe-6.8Al steel. The better properties are shown by Mn containing steel is due to the grain refinement effect **(Pramanik and Suwas 2020).**

2.10 Strength improvement by grain refinement

It is well known that refinement is most preferred method to simultaneously improve both the strength and plasticity of any metallic material. Grain refining of steel can be achieved during or/and after solidification process. Generally, the methodology adopted for achieving grain refinement is by (a) agitation and stirring during solidification, (b) addition of grain refiners in the melt, (c) rapid solidification and (d) severe plastic deformation. Fine ferrite grains can be achieved by offering additional nucleation sites for ferrite or by increasing the driving force for the transformation of ferrite to austenite.

Addition of alloying elements to Fe-Al binary alloys can improve the strength. The alloying elements such as Cr, Co and Mn can improve the strength by solid solution strengthening. Alloying elements such as B, Nb, Ta, Hf and Zr have demonstrated to enhance the tensile strength by precipitation hardening (**Vedula and Stephens 1987, Mendiratta et al. 1987, Maziasz et al. 1996).** It was also reported that addition of oxides also improve the strength by oxide dispersion strengthening (ODS) **(Morris-Munoz 1999, Wolski et al.1996).**

Strength can also be improved by addition of carbides such as SiC, TiC, ZrC, and diborides such as ZrB_2 and TiB_2 in the ferritic low density steels. These metallic particles/precipitates can be added as reinforcements or formed in-situ during the melt. The morphology of these precipitates has tremendous effect on the properties of the steel. The size, shape, volume fraction and distribution of the particulates considerably affect the mechanical behaviour of the lightweight steels. The addition of boron (B) has been tried to improve the ductility of Fe-Al-based alloys.

2.11 Types of reinforcements/particulates

A low-density hard phase with high stability and high-elastic modulus can be effectively used in enhancing the properties of the of lightweight Fe-Al steels by numerous methods. The important property required for the particulate is that it should be thermally and chemically compatible with the matrix. Various particulates such as carbides, oxides and borides can be potential candidates to improve the strength. Carbides and borides are found to be more effective which will be discussed in the following sections, whereas the oxides have very limited use. The selection of the particulates is decided based on the morphology, the availability and its compatibility with the matrix of the steel. Since the development of lightweight steels are based on Fe-Al system (because of their low cost), the cost of the reinforcement along with its lower density is also the main criteria to be considered.

Since the reinforcement (ceramic) is generally brittle, the matrix needs to accommodate the dimensional mismatch occurring due to the difference in strain of matrix and the reinforcement during plastic deformation. The reinforcements need to be highly stable, fine sized and uniformly distributed to improve the properties of the steel. The selection of the composition and their process control to achieve the above parameters play very important role.

Vast majority of the processes banks on the formation of the reinforcement by eutectic or precipitation process. The method used for having the reinforcement in Fe-Al alloys is dependent of the type (eg. Fibre or particulate) and size of the reinforcement. Particulate reinforcement is the process which is significantly used in Fe-Al alloys. Powder or

melting process can be used to make these steels with reinforcement. Mechanical alloying, reaction synthesis and melting process rely mainly on the in-situ formation of the reinforcements. Particulate reinforcements can also be added externally in the form of powders in the melt or in powder processing routes. Fe_2O_3 particulates have been introduced by displacement reaction in Fe-Al alloy matrix to achieve oxide dispersion.

2.11.1 Oxide reinforced Fe-Al alloys

Powder processing of Fe-Al alloys particularly, in aluminides is the most general route opted for oxide reinforced composites. Liquid phase sintering process was used to make Fe-40at%Al alloy composite **(Schniebel and Deevi 2004).** Pre-alloyed powders of Fe-40wt.%Al were mixed with 30wt.%ZrO_2 of <45µm or 15Vol. % Al_2O_3 of <38µm. Due to the thermodynamic instability of ZrO_2 in the molten matrix of Fe-Al alloy, it was found to be unsuitable by liquid phase sintering process. The Al_2O_3 powders could not be wetted by the Fe-Al matrix. Wettability with Fe-Al matrix was achieved after addition of an equal quantity of TiC powders. It is important to note that Ti addition to Fe-40wt.%Al has improved the wettability of the alloy **(Nourbakhsh and Margolin 1991).**

2.11.2 Boride reinforced Fe-Al alloys

The stability of borides of Zr, Ti, Nb and Ta in Fe-Al alloys was examined by **Doucakis and Kumar 1999.** They observed that TiB_2 and ZrB_2 displayed extreme resistance to coarsening. The density of these dispersoids is 4.52 and 6.08 g/cm^3, respectively. Considerable amount of strengthening is obtained by the addition of borides to Fe-Al based alloys without impairing the ductility. At high temperature, Iron boride dissolves in the Fe-Al matrix, hence its use as a dispersoid is not recommended.

Powder metallurgy processing of Fe-Al aluminides with TiB_2 dispersoids has shown good elongation of 11% and yield strength of about 1GPa **(Bordeau 1987).** Rapid solidification process is by melt spinning and rapidly solidifying to get ribbons. The rapidly solidified process generally resulted in finer dispersoids of submicron size. The ZrB_2 addition has resulted in improved strength and ductility though their distribution was not uniform **(Morris and Morris, 1991).**

The powders of Fe, Al, Ti and B were used to prepare Fe-Al-TiB_2 alloy by reactive synthesis using a pseudo HIP process by **Obara et al. 2008.** The usage of pressure during the synthesis resulted in the improvement of ductility probably by reducing the porosity. The powders when sintered in vacuum produce the alloy with reduced volume fraction of pores and also the size of the TiB_2 dispersoids was smaller. In this case, it was noted that the alloy had a dispersoid size in the range of 1-7 μm.

Thus both the ingot and powder processing routes have been used to prepare boride containing Fe-Al alloys. Various stable and more compatible metallic refractory diborides have been used to strengthen Fe-Al alloys. These dispersoids are impervious to coarsening and also expected to refine the matrix grains. Moreover, these dispersoids do not impair ductility. It is expected that the presence of boron may help to improve ductility in Fe-Al alloys.

However, TiB_2 or ZrB_2 powders addition to pre-alloyed Fe-Al powders is not very beneficial because of limited solubility of borides in iron aluminides. This may result in debonding at the interface of boride/matrix at high temperature even in alloys processed by liquid phase sintering thus limiting their potential as structural materials.

2.11.3 Carbide reinforced Fe-Al alloys

These constitute the most investigated of Fe-Al alloys and also the most promising. The low cost of these Fe-Al based alloys is the main advantage because of the low cost sources of raw materials basically steel scrap and commercial grade Al which can be used. The benefits of addition of carbon to ferritic steels have already been addressed in the previous sections. With the addition of carbon in Fe-Al system lead to the formation of stable $Fe_3AlC_{0.5}$ κ-carbide precipitate, which has a preovskite structure as suggested by **Palm and Inden 1995.** This carbide is more stable at low Al content in the ferritic low-density steels. Alloy carbides of high atomic weight or high density such as WC, TaC and MoC are avoided because of their higher density than that of steel. Since density reduction is the main aim with which development of low-density steels started.

The alloying elements distribution in the steel depends on the concentration of the carbon and the corresponding amount of carbide forming element. If the carbon content in the

steel is relatively higher than the alloying element, the later would be completely used up for the formation of respective alloying element carbide. On the other hand, if the carbon content is less compared to the alloying element, then the remaining extra quantity of alloying element after forming carbide will be present in the steel matrix as solid solution or in the form of Laves phase. Alloying elements such as Cu, Ni and Co do not form carbides whereas Mn is weak carbide former. Addition of Si and Mn to Fe-C steel leads to the formation of cementite rather than forming respective metal carbide. Hf, Zr, Nb, Ta, Ti and V are very strong carbide formers even minor quantity of these alloying elements with carbon leads to the formation of carbides whereas Cr, Mo and W are good carbide formers. All these alloying elements Hf, Zr, Nb, Ta, Ti, V Cr, Mo and W have relatively higher enthalpies than iron carbide **(Bhadeshia et al. 2016).** Generally, six forms of metallic carbides are reported in steel such as MC, M_2C, M_3C, $M_{23}C_6$, M_2C_3, M_7C_3 and M_6C, Here M represents respective metallic element. Carbides of the type MC and M_2C (TiC, NbC, WC and Mo_2C) have simple crystal lattice. Whereas other carbides are more complicated ($Cr_{23}C_6$ and Fe_3C). It is to be noted that contribution of carbides in the strength of the steel relies upon the morphology (size and shape) and volume fraction of the precipitates. The finer the size of the precipitate, the higher is its strengthening contribution. The fineness of the carbides is detected by the activation energy barrier for nucleation of the precipitate. This in turn depends on interfacial energy, the free energy of formation and the misfit of the carbide with matrix. Generally, the finest carbides are obtained by MC and M_2C type of carbides (such as TiC, VC, NbC etc.) which are close-packed intermetallic compounds. On the other hand, carbides such as $M_{23}C_6$, M_2C_3, M_7C_3 possess complex crystal structure and the heat of formation is also low. These carbides are reasonably coarser in size.

The volume fraction of the carbides formed depends on the solubility of the metal carbide in the austenite phase as compared to its solubility in ferrite phase. The solubility of Cr, Mo and V carbides is highest in the austenite phase, hence the volume fraction of these precipitates is larger in ferrite. Hence, it is regarded that when strong carbide formers are present in the steel in sufficient quantity, their carbides would form in preference to cementite. Small amount even in micro content of alloying elements such as Al, Ti, Nb and V are very effective in delaying the grain growth since these elements are present as highly dispersed carbides and they require very high temperature to dissolve the carbides

into the solution. It was observed that the solubility of carbides in the austenite increases in the order of NbC, TiC and VC **(Maalekian 2007).**

Depending on the composition of the alloying elements Al, Mn and C in Fe-Mn-Al-C ferritic steel, κ-carbide phase generally forms below 800^0C. In the earlier sections, it has been already presented how the morphology, volume fraction and distribution of the κ-carbide have profound effect on the workability and mechanical properties of these ferritic steels. Effect of various alloying elements such as Si, Mn, Ti, Nb, Mo, Zr and W on the Fe-Al-C alloys with 10.5 to 11wt.% Al was investigated by **Baligidad et al. 2007.** A combination of air induction melting and electroslag refining process was used to melt these alloys, hot-rolled to plates and examined. Considerable solubility was noticed in κ-carbide precipitate as well as ferrite matrix of the alloy for Mn, Mo and W. On the other hand, solubility of Si was very much higher in κ-carbide precipitate. It was observed that Ti, Nb, Mo and Zr lead to the formation of their respective carbides. Addition of Mn, Mo and Zr marginally improved the room temperature ductility. On the other hand, Ti, Nb and W have resulted in poor ductility. Si addition has severely impaired the ductility of the alloy rendering it highly brittle.

The effect of carbide forming alloying elements (Ti, C, Nb and Ta) with respect to strengthening and its stability was investigated on Fe-(7.16 and 13.6)Al-0.216C steel **(Schneider et al. 2005, Falat et al. 2005).** The long duration homogenisation treatment of Fe-7.16Al-0.216C alloy with Nb and Ta have shown the formation of $(Fe,Al)_2Nb$ and $(Fe,Al)_2Ta$ Laves phases. The steel with Ti addition has only shown TiC precipitates whereas steel with vanadium addition has displayed V_4C_3 type of carbide precipitate. The phase formation was predicted for the Fe-7.16Al-0.216C alloy with Nb, Ta, Ti and V as the alloying elements and was noticed to agree with the experimental results.

The role of Nb (1.5 and 3.5wt.%) on Fe-8.5Al and 10.5Al with low carbon was investigated **(Baligidad et al. 2005, Baligidad 2004).** It was observed that addition of Nb leads to the formation of Nb_2C carbide precipitate in addition to κ-carbide precipitates in the ferritic matrix. Additionally, for the alloy with 3.5%Nb, Fe_2Nb Laves phase was noticed.

The influence of Nb and carbon additions on the ferritic Fe-8Al-5Mn steel was investigated **(Zargaran et al. 2014, 2015, Zhou et al. 2018).** Precipitates such as NbC and κ-carbide in ferritic matrix are noticed. Solubility of Mn is observed in the κ-carbide

precipitate and matrix. During hot rolling of the steel, these precipitates (NbC and κ-carbide) are expected to hinder the dynamic recrystallisation of the ferrite grains resulting in elongated grains in the rolling direction. Higher the carbon content (0.05) more is the elongation of the grains compared to the unrecrystallised elongated grains in lower carbon content (0.005 and 0.02) alloy. During annealing process, the κ-carbide precipitates acts as nucleation sites and promote static recrystallisation and help to refine the grains by particle-simulated nucleation (PSN) mechanism **(Humphreys and Hatherly 1995).** Hence, the alloy with 0.05 C show uniformly distributed fine grains as these precipitates retard the growth of the recrystallised grains **(Zargaran et al. 2015).**

In recent times, TiC has also been considered as one of the most essential reinforcing carbide in composites based Fe and Fe–Al matrix because of its excellent combination of properties such as, high modulus, low density, high temperature stability and high hardness. These high modulus and hardness TiC precipitates in Fe-Al based composites drastically improved the important properties such as high temperature strength and wear resistance.

Significant research has been carried out to understand the solidification aspects of TiC precipitates in Fe based alloys and it has been noted that on the whole the evolution of TiC reinforced composite microstructure can be controlled by parameters such as cooling rate in the formation of TiC particle morphology. Various studies have been carried out to prepare composites based on Fe3Al–TiC and FeAl–TiC in vacuum using arc melting or induction melting process **(Terry and Chinyamakobvu 1992, Parashivamurthy et al. 2008).** They focused mainly on the growth morphology of TiC particles. The studies on the in-situ formation of TiC precipitates in Fe-Al ordered and disordered solid solution is very limited **(Khaple et al. 2009, Schneider et al. 2003, Falat et al. 2005, Chaudhary et al. 2015).** It is expected that micro-alloyed high strength steels are basically steels containing small amount of alloying additions such as V, Nb and Ti **(El-Faramawy et al. 2012).** These alloying elements operate as solid solution or form precipitates to suppress the recrystallisation and grain growth behaviour of the austenite. Micro-alloying of carbon steels is usually practised. Grain refinement can be enhanced by using these micro-alloying elements to get better combination of mechanical properties. As the cost of alloying elements such as Nb and V is much higher than Ti, the development of lightweight steels with Ti as alloying element is recently getting more attention. The

effect of Ti (0.05 to 0.23 wt.%) addition on carbon containing steel has been investigated **(El-Faramawy et al. 2012).** It was observed that Ti addition causes considerable grain refinement which is attributed to the formation of TiC or TiN which retards the grain growth during hot processing resulting in decreased ferritic grains. Good improvement in the mechanical properties such as hardness, strength and impact energy was detected by the addition of titanium in the steel.

Effect of Ti and C on as-cast ferritic lightweight steel has been examined **(Chaudhary et al. 2015)**. In this study, the Ti and C content was taken in stoichometrical quantity such that only TiC precipitate forms in the steel. No precipitate is observed in the base steel, whereas primary and secondary TiC precipitates were observed in all the other steels within the ferritic matrix. It was noted that as the carbon and titanium content increased in the alloy, the size and the volume fraction of the TiC precipitate increased. The increase in compressive yield strength is attributed to the composite strengthening caused by higher volume fraction of harder TiC precipitates.

The effect of 0.5wt.%Ti on Mn containing low-density steel (Fe-7Al-32Mn-2.2C) was examined in the cast condition **(Mejía et al 2015)**. JMatPro software was used to predict the physical properties and the phase evolution, which was validated successfully with the experimental results. In this steel a density reduction of 16.3% was reported compared to the density of the conventional steels.

2.12 Summary

Based on the literature discussed in the above sections following inference can be arrived at

1. Fe-Al based ferritic steels are one of the potential materials for lightweightening of structural application, particularly in automobile industry.
2. Fe-7wt.%Al exhibited about 10% reduction in density and considerable improvement in tensile strength compared to the conventional steel used for automobile applications such as interstitial free steel and mild steel etc.

3. It is also observed that Fe-7wt.%Al steel prepared by air induction melting or vacuum induction melting exhibited similar mechanical properties as the Al content is low to cause hydrogen embrittlement.
4. The Fe-Al based ferritic steels exhibited large average grain size in the order of about 1mm. The strength levels of these (300-380 MPa) are also low compared to the other steels used for structural applications.
5. The Fe-Al steel grains can be refined by alloying additions in the form of stable and compatible inoculants such as TiB_2 and ZrB_2 in the melt itself. The effect of these grain refiners on solidification and also thermo-mechancial processing of Fe-7Al based lightweight steel has been attempted.
6. It is illustrated in detail the beneficial effects of addition of carbon to iron aluminides. The literature on low Al containing Fe-Al alloys is very scanty. However, the strength (300-380 MPa) and ductility value (18%) of this steel are still low as compared to other competitive structural materials. Hence, strength improvement of Fe-Al ferritic steels is attempted by the addition of carbon and a systematic study is taken up.
7. It is also understood that stable carbide formers such as Ti and Nb are effective in reducing the grain size and also improving the tensile strength of the Fe-Al alloys. Hence, the effect of in situ formation of these stable carbides is undertaken to improve both the strength of the steel by grain refinement and partitioning of carbon between κ-carbide and metallic carbide such as TiC or NbC by adding Ti and Nb to Fe-7Al steel containing optimum level of carbon.

Chapter 3

EXPERIMENTAL PROCEDURES

Chapter 3 provides the experimental procedure adopted for preparation of the steel of different compositions, processing, chemical, microstructural and mechanical characterization of the different steels.

3.1 Material Selection

Commercially pure raw materials such as iron, mild steel, aluminium, niobium, titanium, graphite and diborides (ZrB_2 and TiB_2) were used for preparing steel pancakes of desired compositions. To study the effect of carbon, at lower levels, graphite was added to the commercially pure iron to make the composition and in case of higher carbon levels, graphite was added to mild steel scrap. The chemical composition of the raw materials used is given in **Table 3.1**. Various steps involved in the preparation, processing and characterization of the steels with different chemical compositions is presented in the form of flowchart (**Fig. 3.1)**.

3.1.1 Melting

The raw materials such as iron, mild steel and aluminium were taken in the form of ingot/rods. These materials were cut into pieces of 10-25 mm thickness. Niobium was taken in the form of rod of 8 mm thickness. Titanium in the form of 10-15 mm thick chunklets was used. Diborides (ZrB_2 and TiB_2) were used in the form of powders (average particle size of 3-6 μm and 2-10 μm, respectively) for preparing steel pancakes of desired compositions.

Table 3.1 The chemical composition of the raw materials used in the study

Raw Material	Chemical Composition (wt.%)
Commercially pure iron	C-0.014, O-0.016, N-0.012, Mn-0.05, Cu <0.025, Ti <0.02, Si-0.016, S-0.003, P-0.08, Balance-Fe
Mild steel scrap	C-0.26, O-0.040, N-0.018, Mn-0.45, Si-0.09, Cu <0.02, Ti <0.05, S-0.014, P-0.02, Balance-Fe
Commercially pure Al	Si-0.16, Fe-0.42, Balance-Al
Ti sponge	C-0.02, N-0.05, O-0.08, Fe-0.12, Ni-0.06, Cr-0.056, Al-0.029, Mn-0.024, Balance-Ti
Commercially pure niobium	C- 0.15, O- 0.5, N- 0.1, H-0.05, Fe-0.05, Ta- 0.5, Ni-0.02, W- 0.2, Balance- Nb
Commercially pure TiB_2	B-21, C-0.32, O-1.5, N-0.25, Fe-0.21, Hf-0.25, Balance- Ti
Commercially pure ZrB_2	B-20, C-0.25, O-1.2, N-0.24, Fe-0.31, Hf-0.24, Balance- Zr

Non-consumable direct current (DC) arc melting process with a thoriated tungsten electrode was used for melting the raw materials. Pieces of iron, aluminium and powders of diborides (ZrB_2 and TiB_2) were premixed. These raw materials were directly placed in the cavity of water cooled crucible. The melt chamber was evacuated to 1×10^{-4} mbar and refilled with argon gas to about 600 mbar pressure. This evacuation and gas refilling cycles were repeated twice. Argon gas at 600 mbar pressure was maintained throughout the melting process. A photograph of the non-consumable button arc melting process along with schematic diagram is shown in **Fig. 3.2.**

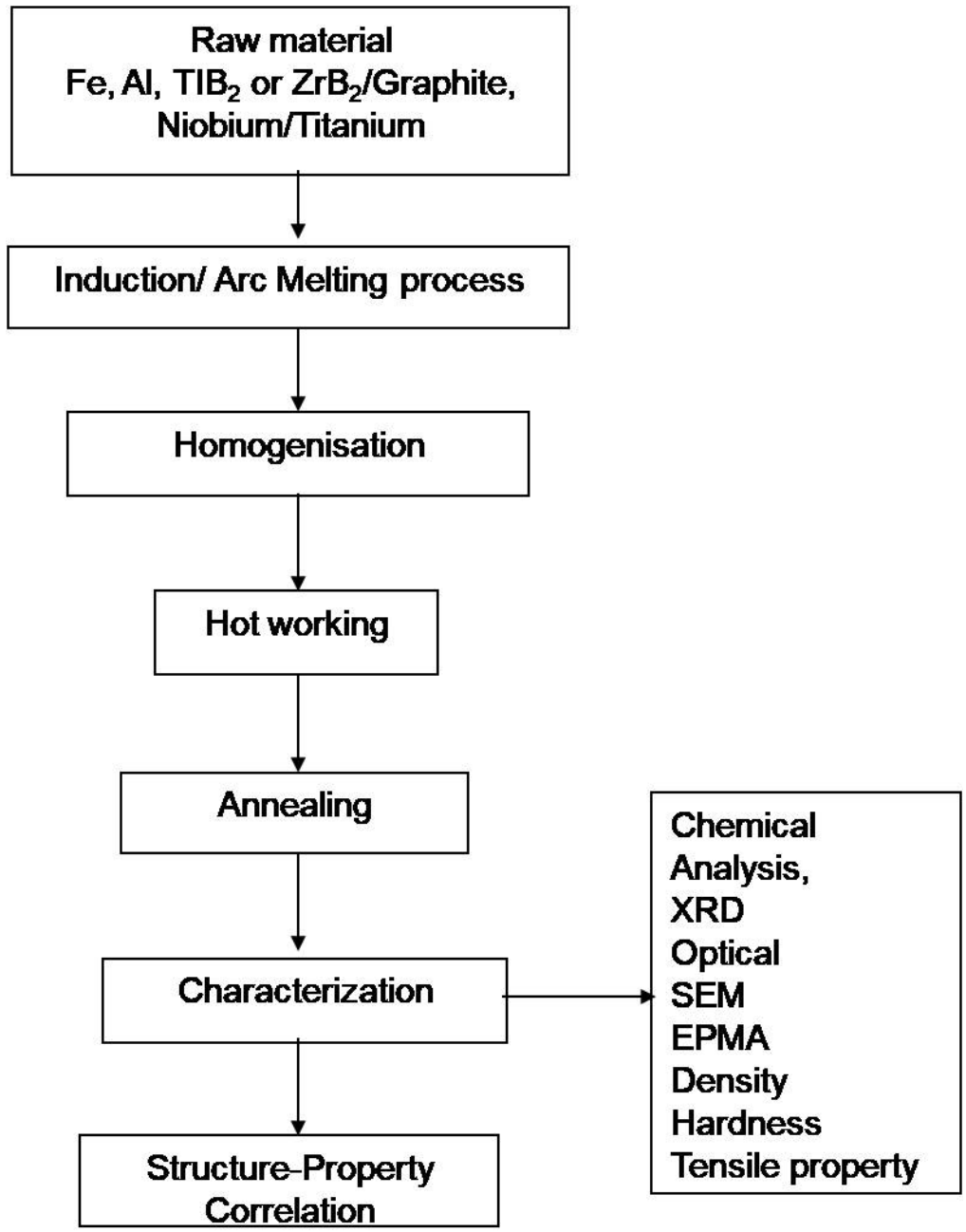

Fig. 3.1 Flow sheet showing the different steps in making and processing lightweight steels with different alloying additions

.

(a)

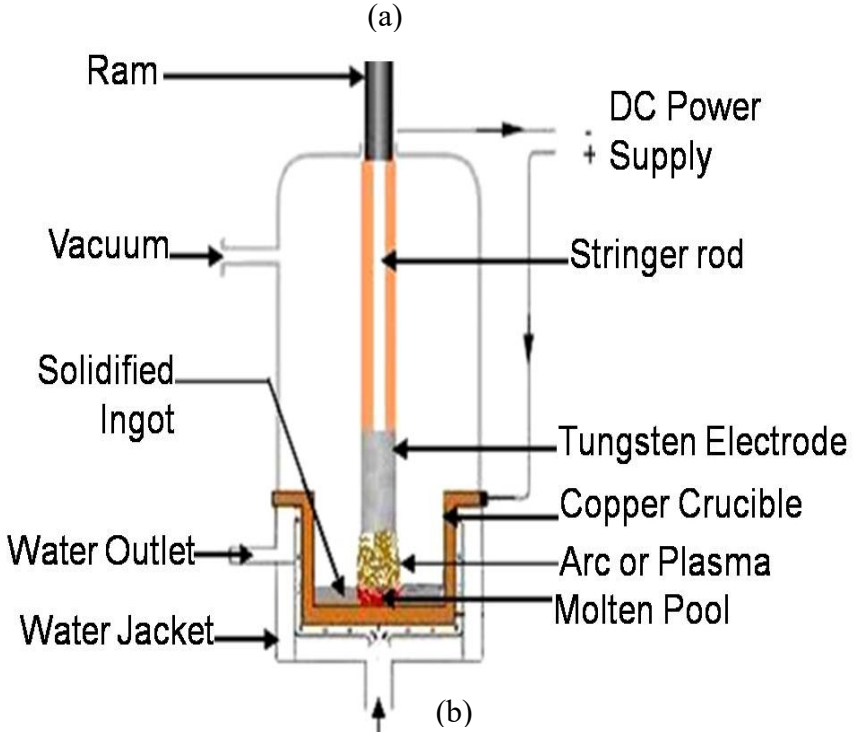

(b)

Fig. 3.2 (a) Photograph of non-consumable arc melting furnace and (b) its schematic diagram

To prevent contamination of the melt from the electrode, a high frequency power source was used to start the arc without contact between the thoriated tungsten electrode and the charge material. The molten metal was allowed to solidify in the water cooled copper crucible into a pancake form. An arc current of 850-900 A and arc voltage of 18-20 V were maintained during melting. The alloy was cast as a pancake of 100 mm diameter and 10 mm thickness in a water-cooled copper crucible. For each composition, the pancake was melted four times by periodically turning it upside down to improve the compositional homogeneity of the samples. A typical representative of the pancake sample is shown in the **Fig. 3.3.**

Fig. 3.3 A photograph of the pan cake melted by non-consumable vacuum arc melting process

For the study of effect of carbon content on Fe-7Al steel, the same raw materials such as commercially pure iron, mild steel scrap, aluminium and graphite were used. The melts were prepared by air induction melting process. The furnace started with (cleaned) iron pieces and after melting iron, a preheated alumina based flux (containing CaF_2, MgO and CaO) was added to cover the molten metal coming in direct contact with the atmosphere. This flux basically prevents the moisture coming in direct contact with the melt. Further other alloying elements such as aluminium and graphite were added into the melt by plunging through the molten flux cover. A photograph of the induction furnace used along with schematic diagram of air induction melting process is shown in **Fig. 3.4**. The melt was top poured into split cast iron moulds of 50 mm diameter. A typical representative of the ingot made by air induction melting process is shown in **Fig. 3.5**.

3.2 Radiography

This is one of the non-destructive testing methods to know the internal quality of the cast ingot. X- ray radiography (5 Curie Co-60 radioactive source) with an exposure factor of about 5 Curie-hour was used to check the defects such as piping, blow holes, porosity and cracks present in the cast pancakes/ingots.

3.3 Thermo-mechanical processing of the alloy

All the ingots/pancakes were homogenized at 1200^0C for 6 hours. These homogenized pancakes were preheated in a hearth furnace at 1100 °C for 1 h. The pre-heated ingots were given about 50 % reduction with one-ton pneumatic forge hammer (**Fig. 3.6**). Further these hot-forged ingots as well as cast pancakes were soaked at 1100 °C for 1 h and hot-rolled using a 2 high reversible DEMAG rolling mill (**Fig. 3.7**) with a reduction in thickness of 1 mm per pass. The samples were subjected to intermediate heating at 1100°C after every three rolling passes.

(a)

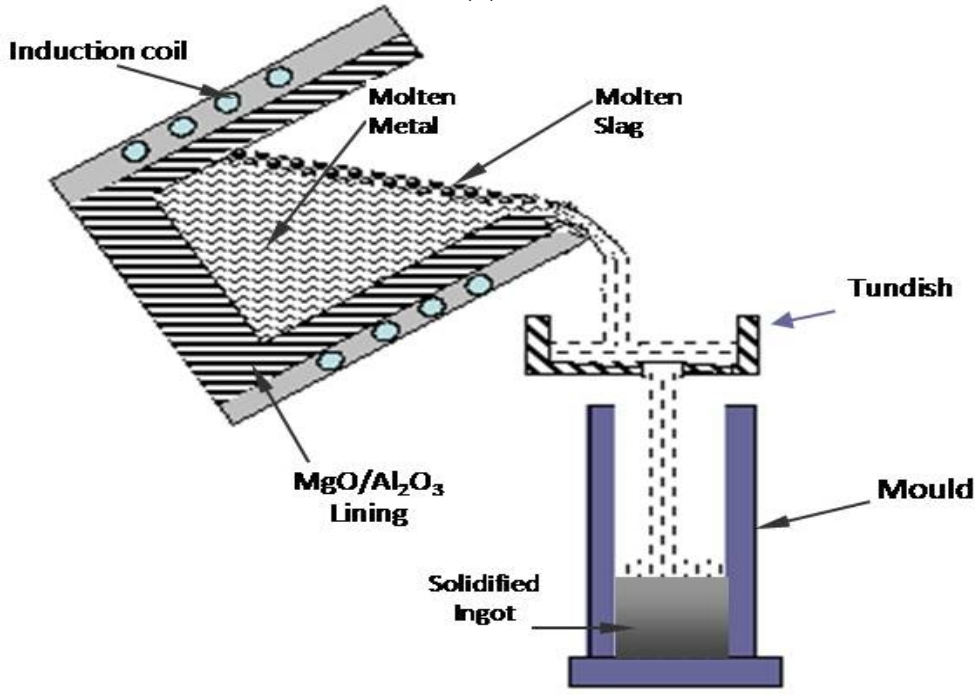

(b)

Fig. 3.4 The air induction melting furnace (a) photograph and (b) schematic diagram of the melting process with flux cover.

Fig. 3.5 A photograph of an ingot produced by an air induction melting process with flux cover

Fig. 3.6 A photograph of the hot deformation of the ingot by a forge hammer

Fig. 3.7 Two high reversible DEMAG rolling mill used in the present study

The final thickness of the ingots after the hot deformation (hot-forged and hot-rolled) (**Fig. 3.8**) was of 12 mm. The final thickness of the hot-rolled pancakes was of 2 mm (**Fig. 3.9**). After hot rolling, samples were cleaned either by surface grinding or pickling in dilute HCl. The hot-rolled and cleaned samples were then annealed at 700 °C for 1 h. The samples were cut in both longitudinal and transverse directions using band saw cutting machine for further analysis.

Fig. 3.8 A photograph of the hot-rolled plate from the ingot of Fe-7Al-0.35C lightweight steel.

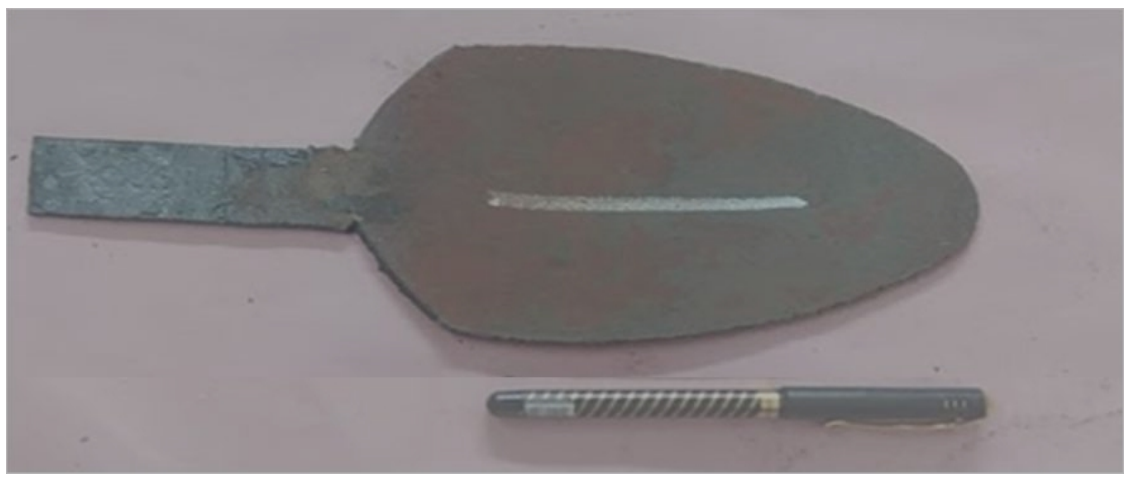

Fig. 3.9 A photograph of the hot-rolled sheet from the pancake of Fe-7Al-0.35C-1Nb lightweight steel.

3.4 Chemical analysis

Manganese, aluminium, silicon, niobium, zirconium and titanium were analyzed using GD-OES technique (Glow Discharge Optical Emission Spectroscopy). CC-444 Leco Carbon and Sulphur Determinator was used to analyse carbon and sulphur contents in the samples. Glow discharge technique was also used to analyse phosphorus content. Oxygen and nitrogen were measured using TC-136 Leco oxygen and nitrogen gas analyzer. Hydrogen analysis was done by RH 444 Leco gas analyzer.

3.5 Density measurement

Density of the hot-rolled and annealed samples was measured based on Archimedes principle using a density measurement kit of Sartorius make. The average of five independent measurements was recorded as the density of the sample.

3.6 ThermoCalc predictions

Thermodynamic calculations were performed to identify phases present at various temperatures and to study phase transformations in the alloys using TCFE6 database of ThermoCalc software. ThermoCalc works on the technique of free energy minimisation. The first and the second derivatives of Gibbs free energy expressions were used for calculating various thermodynamic properties of the system. This software was used to arrive at the equilibrium phase diagram of the alloy system at particular composition. The prediction of the phases and the amount and the type of the phases was compared with the experimental results. It would be appropriate to mention that in the calculation of equilibrium volume fraction of phases (in the present work); the carbides such as $M_{23}C_6$, M_7C_3, cementite etc. are not considered for the calculations as these are based on the kinetics of carbide formation.

3.7 Microstuctural Characterisation

3.7.1 Optical Microscopy

Conventional grinding and polishing were used to prepare the metallographic samples. The samples were mounted using bakelite powders. The mounted samples were initially polished on the belt grinder and subsequently using emery paper of various grits namely 150, 320, 500, 800, 1000 and 1200 to get the surface free from scratches. Further polishing was carried on velvet cloth with diamond paste of different sizes (such as 9µm, 3µm, 1µm and 0.5µm) as the abrasive material to obtain fine finish. The polished samples were ultrasonically cleaned in acetone. The polished sections were subsequently etched with an etchant consisting of 33% HNO_3 + 33% CH_3COOH + 33% H_2O + 1% HF by volume for microstructural examination using optical microscope. Progressive etching was carried out based on observing the degree of dullness of the sample surface. The etched surface was then quickly plunged into a stream of running water and then cleaned with acetone. The etched samples were then observed under optical microscope. The volume fraction of precipitates present in steels was measured using image analyser of Biovis Materials Plus Software attached to the optical microscope. The volume fraction was arrived by measuring the average volume fraction of precipitates at different locations for each alloy.The same software was also used to measure the average grain size of the alloy samples by the linear intercept method.

3.7.2 Scanning electron microscopy studies

Standard metallographic sample preparation techniques as discussed above were used to prepare the samples for scanning electron microscopy (SEM). The unetched metallographic samples were studied in the back scattered electron (BSE) mode and etched samples were studied in the secondary electron (SE) modes of Leo 440I scanning electron microscope (operated at 20 kV). X-ray energy dispersive analyses system (EDAX) attached to this system was used to analyse the elements present in the matrix and precipitates/phases. The EDAX works by simultaneous collection of whole spectrum of all energies and records them electronically. Fracture surfaces of the tensile tested samples were cleaned with acetone and examined to understand the mode of fracture in SE mode using SEM.

3.7.3 Electron probe micro analysis studies

The electron probe micro analysis (EPMA) studies were carried out on polished samples to determine the matrix and precipitate compositions present in the steel samples. The working principle of EMPA is based on wavelength dispersion spectroscopy (WDS). There is sequential measurement of peaks due to the physically dispersed spectrum of X-rays with the crystal. Hence, the chances of overlapping are less unlike as in the case of EDS. A photograph of the EPMA (Make: Cameca and Model: Sx-100) used for the study is shown in **Fig. 3.10.** Quantitative analysis of the elements present in the samples was taken. The line scanning and elemental mapping were also carried out to know the distribution of the elements.

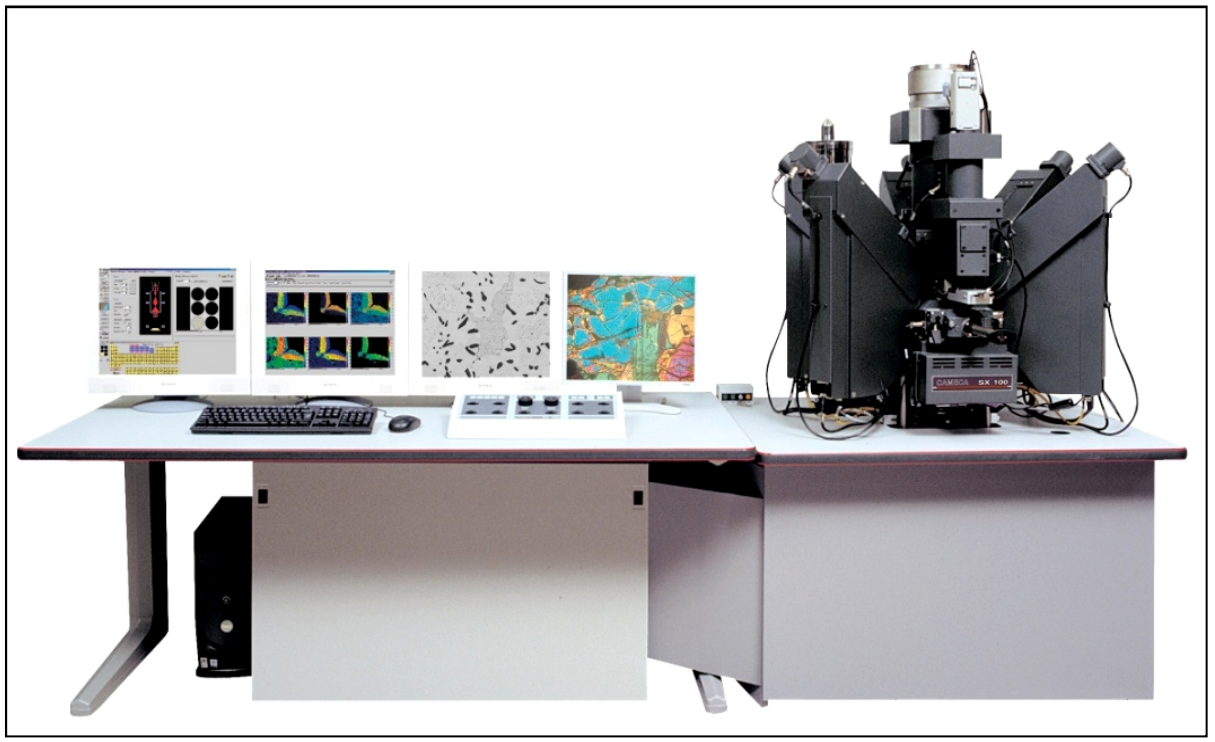

Fig. 3.10 A photograph of Cameca, Sx-100 electron probe micro analyser (EPMA)

3.8 X-ray diffraction analysis

Samples of 8 × 6 × 5 mm^3 thick section were cut from each alloy and mechanically polished up to 800 grit finish for this study. To examine the precipitates and phases present in the low density steel, X-ray diffraction (XRD) of the samples was carried out using a Philips PW3020 diffractometer coupled with graphite monochromator. The samples were irradiated with CuKα radiation obtained from a copper source operated at 40 kV and 30 mA. It is to be noted that the fluorescence problem on ferrous samples with Cu target for XRD measurements was overcome using a graphite monochromator. It is set to reflect/diffract only CuK_{α}. The sample is stationary and the detector moves around the sample. It measures the intensity and position of the peaks which fulfils the Bragg's law. The XRD patterns were recorded in a continuous slow scan mode. The peaks of various phases present in the pattern were indexed using an X'Pert HighScore software which has an inbuilt inorganic JCPDS (Joint Committee on Powder Diffraction Standards).

3.9 Mechanical characterisation

3.9.1 Hardness measurement

The bulk hardness and the microhardness values of all the lightweight steels were measured using Vickers hardness machine and are reported as Vickers hardness number (HV). The hardness value is determined by the ratio P/A. Where, P is the normal applied force and A is surface area formed after indentation. The surface area is determined by using the relation.

$$A = d^2/2 \sin(136^o/2) \approx d^2/1.8544$$

$$HV = P/A = 1.8544*L/d^2$$

Where 'L' applied load in kg and 'd' is the average length of diagonal in mm.

The hardness of metallographic samples was measured in a Leco LV700 Vickers hardness testing machine using a 30 kg load and a dwell time of 10 seconds. Microhardness of individual phases was also measured using an Economet VH 1D micro-hardness machine with 100 g load and a dwell time of 10 seconds. The average of five

independent measurements was recorded as the hardness value for the bulk and the microhardness of the samples.

3.9.2 Tensile testing

ASTM tensile test specimens for room temperature tests were prepared by EDM wire cut machine and polished using 600 grit abrasive. Tensile tests were conducted using an Instron 5500R universal testing machine at an initial strain rate of 1×10^{-3} s^{-1}. Tensile tests were carried out on samples of hot-rolled and annealed sheet conforming to ASTM E-8M. The yield strength (YS), ultimate tensile strength (UTS) and elongation values were also calculated from the tensile curves. The reported values were an average of three tensile tests data for each sample. The fractography of tensile tested alloy samples were observed using the SEM.

Chapter 4

EFFECT OF DIBORIDE ADDITIONS

Chapter 4 describes the effect of inoculants such as diborides (ZrB_2 and TiB_2) on structure-property and improvement of the tensile properties of Fe-7Al lightweight steel

---

4.0 Introduction

The Fe-Al ferritic steels have received more attention in the development of structures particularly for automobiles industry by reducing the density of the steel with addition of lighter alloying element such as Al. As described in the chapter 2, addition of 7wt.%Al in steel gives about 10% reduction in density. These steels (Fe-7Al) exhibited about 18% tensile elongation and yield strength of 300 MPa at room temperature in hot-rolled condition. However, the strength and ductility values are still low as compared to other competitive structural materials **(Herrmann et al. 2003, Rana et al. 2014, Pramanik et al. 2014, Rana 2014.** As discussed in the literature chapter, diborides ($ZrB_2$and TiB_2) have high stability, high elastic modulus and lower density. Hence, an attempt has been made to study the effect of these inoculants (ZrB_2 and TiB_2) additions as grain refiners on microstructure and properties of Fe-7wt.%Al steel.

4.1 The effect of inoculants (ZrB_2 and TiB_2) additions on microstructure of Fe-7Al steel

Two sets of pancakes of 100 mm diameter and 10 mm thickness and each with nominal compositions of Fe-7Al, Fe-7Al-0.5ZrB_2 and Fe-7Al-0.5TiB_2 were prepared by non-consumable electrode DC arc melting process. These pancakes were hot-rolled to 2mm thick sheets, annealed and characterised in the as-cast and annealed condition.

4.1.1 Visual observation and radiography of steel pancakes

All the pancakes were melted using vacuum-arc melting process. Apart from surface undulations typically seen in VAR pancakes, no other defects were present and the surface was smooth. Typical photograph of all the three pancakes with Fe-7Al, Fe-7Al-0.5ZrB_2 and Fe-7Al-0.5TiB_2 compositions are shown in **Fig. 4.1**. Radiography of all the steel samples indicated that pancakes are sound and free from internal defects such as cracks. No surface and edge cracks were observed in the hot-rolled sheets of all the alloys.

4.1.2 Chemical analysis:

The nominal composition and chemical analysis of the pancakes and the various elements present in the pancakes of the three steels are given in **Table 4.1**. From the table it is clear that the recovery of the alloying elements is good.

4.1.3 Microstructural characterisation

The macrostructures of all the three steel pancakes are shown in **Fig. 4.2.** It can be seen from the **Fig. 4.2** that in all the three steel pancakes columnar grains are visible and found to be aligned along the ingot axis. These observations indicate directional solidification from the water cooled bottom to the top surface of samples. During the non-consumable vacuum arc melting process, the cooling of the liquid metal takes place mainly by extraction of heat from the bottom of the pancake. In addition, the continuous heat input above the metal pool due to arcing between non-consumable electrode and liquid metal pool ensures large temperature gradient at the solidifying surface. These factors contribute to directional solidification and producing nearly columnar grain structure.

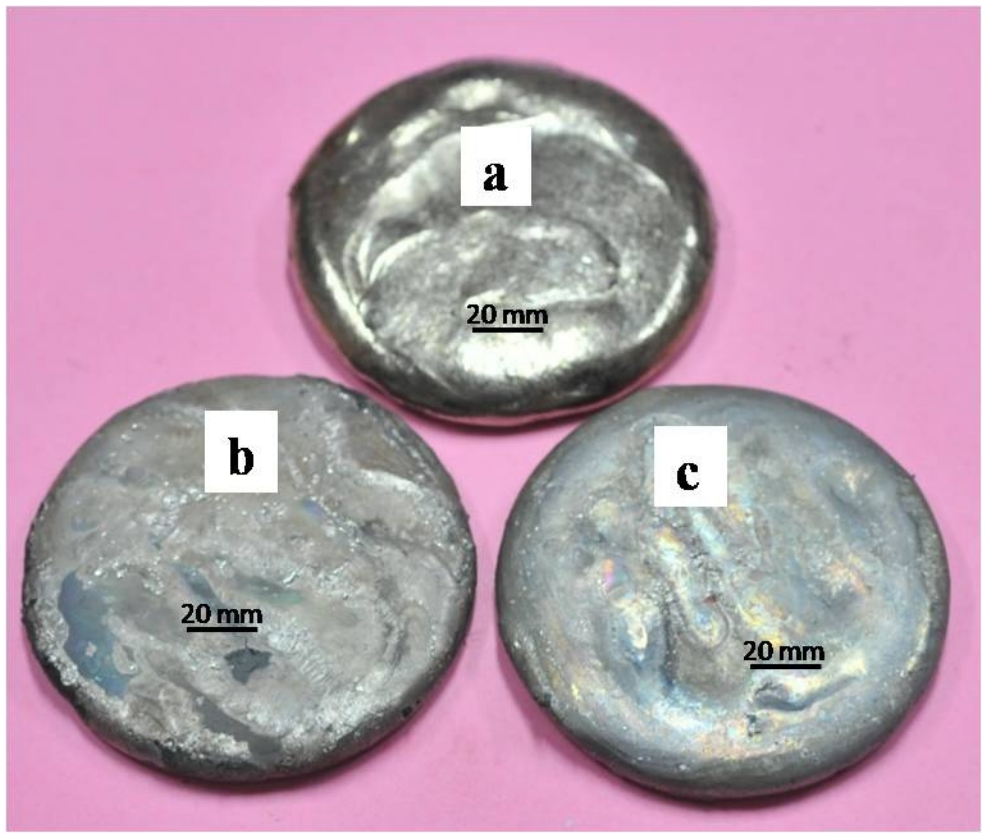

Fig. 4.1 Photograph of 100 mm diameter and 10 mm thick cast pan cakes of (a) Fe-7Al, (b) Fe-7Al-0.5ZrB_2 and (c) Fe-7Al-0.5TiB_2 steel.

Table 4.1: Chemical analysis of lightweight Fe-7Al steels with (ZrB_2 and TiB_2) inoculants.

Sample ID	Steel Composition (wt. %)	C (wt. %)	Mn (wt. %)	Al (wt. %)	Si (wt. %)	P (wt. %)	S (wt. %)	Zr (wt. %)	Ti (wt. %)	B (wt. %)	H ppm	O ppm	N ppm
Steel 1.	Fe-7Al	0.010 ±0.001	0.056 ±0.003	6.91 ±0.01	<0.02	<0.01	0.007 ±0.002	--------	-------	-------	9.7 ±0.2	160	<20
Steel 2.	Fe-7Al-0.5ZrB_2	0.013 ±0.001	0.070 ±0.003	6.97 ±0.01	0.024 ±0.002	<0.01	0.009 ±0.002	0.37 ±0.02	-------	0.09 ±0.02	12 ±2	150	<20
Steel 3.	Fe-7Al-0.5TiB_2	0.011 ±0.001	0.045 ±0.003	7.01 ±0.01	<0.02	<0.01	0.010 ±0.002	------	0.34 ±0.01	0.14 ±0.01	12 ±2	130	50 ±5

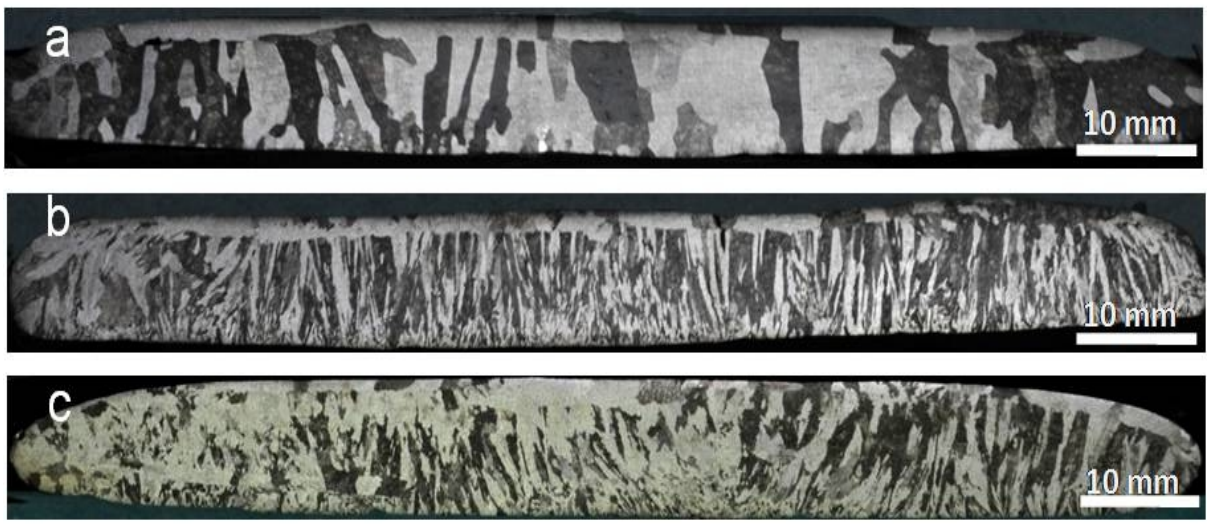

Fig. 4.2 Macrostructure of longitudinal section of 100 mm diameter and 10 mm thick cast pancakes of (a) Fe-7Al, (b) Fe-7Al-0.5ZrB_2 and (c) Fe-7Al-0.5TiB_2 steel.

The grain size of pancakes was measured in the cast as well as hot-rolled and annealed condition using Heyn's linear intercept method. The Fe-7Al steel containing ZrB_2 and TiB_2 inoculants (Steel 2 and 3) exhibited much finer grain structure as compared to the base steel (Steel 1) in all conditions (**Figs. 4.3** and **4.4)**. The average grain size in the as-cast (AC) and hot-rolled and annealed (HRA) conditions are presented in **Table 4.2**. From **Table 4.2,** it can be seen that the grain size of Steel 1 (the cast pancake) is about 895 µm and the grain size reduced to 79 µm in Steel 2 and 72 µm in Steel 3, respectively. Even in the HRA condition, the boride modified steels show finer grain structure than the base steel. Between the two boride modified steels, TiB_2 modified steel has much finer grain structure than the ZrB_2 modified steel (**Table 4.2**).

Campell and Bannister 1975 studied the effect of addition of fine particles (10-100 µm) of stable compounds (oxides, nitrides and borides) of Ti and Zr directly to Fe-3Si steel during electroslag remelting. They observed transition from columnar to equiaxed grain structure as a result of these additions. It was reported that TiB_2 is a good grain refiner for ferrous materials **(Campell and Bannister 1975).** The grain refinement in carbon steels have been attributed to partial dissolution of TiB_2 to give Ti and B in solution. Ti reacts with C present in the steel and TiC precipitates. The TiC particles heterogeneously nucleate new grains during solidification. In the present case, C is almost absent in the steels and therefore TiC aided nucleation is ruled out. However, B in solution possibly provides constitutional undercooling and inhibiting further growth of columnar dendrites.

The mechanism of grain refinement during thermo-mechanical working in Ti containing steels has been extensively studied **(Turkdogn 1996, Pickering 1997, Gladman et al. 1999)**. The grain refinement in these steels has been attributed to grain boundary pinning by carbides, borides, nitrides and carbonitrides of Ti. The reduction in cast grain size is important because hot-workability depends to a large extent on the as cast microstructure. The reduction in grain size after hot rolling and annealing is marginal for the base alloy, which can be attributed to the absence of grain growth inhibiting particles. The ZrB_2 particles seem to inhibit grain growth **(Park et al. 2001)**. Similar trend is observed in the present work by the addition of TiB_2 and ZrB_2.

Formatted[khaple H]: Not Superscript/ Subscript

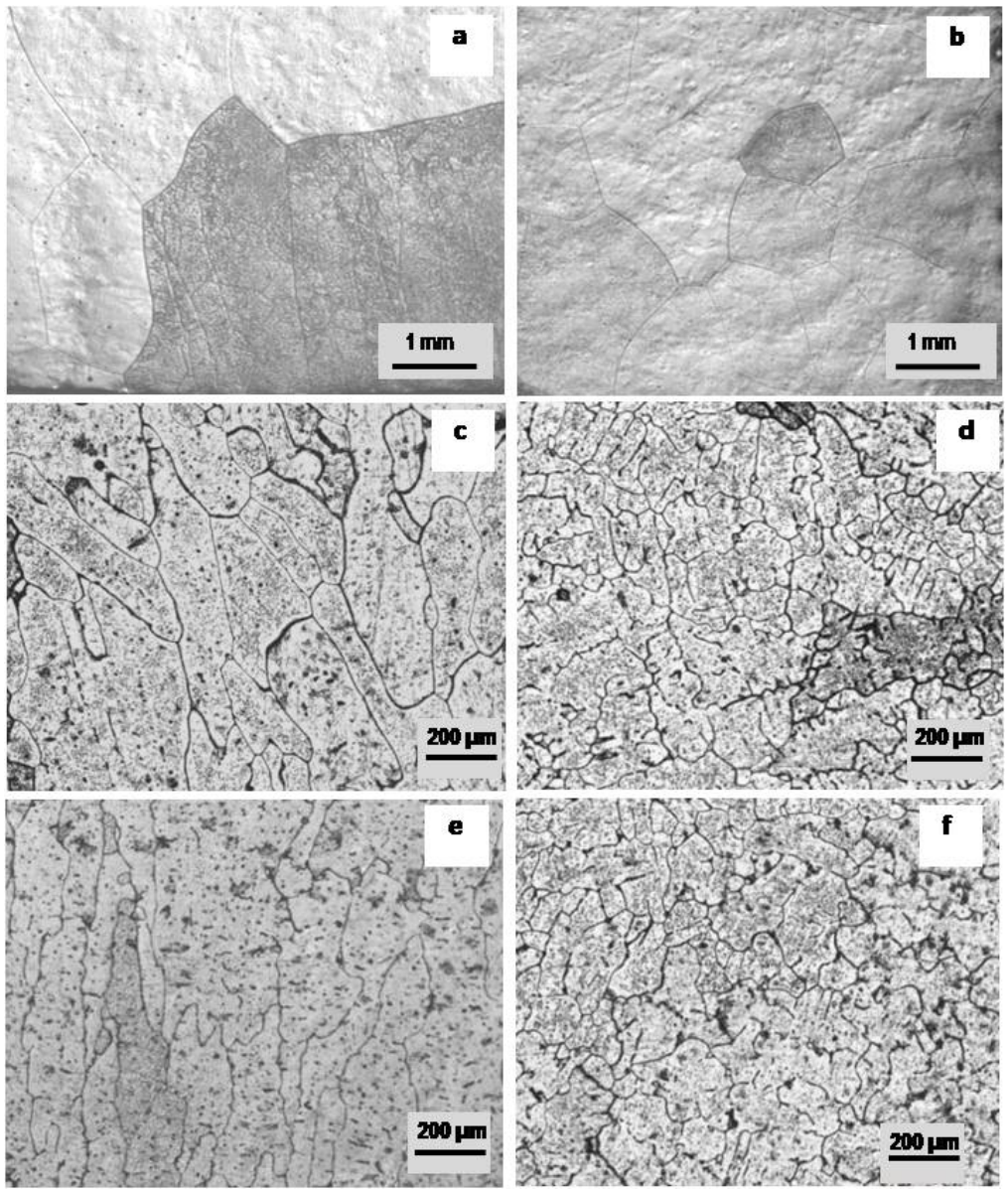

Fig. 4.3 Microstructure of 100 mm diameter and 10 mm thick as solidified pancakes of Fe-7Al based steel (a) longitudinal direction (b) transverse direction, Fe-7Al-ZrB_2 steel (c) longitudinal direction (d) transverse direction and Fe-7Al-TiB_2 steel (e) longitudinal direction (f) transverse direction.

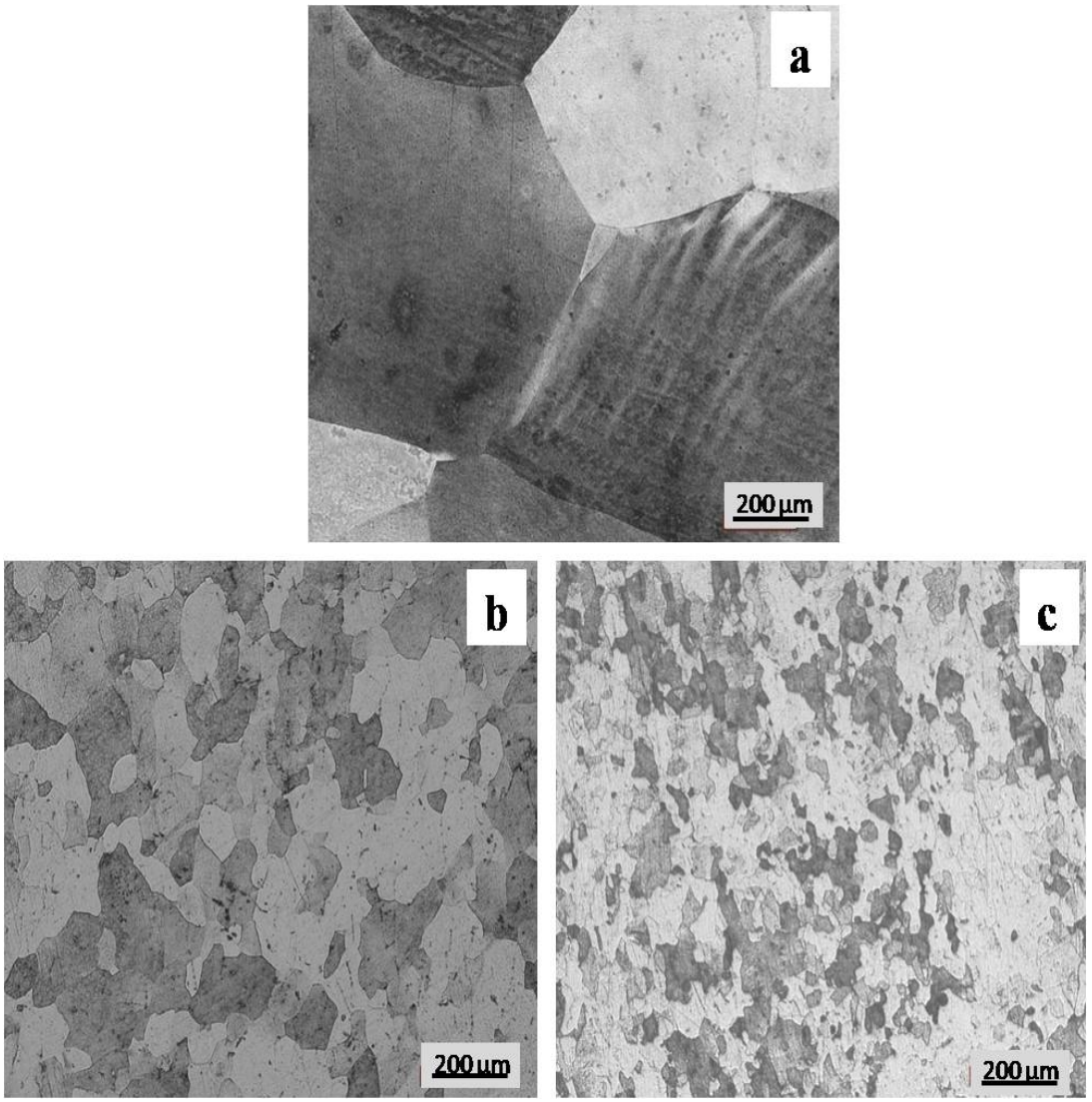

Fig. 4.4 Microstructure of hot-rolled and annealed sheets of (a) Fe-7Al, (b) Fe-7Al-0.5ZrB_2 and (c) Fe-7Al-0.5TiB_2 steel.

Table 4.2 Grain size of the lightweight steels in cast as well as hot-rolled and annealed condition.

Sample ID	Steel nominal composition (wt %)	Grain size (μm)	
		Cast pancake	Hot-rolled and annealed pancake
Steel 1	Fe-7Al	895±28	632±16
Steel 2	Fe-7Al-0.5ZrB_2	79±6	68±5
Steel 3	Fe-7Al-0.5TiB_2	72±4	66±4

In both the diborides (TiB_2 and ZrB_2) modified alloyed, the hot-rolled and annealed grain size is less than the as-cast grain size, highlighting the role of these diborides as grain boundary pinning agent during thermo-mechanical processing

The SEM back scattered electron images of all the three steels in hot-rolled and annealed condition are presented in **Fig. 4.5**. While Fe-7Al microstructure does not show either dark or bright second phase particles, Fe-7Al-ZrB_2 alloy shows presence of bright particles and Fe-7Al-TiB_2 steel shows presence of dark particles. Examination of more areas of the samples showed that the particles are distributed uniformly throughout the matrix in Steels 2 and 3. Further the microstructural and micro-chemical analysis of the ZrB_2 modified steel samples with the help of EDS and EPMA line scanning **(Figs. 4.6 and 4.7)** revealed that the bright particles are enriched in Zr and B, while the matrix contains only Fe and Al. The bright contrast of the particles implies that the average atomic number of the particles is higher than that of the matrix. Since the average atomic number of ZrB_2 (~17) is less than that of Fe-7Al (~24), the bright particles may be non-stoichiometric ZrB_2 composition. However, it is possible that during melting, partial dissolution of B or complete melting/dissolution of boride and re-precipitation in the form of non-stoichiometric boride during subsequent solidification might have taken place, resulting in the formation of a sub-boride with a higher effective atomic number.

In case of the TiB_2 modified steel, micro-chemical analysis by EDS and EPMA line scanning (**Figs. 4.8 and 4.9**) showed that the dark particles are enriched in Ti and B while the matrix showed the presence of Fe and Al. The average atomic number of TiB_2 is about 11, which is much smaller than that of Fe-7Al (about 24) and it represents that these particles being of TiB_2. Although there is strong possibility of dissolution of B in steel during melting, it cannot be verified based on BSE image contrast and micro-chemical analysis alone, since even complete dissolution of B into the steel matrix can only raise the atomic number to that of pure Ti (~22) which is still less than that of Fe-7Al, thus retaining their darker contrast. These boride particles are not observed in the optical micrographs of the respective alloys due to the fact that most of its size is not close to the resolution of optical microscope. The volume fraction of TiB_2 and ZrB_2 particles in Fe-7Al alloy is about 0.94±0.12 and 1.79±0.18 %

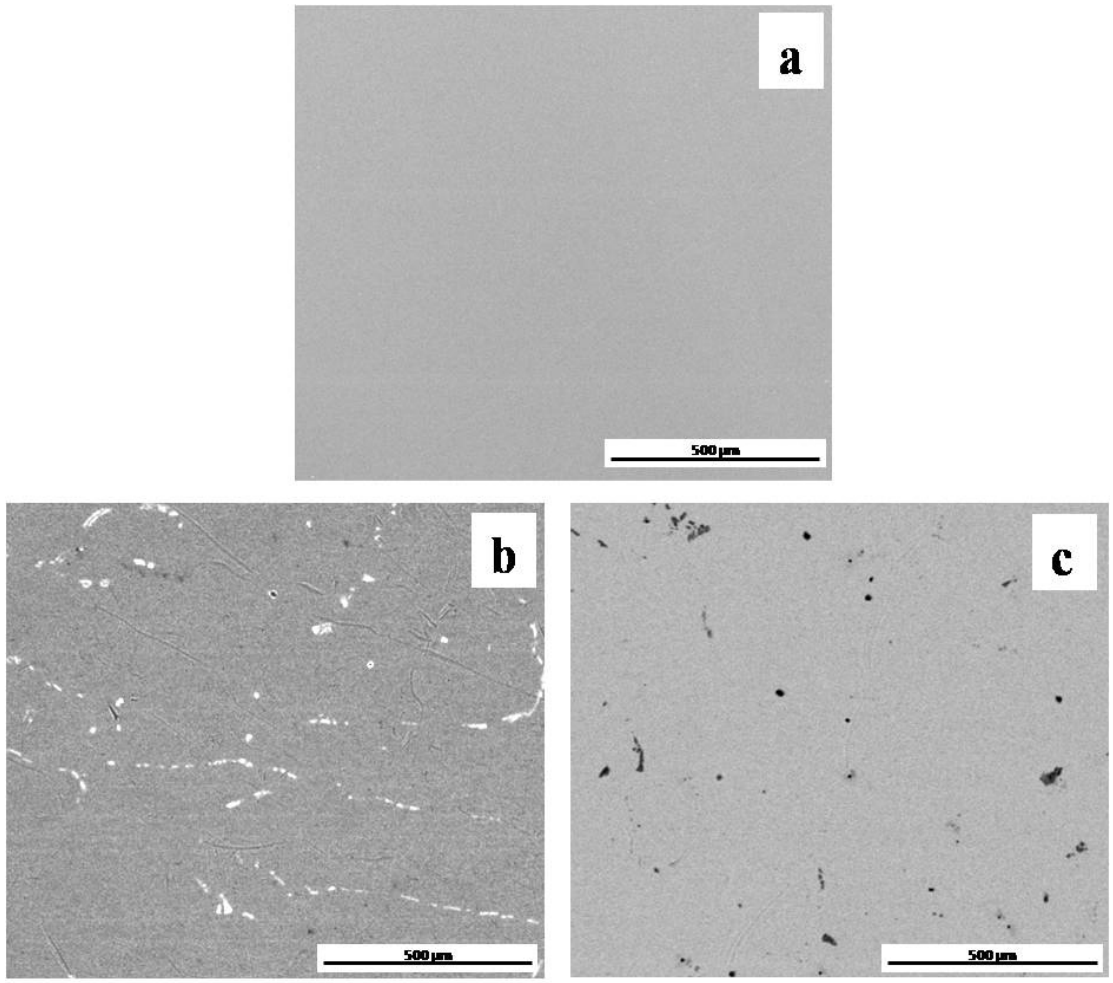

Fig. 4.5 Back scattered electron micrographs of hot-rolled and annealed sheets of (a) Fe-7Al, (b) Fe-7Al-0.5 ZrB_2 and (c) Fe-7 Al-0.5 TiB_2 steel.

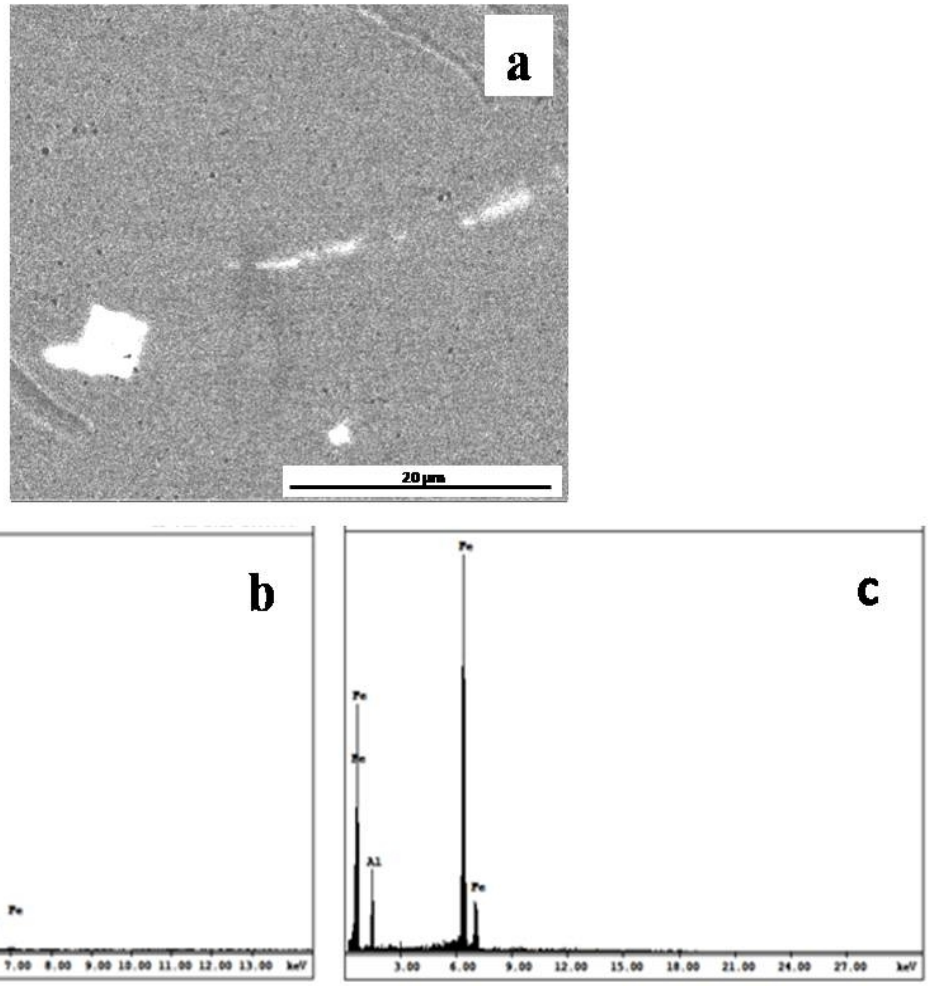

Fig. 4.6 (a) Back scattered electron micrographs of hot-rolled and annealed sheets of Fe-7Al-0.5ZrB_2 steel showing bright particles (b) EDAX analysis of particle showing presence of Zr in the particle and (c) EDAX analysis of the matrix showing the presence of Fe and Al and absence of Zr in the matrix.

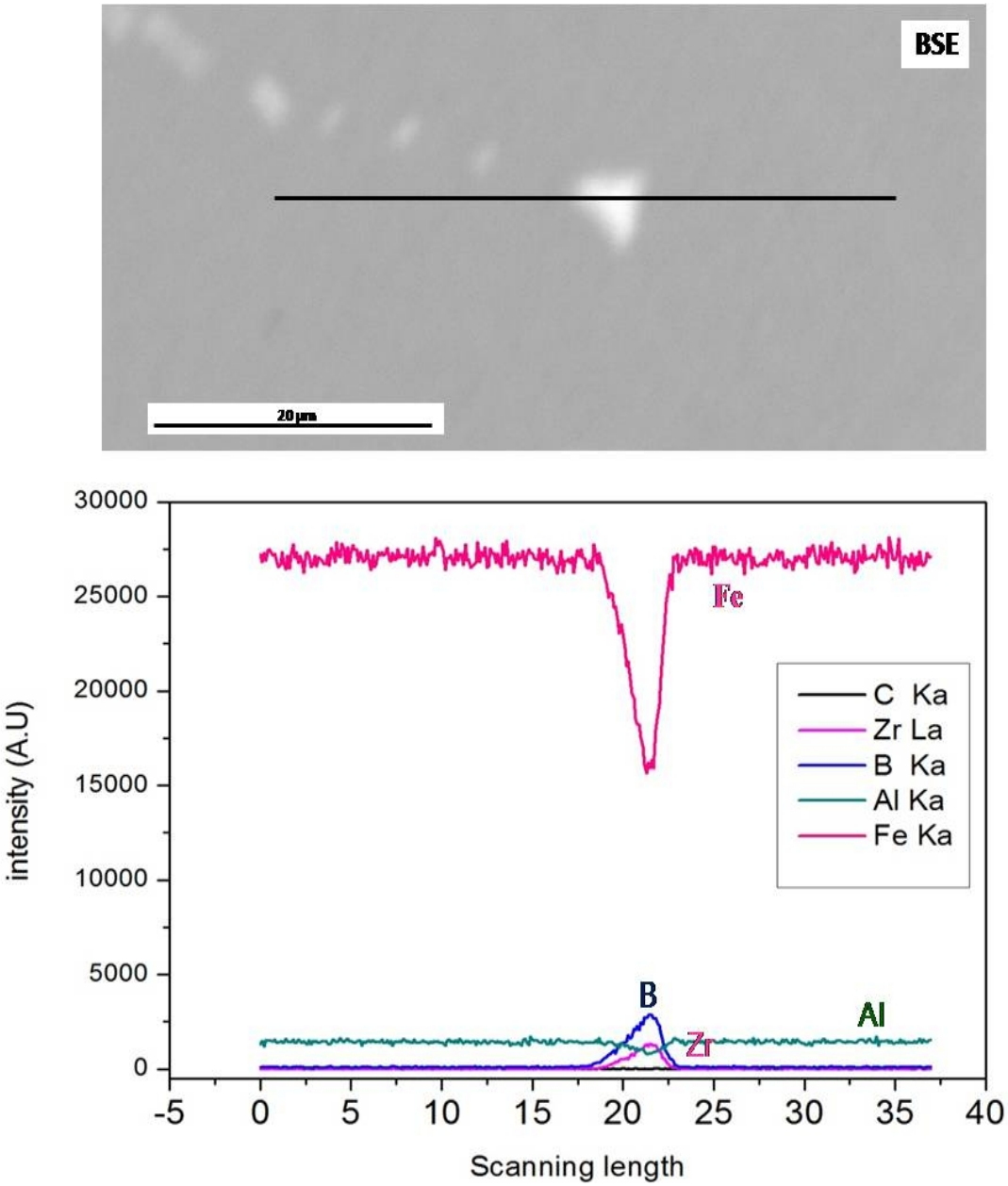

Fig. 4.7 BSE images and line scan of EPMA observed in hot-rolled and annealed Fe-7Al-0.5ZrB_2 steel. Line scan across the particle indicates that the particle is rich in Zr and B.

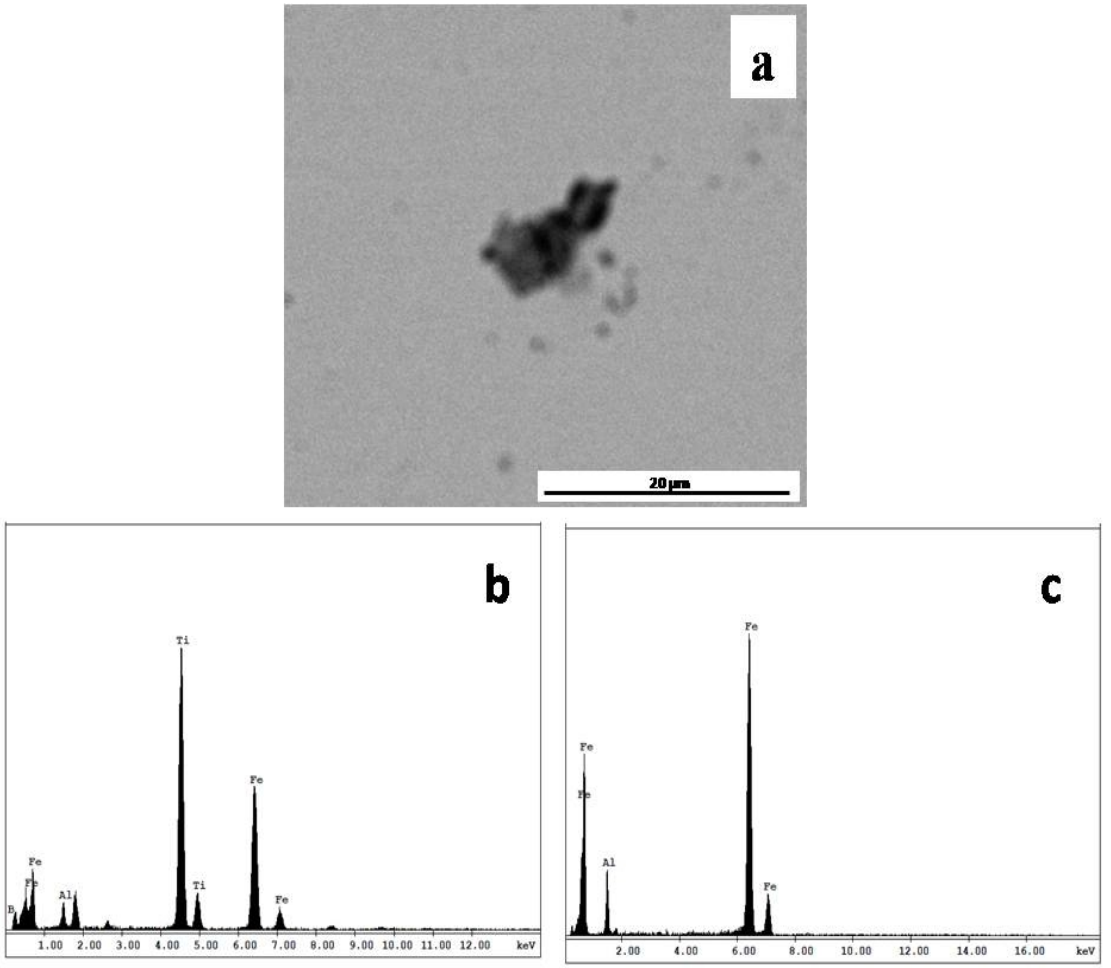

Fig. 4.8 (a) Back scattered electron micrographs of hot rolled and annealed sheets of Fe-7Al-0.5TiB_2 steel showing dark particles (b) EDAX analysis of particle showing the presence of Ti in the particle and (c) EDAX analysis of the matrix showing presence the of Al and Fe and absence of Ti in the matrix

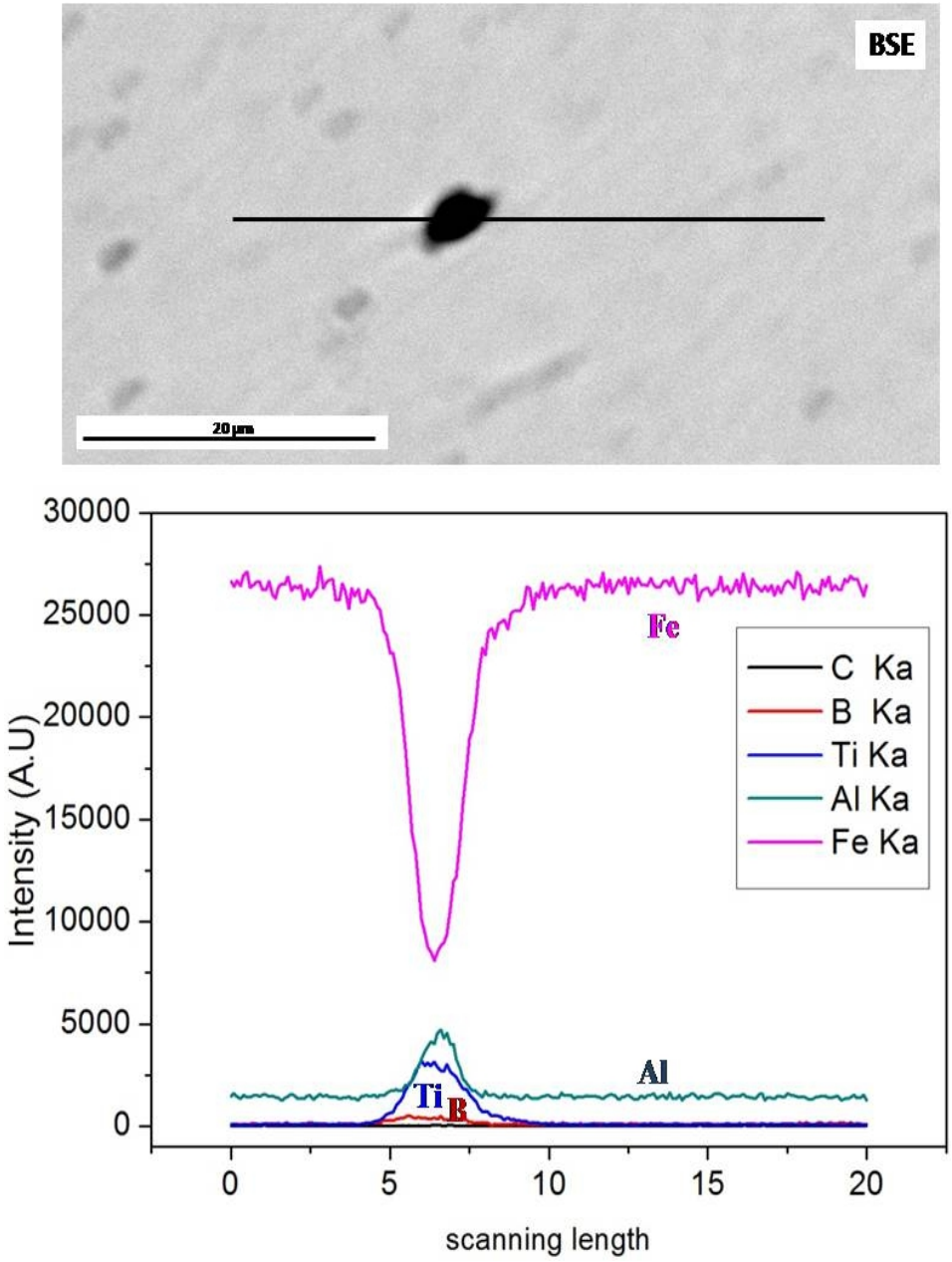

Fig.4.9 BSE image and line scan of EPMA observed in hot-rolled and annealed Fe-7Al-0.5TiB_2 steel. Line scan across the particle indicates that the particle is rich in Ti and B.

The XRD of all the three steels are shown in **Fig. 4.10**. The peaks of the XRD pattern of all the lightweight steels is indexed for α (Fe-Al) phase. The peaks of ZrB_2 in Steel 2 and TiB_2 in Steel 3 were missing in XRD pattern **(Fig. 4.10),** as expected, due to their low concentrations and also since the particles may have been of non-stoichiometric compositions or it is not within the detection limit of XRD.

4.2 The effect of inoculants (ZrB_2 and TiB_2) additions on mechanical properties of Fe-7Al steel

4.2.1 Hardness

The bulk hardness values of all the alloys in hot-rolled and annealed condition are listed in **Table 4.3**. The hardness of steels in as cast condition observed to increase from 154 to 181 HV. Similarly, the hardness of steels further increased from 174 to 193 HV in the hot-rolled and annealed condition. These observations clearly indicate improvement in the hardness of Fe-7Al steel with boride addition as well as hot-rolling and annealing. It can be further noted from the **Table 4.3** that the bulk hardness values of Steels 2 and 3 are marginally higher (5 and 11%, respectively) than that of the base steel (Steel 1), since the hardness of diborides are much higher than the hardness of the Fe-Al ferritic steel. However the contribution from the diboides particles is expected to be lower due to the low volume fraction of these diborides. On the other hand, the hardness imcrease contribution due to grain refinement appears to be predominently higher.

4.2.2 Tensile properties

The engineering stress-strain curves of all the three steels are presented in **Fig. 4.11**. The room temperature tensile properties of the steels in hot-rolled and annealed condition are summarized in **Table 4.4.** It can be seen from **Table 4.4 and Fig. 4.11** that the yield strength (YS) and ultimate tensile strength (UTS) of both the boride particle modified steels are higher than that of the base steel. The YS of Fe-7Al steel increased from 405 to 433 MPa and UTS enhanced significantly from 478 to 547 MPa. This must be due to the grain refinement of steels with boride (ZrB_2 and TiB_2) inoculants addition. Moreover, the strain hardening exponents of the boride added steels are found to be higher (0.1682) compared to the base steel (0.115).

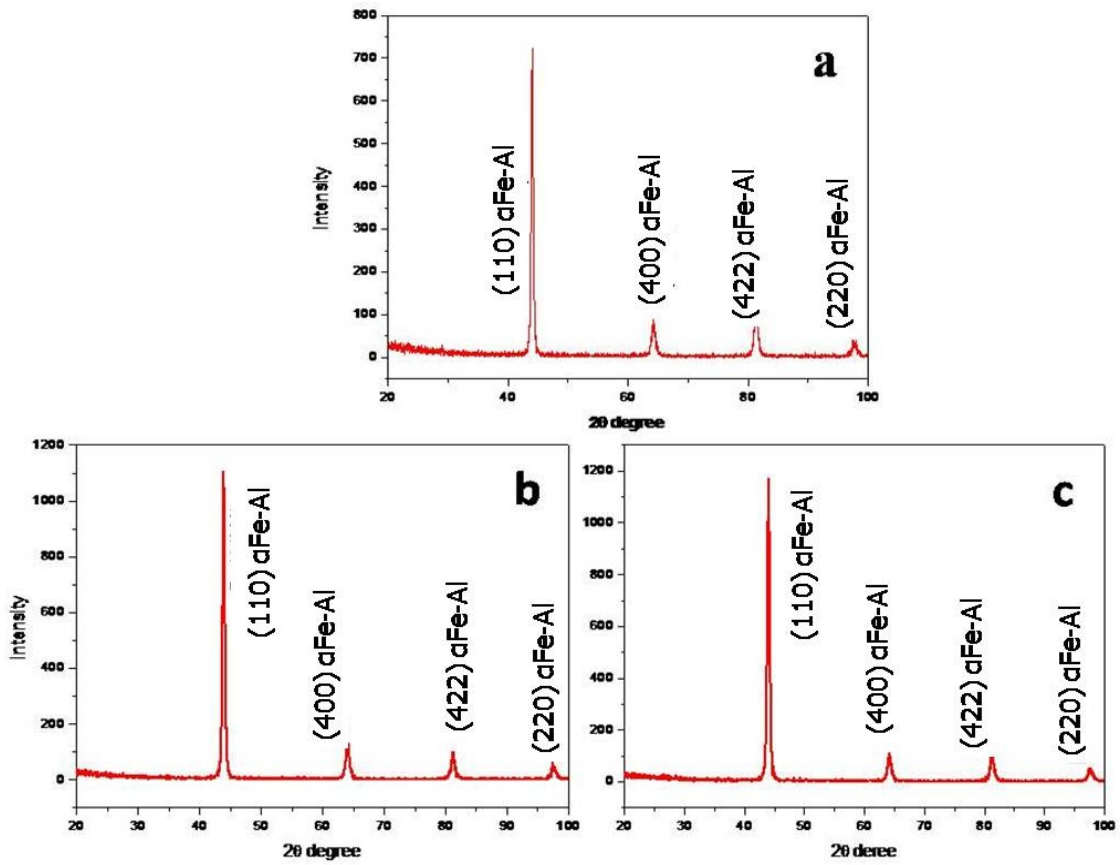

Fig. 4.10: XRD traces using Cu Kα radiation showing bcc peaks in all the steels (a) Fe-7Al, (b) Fe-7Al-0.5ZrB_2 and (c) Fe-7Al-0.5TiB_2

Table 4.3 Bulk hardness of all the three lightweight steels in the as-cast, hot-rolled and annealed condition

Sample ID	Steel Nominal composition (wt.%)	Hardness HV 30	
		As-Cast	Hot-rolled and annealed
Steel 1	Fe-7Al	154±8	174±06
Steel 2	Fe-7Al-0.5ZrB_2	178±10	183±8
Steel 3	Fe-7Al-0.5TiB_2	181±6	193±9

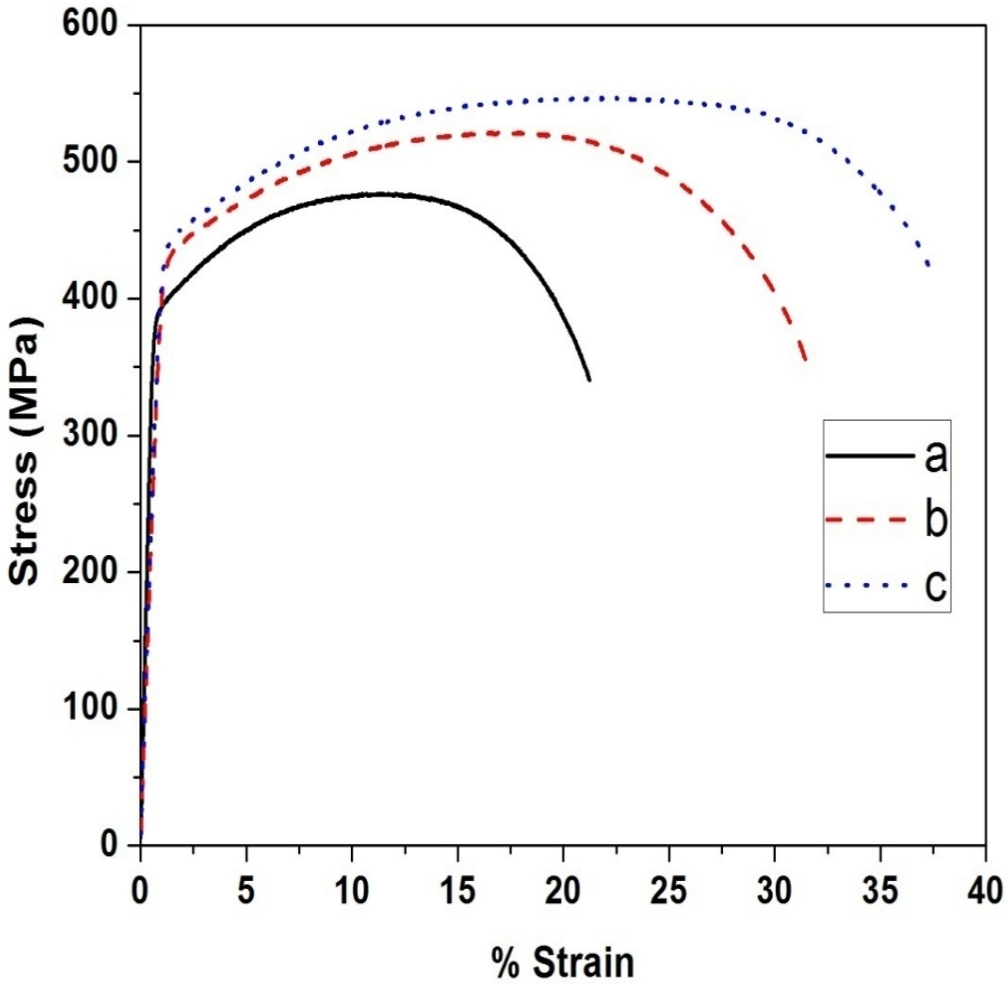

Fig. 4.11 Engineering stress-strain curves of hot-rolled and annealed sheets of (a) Fe-7Al, (b) Fe-7Al-0.5ZrB_2 and (c) Fe-7Al-0.5TiB_2 steel

Table 4.4 Room temperature tensile properties of all the three lightweight steels in hot-rolled and annealed condition

Sample ID	Steel Nominal composition (wt %)	0.2% YS MPa	UTS MPa	Uniform Elongation %	Total Elongation %	Strain hardening exponent (n)
Steel 1	Fe-7Al	405±10	478±12	11.5±1	19±1	0.115±0.002
Steel 2	Fe-7Al-0.5ZrB_2	422±13	541±15	17.5±1	31±1	0.1659±0.003
Steel 3	Fe-7Al-0.5TiB_2	433±14	547±16	21.5±1	38±2	0.1682±0.004

Interestingly, addition of both ZrB_2 and TiB_2 also resulted in significant improvement in room temperature ductility from 19% to 38%. The addition of ZrB_2 resulted in about 63 % improvement in room temperature ductility, whereas addition of TiB_2 gave rise to about 100 % improvement in room temperature ductility over the base alloy. Further, steels containing ZrB_2 and TiB_2 exhibited higher uniform elongations as compared to the base steel as indicated by their higher strain hardening exponent values given in **Table 4.4.** This improvement in room temperature ductility and higher strain hardening ability can be attributed to reduction in grain size (**Table 4.2)** which was caused by the addition of ZrB_2 and TiB_2. It is to be noted that both high uniform elongation and high strain hardenability are positive attributes with respect to deep forming.

4.3 Fractography

The fractographs of hot-rolled and annealed steel sheets after tensile test are shown in **Fig. 4.12.** It can be seen from the fractrographs that the base steel (Steel 1) has failed essentially by cleavage mode. For Fe-Al ferritic steels, fracture is generally by cleavage, where the main resistance to fracture is offered by grain boundaries **(Chen et al. 2015; Calcagnotto et al. 2009).** Further, since the base composition shows coarse grain size in the hot-rolled and annealed condition, low ductility cleavage fracture is expected. On the other hand, tensile fracture surface of steels containing ZrB_2 and TiB_2 is ductile with characteristic dimples, as would be expected in a fine grain material in which the dislocation pile up is less because of smaller grain size. Among the two boride particle modified steels, the size of the dimples in the steel containing TiB_2 is somewhat finer than the size of the dimples observed in the steel containing ZrB_2, explaining higher ductility of the TiB_2 modified steel among the two. The dimple features in the boride particle modified steels indicate that fracture proceeds by classical nucleation, growth and coalescence of micro voids formed by decohesion of ZrB_2/TiB_2 particles from the matrix (**Calcagnotto et al. 2009).**

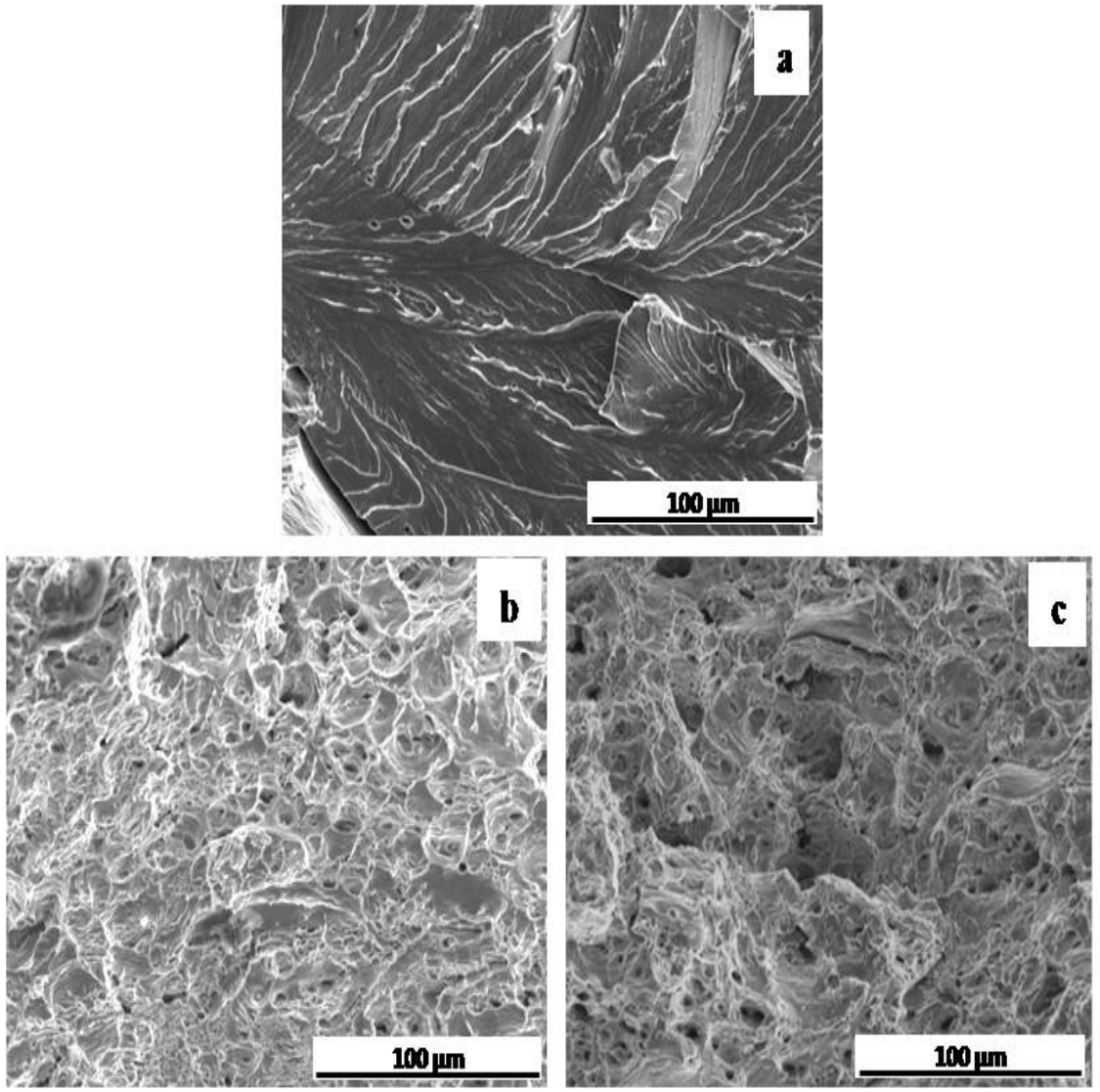

Fig. 4.12 SEM fractrographs of hot-rolled and annealed fracture surface of (a) Fe7Al showing cleavage fracture, (b) Fe-7Al-0.5ZrB_2 and (c) Fe-7Al-0.5TiB_2 both showing dimple fracture.

4.4 Summary

In the present work, the effect of diboride inoculants (ZrB_2 and TiB_2) addition as grain refiners on microstructure and properties of Fe-7wt.% Al steel has been studied. The conclusions of the above work are as follows.

1. Directionally solidified structure was observed in vacuum arc remelted pancakes of steels based on Fe-7Al composition.
2. The base steel (Steel1: Fe-7Al) exhibited single phase microstructure, while those modified with ZrB_2 and TiB_2 particles exhibited two phase microstructure, the additional phases were Ti and Zr diborides, respectively.
3. In the cast condition, the steels containing ZrB_2 and TiB_2 exhibited much finer grain (79 μm and 72 μm) structure as compared to the (695 μm) base steel.
4. Hot rolling and subsequent annealing resulted in further grain size reduction in all the three steels. Higher the as-cast grain size, greater is the grain refinement seen after hot rolling and annealing.
5. Hardness, yield strength, ultimate tensile strength and strain hardening exponent increased in boride particle modified steels compared to the base steel.
6. Significant improvement in room temperature strength (478 to 547 MPa) and ductility (19 % to 38 %) was observed by addition of ZrB_2 and TiB_2 to the base steel, and is attributed to grain refinement occurring during solidification, which is either retained (Fe-7Al-0.5ZrB_2 and Fe-7Al-0.5TiB_2) or increased further after hot rolling and annealing in Fe-7Al-0.5TiB_2 steel.
7. The fractography of Fe-7Al steel indicated cleavage mode of fracture. On the other hand, the fracture surface of Fe-7Al containing ZrB_2 and TiB_2 is ductile with characteristic dimples.

Chapter 5

EFFECT OF CARBON

Chapter 5 provides the *effect of carbon in the wide range (0.012 to 2.2wt.%) on the evolution of microstructure, its impact on mechanical properties and fracture behaviour of Fe-7Al lightweight steel.*

5.0 Introduction

The disordered ferritic (A2) phase in Fe-Al lightweight steels results in good ductility but suffers from lower strength when compared to the other existing structural materials such as heat-resistant stainless steel. Hence, an attempt has been made to study the effect of carbon in the wide range (0.012 to 2.2wt.%) on the evolution of microstructure, its impact on mechanical properties and fracture behaviour of Fe-7Al lightweight steel.

5.1 Influence of carbon (0.012 to 2.2 wt.%) on density and phase evolution of Fe-7Al steel

The nominal composition and the chemical analysis of five steels based on Fe-7wt.%Al with different carbon (0.012 to 2.2 wt.%) contents made by air induction melting process given in **Table 5.1.** All the steel samples with different carbon content could be successfully hot forged and hot-rolled to 12 mm plates. The photograph of the hot-rolled plates is shown in **Fig. 5.1.** The effect of carbon on the density of the Fe-7wt.%Al steels is given in **Table 5.2.** The plot showing the effect of carbon on the variation in density of Fe-7wt.%Al steels is shown in **Fig. 5.2.** The density of steel decreased from 7231.51 to 7103.18 kg/m^3 with the carbon addition. These lightweight steels with carbon addition (upto 2.2wt.%) showed considerable reduction (~ 10%) in density as compared to the traditional steel (7873.24 kg/m^3).

Table 5.1: Chemical composition of Fe-7wt.%Al based lightweight steel with different carbon contents.

Steel Sample	Nominal composition (wt.%)	Steel Composition				
		Al (wt. %)	Si (wt.%)	Mn (wt. %)	S (wt. %)	C (wt. %)
CS1	Fe-7Al-0.012C	6.88	0.18	0.16	0.004	0.012
CS2	Fe-7Al-0.35C	6.78	0.19	0.15	0.004	0.35
CS3	Fe-7Al-0.65C	6.98	0.15	0.12	0.004	0.65
CS4	Fe-7Al-1.5C	7.10	0.18	0.13	0.002	1.50
CS5	Fe-7Al-2.2C	7.11	0.16	0.15	0.005	2.20

Table. 5.2. The density of Fe-7wt.% Al lightweight steel different Carbon content.

Steel Sample	Nominal Composition (wt.%)	Density (gm/cc^3)
CS1	0.012C	7.23151±0.0014
CS2	0.35C	7.21024±0.0020
CS3	0.65C	7.18254±0.0021
CS4	1.5C	7.12591±0.0012
CS5	2.2C	7.10318±0.0018

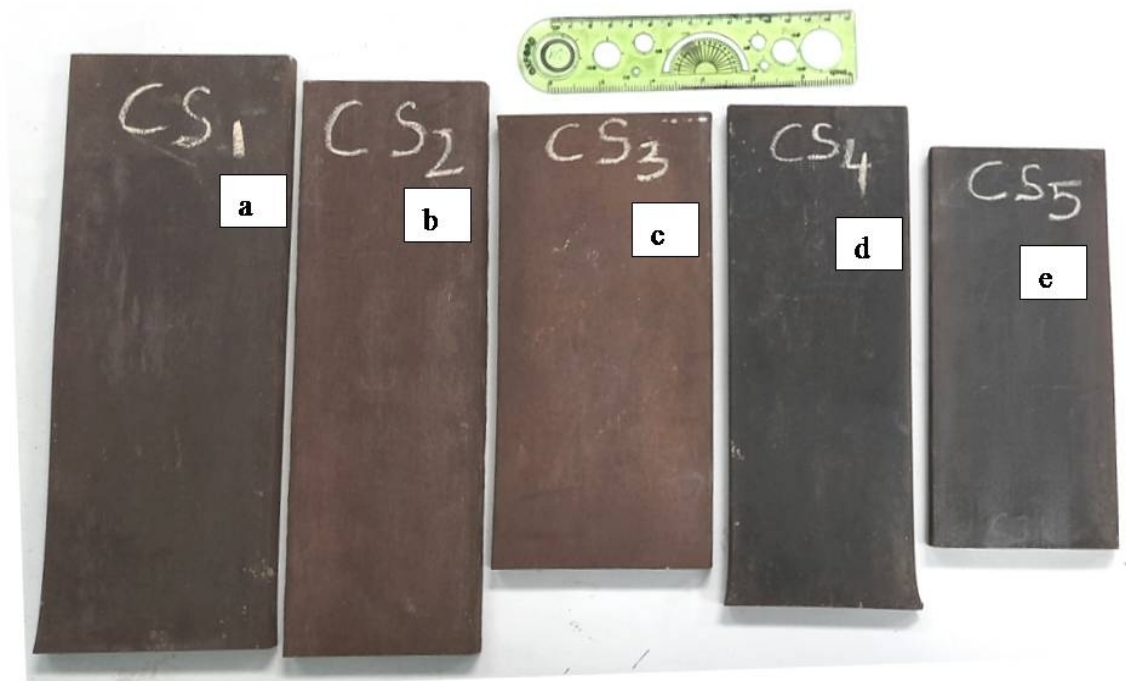

Fig 5.1. Photograph showing the hot-rolled plates of Fe-7wt.%Al based steel with (a) 0.012, (b) 0.35, (c) 0.65, (d) 1.5 and (e) 2.2wt.% carbon.

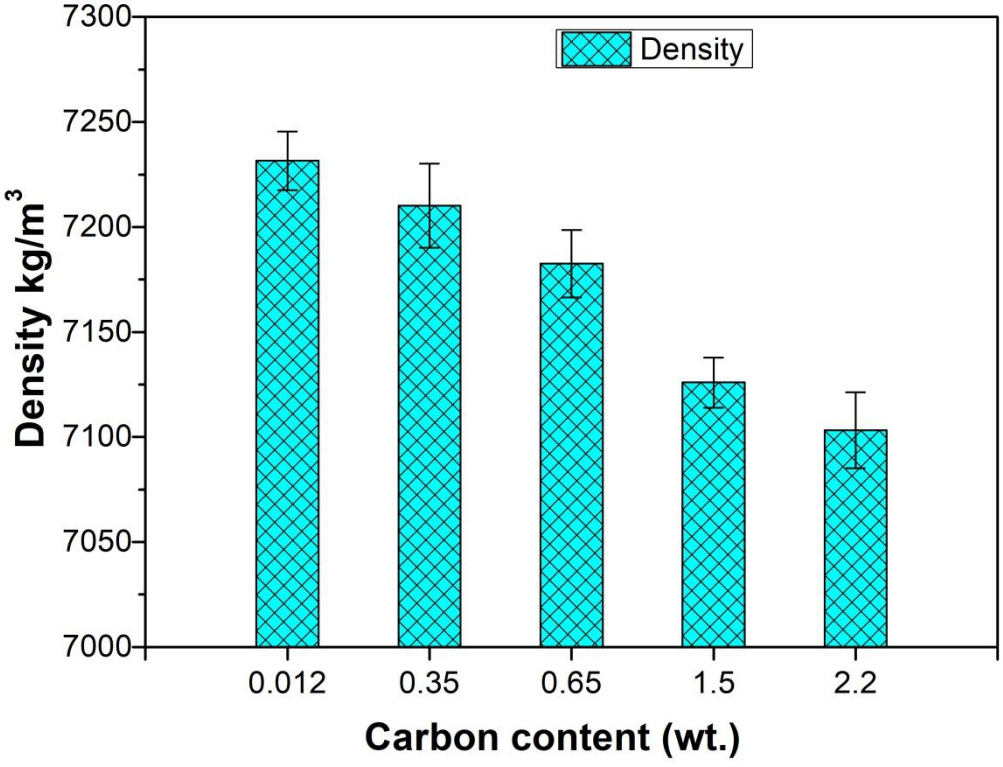

X-ray diffraction revealed the presence of $Fe_3AlC_{0.5}$ (κ-carbide), ferrite (α) and graphite phases in the hot-rolled and annealed steel samples (**Fig. 5.3**). The steel with low carbon of 0.012wt.% (CS1) exhibit single ferrite (α) phases. On the other hand, XRD of steels with carbon content upto 1.5wt.% (CS2, CS3 and CS4) revealed presence of ferrite (α) and $Fe_3AlC_{0.5}$ (κ-carbide) phases within the detection limit of XRD. Additionally, the presence of graphite is seen in steel (CS5) with maximum amount of 2.2wt.% carbon.

5.2 Microstructural analysis

The microstructure of steel sample (CS1) with 0.012wt.% carbon consisted of a single ferrite phase **(Fig. 5.4a).** However, steel sample CS2 with 0.35wt.% carbon revealed presence of significant amount of the second phase in the form of precipitates apart from ferrite **(Fig. 5.4b).** At 0.65wt.% carbon (steel sample CS3), the microstructure exhibits an increased amount of second phase, which exists in the form of bands **(Fig. 5.4c).** When carbon content is further increased to higher levels i.e., 1.5 and 2.2wt.% (Steel CS4 and CS5 respectively), the second phase in the form of very fine precipitates is observed **(Fig. 5.4d and e**). The precipitates being very fine, they could not be resolved by optical microscopy. Additionally, there is a third phase with dark contrast distributed in the matrix of **(Fig. 5.4e)** steel CS5.

Scanning electron micrographs of steels with more than 0.35wt.% C are shown in **Fig. 5.5(a-h)**. Further, as illustrated by secondary electron images **(Fig. 5.5)**, the second phase, which is in the form of small globules in the CS2 steel, while in the form of bands in the steel, CS3 is essentially the κ-pearlite (κ-carbide + ferrite) phase composed of ferrite Fe-Al(α) and κ-carbides ($Fe_3AlC_{0.5}$) as identified by XRD analysis **(Fig. 5.3)**. **Fig 5.5 b, d, f and h** are the micrographs of the steel showing the precipitates respectively at higher magnification. The volume fraction of precipitates present in steel was determined based on the SEM micrographs using Biovis Materials Plus Software (**Table 5.3.).** Volume fraction of the κ-carbide precipitates increases from 12.84 to 57.10% with the increase in carbon in the steel from 0.35 to 2.2wt.%.

.

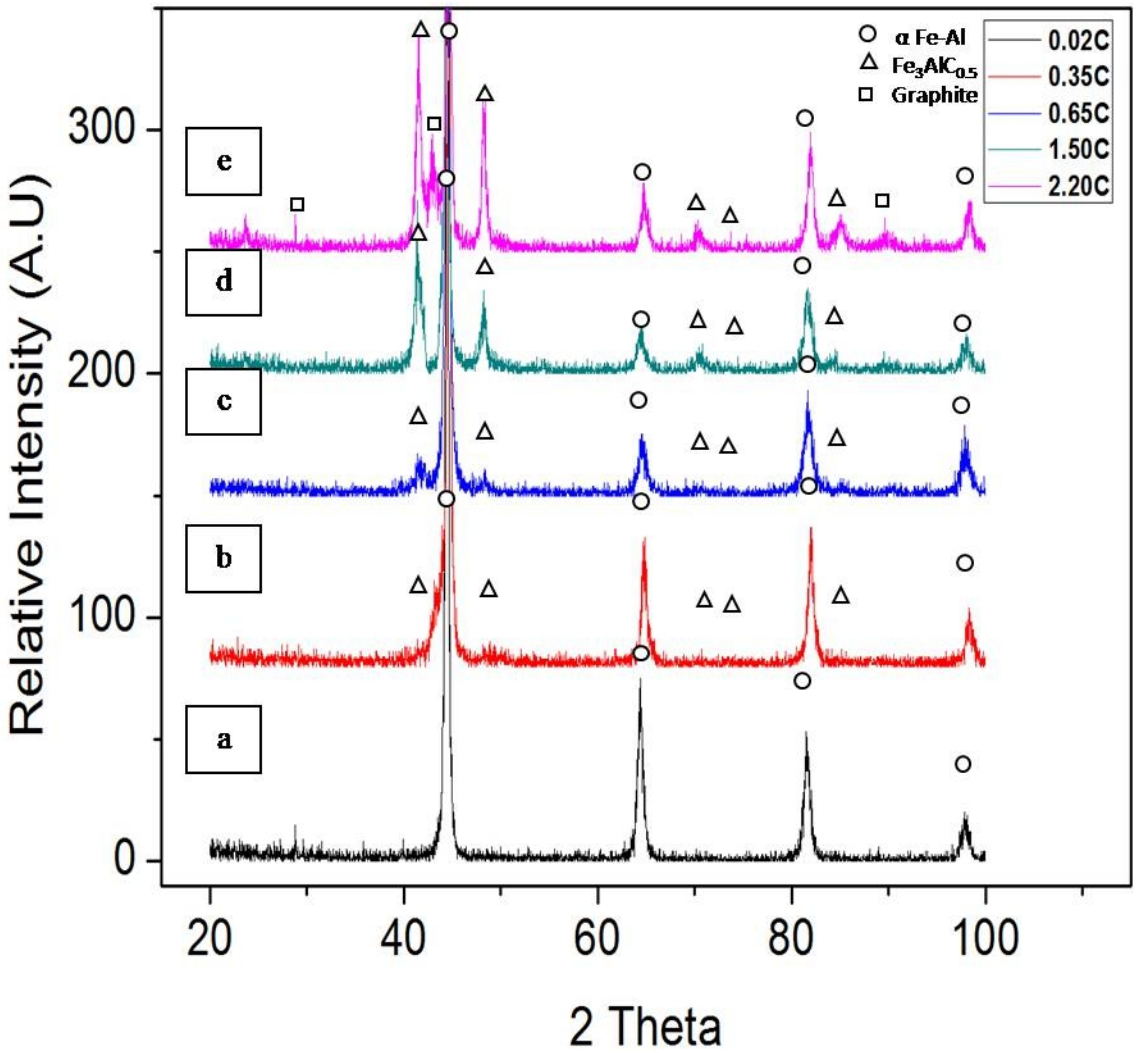

Fig 5.3. XRD traces using Cu-kα radiation showing α(Fe-Al) peaks of hot-rolled and annealed Fe-7wt.%Al based lightweight steel with (a) 0.012, (b) 0.35, (c) 0.65, (d) 1.5 and (e) 2.2wt.% carbon

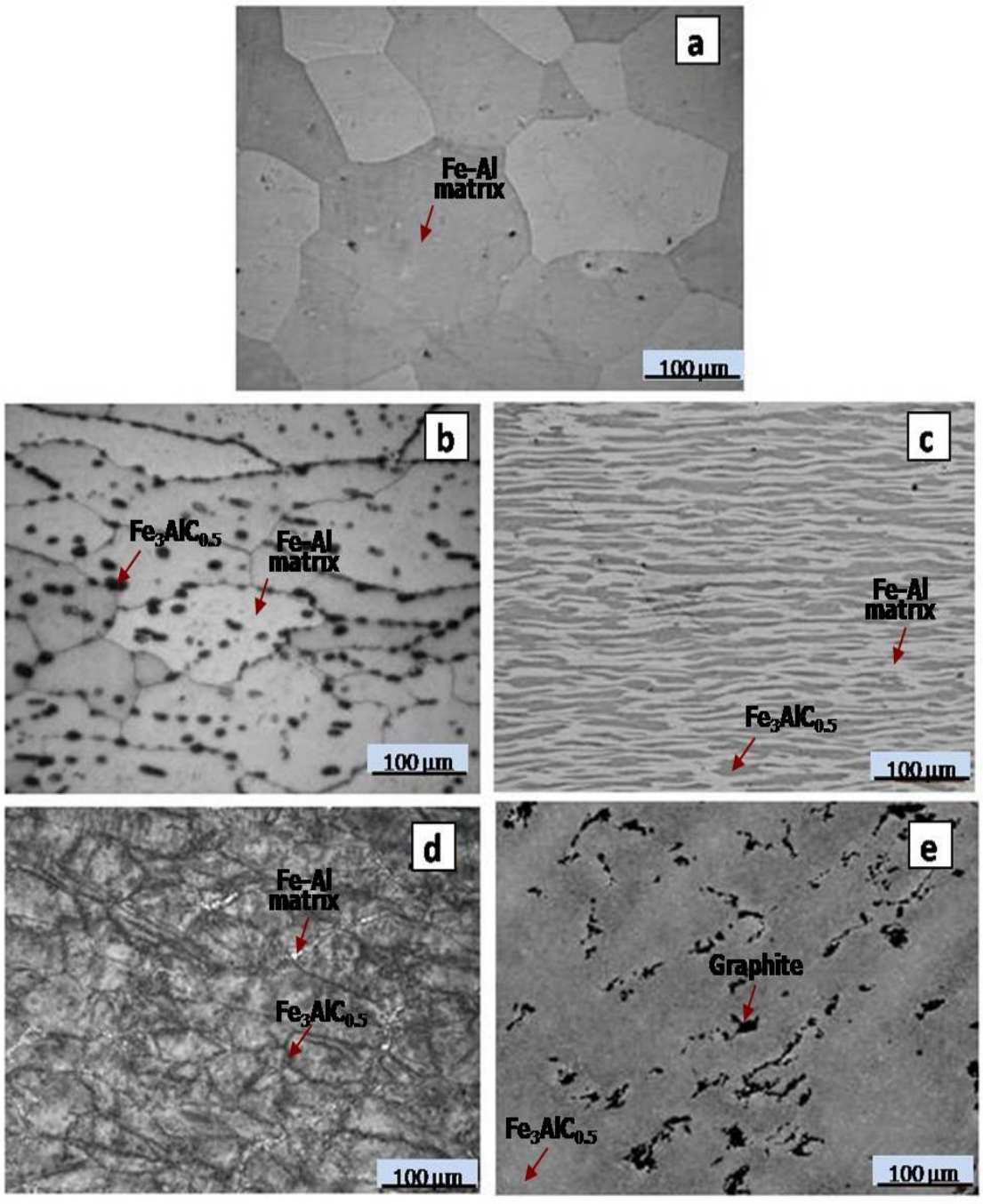

Fig 5.4. Optical micrographs showing the microstructure of Fe-7wt.%Al based steel with (a) 0.012, (b) 0.35, (c) 0.65, (d) 1.5 and (e) 2.2wt.% carbon.

Table. 5.3: Volume fraction of $Fe_3AlC_{0.5}$, graphite and Al in Fe-7wt.%Al based steel, which were calculated and measured.

Steel sample	Steel composition (wt.%)	Al present in the matrix (wt.%) Calculated	Volume fraction of precipitate ($Fe_3AlC_{0.5}$) Calculated	Volume fraction of graphite Calculated	Volume fraction of precipitate ($Fe_3AlC_{0.5}$) Measured	Volume fraction of graphite Measured
CS1	0.012C	7.0	--	--	--	--
CS2	0.35C	5.4	12.46	--	12.84±2	--
CS3	0.65C	4.1	23.13	--	26.04±3	--
CS4	1.5C	0.3	53.40	--	54.64±2	--
CS5	2.2C	Nil	56.97	6.0	57.10±3	6.12±2

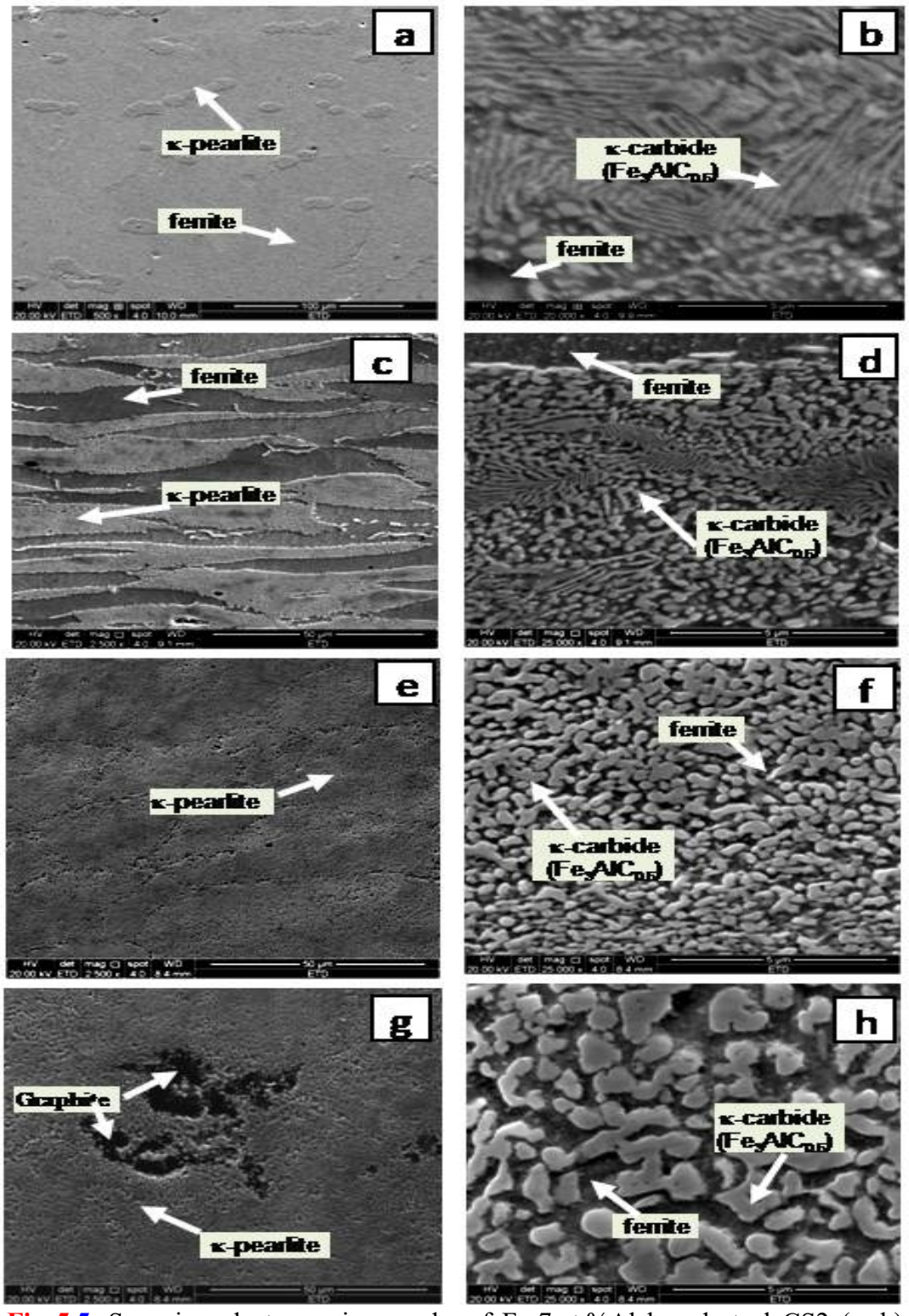

Fig 5.5. Scanning electron micrographs of Fe-7wt.%Al based steel CS2 (a, b), steel CS3 (c, d), steel CS4 (e, f) and steel CS5 (g, h). Micrographs b, d, f and h show precipitates in the steel respectively at higher magnification.

SEM micrographs at higher magnification reveal the distribution of dense, fine spherical and lamellar κ-carbide ($Fe_3AlC_{0.5}$) precipitates inside the globular κ-pearlite of the steel CS2 and inside the κ-pearlite bands of the steel CS3. Further, it can also be noted that with an increase in carbon content from 0.35 to 0.65wt.%, the volume fraction of κ-pearlite increased from 12.84 to 26.04%, while inter-lamellar spacing decreased from 75.20 to 8.30 μm.

On the other hand, the steels CS4 **(Fig. 5.5e and f)** and CS5 **(Fig. 5.5g and h)** exhibited complete κ-pearlite structure consisting of globular κ-carbides in a ferrite matrix. It is to be pointed out that the microstructural features observed in steel CS4 i.e., the complete pearlitic structure is similar to another steel containing 7.16% Al, 1.72% C and 9.98% Mn **(Ishii et al. 2003)**. Further, it is to be noted that the microstructure of steel CS5 also exhibits dark coloured coarse precipitates as illustrated in **(Fig. 5.5g)**. The wavelength dispersive spectroscopy image of Steel CS5 obtained by EPMA analysis is displayed in **Fig. 5.6**. The elemental mapping of Fe, Al and C in the alloy is revealed. The distribution of these elements in the matrix and the precipitates is given by the EPMA line scan analysis of the alloy which is presented in **Fig. 5.7.** WDS image **(Fig. 5.6)** and EPMA line scan **(Fig. 5.7)** of the dark coloured precipitate observed in Steel CS5 steel clearly indicate that they are rich in carbon and resembles one of the basic shapes of graphite. The amount of aluminium available in steel CS5 is sufficient to form only about 57 volume % of $Fe_3AlC_{0.5}$ precipitates for which, the amount of carbon required is about 1.6wt.%. Therefore, the balance 0.6wt.% carbon present as graphite. Similar observations have also been reported earlier in ferritic Fe-Al steel (**Jimenez and Frommeryer 2011)**.

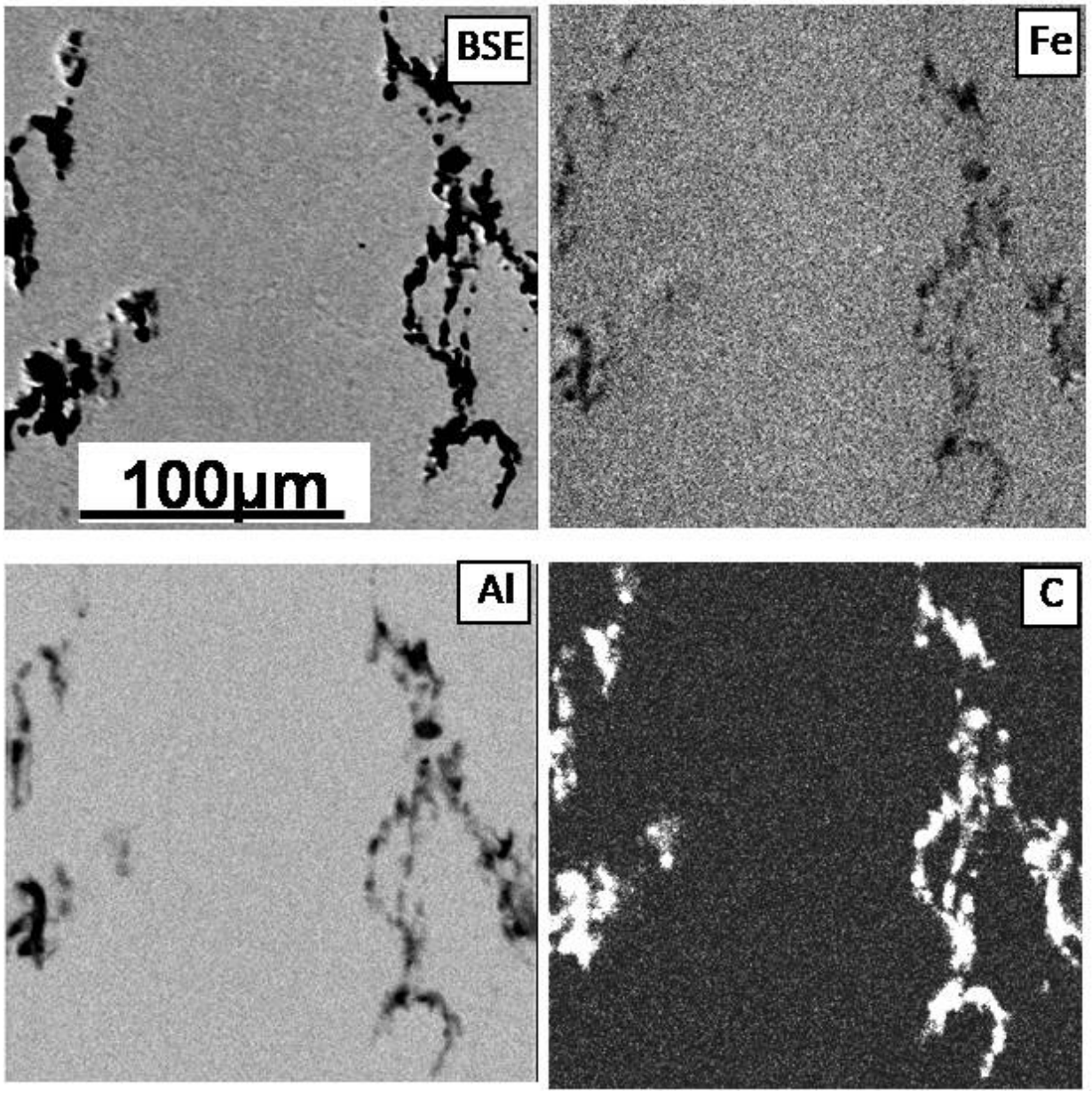

Fig 5.6. Wavelength dispersive spectroscopy (WDS) images observed in EPMA showing the distribution of elements of Fe-7wt.%Al-2.2wt.%C steel.

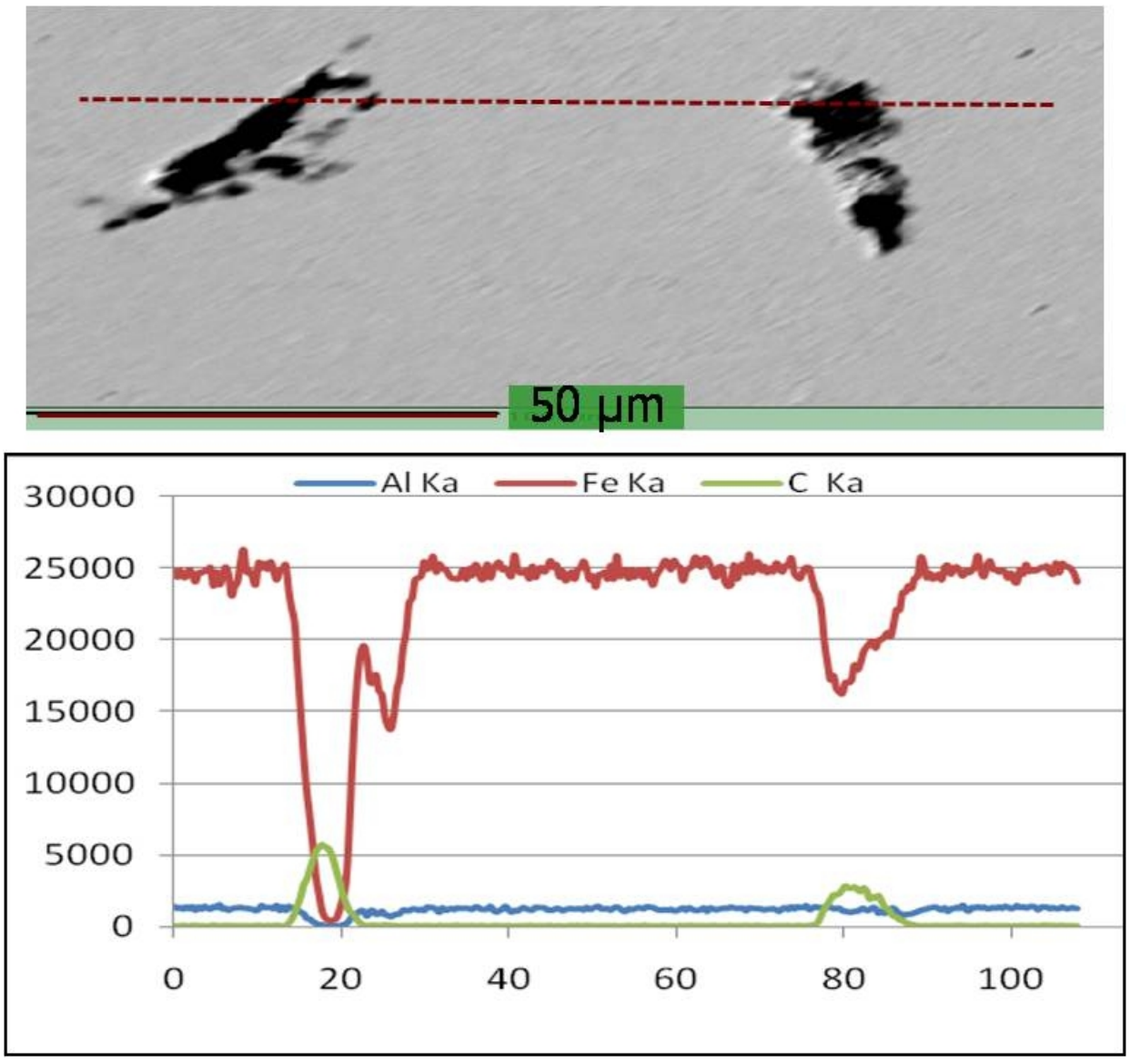

Fig. 5.7. BSE image and line scan of EPMA observed in Fe-7wt.%Al-2.2wt.%C steel

5.3 Mechanical properties

5.3.1 Hardness

The hardness of the matrix, precipitate and the bulk of the steels with different carbon content are summarized in **Table 5.4.** The bulk hardness values were calculated from the micro hardness measurements using the rule of mixtures for the phases present. The micro-hardness of κ-carbide precipitates (585-595HV) obtained here complies with the values reported in the literature **(Baligidad and Satya Prasad 2007, Prakash 2008)**. Also, the calculated volume fraction of precipitates complies with the measured values for all steels. It would thus appear that most of the carbon is present as $Fe_3AlC_{0.5}$ in CS2, CS3 and CS4 steels and $Fe_3AlC_{0.5}$ and graphite in steel CS5 as there is very minimal solubility of carbon in Fe-Al matrix **(Baligidad and Satya Prasad 2007, Palm and Inden 1995, Raghavan 1987).** It is clear that, as Al content in the matrix decreases, the volume fraction of $Fe_3AlC_{0.5}$ phase increases **(Table 5.3)**. Since there is a depletion of Al from the matrix due to the formation of κ-carbide precipitates, the hardness of the matrix decreases **(Table 5.4).** The bulk hardness of the steel increased from 193 to 412 HV whereas the hardness of the matrix decreased from 193 to 140 HV as the carbon content is increased from 0.012 to 2.2wt.%. The bulk hardness increases with an increase in carbon up to 1.5wt.% which is attributed to the increased formation of hard κ-carbide precipitates (from negligible to 54.64%) but with further increase in carbon to 2.2wt.% the increase in the hardness is not significant as it results in only minimal (3.5%) increase in volume fraction of hard $Fe_3AlC_{0.5}$ and, also, leads to the precipitation of small amount (6%) of soft graphite (hardness HV =10). The theoretically calculated bulk hardness using rule of mixtures is found to be only slightly lower than the (experimentally) measured bulk Vickers hardness for all steels studied.

Table. 5.4. The hardness of Fe-7wt.%Al lightweight steel with different carbon content.

Steel Sample	Nominal Composition (wt.%)	Hardness (HV)		
		Bulk Measured (30kg)	Matrix Micro 10 gm	Bulk Calculated
CS1	0.012C	193±5	193±5	193
CS2	0.35C	242±7	176±6	227
CS3	0.65C	275±3	170±3	267
CS4	1.5C	402±6	148±4	384
CS5	2.2C	412±8	140±8	396
Micro-hardness of κ-carbide precipitates:(585-595HV; Graphite:10 HV.				

5.3.2 Tensile properties

The room temperature tensile properties of all the steels with different carbon content are summarized in **Table 5.5**. The stress strain plot of Fe-7Al lightweight steel with different cqaqrbon content is presented in **Fig.5.8.** It can be seen that tensile strength of the steel increases from 486 to 1105 MPa, whereas the yield strength enhanced from 398 MPa to 923 MPa as carbon content is increased from 0.012 to 2.2 wt.%. More than double the increase in the strength is obtained in the steel with the variation of carbon in the above range. However, considerable decrease in the ductility is observed with the increase in carbon content **(Table 5.5)**. The ductility decreased from 21% (with 0.012 wt.%C) to almost nil ductility (at 2.2wt.%C). Significant increase in tensile strength and bulk hardness, while decrease in elongation of all these steels is conceivable. Such observations are related to increase in carbon content which leads to increase in volume percent of κ-pearlite/hard κ-carbide from almost negligible to 57%. Thus, for the present steels it appears that the measured bulk hardness values follow the rule of mixture well which is similar to Fe_3Al based alloys containing carbon **(Baligidad and Satya Prasad 2007, Prakash 2008).**

Formatted[khaple H]: Font: Bold

As presented in Chapter 4, the addition of diborides (ZrB_2 and TIB_2) to Fe-7Al lightweight steel lead to the marginal improvement in yield strength from about 400 MPa to 433 MPa whereas with the addition of carbon significant increase in the yield strength (about 400 to 923 MPa) could be obtained. Moreover, the carbon containing Fe-Al lightweight steels will be much cheaper as the raw material used can be steel scrap. On the other hand, the addition of carbon resulted in drastic drop in ductility. However, the diborides addition had exhibited excellent ductility upto 38% which is one of the important attributes of the formability to make various components. Nevertheless, steel with 0.35wt.%C had exhibited reasonable tensile properties (strength 590 MPa) and about 12% ductility which can be used for lightweightening application with an added advantage of about 10% reduction in density when compared to the conventional steels.

Table. 5.5 The room temperature tensile properties of Fe-7wt.%Al lightweight steel with different carbon content.

teel sample	Nominal Composition (wt.%)	Tensile Strength (MPa)		% Elongation
		UTS	YS	
CS1	0.012C	486±23	398±28	21±2
CS2	0.35C	591±25	450±30	12±2
CS3	0.65C	796±28	610±33	06±2
CS4	1.5C	1000±31	891±36	04±1
CS5	2.2C	1105±34	923±38	01±1

5.4 Mechanisms correlating the hardness and strength with microstructural parameters

In order to understand the underlying mechanism to explain the dependence of yield strength on carbon content, Hall-Petch type equation of the form that relates the strength or hardness to inter-barrier spacing is considered.

$$\sigma_y = \sigma_0 + k_y L^{-1/2} \quad \ldots (1)$$

$$HV = HV_0 + k_H L^{-1/2} \ldots (2)$$

where σ_y is the yield strength and H_V is the bulk Vickers hardness, σ_0 and HV_0 are constants related to the strength and hardness of ferrite phase, k_y and k_H are constants which are characteristic to mean inter-barrier spacing (locking parameter) and L is inter-barrier spacing. Since the microstructure of the steel is evolving with carbon content as already discussed (section 5.2), from complete ferrite, through ferrite plus κ-pearlite to complete κ-pearlite and finally to globular κ-carbides in ferrite matrix, different type of barriers to dislocation in different steels are to be considered to verify the validity of the above relationships.

A schematic of various phases in steels with 0.35 to 2.2 wt.% carbon and their respective inter-barrier spacing are given in **Fig. 5.8**. As shown in **Figs. 5.3 and 5.4** as well as schematically illustrated in **Fig. 5.8**, the appropriate barriers in different steels are identified as follows. In case of steels CS2 **(Fig. 5.8a)** and CS3 steels **(Fig. 5.8b),** κ-pearlite being harder phase the inter-pearlite phase spacing as marked in **Fig. 5.8**, is considered as 'L'. On the other hand, in steels CS4 and CS5 steels, the inter-carbide ($Fe_3AlC_{0.5}$) spacing is taken as 'L'. Based on this analysis, both yield strength and bulk hardness data of different steels are plotted as a function of inter-barrier spacing as shown in **Fig. 5.9** and the data are fitted according to equations 1 and 2 for yield strength and hardness, respectively. It is interesting to observe that both yield strength and hardness data correlate with the inter-barrier spacing reasonably well thereby supporting the proposed supposition of barriers in steels with different carbon content as well as strength or hardness dependence on inter-barrier spacing.

The values of σ_0, k_y, HV_0 and k_H of the present alloys obtained from the fitting of the data to the above equations are ~435 MPa, 245 MPa, 234 HV and 110 HV respectively. The yield strength of the Fe-7Al (α) steel i.e., CS1 steel in of the present study was determined to be ~400MPa, which is fairly close to the value of σ_0 i.e., ~435 MPa obtained from the intercept of the plot shown in **Fig. 5.9.**

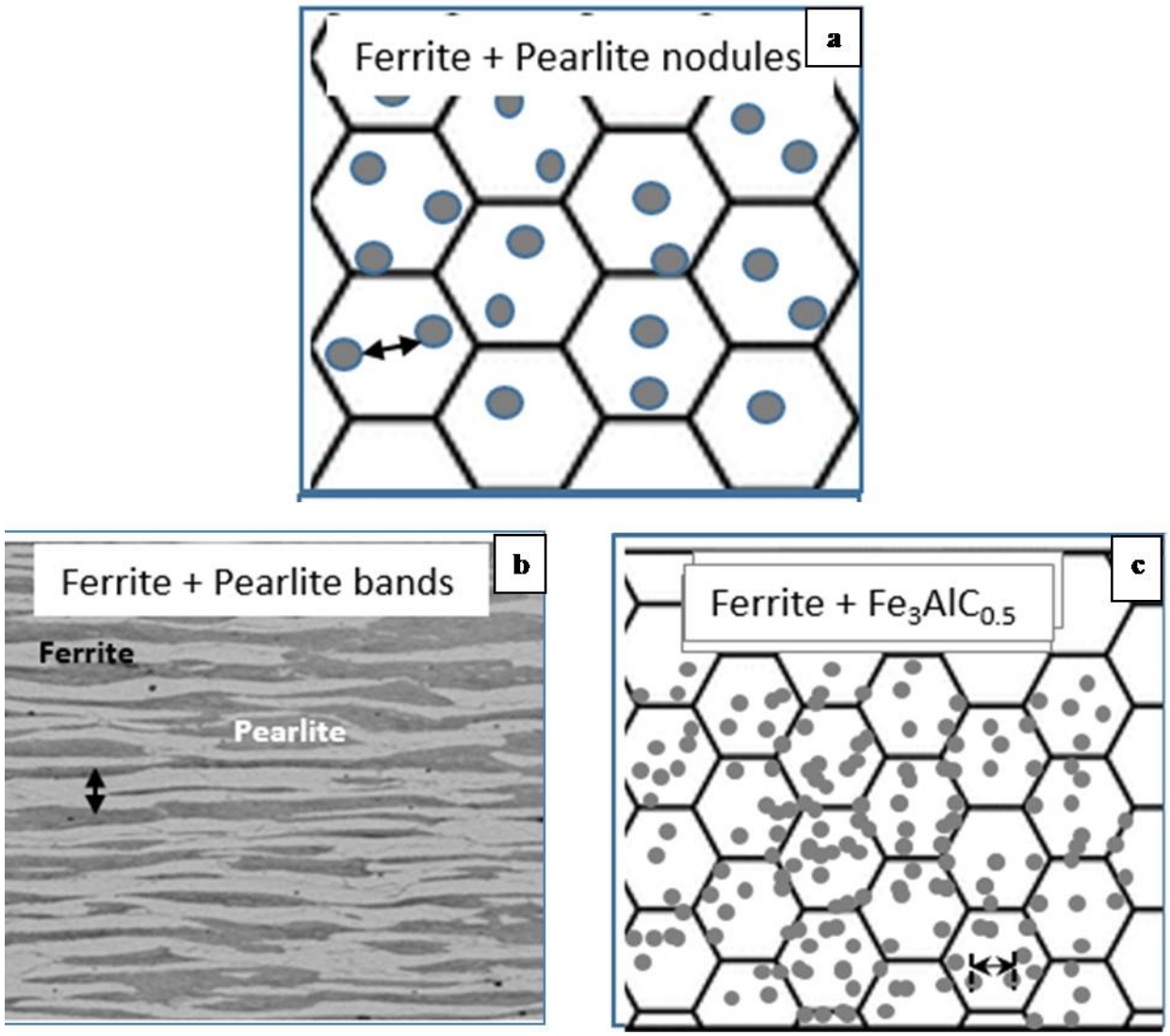

Fig. 5.8. Schematic of various phases present in steels (a) CS2, (b) CS3, (c) CS4 and CS5 and their respective inter-barrier spacing. It is the average spacing of κ-pearlite nodule in the steel CS2, average spacing of κ-pearlite bands in the steel CS3 and the average carbide spacing in the steels CS4 and CS5.

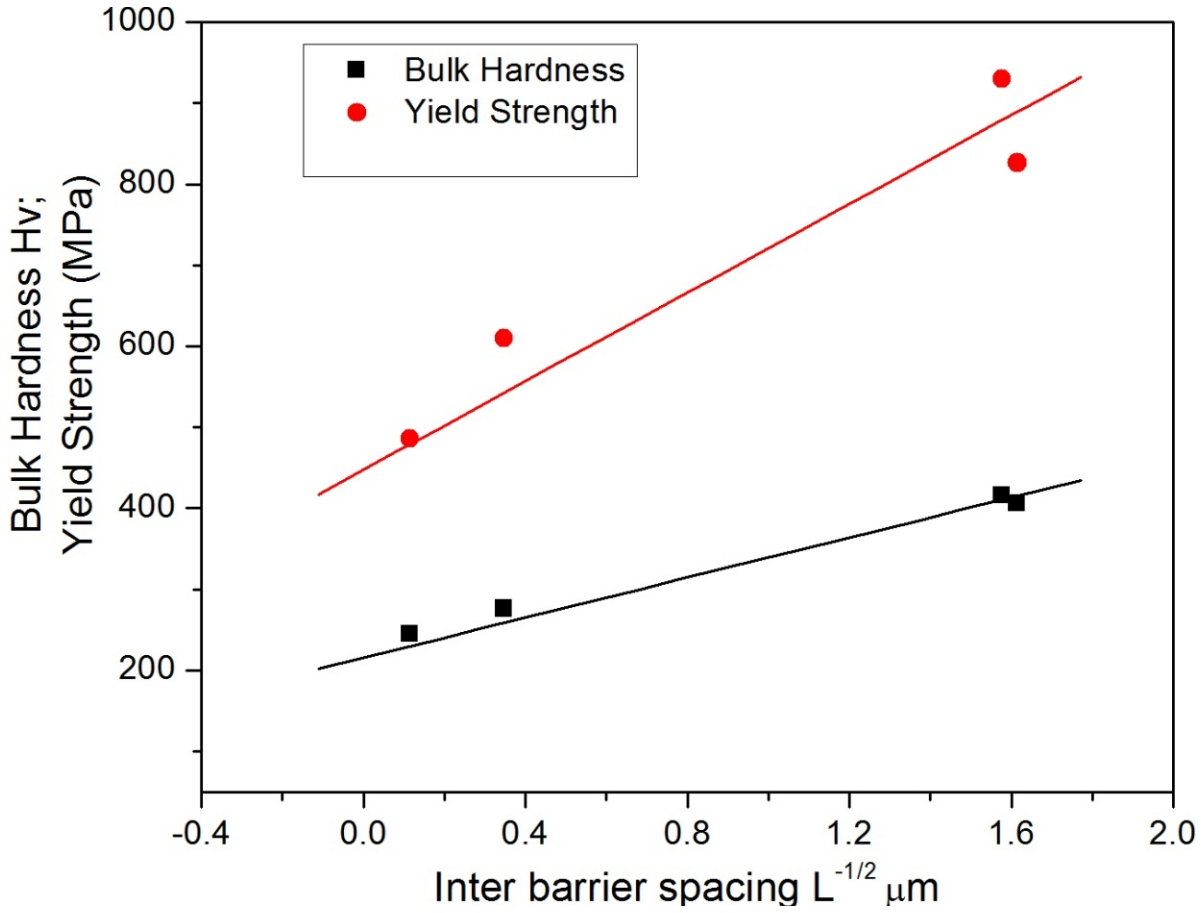

Fig. 5.9. Plot of yield strength and bulk hardness as a function of inverse square root of an average inter-barrier spacing L of different steels.

It may be worth mentioning here that similar observations have also been reported earlier in a Fe-Mn-Al-C alloy with ~1.72 %C **(Ishii et al. 2003).** exhibiting complete κ-pearlite structure with inter-carbide spacing being varied through different heat treatments. The value of σ_0 reported in this steel is ~477 MPa, which is marginally higher than σ_0 i.e., ~435 MPa obtained in the present study. The higher value reported may be attributed to the presence of Mn in the Fe-Mn-Al-C alloy **(Ishii et al. 2003)**.

5.5 Fracture behaviour

Fracture features of tensile samples of all the Fe-7Al based lightweight steels with different carbon content are presented in **Fig. 5.10**. Steels with 0.012 to 0.35wt.% carbon displayed coarse cleavage facets while mixed mode features (fine dimples and smaller cleavage steps) are observed in 0.65 to 2.2wt.% carbon steels.

Fracture is generally by cleavage in ferritic (Fe-Al) steels where grain boundaries act as the main resistance to dislocation motion **(Chen and Cao 2015, Calcagnotto et al. 2009)**. Thus, low carbon Fe-Al steels are expected to fail by cleavage as these steels have coarse grain size and the resistance is caused by a large number of dislocation pile-ups at the grain boundary which leads to coarse cleavage fracture **(Chen and Cao 2015)**. The lower spacing of the inter-pearlite nodule or $Fe_3AlC_{0.5}$ carbide in steel CS3, CS4 and CS5 within the grain has effectively reduced the dislocation pile-up length which resulted in smaller cleavage steps and fine dimples. With increase in carbon content there is a progressive decrease in ductility and is due to increased incidence of void nucleation and premature interlinkage of voids nucleated at carbide-matrix interface. Hence steel with higher carbon 2.2wt.% exhibited very low ductility.

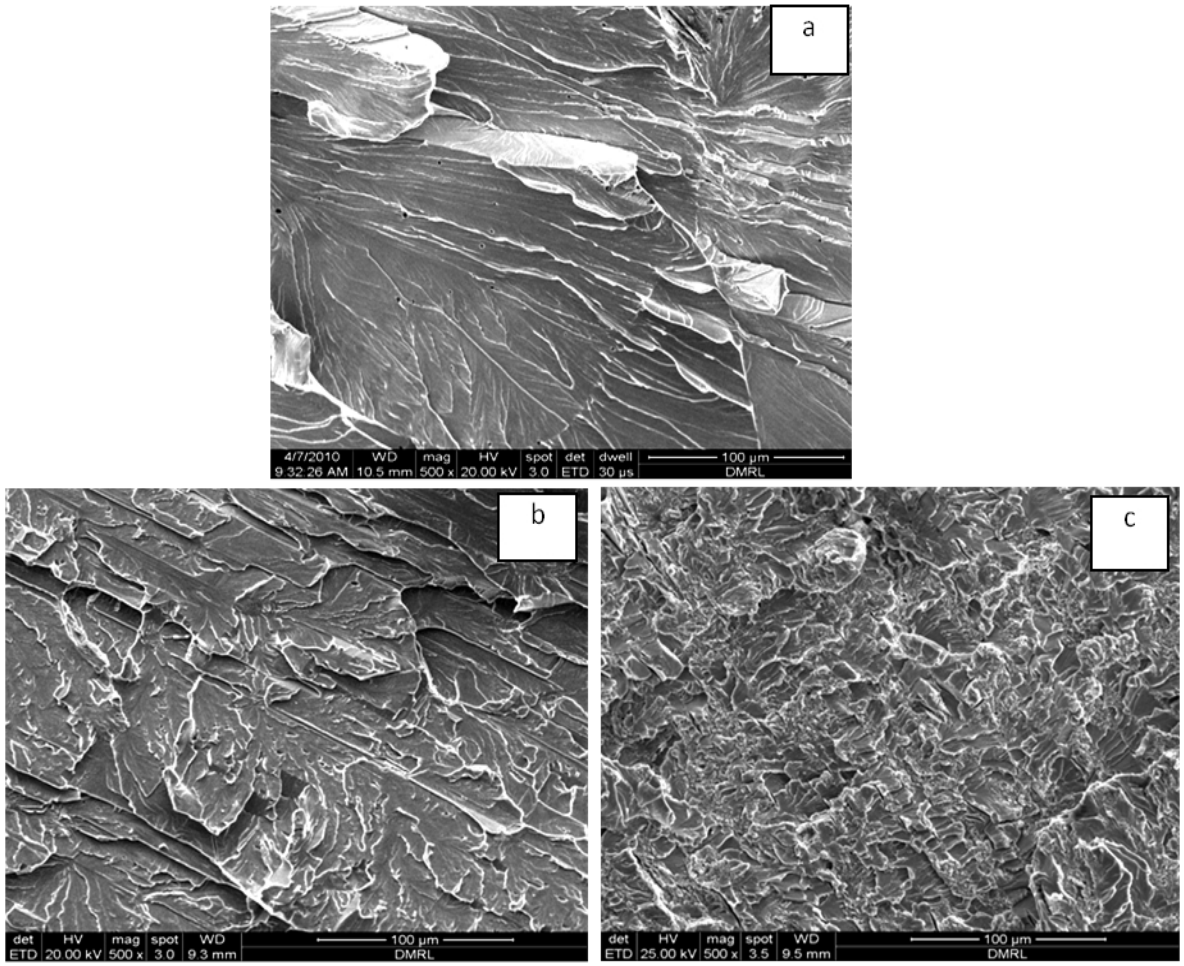

Fig. 5.10. SEM photographs showing the tensile fracture of Fe-7wt.%Al based steel with (a) 0.012, (b) 0.35, (c) 0.65, (d) 1.5 and (e) 2.2wt.% carbon

5.6 Comparison of properties of ferritic lightweight steels containing carbon

Steels based on Fe-Al system are inherently ductile, but steels with Al greater than 7wt.% suffer from environmental embrittlement during melting, processing as well as during testing of the steels **(Rana 2014, Rana et al. 2014, Pramanik and Suwas 2014, Khaple et al. 2010). Fig. 5.11** gives the properties of steels with different Al as well as with small Mn content albeit with similar carbon content. Further, these steels are processed under similar conditions. As presented in **Fig. 5.11** steels a, b and c with 9wt.%Al exhibited poor ductility as these steels are prone to environmental embrittlement. Steels d and e with a small content of Mn content (4-6 wt.%) have shown a good combination of tensile properties as the Mn has the solubility in both the matrix as well as κ-carbide precipitates and enhances the properties by solid solution strengthening. Nevertheless, these steels suffer from processing problem in that they were prone to cracking during hot-rolling **(Sang et al. 2010, Seung et al. 2011, Sohn et al. 2013)**. Steels 'f, g, i, k and l' are the steels of present research. Steel 'g' with 0.35wt.%C has shown a good combination of strength and ductility. The ductility of this steel in hot-rolled and annealed condition is over 12% which is the minimum ductility required for the formability operation of the steels **(Davis 2012).** Steels with higher carbon content (C > 0.5wt.%) have shown better tensile strength but suffer from poor ductility which can be attributed exclusively to the increase in volume fraction of very hard κ-carbide precipitates.

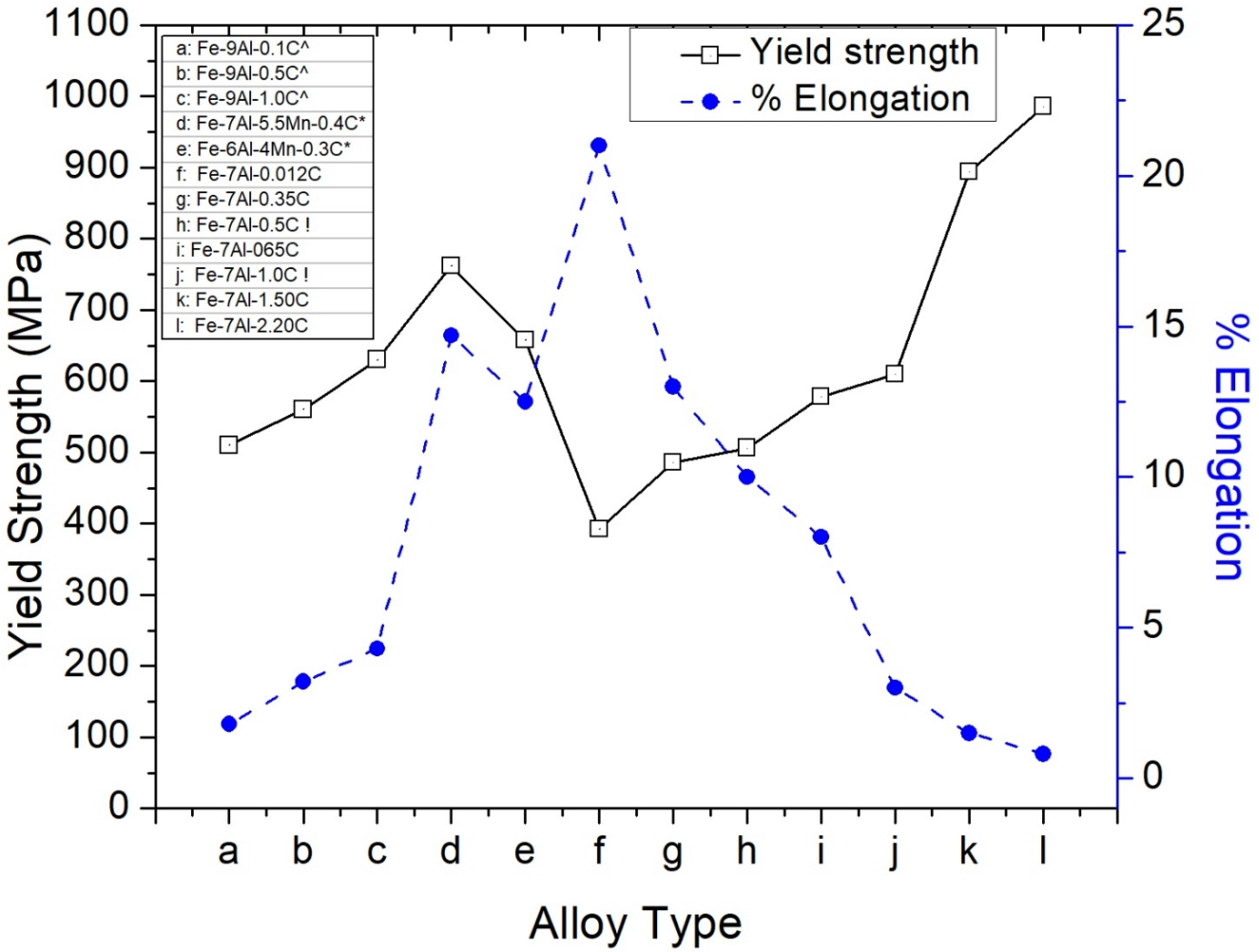

Fig. 5.11. Comparison of yield strength and ductility of lightweight steels from literature (**Baligidad and Satya Prasad 2007**-^, **Sang, et al. 2010**-* and **Khaple et al. 2015** –i)

5.7 Summary

1. Fe-7wt.%Al based steel with all carbon levels (0.012 to 2.2wt.%) could be hot-rolled successfully.
2. Steel with 0.012wt.%C exhibit a single-phase microstructure of Fe-Al(α) whereas steels with 0.35wt.%C and 0.65wt.%C exhibit a two-phase microstructure containing ferrite and κ-pearlite. The steels with 1.5wt.%C and 2.2wt.%C exhibited complete κ-pearlite structure and consisting of the dispersion of globular $Fe_3AlC_{0.5}$ carbides in a matrix. In addition, the microstructure of the steel with 2.2wt.%C revealed a very small volume fraction of graphite phase.
3. Bulk hardness as well as tensile strength increased significantly with an increase in carbon content. The yield strength, as well as hardness of the steels with different carbon content, can be correlated well with the inter-barrier spacing in different steels.
4. Steel with 0.012wt.%C exhibited excellent (21% elongation) ductility. However, the addition of higher amount of carbon has resulted in significant reduction in ductility (21 to 0.8%).
5. Progressively decrease in ductility of steel samples can be attributed to increased incidence of void nucleation and premature interlinking of voids nucleated at carbide-matrix interface.

Chapter 6

EFFECT OF NIOBIUM ON Fe-7Al-0.35C STEEL

Chapter 6 describes the effect of Nb (0.2, 0.4, 0.7 and 1wt.%) on structure-property correlation and fracture behaviour of Fe-7Al-0.35C based lightweight steel.

6.0 Introduction

As discussed in the Chapter 5, addition of 0.35wt.%C to Fe-7Al steel has resulted in more than 12% ductility which is the minimum requirement for the formability operation of the steels. With an aim of improving the tensile properties of the steel further by grain refinement through in-situ formation of NbC precipitates, the effect of Nb (0.2 to 1wt.%) addition on Fe-7Al-0.35C was studied. In order to predict the formation of phases on Nb addition, thermodynamic calculations were performed using ThermoCalc software and compared with the experimental results. Earlier attempts to add Nb to low-density steels resulted in very low ductility (**Schneider et al. 2003, Baligidad 2004, Baligidad 2004, Falat et al. 2005)** which may be related to susceptibility of these alloys due to hydrogen embrittlement. Their main objective was to improve the high temperature properties of higher Al containing Fe-Al alloys (7.8 wt.% **Falat et al. 2005,** 8.5 and 10.5 wt.% **Baligidad 2004, Baligidad 2004)** with higher Nb content to have niobium carbide and Laves phases.

6.1. Effect of Nb (0.2 to 1 wt.%) on chemical composition and phase evolution of Fe-7Al-0.35C steel

Chemical compositions of the steels with different niobium content are given in Table 6.1. The recovery of the alloying elements such as Al and Nb is good since the melting of the

steels are carried out in controlled atmosphere. Radiography studies confirm that the pancakes are free from internal cracks and porosity.

Table 6.1 Chemical composition of Fe-7Al-0.35C based lightweight steel with different niobium contents.

Steel Sample	Steel composition					
	Al (wt. %)	Mn (wt. %)	S (wt. %)	Si (wt. %)	C (wt. %)	Nb (wt. %)
NS1	6.8±0.2	0.04	0.014	0.43	0.33 ±0.02	0.2 ±0.04
NS2	7.0±0.2	0.06	0.015	0.48	0.32±0.01	0.4 ±0.05
NS3	6.6±0.3	0.05	0.019	0.51	0.35±0.01	0.7 ±0.05
NS4	6.8±0.1	0.08	0.016	0.36	0.34±0.02	1.0 ±0.06

The X-ray diffraction of Fe-7Al-0.35C based steel sample with different niobium content revealed the presence of $Fe_3AlC_{0.5}$ (κ-carbide) (**Fig. 6.1)** and ferrite (α) at all the niobium levels. The peaks related to the addition of Nb were missing in XRD pattern of all the steel compositions, as expected, due to their low concentrations and also since the particles may have been of non-stoichiometric compositions or they may be not within the detection limit of XRD.

6.1.1 Phase Prediction by ThermoCalc

The predicted equilibrium phase diagram of Fe-7Al-0.35C with varying Nb contents using ThermoCalc software is displayed in **Fig. 6.2.** The various phases and their amounts present in these steels containing 0 to 1 wt.% Nb at different temperatures as calculated by using thermodynamic database are given in **Figs. 6.3a-e.** The solidification of the steels with niobium content starts at 1484^0C. The NbC precipitation starts form the liquid, while the κ-carbide ($Fe_3AlC_{0.5}$) forms at 812^0C. Based on the Nb content, the NbC formation temperature changes and for the content 0.2 to 1wt.% of Nb, the NbC formation temperature is in the range of 1430°C to 1462°C. The austenite phase is observed between 1410^0C and 810^0C. At room temperature ferrite (α), κ-carbide and NbC precipitates are the stable phases. Since the solubility of NbC is high in austenite (**Gladman 1997, Speer et al. 2016, Ray 2004)**, further NbC precipitation occurs during the transformation from austenite to ferrite. From **Fig. 6.2**, it can be seen that the eutectic occurs at 0.083 wt.% of Nb at 1405^0C for Fe-7Al-0.35C steel. In the steels with 0.083wt.%Nb and above NbC precipitate formation starts from liquid **(Fig. 6.3 a-e).** At lower levels of Nb (<0.083 wt.%), the NbC precipitate formation starts from austenite. At 1wt.% Nb, the niobium carbide formed is very coarse and is in the order of 5-6 μm. Similar observations have been reported for steels containing high carbon and high niobium **(Speer et al. 2016, Ray 2004, Hecht et al. 2018).**

6.2 Microstructural characterisation

Lightweight steels based on Fe-7Al-0.35C with niobium content from 0.2 to 1wt.% exhibited a dendritic microstructure with significant amount of precipitates in the cast

condition which is shown in **Fig. 6.4.** Back scattered electron micrographs of as-cast Fe-7Al-0.35C steel with different niobium content are displayed in **Fig. 6.5.**

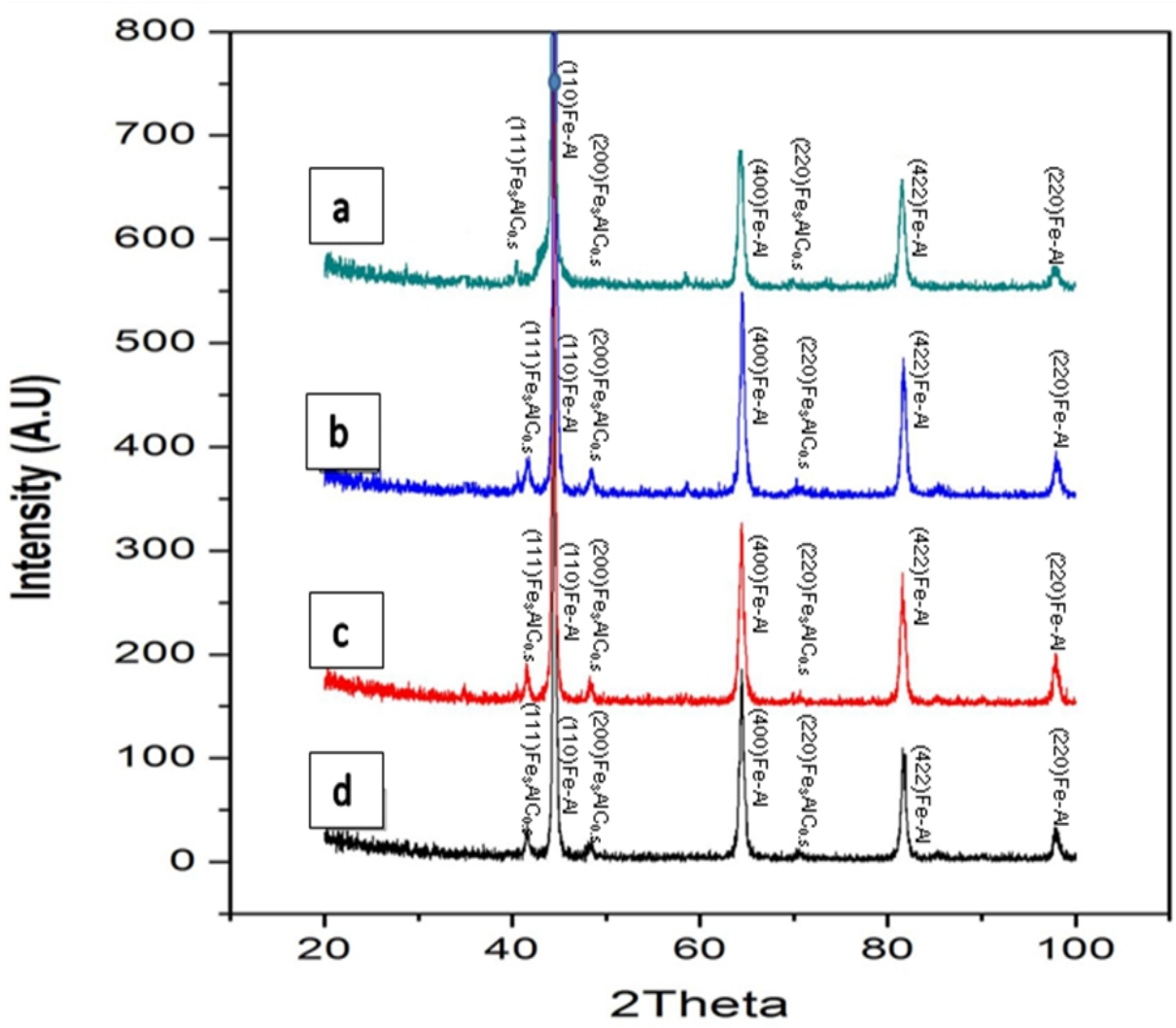

Fig. 6.1. XRD patterns using Cu-kα radiation showing Fe-Al and $Fe_3AlC_{0.5}$ peaks in Fe-7Al-0.35C steel with (a) 0.2, (b) 0.4, (c) 0.7 and (d) 1.0wt.% niobium.

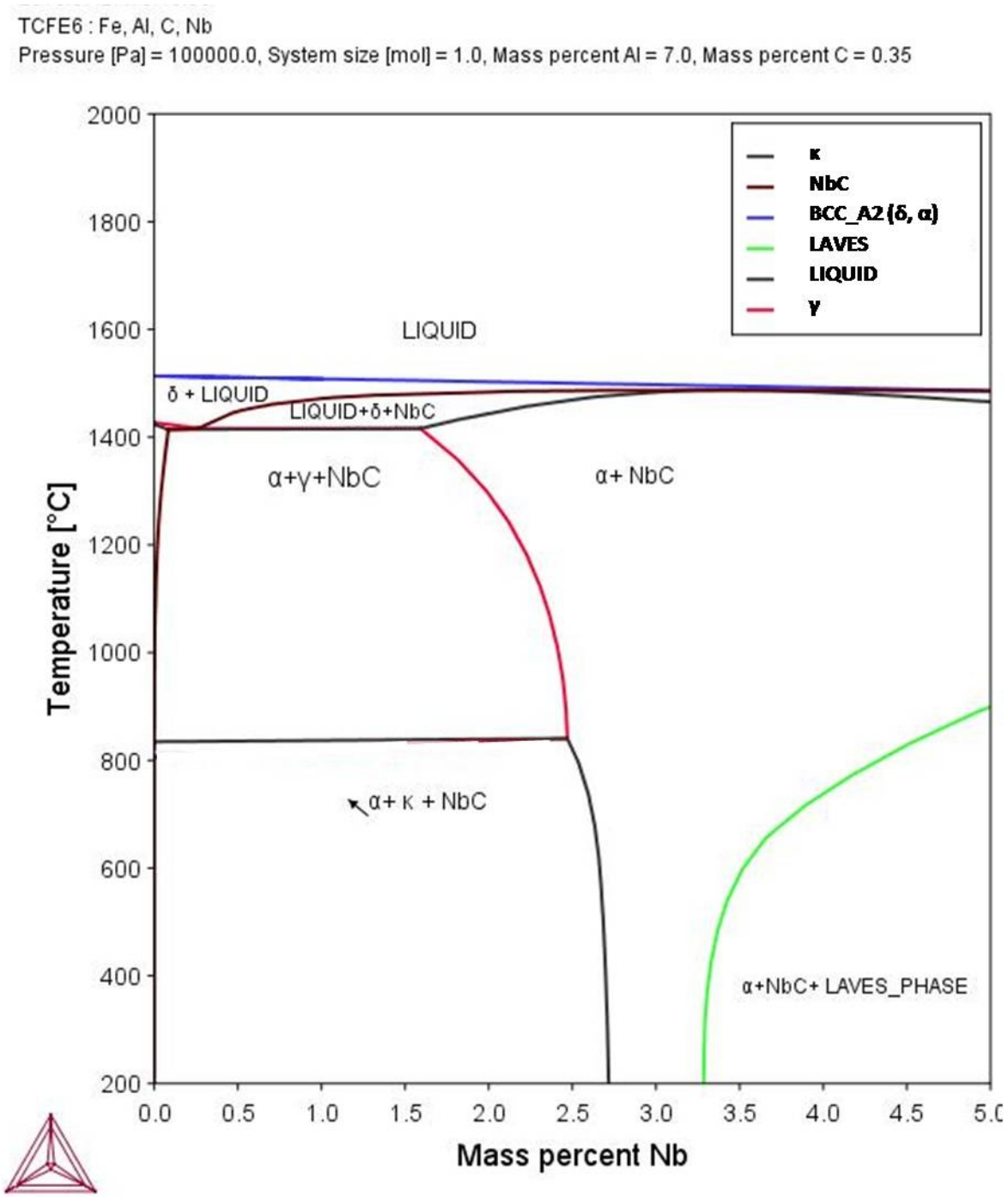

Fig. 6.2. Equilibrium phase diagram of Fe-Al-C-Nb with fixed contents of (7%) Al, (0.35%) C and varying Nb content as predicted by using ThermoCalc.

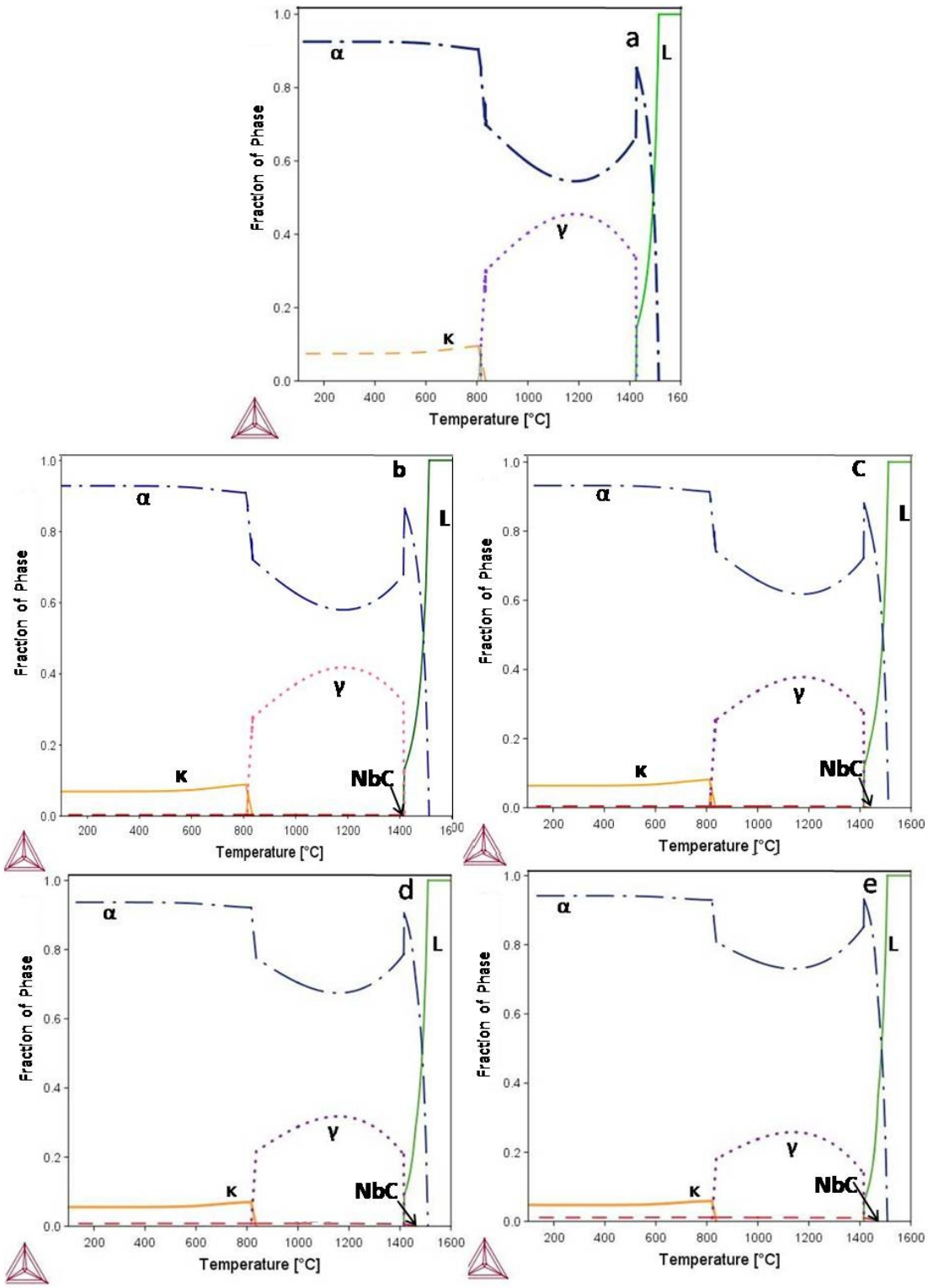

Fig. 6.3. Amount of various phases in Fe-7Al-0.35C steel as a function of temperature as predicted by ThermoCalc with (a) 0, (b) 0.2, (c) 0.4, (d) 0.7 and (e) 1.0 wt.%

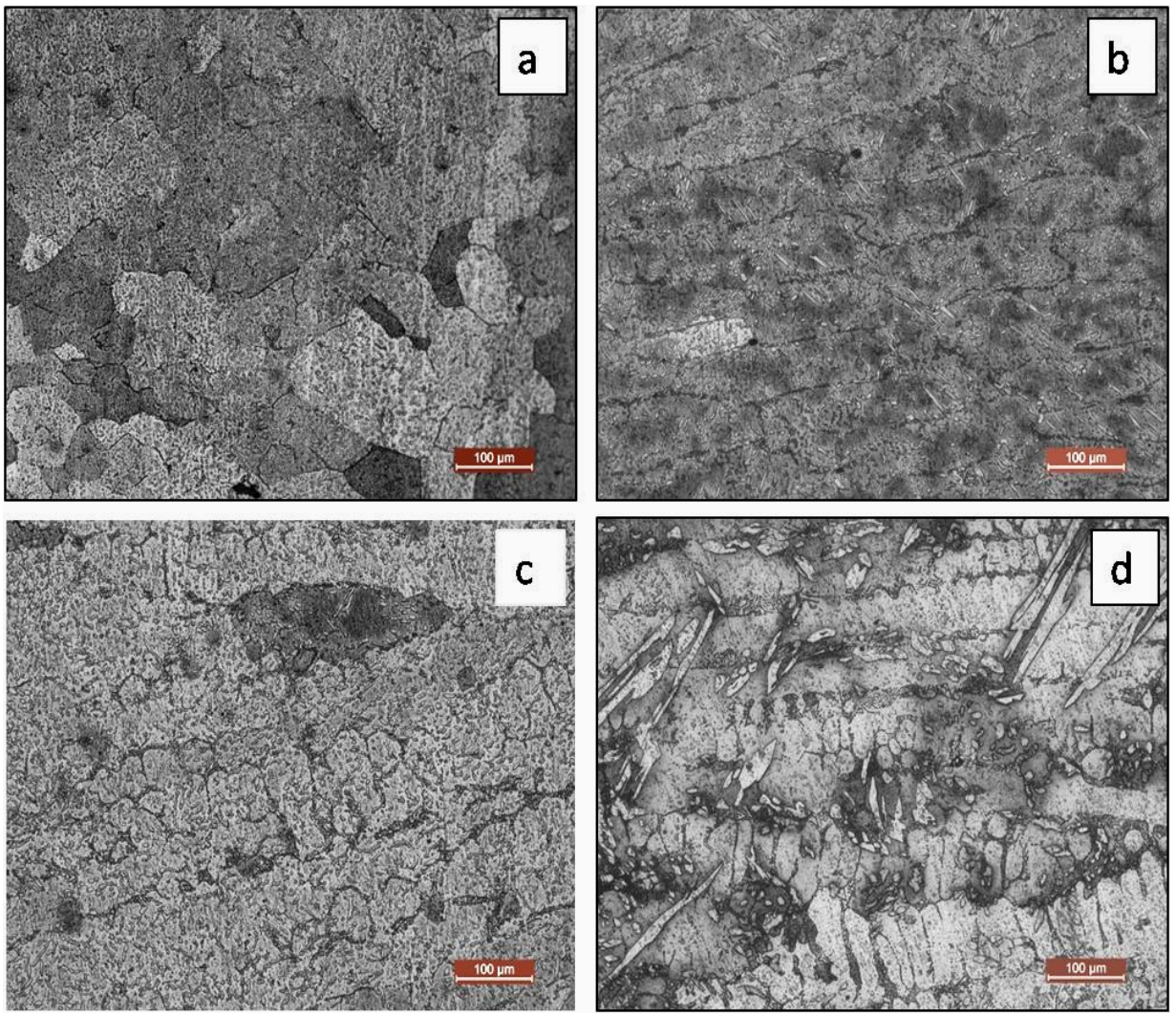

Fig. 6.4. Optical micrographs showing the as-cast microstructure of Fe-7Al-0.35C steel with (a) 0.2, (b) 0.4, (c) 0.7 and (d) 1.0 wt.% niobium.

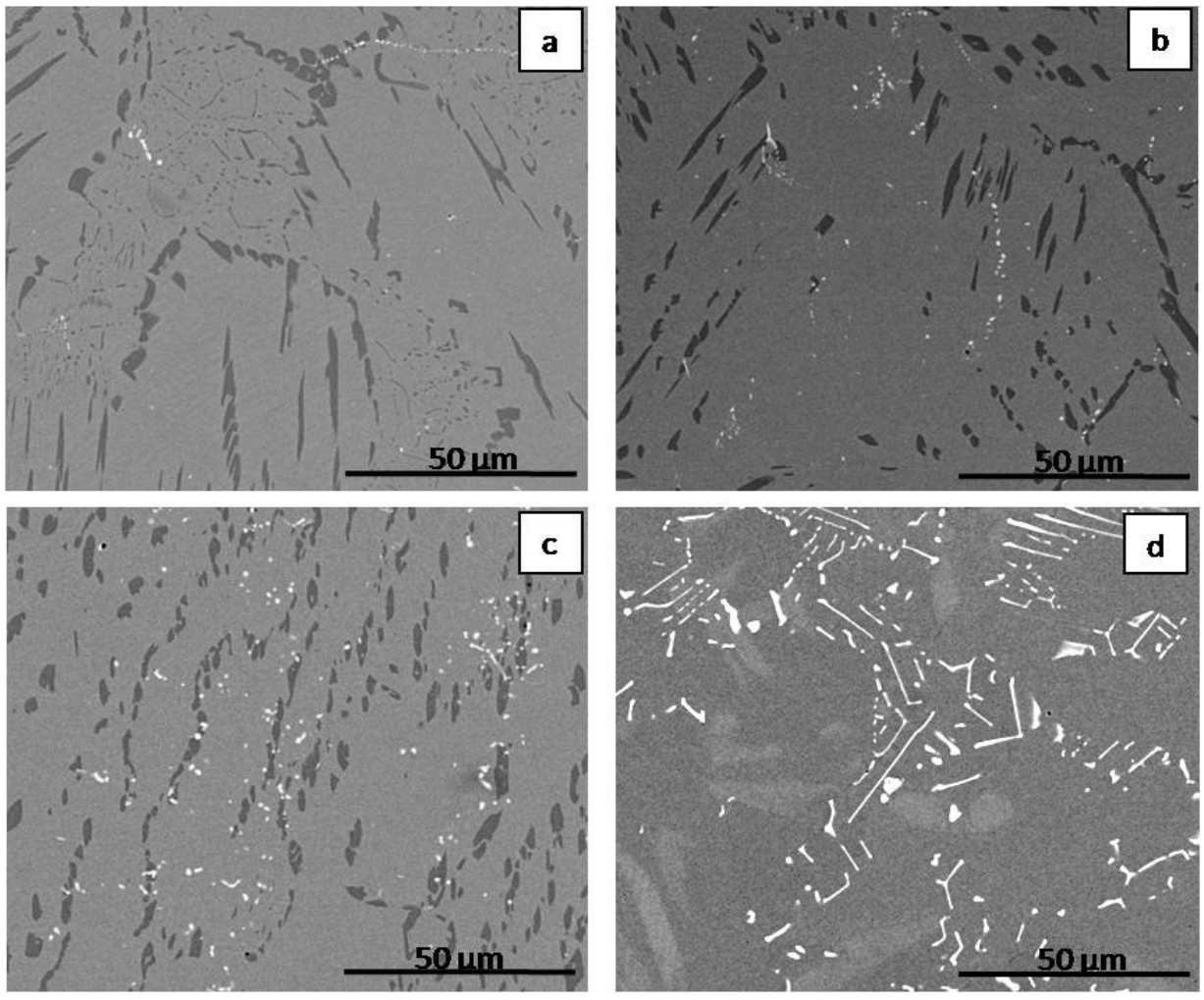

Fig. 6.5. Back-scattered electron micrographs showing the distribution of precipitates (bright are rich in Nb and C, and grey are $Fe_3AlC_{0.5}$ precipitates) microstructure of as-cast Fe-7Al-0.35C steel with (a) 0.2, (b) 0.4, (c) 0.7 and (d) 1.0 wt.% niobium.

Two types of precipitates (grey and bright) are observed (**Fig. 6.5).** As the niobium content increases, the volume fraction of the bright precipitates increases. SEM analysis has shown that the bright phase is rich in Nb and C. The grey phase is identified as $Fe_3AlC_{0.5}$, which is also confirmed from the XRD analysis. In alloys containing upto 0.7 wt.% Nb, the BSE, SEM micrographs reveal globular bright precipitates. In the 1 wt.% Nb alloy, thin needle-shaped bright precipitates are observed.

All the Fe-7Al-0.35C steel pancakes containing Nb content from 0.2 to 1 wt.% could be successfully hot-rolled from 10 mm to 2 mm thickness. The steel pancakes in the present work could easily be hot-rolled without any cracking. In contrast, Fe-Mn-Al-C alloys with similar Al and C contents have been reported with cracking on hot rolling **(Shin et al. 2010, Shon et al. 2013, Han et al. 2011).** The obtainment of crack free steels may be due to intermediate heating of samples after every three passes during rolling that is practised in the present work. This practise also ensures a more homogeneous microstructure and avoids the significant banding reported in earlier works **(Shin et al. 2010, Han et al. 2011).**

A microstructure consisting of niobium carbide and Laves phases in the ferrite matrix has been reported for Fe-(7.8 to 8.5 Al) alloys containing different carbon and niobium **(Schneider et al. 2003, Baligidad 2004).** The presence of Laves phases is highly detrimental as it can lead to loss in ductility. In the present study, Laves phases were not observed. This may be ascribed to the much higher C/Nb ratio maintained in the present study (1.75 to 0.35) as compared to a much lesser value (0.06) reported in the literature **(Schneider et al. 2003, Baligidad 2004).**

Fig. 6.6 shows the optical microstructures of the hot-rolled steel samples with different Nb contents. All samples exhibit recrystallized grains. The average grain size of all the steels with different Nb content is summarised in **Table 6.2.** As the Nb content increased from 0.2 to 1 wt.%, the average grain size decreased from about 320 µm to about 80 µm **(Table 6.2).** The recrystallized grains could also be observed in the BSE SEM micrographs of the hot-rolled steels **(Fig. 6.7).** In the alloy with 1%Nb, the morphology of Nb-carbides changes from needle to globular after hot-rolling. The EPMA analysis of the matrix and precipitates is summarized in **Table 6.3**. No Nb could be detected in the matrix and grey precipitates. The EPMA line scanning of the matrix, grey and the bright

precipitates is as shown in **Fig. 6.8.** The bright precipitates are found to be enriched in Nb and C **(Fig. 6.8).** Based on ThermoCalc results, these can be realised as NbC precipitates. The volume fraction of both the grey and the niobium carbide precipitates are given in **Table 6.4.** The results **(Table 6.4)** show that the volume fraction of NbC is very small (<4 %) in all the alloys. Thus its presence could not be detected in XRD due to its detection limit.

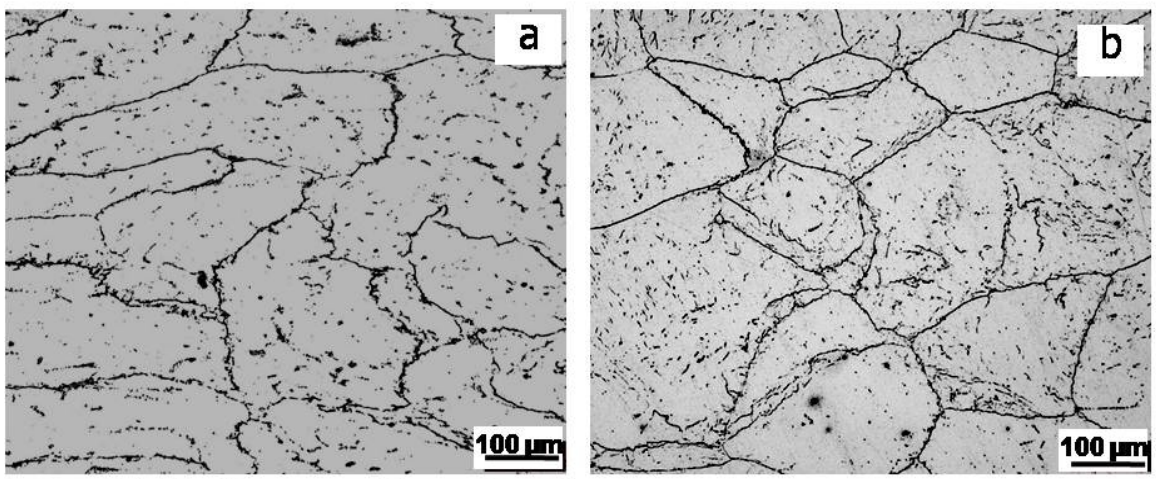

Fig. 6.6. Optical micrographs showing the microstructure of hot-rolled Fe-7Al-0.35C steel with (a) 0.2, (b) 0.4, (c) 0.7 and (d) 1.0 wt.% niobium.

Table 6.2 The variation in average grain size of Fe-7Al-0.35C based lightweight steels with different niobium content in the hot-rolled and annealed condition

Steel Sample	Nominal composition (wt.%)	Average Grain Size (μm)
NS1	Fe-7Al-0.35C-0.2Nb	320±16
NS2	Fe-7Al-0.35C-0.4Nb	280±14
NS3	Fe-7Al-0.35C-0.7Nb	140±8
NS4	Fe-7Al-0.35C-1.0Nb	80±4

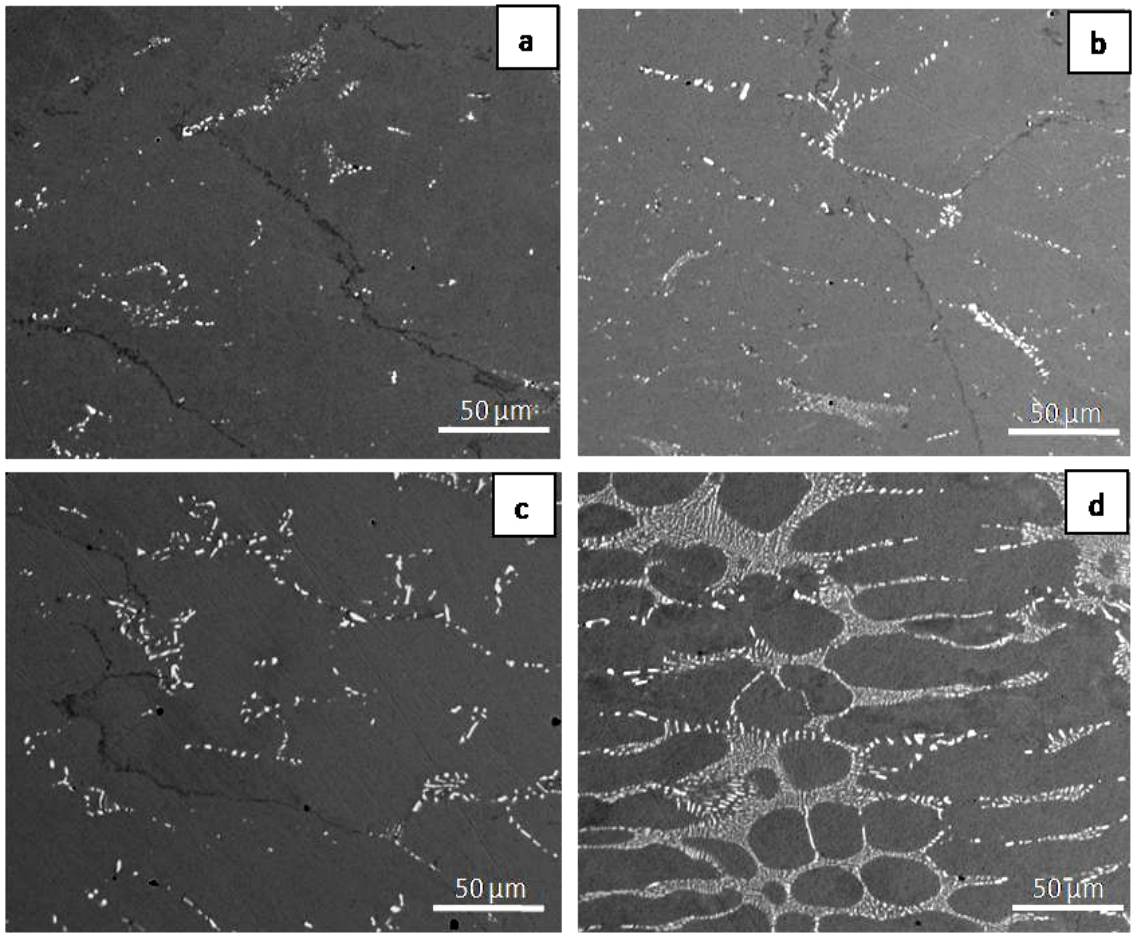

Fig. 6.7. BSE micrographs of hot-rolled Fe-7Al-0.35C steel showing the distribution of precipitates (bright are rich in Nb and C, and grey are $Fe_3AlC_{0.5}$ precipitates) with (a) 0.2 and (b) 0.4, (c) 0.7 and (d) 1.0 wt.% niobium.

Table 6.3 Electron Probe Micro Analysis (EPMA) of phases present in lightweight steel with different niobium content

Steel	Nominal composition (wt.%)	Elements	Matrix wt.%	Precipitate 1 (grey) wt.% ($Fe_3AlC_{0.5}$)	Precipitate 2 (white) wt.% (Niobium carbide)
NS1	Fe-7Al-0.35C-0.2Nb	Fe Al C Nb	93.10 6.90 --- ---	82.10 14.30 3.60 ---	3.98 ---- 10.84 85.06
NS2	Fe-7Al-0.35C-0.4Nb	Fe Al C Nb	92.80 7.20 --- ---	82.10 14.52 3.48 ----	3.12 ---- 10.98 85.90
NS3	Fe-7Al-0.35C-0.7Nb	Fe Al C Nb	93.38 6.62 --- ---	82.04 14.70 03.26 ----	2.82 ----- 11.06 86.12
NS4	Fe-7Al-0.35C-1.0Nb	Fe Al C Nb	93.17 6.83 --- ---	82.00 14.80 03.20 ----	2.21 ---- 11.43 87.16

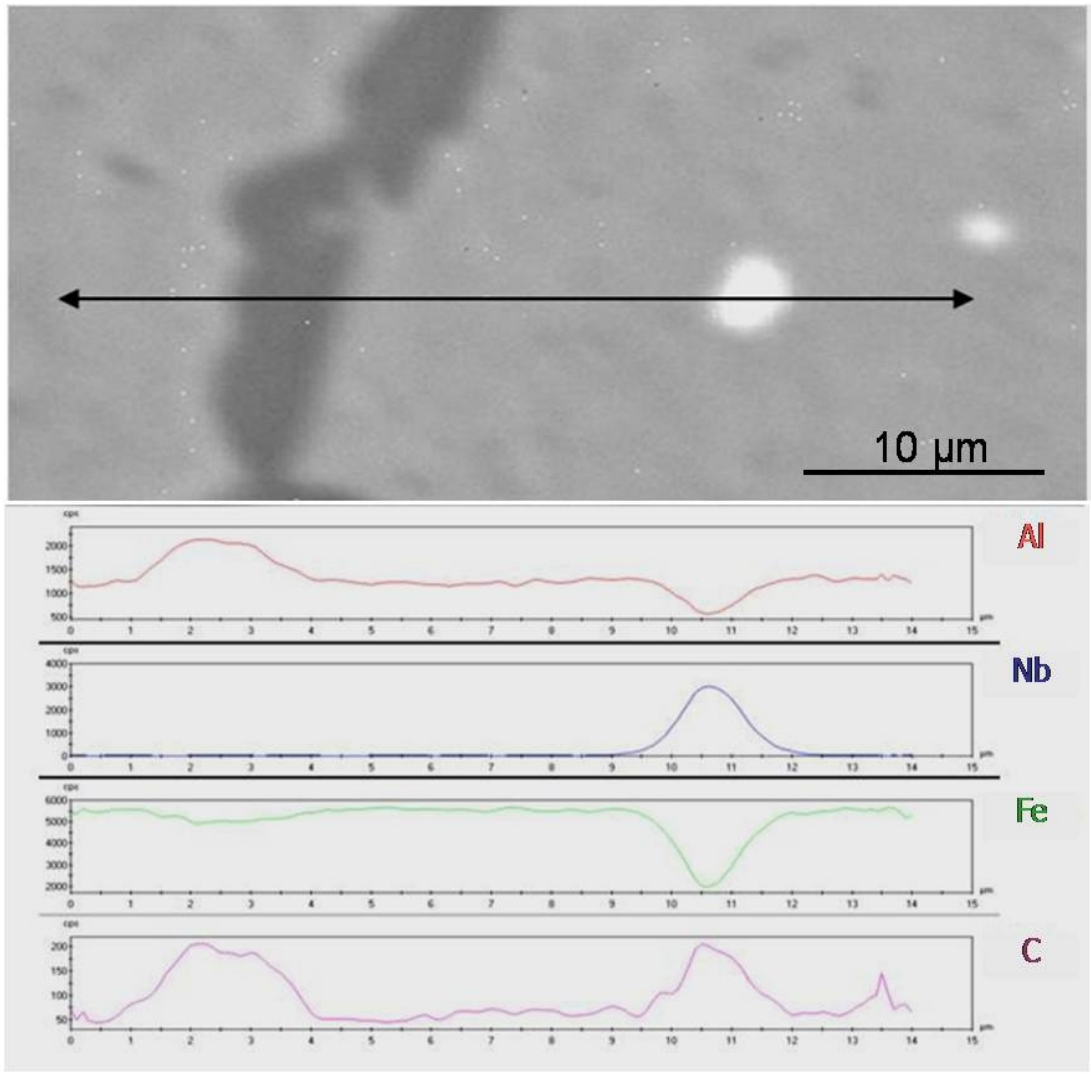

Fig. 6.8. BSE image and line scan of EPMA observed for the elements present in the bright precipitate and matrix of hot-rolled Fe-7Al-0.35C with 0.7wt.% niobium.

Table 6.4 Volume fraction of phases present in hot-rolled lightweight steels with different niobium content

Steel sample	Nominal Steel Composition (wt.%)	Volume fraction of phases (%)				
		Predicted by ThermoCalc		Measured using image analyser		
		$Fe_3AlC_{0.5}$ (κ carbide) Precipitate	Niobium carbide precipitate	$Fe_3AlC_{0.5}$ (κ carbide) Precipitate	Niobium carbide precipitate	α Fe-Al (Matrix)
NS1	Fe-7Al-0.35C -0.2Nb	11.82	0.38	12.82±0.1	0.86±0.1	86.46±0.1
NS2	Fe-7Al-0.35C -0.4Nb	10.41	0.64	12.64±0.2	1.08±0.3	86.15±0.4
NS3	Fe-7Al-0.35C -0.7Nb	09.83	0.88	12.32±0.2	3.04±0.2	84.84±0.3
NS4	Fe-7Al-0.35C -1.0Nb	08.07	1.86	12.04±0.1	3.42±0.3	84.62±0.5

At room temperature, the type of the phases (ferrite (α), κ-carbide and NbC precipitates) predicted by the ThermoCalc **(Fig. 6.3)** agrees well with the type of phases from the experimental results **(Fig. 6.8, Tables 6.3 and 6.4).**The volume fraction of the precipitates predicted by phase diagram is low compared to the volume fraction measured from micrographs **(Table 6.4)** Nevertheless, it is following the similar increasing trend for niobium carbide precipitate. In a different work, the phases formed with titanium additions to Fe-7Al-0.35C alloy have also been successfully predicted **(Khaple et al. 2018)** using ThermoCalc.

The microstructure is significantly refined on hot working **(Figs. 6.6 and 6.7).** As the niobium content increased, the ferrite grain size in the hot-rolled steels decreased significantly. This is because of the formation of fine niobium carbides at the ferrite boundaries. The rolling temperature of 1100^0C was in the intercritical (ferrite + austenite) region **(Palm et al. 1995, Raghavan 1987)** where the perovskite carbide dissolves and only niobium carbide is present. This agrees well with the prediction of phases from the equilibrium diagram calculated by ThermoCalc **(Figs. 6.2 and 6.3).** This is also supported by the reported stability of niobium carbides above 1200^0C **(Zargaran et al. 2014, 2015).**

In conventional steels, dynamic recrystallisation of austenite is delayed by the addition of strong carbide formers such as Nb **(Deardo 2003, Akben et al. 1981)**. On similar note, the addition of niobium to Fe-7Al-0.35C may be expected to retard dynamic recrystallisation in the present low-density steels during hot rolling. As discussed above, the precipitation of NbC occurs well above the hot rolling temperature. In the case of alloy with 0.2wt.% Nb the low volume fraction (0.86%) of NbC particles resulted in coarse grain size (320 μm). This is attributed to the insufficient number of NbC particles present. As the Nb content is increased to 1wt.%, there is a four-fold increase in the volume fraction (to 3.42%) of NbC precipitates. This restricts grain growth (Fig. 6.6) and lead to fine grain size (80 μm). The size of NbC precipitates is in the range of 0.3 to 6 μm which may retard the grain growth. The EPMA line scan did not detect niobium in the matrix or in the κ-carbide precipitates. As the Nb content increased, more carbon is consumed in the formation of niobium carbide and subsequently volume fraction of the perovskite carbide decreased **(Table 6.4).**

6.3 Mechanical property characterisation

Fig. 6.9 shows engineering stress-strain curves of all the alloys in the hot-rolled condition. The plot of logarithmic stress vs. logarithmic plastic strain in the uniform deformation region is shown in **Fig. 6.10.** The values of strain hardening exponent 'n' and strength coefficient 'k' were determined assuming a power law relationship ($\sigma = k\varepsilon^n$) between logarithmic stress and logarithmic strain. The results are presented in **Table 6.5.** The strain hardening exponent remains largely unaffected by Nb addition; however, the strength coefficient increases from 798 to 1344 MPa **(Fig. 6.10 and Table 6.5).** The hardness increases significantly from 246 to 402 HV as the Nb content in the steel is increased from 0.2 to 1 wt.% **(Table 6.5).** Further, yield strength and tensile strength also increase with the increase in Nb content **(Fig. 6.9 and Table 6.5).** A significant increase (about 80%) in the yield strength is evident on increasing Nb content from 408 MPa at 0.2 wt.% Nb to 735 MPa at 1.0 wt.% Nb. The tensile strength of steels also increased from 502 MPa to 862 MPa with addition of Nb (upto 1.0 wt.%). This is accompanied by a decrease in tensile elongation from 30% to 20 %. These results are clear indication of obtainment of moderate strength and good amount of ductility in this class of lightweight steels with Nb addition.

6.4 Fractography

The 0.2 wt.% Nb alloy exhibited cleavage failure while the alloys with higher Nb content exhibited mixed mode features comprising transgranular cleavage and ductile dimples **(Fig. 6.11).** It is well known that coarse-grained ferritic steels mainly fracture by cleavage **(Chen et al. 2015)**. The resistance to cleavage is mainly provided by grain boundaries **(Chen et al. 2015, Calcagnotto et al. 2009)**. Stress at the crack tip increases with the reciprocal root of the grain diameter. The plastic strain needed for fracture of a grain increases with decreasing grain size. This may be explained by a large number of dislocation pile-up at a grain boundary which leads to coarse cleavage fracture **(Chen et al. 2015)**. This is observed in the steel with 0.2 wt.% Nb **(Fig. 6.11a).** A mixed mode fracture surface is exhibited by the alloys with 0.4 to 1wt.% Nb which consists of finer dimples and shorter cleavage steps **(Fig. 6.11b-d).** This is attributed to the finer grain size displayed by the alloy with higher Nb content **(Fig. 6.6, Table 6.2).** Further, a large number of fine precipitates (NbC and κ-carbides) effectively reduce the dislocation pile-

up length thereby reducing the size of the cleavage steps. Although, the 0.2wt.% Nb steel exhibited cleavage failure **(Fig. 6.11a),** it displays adequate ductility (30 %). As the Nb content increases the volume fraction of hard niobium carbide precipitates increases **(Table 6.3).** Hence, it lead to the reduction in ductility of the steel from 30 to 20%.

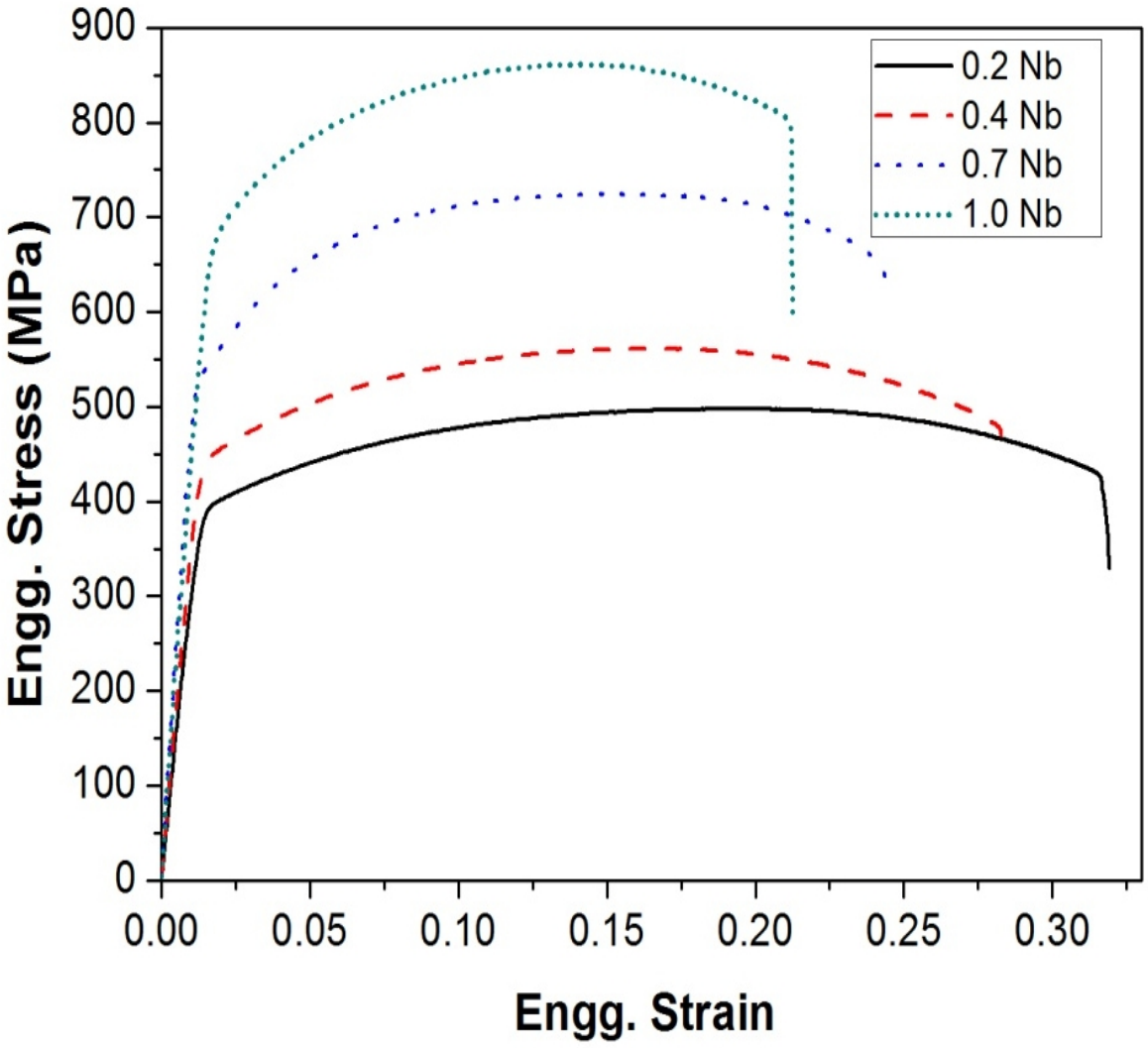

Fig. 6.9. Engineering stress–strain curves for tensile samples of hot-rolled Fe-7Al-0.35C steel with different niobium content.

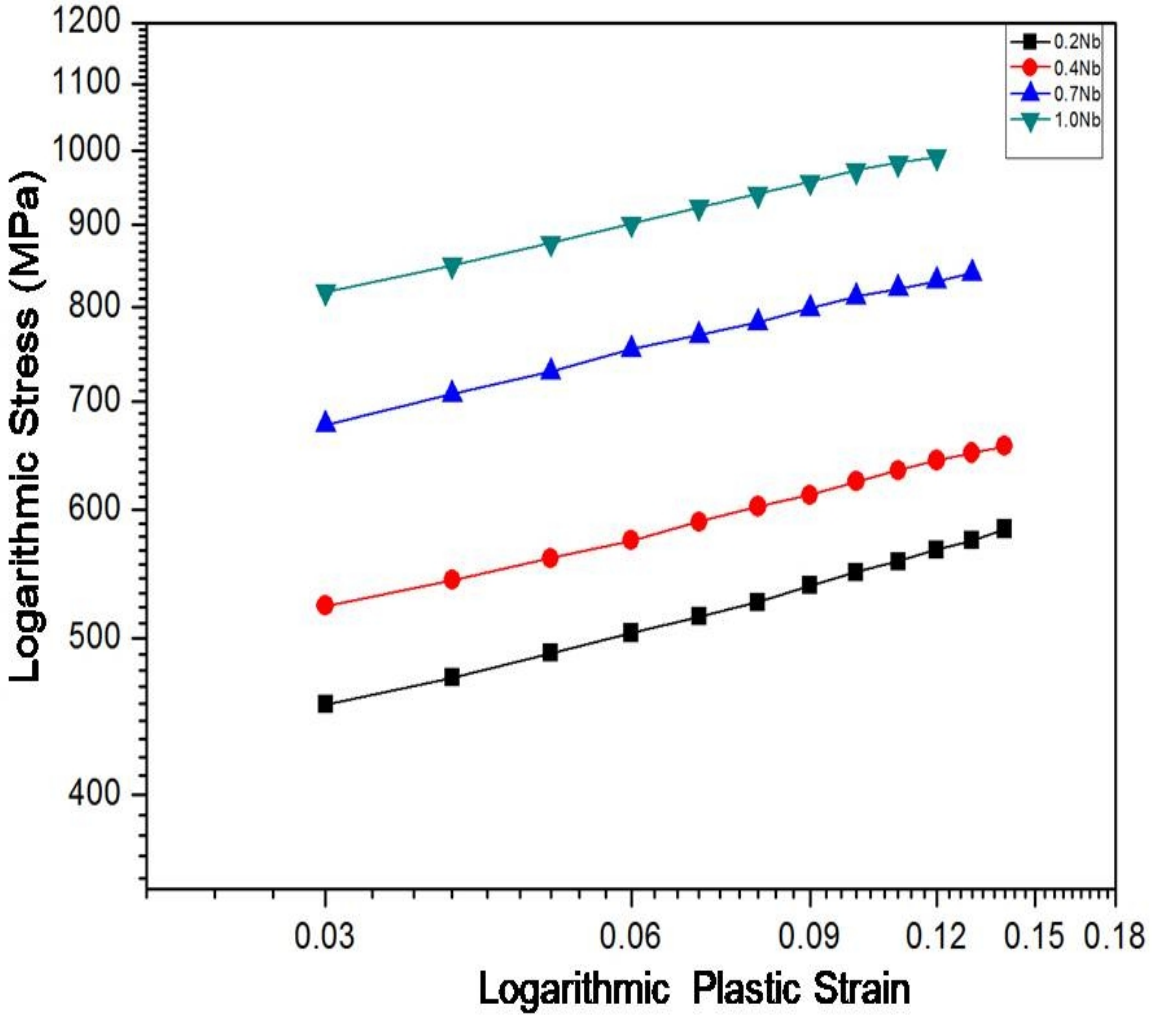

Fig. 6.10. Plot of logarithmic stress–logarithmic plastic strain curves of hot-rolled Fe-7Al-0.35C steel with different niobium content.

Table 6.5 Variation of bulk hardness, strain hardening exponent and strength coefficient in lightweight steels with different niobium content

Steel	Composition Nb (wt.%)	Bulk hardness (HV_{30})	Strain hardening exponent (n)	Strength coefficient K (MPa)
NS1	Fe-7Al-0.35C -0.2Nb	246±10	0.1643±0.001	798±1.8
NS2	Fe-7Al-0.35C -0.4Nb	282±14	0.1547±0.002	885±1.6
NS3	Fe-7Al-0.35C -0.7Nb	336±18	0.1472±0.003	1137±1.7
NS4	Fe-7Al-0.35C -1.0Nb	402±22	0.1408±0.002	1344±1.5
The measured micro hardness of $Fe_3AlC_{0.5}$ precipitates: 585±12 $HV_{0.1}$ and Niobium carbide: 2040±18 $HV_{0.1}$				

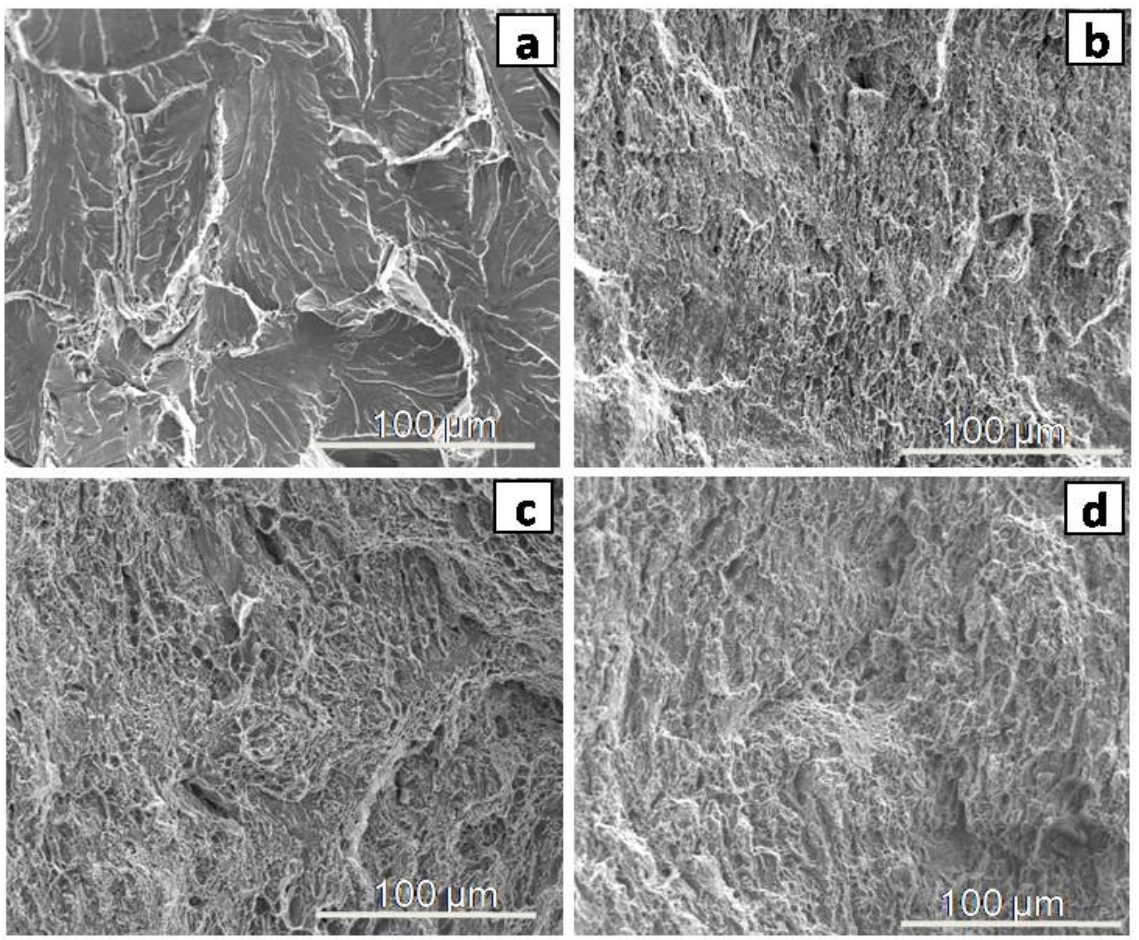

Fig. 6.11 SEM fractographs of hot-rolled Fe-7Al-0.35C steel with showing the cleavage features for (a) 0.2, mixed mode fracture with smaller cleavage length observed for (b) 0.4, (c) 0.7 and (d) 1.0 wt.% niobium.

6.5 Comparison of tensile properties of Fe-Al-C based lightweight steels

The tensile test results of the present work are compared with Fe-Al based lightweight steels containing different carbon and niobium levels **(Table 6.6).** It can be observed that steels containing higher aluminium (8.5 and 10.5 wt.%) with carbon and different niobium contents have shown high strength but poor ductility (**Baligidad 2004, Baligidad 2004).** This may be because these steels are prone to environmental embrittlement due to the presence of Al **(Satya Prasad et al. 2014, Khaple et al. 2010, Sikka et al. 1993).** The reduced ductility may also be attributed to the ordering effect **(Frommeyer et al. 2000, Satya Prasad et al. 2014, Khaple et al. 2010, Herrmann et al. 2003).** The Fe-7%Al-0.35%C alloy processed by air induction melting under flux cover has been reported to have exhibited only 13.5% elongation **(Satya Prasad et al. 2014)**. The improved mechanical properties obtained in the present work are also attributed to the use of a controlled atmosphere during melting. It has also been demonstrated that a range of tensile properties is attainable by varying niobium content to Fe-7Al-0.35C steel. Use of controlled atmosphere appears critical from the present results. Melting process such as vacuum induction melting and vacuum arc melting are well established industrially and hence can be practised for producing low-density steels containing carbon and niobium on a tonnage scale.

Table 6.6 The tensile properties of the present steels along with various Fe-Al-C based lightweight steels

Sl. No.	Steel composition	Melting Process	Processing condition	Room Temperature tensile properties			References
				UTS (MPa)	YS (MPa)	% El.	
1	Fe-8.5Al-0.1C	AIMFC + ESR	80 mm dia. ingot hot rolled to 12 mm thickness	554	515	1	**(Baligidad 2004)**
2	Fe-8.5Al-0.1C-1.5Nb	AIMFC + ESR	80 mm dia. ingot hot rolled to 12 mm thickness	686	550	6.3	**(Baligidad 2004)**
3	Fe-10.5Al-0.9C	AIMFC + ESR	80 mm dia. ingot hot rolled to 12 mm thickness	980	820	3.0	**(Baligidad 2004)**
4	Fe-10.5Al-0.9C-2Nb	AIMFC + ESR	80 mm dia. ingot hot rolled to 12 mm thickness	868	781	1.0	**(Baligidad 2004)**
5	Fe-7.8Al-0.23C-3.59Nb	VIM	32 mm diameter cast ingot	700	-	7.5	**(Falat et al. 2005)**
6	Fe-8Al-5Mn-0.017C	VIM	Ingot hot rolled to 70 mm to 20mm plate; warm rolled to 3 mm, 1.5 mm sheet, finally cold rolled to 1 mm and annealed	592.2	484	35.9	**(Shon et al. 2013)**
7	Fe-8Al-5Mn-0.1C-0.1Nb	VIM	Ingot hot rolled to 70 mm to 20mm plate; warm rolled to 3 mm, 1.5 mm sheet, finally cold rolled to 1 mm and annealed	694	600	30.7	**(Shon et al. 2013)**
8	Fe-7Al-0.35C	AIMFC	80 mm dia. ingot hot rolled to 12mm thickness	510	476	13.5	**(Satya Prasad et al. 2014)**
9	Fe-7Al-0.35C-0.2Nb	VAR	10 mm thick pan cakes, hot rolled to 2 mm thickness	502	408	30.2	Present work
10	Fe-7Al-0.35C-0.4Nb	VAR	10 mm thick pan cakes, hot rolled to 2 mm thickness	560	483	25.8	Present work
11	Fe-7Al-0.35C-0.7Nb	VAR	10 mm thick pan cakes, hot rolled to 2 mm thickness	684	581	22.5	Present work
12	Fe-7Al-0.35C-1.0Nb	VAR	10 mm thick pan cakes, hot rolled to 2mm thickness	862	735	20.1	Present work
(AIMFC: Air Induction Melting with Flux Cover, ESR: Electroslag Refining , VIM: Vacuum Induction Melting, VAR: Vacuum Arc Melting)							

6.6 Summary

1. The Fe-7Al-0.35C based lightweight steels (with 0.2% to 1% niobium) are successfully hot-rolled without any evidence of cracking or band formation. After 80% reduction, all the samples exhibited recrystallized grains.
2. The microstructure of steel (with different amounts of Nb) consists of ferritic matrix (α) with $Fe_3AlC_{0.5}$ (k-carbide) and NbC precipitates. The volume fraction of NbC precipitates increased with an increase in niobium content. The phases predicted using ThermoCalc agree well with the experimental results.
3. A significant increase in strength and hardness is observed with increasing Nb-content. This is attributed to the cumulative contribution from the increase in the volume fraction of the fine NbC carbides and the resulting grain refinement. All the compositions resulted significant (>20 %) tensile elongation.
4. It is also demonstrated that the use of a controlled atmosphere during melting may be necessary in the successful processing of Al containing lightweight steels. Otherwise, the low ductility is unavoidable for the steels with Nb processed in the unprotected atmosphere. In addition, it is also important to maintain a high C/Nb ratio to avoid the formation of Laves phases.

Chapter 7

EFFECT OF TITANIUM ON Fe-7Al-0.35C STEEL

Chapter 7 deals with the effect of titanium on the evolution of microstructure, its impact on mechanical properties and fracture behaviour of Fe-7Al-0.35C based lightweight steel.

7.0 Introduction

As discussed in the chapter 5, Fe-7 Al-0.35 C based steel has exhibited good combination of tensile properties (yield strength of 450 MPa and 12% ductility). With an aim of improving both the strength and ductility of these steels, it is of current interest to explore the potential of titanium as an alloying element by the partitioning of carbon between the carbide formers in Fe-7Al-0.35C based lightweight ferritic steel. In this work the formation of Laves phase is avoided as the formability of the steel is drastically affected by the presence of these phases.

7.1 The effect of Ti addition on the chemical composition and the density of Fe-7Al-0.35C lightweight steel

Non-consumable DC arc-melting process was used to melt the pancakes with four levels of titanium in the range of 0.2, 0.5, 0.75 and 1wt.%. These pancakes were hot-rolled to 2mm thick sheets subsequently annealed and characterised **(Fig. 7.1)**.

Fig 7.1. Photograph showing the hot-rolled sheets of Fe-7Al-0.35C steel with (a) 0.2, (b) 0.5, (c) 0.75 and (d) 1.0 wt.% titanium.

7.1.1 Chemical analysis:

The chemical compositions of the steels melted are given in **Table 7.1**. The recovery of the alloying elements particularly Al and Ti is good. The chemical composition of the pancakes is more homogenous as melting was done four times for every pancake, each time the pancake was turned upside down.

7.1.2 Density measurement

The density of hot-rolled steels is given in **Table 7.2**. As the titanium content increases from 0.2 to 1wt.%, a reduction in the density is observed in the steels from 7101 kg/m^3 to 7144 kg/m^3. These lightweight steels with different titanium content show a considerable reduction in density (~ 10%) compared to the traditional steel (7873 kg/m^3) as the alloying elements used in the melt of these steels are of lower density (Ti-4420 kg/m^3, Al-2700 kg/m^3, C-2250 kg/m^3) compared to the pure iron 7874 kg/m^3. This is one of the important aspects for the development of structural steels particularly for the automobile industry, where light weighting of the components is in ever increasing demand.

7.2 Visual observation and radiography of steel pancakes

The radiography studies confirmed that the pancakes are free from internal cracks and porosity. This is in contrast to the Fe-8.5 Al-0.1 C ingots prepared by air induction melting process, which was reported to have micro cracks **(Baligidad 2004).** This is attributed to the low Al content present in the present steels and also type of the melting route (VAR) which makes the melt with very low level of hydrogen. The hot rolling of the pancakes was carried out with more than 80% reduction and it was successful without defects such as cracks etc unlike edge and surface cracks reported in Mn containing low density steel with similar aluminium and carbon content (**Han et al. 2011)**.

.

Table 7.1 The chemical composition of Fe-7Al-0.35C based lightweight steel with different titanium content

Steel Sample	Steel composition							
	Al (wt.%)	Si (wt.%)	Mn (wt.%)	S (wt.%)	C (wt.%)	H (ppm)	N (ppm)	Ti (wt.%)
TS1	6.92 ±0.4	0.42	0.08	0.016	0.36 ± 0.02	4.1±2	<20	0.2 ± 0.04
TS2	7.20 ±0.5	0.50	0.05	0.014	0.33 ± 0.01	3.6±3	<20	0.5 ± 0.03
TS3	7.16 ±0.6	0.38	0.04	0.016	0.32 ± 0.03	4.2±1	<20	0.75 ± 0.05
TS4	6.98 ±0.2	0.53	0.06	0.019	0.30 ± 0.02	3.8±1	<20	1.0 ± 0.08

Table 7.2 The variation in density of Fe-7Al-0.35C based lightweight steel with different titanium content

Steel Sample	Chemical Composition (wt.%)Ti	Density (kg/m^3)
TS1	0.2 ±0.04	7145
TS2	0.5 ±0.03	7121
TS3	0.75 ±0.05	7115
TS4	1.0 ±0.08	7101

7.3 Phase prediction by ThermoCalc

ThermoCalc software was used to predict the equilibrium phase diagram of Fe-7Al-0.35C with varying titanium contents and is given in **Fig. 7.2.** The distribution of various phases formed and their amounts as a function of temperature in these steels containing 0 to 1 wt.% titanium which was done using ThermoCalc are as shown in **Figs. 7.3a-e**. It is important to note that in these calculations, the ferrite, austenite, carbides and Laves phases are the possible phases considered. Also, the phases such as graphite and ordered B2 are not considered. From **Fig 7.2 and Fig. 7.3,** it is clear that the solidification of these steels starts at about 1498^0C. The TiC precipitation starts form the liquid, while the κ-carbide ($Fe_3AlC_{0.5}$) forms at about 818^0C. Based on the amount of titanium present in the steel, the TiC formation temperature changes and for the content of 0.2 to 1 wt. % Ti, the TiC formation temperature varied in the range of 1458-1497°C. The austenite phase is observed between 1405^0C and 815^0C. The TiC is also formed from the austenite phase. This is also supported by the higher solubility of TiC in the austenite phase than in the ferrite phase **(Baker 2019).** At room temperature ferrite (α), κ-carbide and TiC precipitates are the stable phases present in the steel with the different amounts of titanium.

7.4 Microstructure and phase analysis

The optical microstructures of the hot-rolled steel samples with different titanium content are shown in **Fig. 7.4**. Recrystallized grains are observed in all the samples. Grain refinement is evident by the addition of Ti in all the steels. This variation in the average grain size with different titanium content is given in **Table 7.3**. The average grain size of steel significantly reduced from 162 to 48 μm with the increasing addition of Ti. The recrystallized grains could also be observed in the backscattered electron (BSE) SEM micrographs of the hot-rolled steels (**Fig. 7.5**). Significant amount of precipitates are observed in the microstructure of all the samples. Two types of precipitates namely grey colour (needle-shaped) and dark colour (cuboidal and acicular-shaped) precipitates are observed in the matrix. The X-ray diffraction of the Fe-7Al-0.35C based steel with varying titanium content is presented in **Fig. 7.6.** The peaks corresponding to $Fe_3AlC_{0.5}$ (κ-carbide) and ferrite (α) are observed in all the samples. The effect of Ti addition on the

formation of any compounds could not be detected in XRD due to very low volume fraction of these compounds and it is beyond the detection limit of XRD technique. As the titanium content increases in the steel, the volume fraction of the dark colour precipitates increases (**Fig. 7.5**). The dark phase is rich in Ti and C. The grey phase is confirmed as $Fe_3AlC_{0.5}$ from XRD.

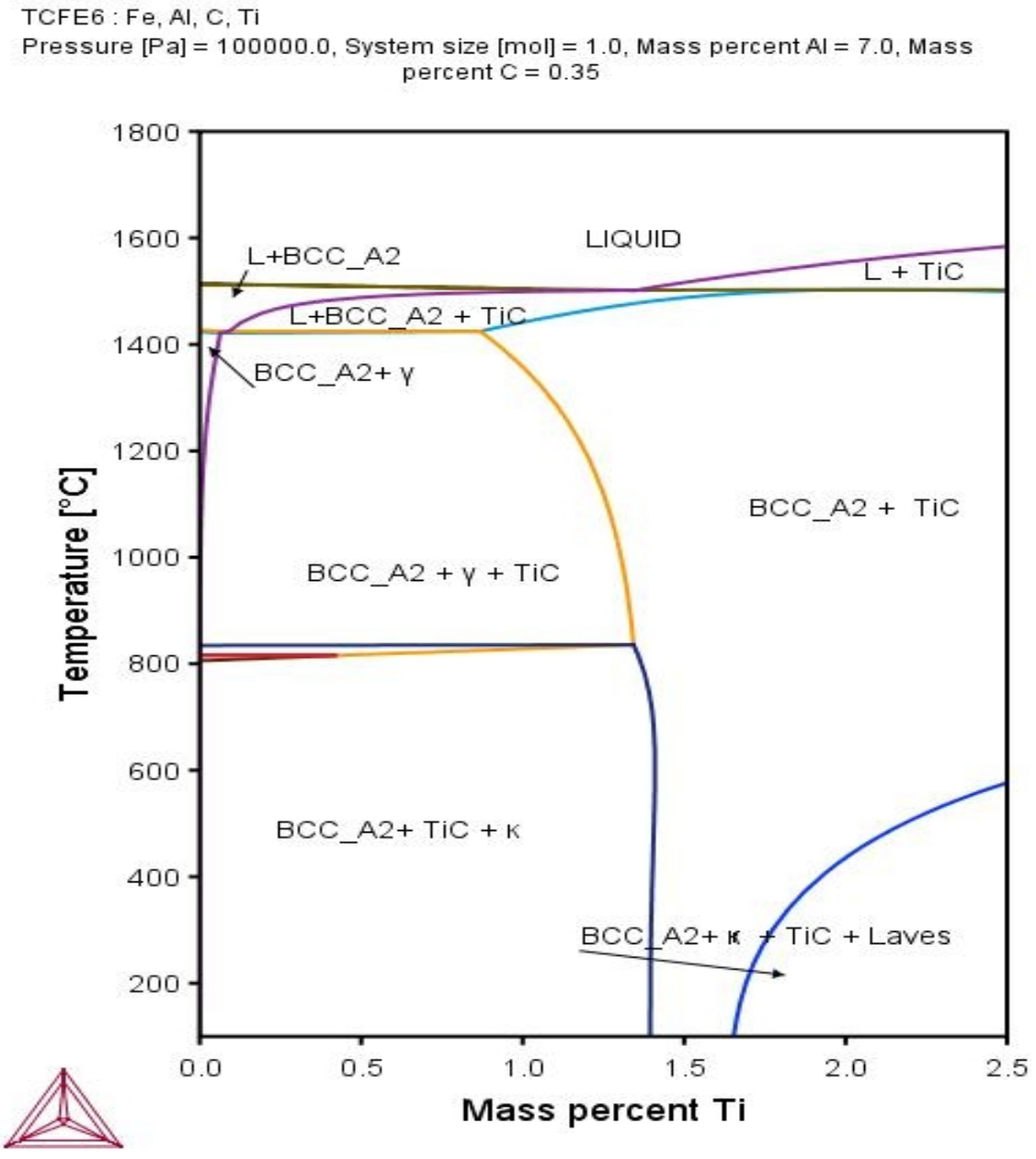

Fig. 7.2. The equilibrium phase diagram of Fe-Al-C-Ti at fixed contents of (7%) Al, (0.35%) C and varying Ti content as predicted by using ThermoCalc.

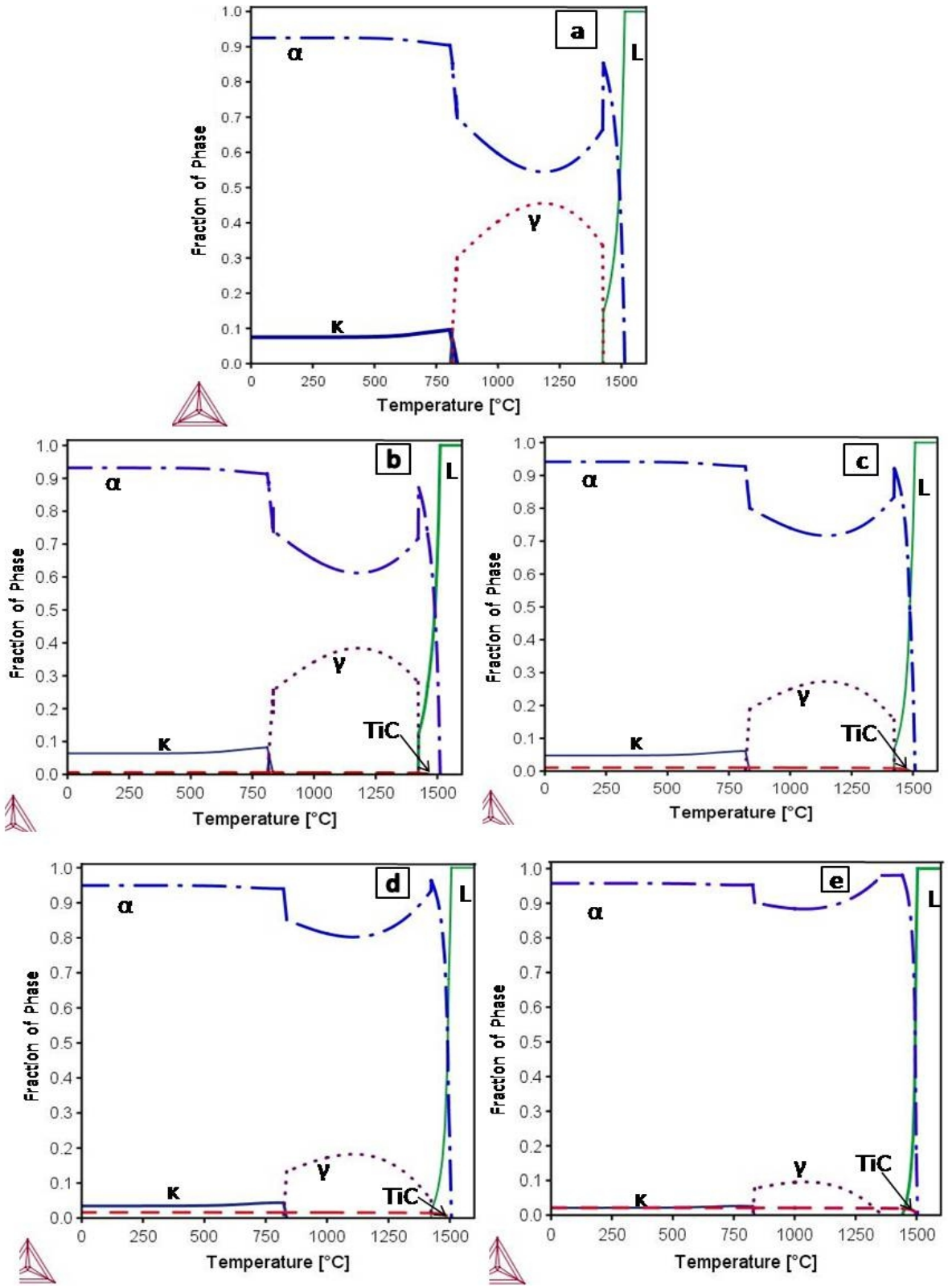

Fig. 7.3. Amount of various phases in Fe-7Al-0.35C steel as a function of temperature as predicted by ThermoCalc with (a) 0 (b) 0.2, (c) 0.5 (d) 0.75 and (e) 1.0 wt.% titanium.

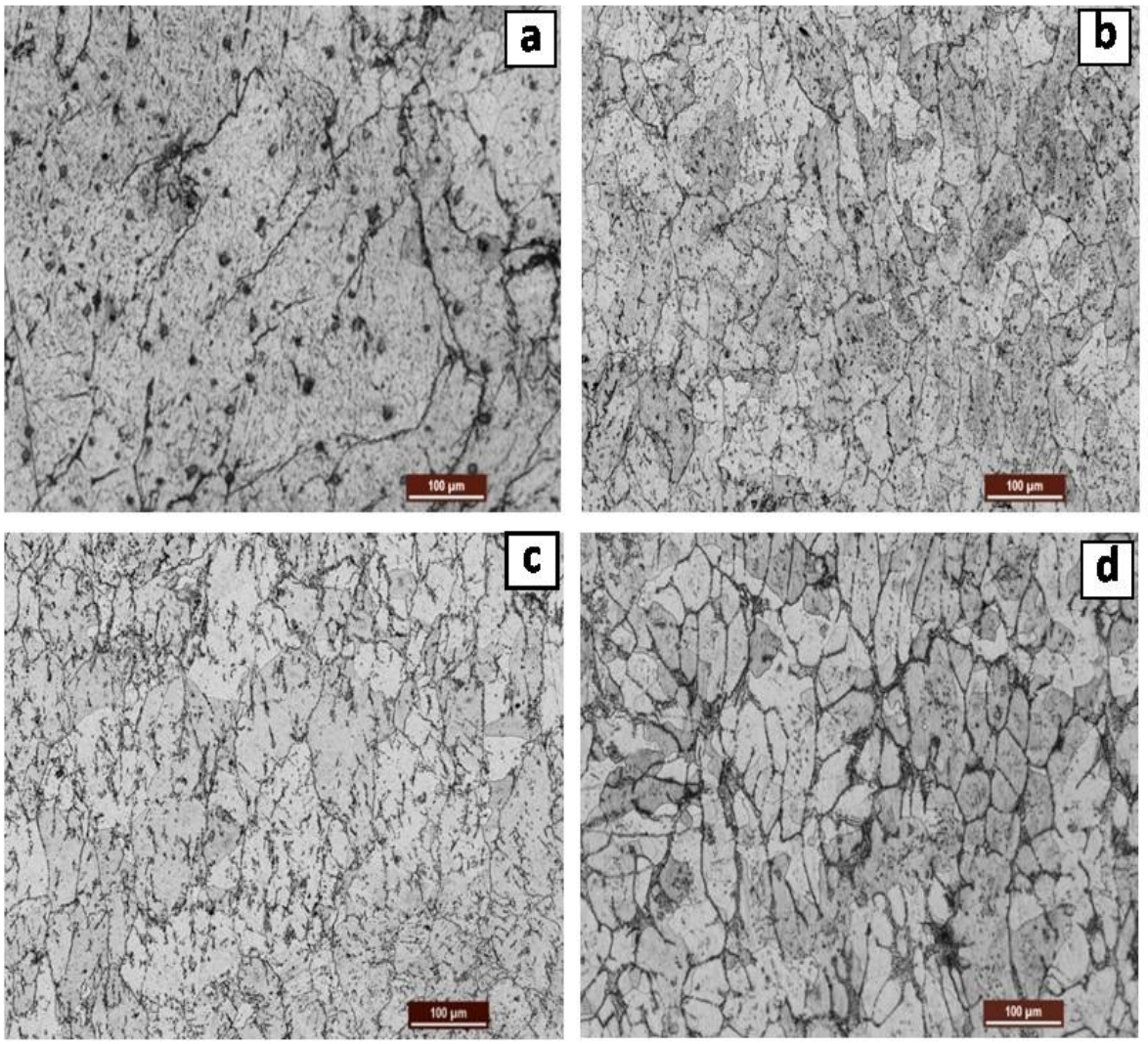

Fig. 7.4. Optical micrographs showing the microstructure of hot-rolled Fe-7Al-0.35C steel with (a) 0.2, (b) 0.5, (c) 0.75 and (d) 1.0 wt.% titanium.

Table 7.3 The average grain size of Fe-7Al-0.35C based lightweight steel with different Ti content in the hot-rolled and annealed condition.

Steel Sample	Composition (wt.%) Ti	Average grain size (μm)
TS1	0.2 ±0.04	162
TS2	0.5 ±0.03	78
TS3	0.75 ±0.05	62
TS4	1.0 ±0.08	48

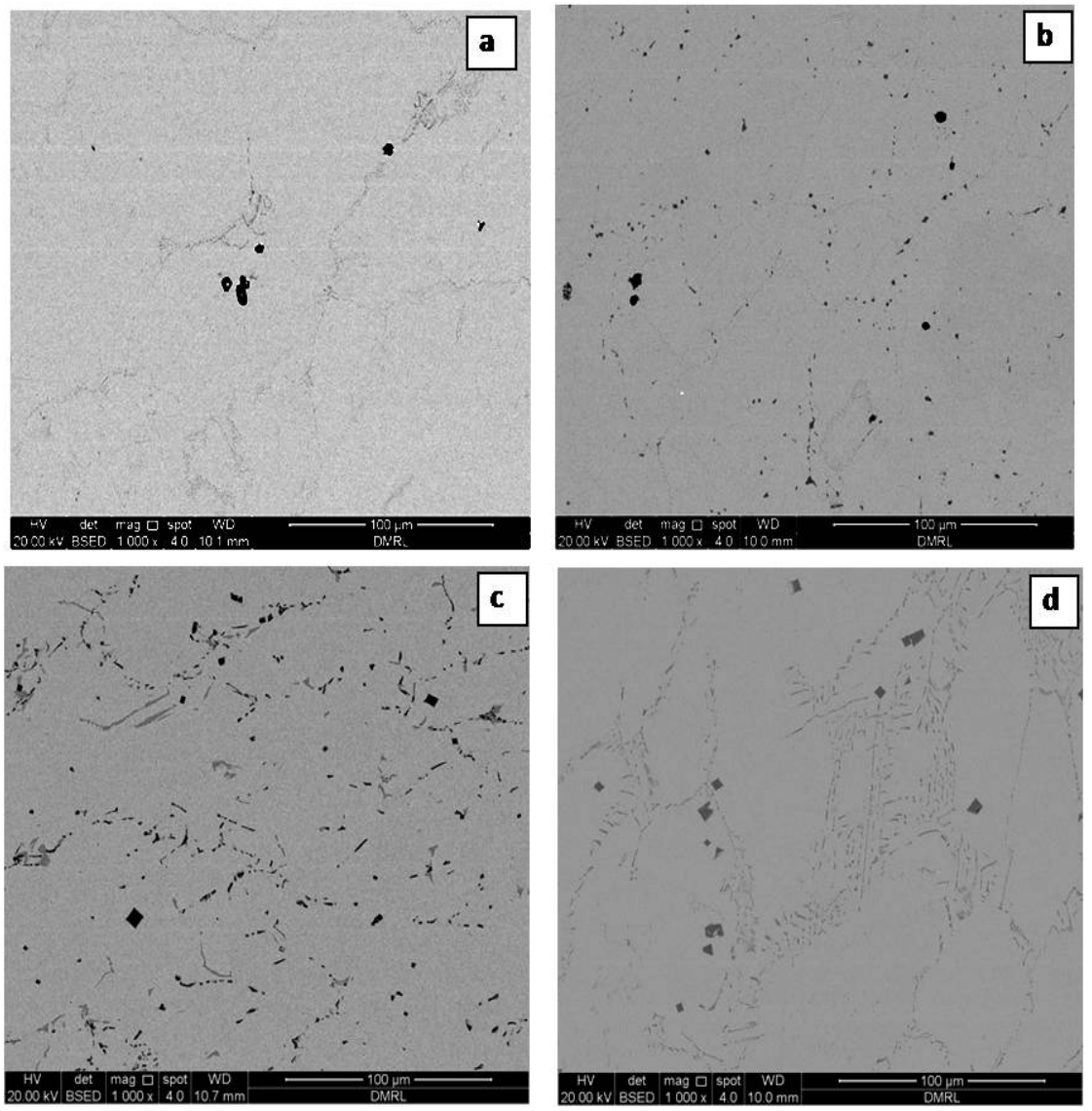

Fig. 7.5 Back-scattered electron micrographs showing the distribution of precipitates (dark are rich in Ti and C), and grey ($Fe_3AlC_{0.5}$) in Fe-7Al-0.35C steel with (a) 0.2, (b) 0.5, (c) 0.75 and (d) 1.0wt. %. titanium.

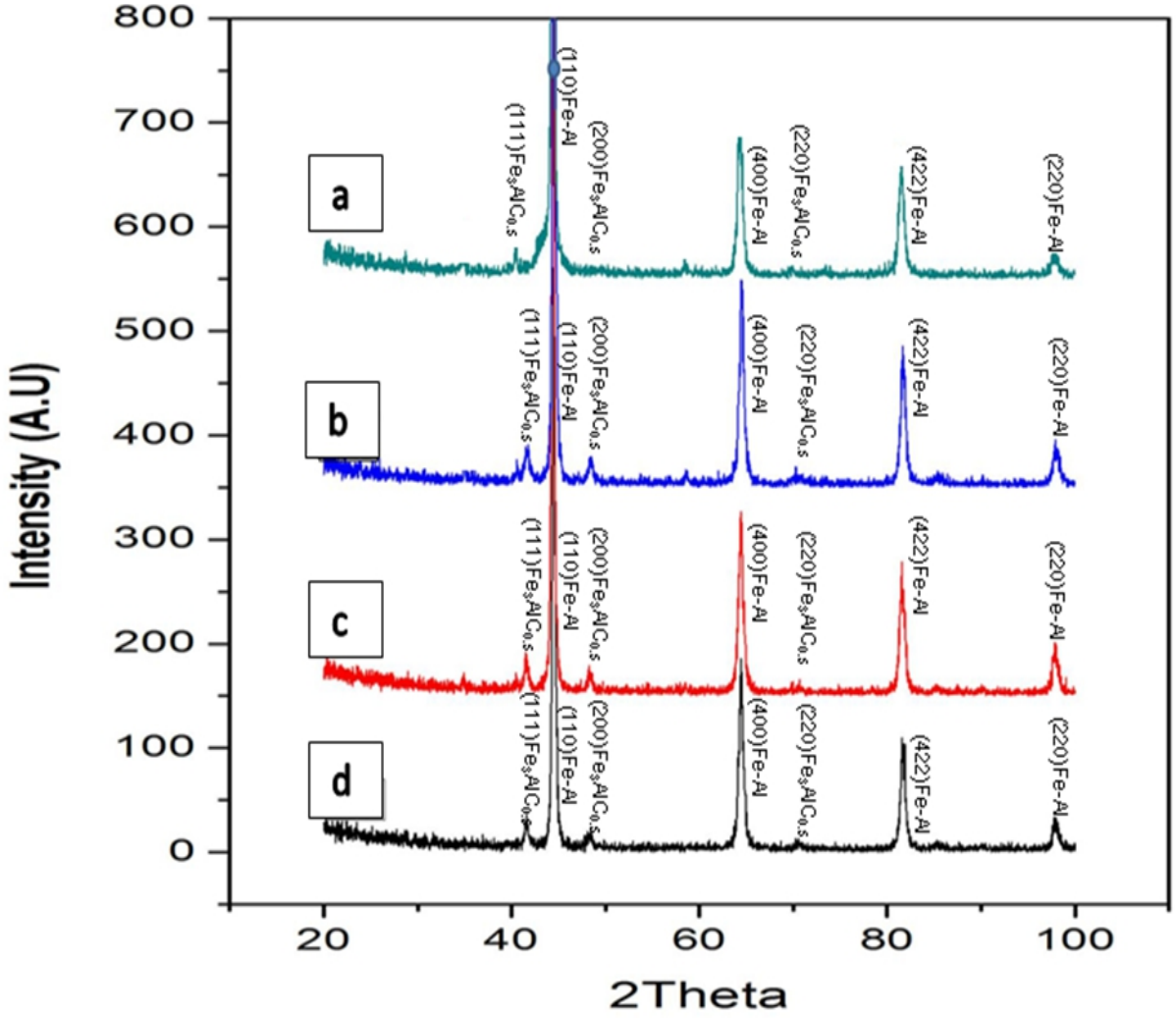

Fig. 7.6 XRD patterns using Cu-kα radiation showing peaks of α(Fe-Al) and $Fe_3AlC_{0.5}$ in Fe-7Al-0.35C steel with (a) 0.2, (b) 05, (c) 0.75 and (d) 1.0 wt.% titanium.

The electron probe micro-analysis (EPMA) results of the matrix, grey and dark precipitates of all the steel samples with varying titanium content is summarized in **Table 7.4**. Ti could not be detected in the matrix and grey precipitates. The dark precipitates are found to be enriched in Ti and C. Back scattered electron (BSE) image and line scan of EPMA observed for the elements present in the precipitates and matrix for Fe-7Al-0.35C steel with 0.7 wt.% titanium is shown in **Fig. 7.7**. The results from the EPMA line scan indicate that there is no solubility of titanium in the matrix or in the grey precipitates. Based on ThermoCalc results and the EPMA analysis, the dark precipitates are confirmed as TiC precipitates. Similar observation of TiC precipitates is reported in carbon containing Fe_3Al based alloys with titanium additions **(Ko and Hanada 1999, Baligidad et al., 1997). Schneder et al. (2003)** have reported the formation of TiC precipitates in the Fe-7.87Al-3.59 Ti-0.23 C alloy. The volume fraction of the precipitates and the matrix measured from the image analyser software is given in **Table 7.5** along with the predicted volume fraction of the precipitates of all the compositions. The volume fraction of phases from image analyser shows that the volume fraction of TiC precipitates increased (0.38, 0.81, 1.37 and 1.75%) whereas volume fraction of κ-carbide precipitates decreased (7.35, 6.41, 5.38 and 5.10%) with increase in Ti (0.2, 0.5, 0.75 and 1%) content. Since the volume fraction of TiC precipitates is very small (<2%) in all the steels, its peaks are not detected with XRD. As the Ti increased, more carbon was used up in the formation of TiC precipitates and it is in the ratio of 1:4.

The phases such as ferrite (α), κ-carbide and TiC precipitates at room temperature are predicted by using ThermoCalc **(Fig. 7.2 and Fig. 7.3)** in all the steels with different titanium content which agrees well with the type of phases from the experimental results **(Fig.7.5, Table 7.4 and Fig 7.6).** The volume fraction of the precipitates predicted by phase diagram is low when compared to the volume fraction measured from micrographs **(Table 7.5).** Nevertheless, it is following the similar increasing trend for titanium carbide precipitate. In a different work, the phases formed with Ti additions to Fe-7Al-0.35C alloy have also been successfully predicted **(Khaple et al. 2020)** using ThermoCalc.

The addition of Ti (0.2 to 1 wt.%) to Fe-7Al-0.35C steel resulted in significant reduction in average grain size from 162 µm to 48 µm which is significantly refined **(Fig. 7.4 and Table 7.3).** This is because of the formation of fine titanium carbides at the ferrite

boundaries. The rolling temperature of 1100^0C was in the intercritical (ferrite + austenite) region **(Palm et al. 1995)** where the perovskite carbide dissolves and only titanium carbide is present. This agrees well with the prediction of phases from the equilibrium diagram calculated by ThermoCalc **(Figs. 7.2 and 7.3).** The presence of increased amount of titanium in the steel, leads to the more amount of TiC precipitate formation in the austenite grain which retards the grain growth resulting in more refined ferritic grains. Ti in steel is generally added for grain refinement. This is also due to the increasing amount of titanium carbides formation at the ferrite boundaries with increasing Ti content. In conventional steels, dynamic recrystallisation of austenite is delayed by the addition of strong carbide formers such as Ti **(Akben et al. 1981)**. In the similar way the presence of Ti in the form of TiC in the present steels are expected to retard dynamic recrystallisation during hot rolling. As discussed earlier, the TiC precipitation occurs at high temperature (above 1450^0C) which is well above the hot rolling temperature. As the volume fraction of TiC precipitates is very low (0.38%) in case of steel with 0.2 wt.% Ti, it resulted in coarse grain size (162 μm). This is attributed to the presence of insufficient number of TiC particles. As the Ti content increased to 1wt.%, there is more than four-fold increase in the volume fraction (1.75%) of TiC precipitates. This restricts grain growth (**Fig. 7.4**) and lead to more refined grains (48 μm).

Table 7.4 Electron probe micro analysis of the precipitates and the matrix present in the Fe-7Al-0.35C steel with different Ti content.

Steel Sample	Composition (wt.%)Ti	Elements	Matrix wt.(at).%	Precipitate 1 (grey)wt.(at).% $Fe_3AlC_{0.5}$	Precipitate 2 (dark) wt.(at).% TiC
TS1	0.20±0.04	Fe Al C Ti	93.10(86.70) 06.9(13.3) --- ---	82.10(63.92) 14.30(23.04) 03.60 (13.04) ---	---- ---- 19.32(49.43) 77.68(49.01)
TS2	0.50±0.03	Fe Al C Ti	92.80(86.16) 07.20(13.84) --- ---	82.10(64.44) 14.52(23.42) 03.48(12.61) ---	---- ---- 19.46(49.49) 77.72(49.82)
TS3	0.75±0.05	Fe Al C Ti	92.68(85.95) 07.32(14.05) --- ---	82.04(64.27) 14.70(23.84) 03.26(12.88) ---	---- ---- 19.58(49.58) 77.78(49.52)
TS4	1.0±0.08	Fe Al C Ti	92.64(85.88) 07.36(14.12) --- ---	82.00(64.44) 14.80(23.96) 03.20(11.92) ---	---- ---- 19.89(50.02) 77.83(49.98)

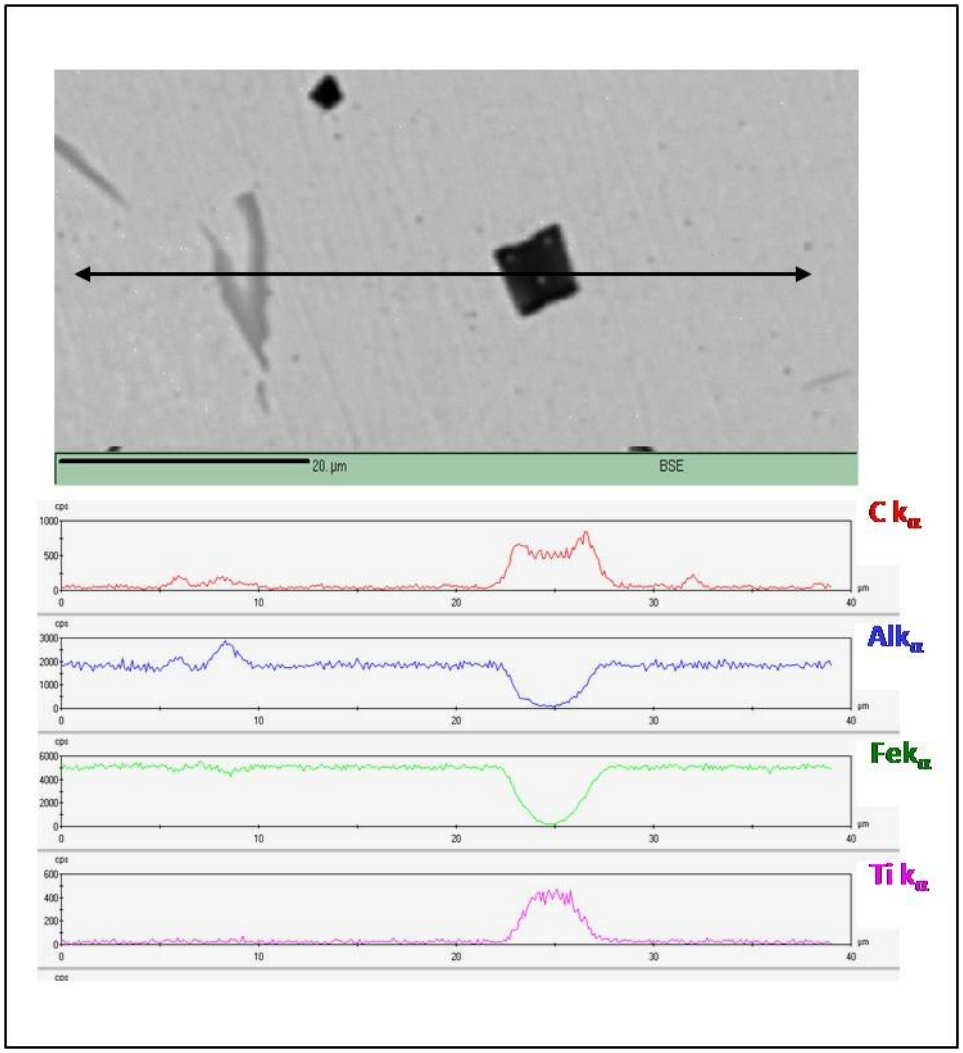

Fig. 7.7. BSE image and EPMA line scan observed for the elements present in the gray, dark precipitates and matrix of hot-rolled Fe-7Al-0.35C with 0.75 wt.% titanium.

Table 7.5 Volume fraction of phases present in hot-rolled Fe-7Al-0.35C steel with different titanium content

Steel Sample	Nominal Steel Composition (wt.%)	Volume fraction of phases (%)				
		Predicted by ThermoCalc		Measured using image analyser		
		$Fe_3AlC_{0.5}$ (κ carbide) Precipitate	Titanium carbide precipitate	$Fe_3AlC_{0.5}$ (κ carbide) Precipitate	Titanium carbide precipitate	α Fe-Al (Matrix)
TS1	Fe-7Al-0.35C -0.20±0.04Ti	8.12	0.36	7.53±0.8	0.38±0.6	89.46± 0.1
TS2	Fe-7Al-0.35C -0.50±0.03 Ti	7.34	0.68	6.41±0.6	0.81±0.3	90.15± 0.4
TS3	Fe-7Al-0.35C -0.75±0.05 Ti	06.83	1.10	5.38±0.4	1.37±0.5	91.04± 0.3
TS4	Fe-7Al-0.35C -1.0±0.08Ti	05.48	1.52	5.10±0.5	1.75±0.4	91.62± 0.5

7.5 Mechanical properties characterisation

The mechanical properties such as hardness, tensile strength and ductility of Fe-7Al-0.35C based lightweight steels with different titanium content are summarized in **Table 7.6.** As can be seen from **Table 7.6**, the bulk hardness and tensile strength increased with increase in Ti whereas ductility decreases. The hardness increased significantly from 243 to 318 HV as the Ti content in the steel increased from 0.2 to 1 wt.%. This increase in hardness & strength and decrease in ductility are attributed to the high hardness of TiC precipitates (3010 HV) compared to medium hardness of κ-carbides (528 HV) and very low hardness of matrix (190 HV). The increase in strength is also partly due to grain refinement. The increase in strength (from 480 to 615 MPa) of these steels is contributed by the grain refinement from 162 μm to 48 μm (**Fig. 7.4 and Table 7.3**) which is occurring in hot-rolled samples as the Ti content is increased from 0.2 to 1.0 wt.%.

The Gibbs free energy of formation of different products with temperature is given in **Fig. 7.8**. The lower the free energy, higher is the chances of forming that product. From the **Fig. 7.8,** it is also clear that TiC phase is formed at higher temperature and also, initially all the carbon is used up for the formation of TiC and left over carbon is used to form Fe_3AlC carbide. Hence with the increase in titanium content in the steel, more TiC is formed. It leads to higher volume fraction of TiC precipitate which is more stable at the hot deformation temperature (1100^0C) leading to higher grain refinement. Since TiC is expected to form well above 1450^0C, directly from the liquid it leads to the formation of TiC of cuboidal shape which are also known as primary TiC precipitates. The solubility of TiC is high in the austenite phase of the steel and lower in the ferrite **(Fig. 7.9)**. TiC precipitates out from the solid austenitic phase resulting in very fine precipitates which are known as secondary TiC precipitates **(Ko and Hanada 1999, Parashivamurthy 2008).** The cuboidal shape TiC precipitates are highly detrimental to the tensile properties of the steel as the sharp corners of the precipitate act as stress concentration region which acts as the crack nucleation point.

Table 7.6 Bulk hardness and tensile properties of Fe-7Al-0.35C steel with varying titanium content.

Steel Sample.	Nominal Steel Composition (wt.-%)	Hardness (HV) 30 kg load	Ultimate Tensile Strength (MPa)	Yield Strength (MPa)	% Elongation.
TS1	Fe-7Al-0.35C -0.20±0.04Ti	243±03	480±18	408±14	28.6±1.2
TS2	Fe-7Al-0.35C -0.50±0.03 Ti	271±04	518±23	440±16	24.8±0.9
TS3	Fe-7Al-0.35C -0.75±0.05 Ti	294±06	571±25	510±19	23.1±0.7
TS4	Fe-7Al-0.35C -1.0±0.08Ti	318±05	615±28	568±22	18.4±0.5
Measured micro-hardness of $Fe_3AlC_{0.5}$ precipitates:582±15 HV and TiC 3010±106 $HV_{0.1}$					

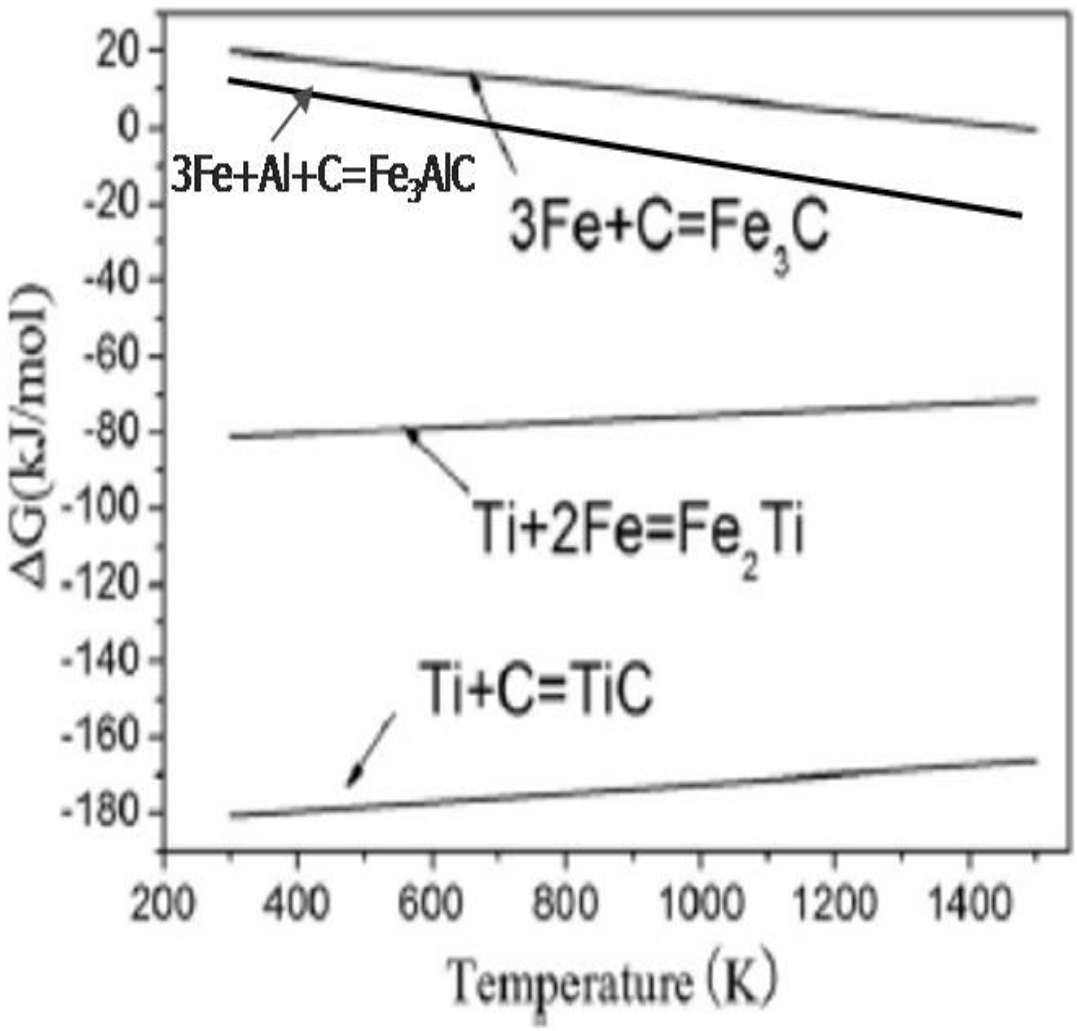

Fig. 7.8. The Gibbs free energy of formation of various products at different temperature (**Parashivamurthy et al. 2008**)

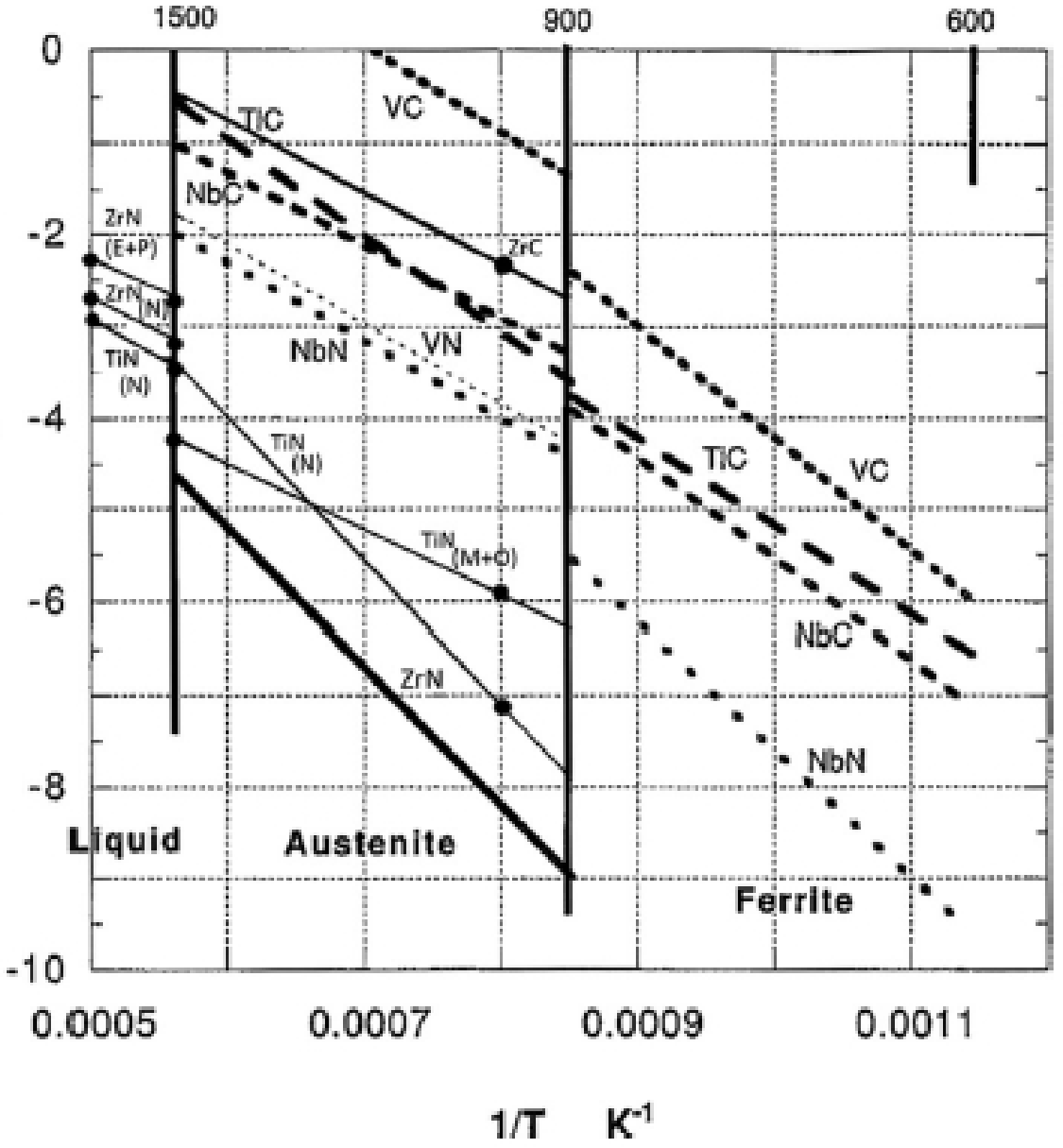

Fig. 7.9. Solubility products of carbides and nitrides as a function of temperature in steels **(Baker 2019)**

7.6 Fracture behaviour

Fig. 7.10 depicts the fracture characteristics of tensile samples of all Fe-7Al-0.35C based lightweight steels with varying titanium content. The fracture surfaces of the tensile tested steel samples with lower titanium content (0.2 percent) show coarse cleavage facets (**Fig. 7.10a**), whereas those of the steels with higher titanium content (0.5 to 1.0 percent) show mixed mode features with smaller cleavage steps and fine dimples **(Fig. 7.10 b-d).**

Cleavage fracture is common in Fe-Al ferritic steels with a coarse gain structure **(Chen et al. 2015**). Grain boundaries provide the most resistance to cleavage (**Chen et al. 2015, Calcagnotto et al. 2009**). The reciprocal root of the grain diameter increases stress near the fracture tip. The amount of plastic strain required to fracture a grain rises as grain size decreases. A high number of dislocations build up at a grain boundary, results in coarse cleavage fracture (**Chen et al. 2015**). This is shown in steel with a Ti content of 0.2 wt% (**Fig. 7.10a**). Alloys with 0.5 to 1 wt. percent Ti have a mixed mode fracture surface, which is made up of finer dimples. This can be due to the alloys with greater Ti content having finer grain sizes (**Fig. 7.3, Table 7.3**). In addition, a significant number of fine precipitates (TiC and -carbides) significantly minimise dislocation pile-up length, resulting in smaller cleavage stages. Despite cleavage failure, the 0.2wt.% Ti steel has acceptable ductility (28 percent). The reduction in ductility from 28 to 18.6% was caused due to increase in the volume fraction of hard TiC component (**Table 7.5**).

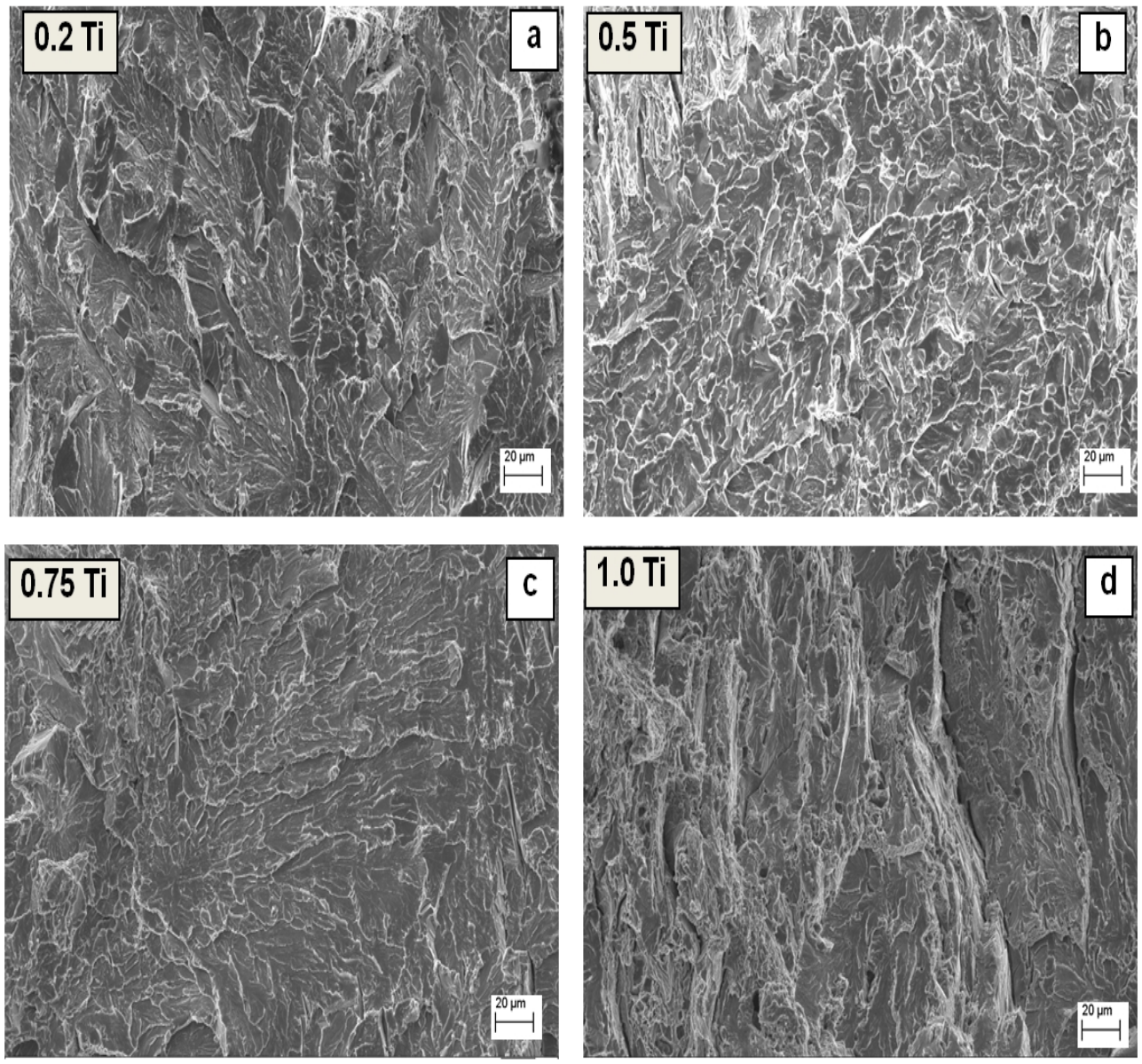

Fig. 7.10. SEM fractographs of Fe-7Al-0.35C steel showing the cleavage features for (a) 0.2, mixed mode fracture with smaller cleavage length observed for (b) 0.5, (c) 0.75 and (d) 1.0 wt.% titanium

7.7 Comparison of tensile properties of Fe-Al-C based lightweight steels containing titanium

The current study's tensile test findings are compared to Fe-Al based lightweight steels with various carbon and titanium levels (**Table 7.7**). Steels with increased aluminium (7.8 and above) percentage, as well as carbon and titanium content, have exhibited great strength but low ductility (**Baligidad 2004, Falat 2005**). This might be owing to the fact that certain steels are susceptible to environmental embrittlement due to the presence of Al (**Satya Prasad et al. 2014, Sikka et al. 1993**). The ordering effect might also be to blame for the lower ductility (**Khaple et al. 2010, Herrmann et al. 2003**).

Only 13.5 percent elongation was recorded for the Fe-7Al-0.35C alloy treated by air induction melting under flux cover (**Satya Prasad et al. 2014**). The use of a regulated environment during melting is also credited with the better mechanical characteristics reported in this study. It has also been established that altering the titanium content in Fe-7Al-0.35C steel may provide a variety of tensile characteristics. The use of a controlled environment appears to be crucial in the current results, which include the addition of more reactive alloying elements such as Ti to the melt. Vacuum induction melting and vacuum arc melting are well-known commercial melting processes that may be used to produce lightweight steels incorporating carbon and titanium on a large scale.

Table 7.7 The tensile properties of the present steels along with various Fe-Al-C based lightweight steels.

Sl. No.	Steel composition (wt.%)	Melting Process	Processing condition	Room Temperature tensile properties			References
				UTS (MPa)	YS (MPa)	% El.	
1	Fe-8.5Al-0.1C	AIMFC + ESR	50 mm dia. ingot hot rolled to 12 mm thickness	554	515	1	**(Baligidad 2004)**
2	Fe-10.5Al-0.7C	AIMFC + ESR	50 mm dia. ingot hot rolled to 12 mm thickness	833	720	1.8	**(Baligidad 2007)**
3	Fe-10.5Al-0.7C-2Ti	AIMFC + ESR	50 mm dia. ingot hot rolled to 12 mm thickness	637	592	1.2	**(Baligidad 2007)**
4	Fe-7.8Al-0.23C-3.59Ti	VIM	32 mm diameter cast ingot	-	420	3.3	**(Falat et al. 2005)**
5	Fe-7Al-0.35C	AIMFC	50 mm dia. ingot hot rolled to 12mm thickness	510	476	12	**(Satya Prasad et al. 2014)**
6	Fe-7Al-0.35C-0.2Ti	VAR	10 mm thick pan cakes, hot rolled to 2 mm thickness	480	408	28.6	Present work
7	Fe-7Al-0.35C-0.5Ti	VAR	10 mm thick pan cakes, hot rolled to 2 mm thickness	518	440	24.8	Present work
8	Fe-7Al-0.35C-0.75Ti	VAR	10 mm thick pan cakes, hot rolled to 2 mm thickness	571	510	23.1	Present work
9	Fe-7Al-0.35C-1.0Ti	VAR	10 mm thick pan cakes, hot rolled to 2mm thickness	615	568	18.4	Present work
(AIMFC: Air Induction Melting with Flux Cover, ESR: Electroslag Refining , VIM: Vacuum Induction Melting, VAR: Vacuum Arc Melting)							

7.8 Summary

1. The Fe-7Al-0.35C based low-density steels containing 0.2% to 1% titanium could be successfully hot-rolled without any cracking (with about 80% reduction). All the steel samples exhibited recrystallized grains.
2. Fe-7Al-0.35C based low density steel with different titanium content exhibited two type of TiC precipitates, (dark cuboidal and dark acicular type) along with grey coloured needle-shaped κ-carbide precipitate in a ferrite matrix. The amount and type of phases as predicted by ThermoCalc in Fe-7Al-0.35C-1Ti steel agrees well with the experimental work.
3. The volume fraction of TiC precipitates increased from 0.38 to 1.75 with an increase in titanium content. Also it resulted in grain refinement from 162μm to 48μm which is significant to improve mechanical properties.
4. . A significant increase in hardness (243 to 318 HV) and strength (480-615 MPa) is observed with increasing Ti-content. This is attributed to the cumulative contribution from the increase in the volume fraction of the fine TiC carbides and the resulting grain refinement. All the compositions resulted significant (>18 %) tensile elongation.

Chapter 8

CONCLUSIONS AND SCOPE FOR FUTURE WORK

8.1 Conclusions

Systematic studies were undertaken to understand the effect of alloying addition such as diborides (TiB_2 and ZrB_2) and carbon (0.012 to 2.2wt.%) on Fe-7Al based lightweight steel. Effect of Nb and Ti on the Fe-7Al-0.35C steel has been studied as well. The focus was mainly on the preparation, thermo-mechanical processing and alloy chemistry of the lightweight steels and subsequently understand their effect on microstructure and mechanical properties of these steels.

The conclusions that emerge from this thesis: alloying additions play a key role in influencing the evolution of the microstructure and its effect on the mechanical properties of lightweight steels.

1. Addition of diborides (TiB_2 and ZrB_2) to base (Fe-7Al) lightweight steel resulted in significant grain refinement in the cast as well as in the hot-rolled and annealed condition compared to the base alloy. Considerable improvement in ductility (19 % to 38 %) was observed which was attributed to grain refinement occurring during solidification, as well as after hot rolling and annealing. On the other hand, marginal improvement in hardness (154 to 180 HV) and tensile strength (478 to 547 MPa) was observed.

2. Addition of carbon (0.012 to 2.2)wt.% to Fe-7Al steel resulted in the evolution of different morphology of $Fe_3AlC_{0.5}$ carbides in the Fe-Al(α) matrix. Addition of upto 0.35wt.%C resulted in a two-phase microstructure containing ferrite and κ-pearlite. With further addition of 0.65 and 1.5wt.%C the alloys composed of complete κ-pearlite structure consisting of the dispersion of globular $Fe_3AlC_{0.5}$ carbides in a matrix. In addition, the steel with 2.2wt.%C exhibited a very small volume fraction of graphite phase. The Fe-7Al steel with 0.35wt.%C

demonstrated a good combination of strength (450±30MPa) and ductility (12±1.7). The ductility of this steel is over 12% which is the minimum requirement for the formability operation of the steels.

3. Addition of niobium to Fe-7Al-0.35C alloy has resulted in the formation of NbC and $Fe_3AlC_{0.5}$ (k-carbide) precipitate in ferritic matrix. The average grain size is reduced from 320 to 80µm. The phases predicted using ThermoCalc agreed well with the experimental results. A significant increase in hardness (246 to 402 HV) and tensile strength (502 to 862 MPa) was observed on increasing Nb-content. This is attributed to the cumulative contribution from the increase in the volume fraction of the fine NbC carbides and the resultant grain refinement. All the compositions revealed significant (>20 %) tensile elongation.

4. Addition of titanium to Fe-7Al-0.35C alloy resulted in the in-situ formation of carbide precipitates namely TiC and $Fe_3AlC_{0.5}$ (k-carbide) in ferritic matrix. The average grain size was reduced from 162 to 48 µm. In this case also, the type of the phases predicted using ThermoCalc agreed well with the experimental results. Considerable increase in hardness (243 to 318 HV) and tensile strength (480 to 615 MPa) was evident with increasing amount of titanium. This is attributed to the cumulative contribution from the increase in the volume fraction of the fine TiC carbides and the grain refinement. All the compositions exhibited significant (>18 %) tensile elongation.

8.2 Scope for future work

The systematic study of the following areas of Fe-7Al based lightweight steel can be further explored

1. Since these steels are mainly used for automobile applications, the workability and formability studies can be taken up.
2. These steels have a texture effect which strongly affects the properties of the steel in application. Hence, detailed future study on the texture of the steels can be done.
3. The addition of Al to steel improves the corrosion properties similar to the behaviour of Cr in stainless steel. A detailed study on the corrosion of these

new class of steels is a very potential area to expand new understanding of the system.

4. Effect of other alloying elements such as silicon, vanadium and zirconium etc. can be attempted.

REFERENCES

1. Akben M. G., Weiss I. and Jones J .J. 1981 Dynamic precipitation and solute hardening in a V microalloyed steel and two Nb steels containing high levels of Mn. *Acta Metal.* **29**, 111–121.
2. Baker I. and Gaydosh D. J. 1987 Flow and fracture of Fe-Al *Mater. Sci. Eng.* **96** 147–158.
3. Baker T. N. 2019 Titanium microalloyed steels *Ironmaking and steelmaking*, **46** 1, 1–55.
4. Baligidad R. G. and Satya Prasad V. V. 2007 Melting, processing and properties of Fe-Al-C alloys. *Trans. Indian Inst. Met.* **5** 451–461.
5. Baligidad R. G., Radhakrishna A. and Prakash U. 1998 Mechanical properties of high carbon Fe3Al-based intermetallic alloys. *Mater. Sci. Eng. A* **257** 235-239.
6. Baligidad R. G. 2004 Effect of niobium on microstructure and mechanical properties of hot-rolled Fe-8.5 wt% Al-0.1 wt% C alloy. *J. Mater. Sci.* **39** 5599–5602.
7. Baligidad R. G. 2004 Effect of niobium on microstructure and mechanical properties of high carbon Fe–10.5wt.%Al alloys. *Mater. Sci. Eng. A* **368** 131–138.
8. Bartlett L., Aken V. D. 2014 High manganese and aluminum steels for the military and transportation industry. *JOM* **66** 91, 1770–1784.
9. Bausch M., Samek L., Hofmann H., Didier M., Frommeyer G., Soler M., Balichev E. 2009 Ultra high-strength and ductile FeMnAlC light-weight steels. *Final Report RFCS Grant No. RFSR-CT*-2006-00027.
10. Bhadeshia H. K. D. H, Honeycombe R. W. K. 2006 Steels: Microstructure and Properties, Elsevier Ltd., UK .
11. Bohnenkamp U, Sandström R. 2000 Evaluation of the density of steels. *Steel Res.* **71** 88–93.
12. Bordeau R. D. 1987 Development of iron aluminides, Technical report no. AFWAL-TR-87-4009, Materials Laboratory, Air Force Wright Aeronautical Laboratories, Wright-Patterson air force base, Ohio, USA.

13. Br¨ux U., Frommeyer G., Jimenez J. 2002 Light-weight steels based on iron-aluminium-influence of micro alloying elements (B, Ti, Nb) on microstructures, textures and mechanical properties. *Steel Research* **73** 543-548.
14. Buckholz S. A., Van Aken D. C., Bartlett L. N. 2013 On the influence of aluminum and carbon on abrasion resistance of high manganese steels. *AFS Trans*; **121** 495-510.
15. Castan C., Montheillet F., Perlade A. 2013 Dynamic recrystallization mechanisms of an Fe–8% Al low density steel under hot rolling conditions, *Scripta Mater.***68** 6, 360-364
16. Cai Z, Ding H, Ying Z, Misra R. D. K. 2014 Microstructural evolution and deformation behaviour of a hot-rolled and heat treated Fe-8Mn-4Al-0.2C steel. *J Mater Eng Perform* **23** 1131–1137.
17. Calcagnotto M., Ponge D., Adachi Y., Raabe D. 2009 Proceedings of the 2nd International Symposium on Steel Science (ISSS 2009) Oct. 21-24, Kyoto, Japan: The Iron and Steel Institute of Japan.
18. Campbell J. and Bannister J. W. 1975 Grain refinement of electroslag remelted iron alloys, *Metals Technol.,* **9** 409–415.
19. Slater C., Hollyhoke N. and Davis C. 2019 The influence of alloy composition on the as-cast grain structure in near net shape low-density steels, *Ironmaking and SteelmakingProcesses, Products and Applications.* **46**, 8,725–730.
20. Castan C, Montheillet F, Perlade A. 2013 Dynamic recrystallization mechanisms of an Fe–8% Al low density steel under hot rolling conditions. *Scripta Mater.***68** 360–364.
21. Chaudhary S., Khaple S., Satya Prasad V.V., Baligidad R. G. 2015 Effect of Titanium and Carbon on Microstructure and Mechanical Properties of Disordered Solid Solution Fe–7wt%Al Alloy. *Trans Indian Inst Met* **68** 809–815.
22. Chen J. H. and Cao R. 2015 Micromechanism of cleavage fracture of metals A comprehensive microphysical model for cleavage cracking in metals; Elsevier publication, 81–85.
23. Chen S., Rana R., Haldar A. and Ray R. K. 2017 Current state of Fe-Mn-Al-C low density steels. *Prog. Mater. Sci.* **89** 345–391.
24. Cheng W.C., Song Y.S., Lin Y.S., Chen K.F., Pistorius P.C. 2014 On the eutectoid reaction in a quaternary Fe-C-Mn-Al alloy: austenite ferrite + kappa-carbide + M23C6 carbide. *Metall. Mater. Trans. A***45** 1199–216.

25. Chu C.M., Huang H., Kao P.W., Gan D. 1994 Effect of alloying chemistry on the lattice constant of austenitic Fe-Mn-Al-C alloys. *Scripta Metall. Mater.* **30** 505–508.
26. Connétable D., Lacaze J., Maugis P., Sundman B. 2008 *Calphad* **32** 361–370.
27. Crimp M. A. and Vedula K. 1986 Effect of boron on the tensile properties of B2 FeAl. *Mater. Sci. Eng.* A **78**, 193–200.
28. Davies R.G. 1963 An X-ray and dilatometric study of order and the ‘‘K-state” in iron-aluminium alloys. *J Phys Chem Solids* **24** 985–988.
29. Davis C. L., Mukhopadhyay P., Strangwood M., Potter M., Dixon S., Morris P. F. 2008 Comparison between elastic modulus and ultrasonic velocity anisotropy with respect to rolling direction in steels. *Ironmaking Steelmaking***35** 359–366.
30. Deardo A. J. 2003 Niobium in modern steels. *Inter. Mater. Rev.* **48** 6, 371–402.
31. Doucakis T. and Kumar K. S. 1999 Formation and stability of refractory metal diborides in an Fe_3Al matrix. *Intermetallics* **7** 765–777.
32. El-Faramawy Hoda S., Ghali Saeed N., Eissa Mamdouh M. 2012 Effect of Titanium Addition on Behavior of Medium Carbon Steel. *Journal of Minerals and Materials Characterization and Eng.11* 1108–1112
33. Etienne A, Massardier-Jourdan V, Cazottes S, Garat X, Soler M, Zuazo I. 2014 Ferrite effects in Fe-Mn-Al-C triplex steels. *Metall Mater Trans A***45** 324–334.
34. European Commission, Reducing CO_2 emission from passenger cars. http://ec.europa.eu/clim a/policies/transport/vehicles/cars/index_en.htm.
35. Falat L., Schneider A., Sauthoff G., Frommeyer G. 2005 Mechanical properties of Fe–Al–M–C (M=Ti, V, Nb, Ta) alloys with strengthening carbides and Laves phase. *Intermetallics* **13** 1256–1262.
36. Frommeyer G, Brüx U, Neumann P. 2003 Supra-ductile and high-strength manganese-TRIP/TWIP steels for high energy absorption purposes. *ISIJ Int.* **43** 438–446.
37. Frommeyer G, Brüx U. 2006 Microstructures and mechanical properties of high-strength Fe–Mn–Al–C light-weight triplex steels. *Steel Res Int.* **77** 627–633.
38. Frommeyer G., Drewes E. J. and Engl B. 2000 Physical and mechanical properties of iron aluminium-(Mn, Si) lightweight steels. *La Rev De Métallurgie-CIT***10** 1245–1253.
39. Gaydosh D. J., Draper S. L., Nathal M. V. 1989 Microstructure and tensile properties of Fe-40 At. pct Al alloys with C, Zr, Hf, and B additions. *Metall. Trans. A***20**, 1701–1714.

40. Gladman T. 1997 The physical metallurgy of microalloyed steels., First Edit. London: Maney Publishing, 1–363.
41. Gladman T., Fourlaris G. and Talafi-Noghani M. 1999 Grain refinement of steel by oxidic second phase particles. *Mater., Sci. Technol.* **15** 1414–1423.
42. Goretskii G. P., Gorev K. V. 1990 Phase equilibria in Fe-Mn-Al-C alloys. *Russian Met*. **2** 217–221.
43. Gutierrez-Urrutia I, Raabe D. 2013 Influence of Al content and precipitation state on the mechanical behaviour of austenitic high-Mn low-density steels. *Scripta Mater*. **68** 343–347.
44. Ha M.C., Koo J.M., Lee J. K., Hwang S. W., Park K.T. 2013 Tensile deformation of a low density Fe–27Mn–12Al–0.8C duplex steel in association with ordered phases at ambient temperature. *Mater. Sci. Eng. A* **586** 276–283.
45. Han S.Y., Shin S.Y., Lee S., Kim N. J., Kwak J-H, Chin K-G. 2011 Effect of carbon content on cracking phenomenon occurring during cold rolling of three light-weight steel plates, *Metall. Mater. Trans. A* **42** 138–146.
46. Han S. Y., Shin S. Y., Lee H. J., Lee B. J., Lee S., Kim N. J., Kwak J.H. 2012 Effects of annealing temperature on microstructure and tensile properties in ferritic lightweight steels. *Metall. Mater. Trans. A***43** 843–853.
47. Han S.Y., Shin S.Y., Lee S., Kim N.J., Kwak J.H., Chin K.G. 2010 Effect of carbon content on cracking phenomenon occurring during cold rolling of three light-weight steel plates. *Metall. Mater. Trans. A***42** 138–146.
48. Hecht M. D., Webler B. A., Picard Y. N. 2018 Effects of Nb modification and cooling rate on the microstructure in an ultrahigh carbon steel. *Metall. Mater. Trans. A***49** 2161–2172.
49. Heo Y-U, Song Y-Y, Park S-J, Bhadeshia H. K. D. H, Suh D-W 2012 Influence of silicon in low density Fe-C-Mn-Al Steel. *Met. Mater. Trans. A,* **43** 1731–1735.
50. Herrmann J, Inden G, Sauthoff G. 2003 Deformation behaviour of iron-rich iron-aluminium alloys at low temperatures. *Acta Mater.* **51** 2847–2857.
51. Ishii H., Ohkubo K., Miura S. and Tetsuo M. 2003 Mechanical properties of α+κ two-phase lamellar structure in Fe-Mn-Al-C Alloy *Mater. Trans.* **44** 9 1679–1681.
52. Howell R. A., Van Aken D. C. 2009 A literature review of age hardening Fe-Mn-Al-C alloys. *Iron Steel Tech.* **6** 193–212.

53. Hwang S.W., Ji J.H., Lee E.G., Park K.T. 2011 Tensile deformation of a duplex Fe–20Mn–9Al–0.6C steel having the reduced specific weight. *Mater. Sci. Eng. A* **528** 196–203.
54. Ishida K, Ohtani H, Satoh N, Kainuma R, Nishizawa T. 1990 Phase equilibria in Fe-Mn-Al-C alloys. *ISIJ Int.* **30** 680–686.
55. Jeong J, Lee C. Y., Park I. J., Lee Y. K. 2013 Isothermal precipitation behaviour of j-carbide in the Fe–9Mn–6Al–0.15C lightweight steel with a multiphase microstructure. *J Alloys Compd* **574** 299–304.
56. Jimenez J. A. and Frommeryer G. 2011 The ternary iron aluminum carbides *J. Alloys Compd*. **509** 6 2729 –2733
57. Jung I.C., Cho L, De Cooman B. C. 2015 In situ observation of the influence of Al on deformation-induced twinning in TWIP steel. *ISIJ Int***55** 870–876.
58. Kartikasari R. 2014 Effect of aluminum content on microstructure and corrosion behavior of as cast Fe-Al-C alloys lightweight steel. *Int. J. Appl. Eng. Res.* **9**(13), 2241–2249.
59. Khaple S., Baligidad R. G., Satya Prasad V. V., Satyanarayana D. V. V. 2015 Microstructure and mechanical properties of Fe-7Al based lightweight steel containing carbon. *Mater. Sci. Technol.,* **31** 12, 1408–1416.
60. Khaple S., Baligidad R. G., Sankar M. and Satya Prasad V. V. 2010 Structure and properties of Fe–(3–7wt.%)Al–0.5 wt.%C alloys. *Mater. Sci. Eng. A* **527** 7452–7456.
61. Khaple S., Baligidad R. G., Sankar M. and Satya Prasad V. V. 2010 Effect of melting process and aluminium content on microstructure and mechanical properties of Fe-Al alloy. *ISIJ. Int.* **50** 10, 1483–1487.
62. Khaple S., Satya Prasad V. V., Golla B. R. 2018 Microstructural characterisation of Ti containing Fe-7Al-0.35C based low density steel. *Trans. Indian Inst. Met.* **71** 11, 2713–2716.
63. Khaple S., Satyanarayana D. V. V., Satya Prasad V. V., Golla B. R. 2019 Evolution of microstructure with increasing carbon content and its effect on mechanical properties of disordered iron–aluminium alloy. *Bull. Mater. Sci.* **42** 234–243
64. Khaple S, Satya Prasad V. V., Golla B. R., Baligidad R. G., Gokhale A. A. 2017 Effect of TiB2 and ZrB2 additions on structure and properties of Fe-7Al based light weight steel. *Mater. Sci. Eng. A* **697**, 167-176.

65. Khaple, S., Prakash, U., Golla B. R., Satya Prasad V. V. 2020 Effect of Niobium Addition on Microstructure and Mechanical Properties of Fe–7Al–0.35C Low-Density Steel. Metallogr. Microstruct. Anal. **9,** 127–139.
66. Kim H, Suh D. W., Kim N. J. 2013 Fe–Al–Mn–C lightweight structural alloys: a review on the microstructures and mechanical properties. *Sci Tech Adv Mater* **14** 1–11.
67. Kim M. S., Kang Y. B. 2015 Development of thermodynamic database for high Mn–high Al steels: phase equilibria in the Fe–Mn–Al–C system by experiment and thermodynamic modelling. *Calphad* **51** 89–103.
68. Ko S. H, and Hanada S. 1998 In-situ production and microstructures of iron aluminide/TiC composites. *Intermetallics* **7** 947–955.
69. Koster W., Tonn W. 1933 The iron corner of the iron-manganese-aluminum system. *Arch Eisenhüttenwes* **7** 365–366
70. Kubaschewski O. 1982 Iron-binary phase diagrams. 1st ed. Berlin: Springer-Verlag.
71. Lai H. J., Wan C. M. 1989 The study of work hardening in Fe-Mn-Al-C alloys. *J Mater. Sci.* **24** 2449–2453
72. Lee S., Jeong J., Lee Y. K. 2015 Precipitation and dissolution behaviour of j-carbide during continuous heating in Fe-9.3Mn-5.6Al-0.16C lightweight steel. *J Alloys Compd.* **648** 149–153.
73. Lehnhoff G. R., Findley K. O., De Cooman B. C. 2014 The influence of Si and Al alloying on the lattice parameter and stacking fault energy of austenitic steel. *Scripta Mater.* **92** 19–22.
74. Lin C. L., Chao C. G., Juang J. Y., Yang J. M., Liu T. F. 2014 Deformation mechanisms in ultrahigh-strength and high-ductility nanostructured FeMnAlC alloy. *J Alloys Compd* **586** 616–620.
75. Liu C. T., Lee E. H., McKamey C. G. 1989 An environmental effect as the major cause for room-temperature embrittlement in FeAl. *Scripta metall.* **23** 875–880.
76. Maalekian Mehran 2007 The Effects of Alloying Elements on Steels (I). Technische Universitat Graz.
77. Marceau R. K. W., Ceguerra A. V., Breen A. J., Palm M., Stein F., Ringer S. P., Raabe D. 2015 Atom probe tomography investigation of heterogeneous short-range ordering in the ‘komplex’ phase state (K-state) of Fe-18Al (at.%). *Intermetallics* **64** 23–31.

78. Marcinkowski M. J., Taylor M. E. 1975 Relationship between atomic ordering and fracture in Fe-Al alloys. *J Mater Sci.* **10** 406–414.
79. Maziasz P. J., Goodwin G. M., Alexander D. J., Viswanathan S., Deevi S. C., (Eds.), 1996 Proceedings of the International Symposium on Nickel and Iron Aluminides: Processing, Properties and Applications. ASM International, Cleveland, OH, 157.
80. Mejía I., Díaz-Martínez G., and Bedolla-Jacuinde A. 2016 Metallographic characterization of a Ti-containing low-density Fe-Mn-Al-C Steel in As-Cast Condition. MRS Proceedings 1812 47–52.
81. Mendiratta M. G., Ehlers S. K., Dimiduk D. M, Kerr W. R., Mazdiyasni S., Lipsitt H. A., 1987 A review of recent developments in Iron aluminides. *Mater. Res. Soc. Symp. Proc.*, 81 393
82. Morris D. G., Morris M. A. 1991 Mechanical properties of FeAl-ZrB_2 alloys prepared by rapid solidification. *Acta Mater.***39** 1771–1779.
83. Morris D. G., Munoz-Morris M. G., Requejo L. M. 2007 Work hardening in Fe–Al alloys. *Mater. Sci. Eng. A* **460–461** 163–173.
84. Morris-Munoz M. A. 1999 Creep deformation of oxide-dispersion-strengthened Fe-40Al intermetallic:thermal and athermal contributions. *Intermetallics* **7** 653–661.
85. Nourbakhsh S., Margolin H. 1991 Processing of continuous ceramic fibre reinforced intermetallic composites by pressure casting, composites. *Mater. Sci. Eng. A* **144** 133–141.
86. Obara Y., Kudoh M., Matsuura K. 2008 Pseudo-HIP combustion synthesis of Fe_3Al-TiB_2 composites. *Mater. Trans.***49** 1168–1174.
87. Palm M., Inden G. 1995 Experimental determination of phase equilibria in the Fe-Al-C system. *Intermetallics* **3**, 443–454.
88. Pang L., Kumar K. S. 1998 Mechanical behavior of an Fe–40Al–0.6C alloy. *Acta Mater.***46** 4017–4028.
89. Parashivamurthy K. I., Sampatha kumaran P., Seetharamu S. 2008 In-situ TiC precipitation in molten Fe-C and their characterization *Crystal Research Technology.* **43** 6 674-678
90. Park J-W, Jee K-K and Jung W-S. 2001 Elevated temperature deformation behavior of low carbon Zr-B steel, *Scripta mater.* **44** 587–592.

91. Park K. T., Jin K. G., Han S. H., Hwang S. W., Choi K, Lee C. S. 2010 Stacking fault energy and plastic deformation of fully austenitic high manganese steels: effect of Al addition. *Mater. Sci. Eng. A* **527** 3651–3661.
92. Park S. J., Hwang B, Lee K. H., Lee T. H., Suh D. W., Han H. N. 2013 Microstructure and tensile behaviour of duplex low-density steel containing 5 mass% aluminium. *Scripta Mater.***68** 365–369.
93. Pickering F. B. 1997 Overview of titanium microalloyed steels, (ed. T. N. Baker), 10-32, London, The Institute of Materials.
94. Prakash U. 2008 Development of iron aluminides containing carbon. *Indian Inst. Met.***61** 193-199.
95. Pramanik S. and Suwas S. 2014 Low-density steels: the effect of Al addition on microstructure and properties. *JOM* **66** 9, 1868–1876.
96. Pramanik S and Suwas S. 2020 Effect of Cr and Mn addition on the microstructure, texture and mechanical properties of ternary low-density steels Journal of Materials Engineering and Performance **29** 4435–4445.
97. Pramanik S., Suresh K., Anupama A. V., Balaram S., Suwas S. 2018 Strengthening mechanisms in Fe-Al based ferritic low-density steels. *Mater. Sci. Eng. A* **712** 574–584.
98. Prescott R., Graham M. J. 1992 The formation of aluminum oxide scales on high-temperature alloys. *Oxid Met.* **38** 233–254.
99. Raghavan V 1987 Phase diagrams of ternary iron alloys Part I *ASM Metals* Park OH USA.
100. Rana R., Lahaye C. and Ray R. K. 2014 Overview of lightweight ferrous materials: strategies and promises *JOM* **66** 1734–1746.
101. Rana R., Liu C., Ray R. K. 2014 Evolution of microstructure and mechanical properties during thermomechanical processing of a low-density multiphase steel for automotive application. *Acta Mater.* **75** 227–245.
102. Rana R., Loiseaux J., Lahaye C. 2012 Microstructure, mechanical properties and formability of a duplex steel. *Mater Sci Forum* **706-709** 2271–2271.
103. Rana R. 2014 Low density steels. *JOM* **66** 9 1730–1733.
104. Rana R. and Liu C. 2013 Thermoelectric power in low-density interstitial-free iron-aluminium alloys. Philos. Mag. Lett. 93 502–511.
105. Rana R., Liu C. and Ray R. K. 2013 Low density low carbon Fe–Al ferritic steels. *Scr. Mater.* **68** 354–359.

106. Ray A. 2017 Niobium microalloyed rail steels. *Mater. Sci. Technol.* **33** 13 1–17.
107. Ray R., Panchanathan V., Isserow S. 1983 Microcrystalline Iron-Base Alloys Made Using a Rapid Solidification Technology. *JOM* **35** 30–36.
108. Rigaut V, Daloz D, Drillet J, Perlade A, Maugis P, Lesoult G. 2007 Phase equilibrium study in quaternary iron-rich Fe–Al–Mn–C alloys. *ISIJ Int.* **47** 898–906.
109. Sanders W., Sauthoff G. 1997 Deformation behaviour of the perovskite type phases in the system Fe-NiAl-C: I Strength and ductility of Ni_3AlX and Fe_3AlX alloys with various microstructures. *Intermetallics* **5** 361–375.
110. Sang to shin Shin Y. S., Lee H., Han S. Y., Seo C-H , Choi K., Lee S., Kim N. J., Kwak J-H, Chin K-G. 2010 Correlation of microstructure and cracking phenomenon occurring during hot rolling of lightweight steel plates. *Metall. Mater. Trans. A***41** 138–148.
111. Satya Prasad V.V., Khaple S., Baligidad R.G. 2014 Melting, processing, and properties of disordered Fe-Al and Fe-Al-C based alloys. *JOM*, **66**, 9 1786–1793.
112. Schneider A, Falat L. and Sauthoff G. 2005 Microstructures and mechanical properties of Fe 3Al-based Fe–Al–C alloys. *Intermetallics* **13** 1322–1331.
113. Schneider A., Falat L., Sauthoff G., Frommeyer G. 2003 Constitution and microstructures of Fe-Al-M-C-(M=Ti,-V,-Nb,-Ta) alloys with carbides and Laves-phase. *Intermetallics* **11** 443–450.
114. Schniebel J. H., Deevi S. C., 2004 Processing and properties of iron aluminide composites containing oxide particles, *Mater. Sci. Engg. A* **364**, 166–170.
115. Schniebel J.H, Carmichael C.H., Specht E.D., Subramanian R., 1997 Liquid-phase sintered iron aluminide-ceramic composites. *Intermetallics* **5** 61–68.
116. Seo C.H, Kwon K.H., Choi K, Kim K.H., Kwak J.H., Lee S, Kim N.J. 2012 Deformation behaviour of ferrite–austenite duplex lightweight Fe–Mn–Al–C steel. *Scripta Mater.* **66** 519–522.
117. Seol J. B., Raabe D, Choi P, Park H. S., Kwak J. H., Park C. G. 2013 Direct evidence for the formation of ordered carbides in a ferrite-based low-density Fe–Mn–Al–C alloy studied by transmission electron microscopy and atom probe tomography *Scripta Mater.* **68** 348–353.
118. Seung-Woo Seo First Principles Calculation on Thermodynamic properties and magnetism of κ-carbide and Monte Carlo Cell gas model Phd Thesis 2010.

119. Seung Y. H, Sang Y. S, Sunghak L, Nack J. K., Jai-Hyun K., Kwang-Geun C. 2011 Effect of Carbon Content on Cracking Phenomenon Occurring during Cold Rolling of Three Light-Weight Steel Plates. *Metall. Mater. Trans. A***42** 138–146.

120. Shin S. Y., Lee H, Han S. Y., Seo C-H., Choi K, Lee S, Kim N. J., Kwak J-H. and Chin K-G. 2010 Correlation of microstructure and cracking phenomenon occurring during hot rolling of lightweight steel plates. *Metall. Mater. Trans. A***41** 138–148.

121. Sikka V. K., Viswanathan S. and Vyas S. 1993 Acceptable aluminum additions for minimal environmental effect in iron aluminides, High Temperature Ordered Intermetallic Alloys V, ed. Baker I., Darolia R., Whittenberger J. D. and Yoo M. H.: Mat. Res. Soc., Pittsburgh, PA, 288, 971–976.

122. Sohn S. S., Lee B-J., Lee S., Kwak J-H. 2013 Effects of aluminum content on cracking phenomenon occurring during cold rolling of three ferrite-based lightweight steel. *Acta Mater.* **61**, 5626–5635.

123. Sohn S. S., Choi K, Kwak J-H, Kim N. J, Lee S. 2014 Novel ferrite–austenite duplex lightweight steel with 77% ductility by transformation induced plasticity and twinning induced plasticity mechanisms. *Acta Mater.* **78** 181–189.

124. Sohn S.S, Lee B-J., Lee S, Kwak J-H. 2014 Effect of Mn addition on microstructural modification and cracking behaviour of ferritic light-weight steels. *Metall. Mater. Trans. A* **45** 5469–5485.

125. Sohn S. S., Lee B. J., Lee S, Kwak J H. 2013 Effects of aluminium content on cracking phenomenon occurring during cold rolling of three ferrite-based lightweight steel. *Acta Mater.***61** 5626–5635.

126. Sohn S.S., Song H., Suh B.C., Kwak J-H., Lee B-J., Kim N.J., Lee S. 2015 Novel ultra-high-strength (ferrite + austenite) duplex light weight steels achieved by fine dislocation substructures (Taylor lattices), grain refinement, and partial recrystallization. *Acta Mater.* **96** 301–310.

127. Speer J. G., Araujo A. L., Matlock D. K., de Moor E. 2016 Nb-Microalloying in Next-Generation Flat-Rolled Steels: An Overview. *Materials Sci. Forum Thermac***879** 1834–1840.

128. Springer H, Raabe D. 2012 Rapid alloy prototyping: Compositional and thermo-mechanical high throughput bulk combinatorial design of structural materials based on the example of 30Mn–1.2C–xAl triplex steels. *Acta Mater.* **60** 4950–4959.

129. Stoloff N. S. 1998 Iron aluminides: present status and future prospects. *Mater. Sci. Eng. A* **258** 1–14.

130. Suh D.-W., Kim N. J. 2013 Low-density steels. *Scripta Mater*. **68** 6, 337–338.

131. Syahrila, Rawlings R. D. 2002 Effect of thermomechanical treatment on the properties of Fe-11Al and Fe-14Al alloys. *Journal of Material Science,* **37** 1823–1830.

132. Terry B. S., Chinyamakobvu O. S. 1992 Dispersion and reaction of TiC in liquid iron alloys. *Mater. Sci. Technol.***8** 399–405.

133. Turkdogn E. T. 1996 Fundamentals of Steelmaking, **316**, London, The Institute of materials.

134. Umakoshi Y. and Yamaguchi M. 1980 Deformation of FeAl single crystals at high temperature. *Phil. Mag. A***41**, 573-588.

135. Vedula K.V., Stephens J. R. 1987 Indentation creep studies of iron aluminide intermetallic alloy. *Mater. Res. Soc. Symp. Proc*. **81** 381–390.

136. Vyas S., Viswanathan S. and Sikka V. K. 1992 Effect of aluminum content on environmental embrittlement in binary iron-aluminum alloys. *Scripta. Metall. Mater.* **27** 185–190.

137. Wolski K., Therenot F., Coze J. L. 1996 Effect of nanometric oxide dispersion on creep resistance of ODS-FeAl prepared by mechanical alloying. *Intermetallics* **4** 299–307.

138. Woo S. D, Kim N. J. 2013 Viewpoint set 53: low density steels. *Scripta Mater.* **68** 337–338.

139. Wu Z.Q., Ding H, Li H. Y., Huang M. L., Cao F. R. 2013 Microstructural evolution and strain hardening behaviour during plastic deformation of Fe–12Mn–8Al–0.8C steel. *Mater. Sci. Eng. A* **584** 150–155.

140. Yang F, Song R, Li Y, Sun T, Wang K. 2015 Tensile deformation of low density duplex Fe–Mn–Al–C steel. *Mater. Des*. **76** 32–39.

141. Yang M .X., Yuan F .P, Xie Q., Wang Y., Ma E, Wu Xiaolei L. 2016 Strain hardening in Fe-16Mn-10Al-0.86C-5Ni high specific strength steel. *Acta Mater.* **109** 213–222.

142. Yoo J. D., Park K. T. 2008 Microband-induced plasticity in a high Mn–Al–C light steel. *Mater. Sci. Eng. A* **496** 417–424.

143. Zargaran A., Kim H. S., Kwak J. H., Kim N. J. 2014 Effect of Nb and C additions on the microstructure and tensile properties of lightweight ferritic Fe-8Al-5Mn alloy. *Scr. Mater.* **89** 37–40.

144. Zargaran A., Kim H. S., Kwak J. H., Kim N. J. 2015 Effect of C content on the microstructure and tensile properties of lightweight ferritic Fe-8Al-5Mn-0.1Nb alloy. Met. Mater. Int. **21** 1, 79–84.

145. Zhang L, Song R, Zhao C, Yang F, Xu Y, Peng S. 2015 Evolution of the microstructure and mechanical properties of an austenite–ferrite Fe–Mn–Al–C steel. *Mater. Sci. Eng. A* **643** 183–193.

146. Zhang L, Song R, Zhao C, Yang F. 2015Work hardening behaviour involving the substructural evolution of an austenite–ferrite Fe–Mn–Al–C steel. *Mater. Sci. Eng. A* **640** 225–234.

147. Zhao C, Song R, Zhang L, Yang F, Kang T. 2016 Effect of annealing temperature on the microstructure and tensile properties of Fe–10Mn–10Al–0.7C low density steel. *Mater Des.* **91** 348–360.

148. Zuazo I., Hallstedt B., Lindahl B., Selleby M., Soler M., Etienne A., Perlade A., Hasenpouth D., Massardier-jourdan V., Cazottes S. Kleber X. 2014 Low-Density Steels: Complex metallurgy for automotive applications, *JOM* **66** 9, 1747–1758.

149. Lee H. W., Kim G. and Park S. H. 2010 Lightweight steel solutions for automotive industry Editors: . Barlat F., Moon Y. H., and Lee M .G. *NUMIFORM 2010, Proceedings of the 10th International Conference*, 1 55-62.

150. Humphreys F. J., Hatherly M. 1995 Recrystallization and related annealing phenomena, second edition, Elsevier, Oxford.

LIST OF PUBLICATIONS

Journal Publications

1. **Shivkumar Khaple,** V.V. Satya Prasad, Brahma Raju Golla, R.G. Baligidad, A. A.Gokhale, '*Effect of TiB_2 and ZrB_2 additions on structure and mechanical properties of Fe-7Al based light weight steel'* Material Science & Engineering A 697 (2017) 167-176. (Impact factor: 3.5).

2. **Shivkumar Khaple,** V.V. Satya Prasad, Brahma Raju Golla, '*Microstructural Characterisation of Ti Containing Fe-7Al-0.35C Based Low-Density Steel'* Transactions of Indian Institute of Metals' Vol. 71 (11) 2018, 2713–2716. (Impact factor: 1.185).

3. **Shivkumar Khaple,** V.V. Satya Prasad, D. V. V. Satyanarayana, Brahma Raju Golla, '*Evolution of Microstructure with Increasing Carbon Content and Its Effect on Mechanical Properties of Disordered Iron-Aluminium Alloy'* Bulletin of Materials Science, vol 42 (2019): 234. (Impact factor: 1.3).

4. **Shivkumar Khaple**, Ujjwal. Prakash, Brahma Raju Golla, V.V. Satya Prasad, '*Effect of niobium content on microstructure and mechanical properties of Fe-7Al-0.35C based low density steel'* Metallography, Microstructure, and Analysis Vol.9, (2020)127–139 (Impact factor: 1.08)

National and International Conferences

5. **Shivkumar Khaple,** V.V. Satya Prasad, Brahma Raju Golla *'Microstructural Characterisation of Ti containing Fe-7Al-0.35C based low density steel'.* International conference on solidification science and processing,(ICSSP), 19-22 Nov 2018, Trivandrum, Kerala

6. **Shivkumar Khaple,** V.V. Satya Prasad, Brahma Raju Golla, '*Role of titanium on microstructure and mechanical properties of Fe-7Al-0.35C based light weight steel'*, 71th ATM-NMD, Indian Institute of Metals , 14-17 Nov- 2017, Goa, India.
7. **Shivkumar Khaple,** V.V. Satya Prasad, R.G. Baligidad, Brahma Raju Golla '*Effect of niobium on microstructure of light weight steel based on Fe-7Al-0.35C'* ISRS-2016, IIT Chennai.
8. **Shivkumar Khaple,** V.V. Satya Prasad, R.G. Baligidad, D. V. V. Satyanarayana, Brahma Raju Golla, *'Effect of carbon on microstructure and mechanical properties of Fe-7Al based lightweight steel',* 69th ATM-NMD, Indian Institute of Metals , 14-17 Nov- 2015, Coimbaiore, India.

Materials Science & Engineering A 697 (2017) 167–176

Contents lists available at ScienceDirect

Materials Science & Engineering A

journal homepage: www.elsevier.com/locate/msea

Effect of TiB_2 and ZrB_2 additions on structure and properties of Fe-7Al based light weight steel

Shivkumar Khaple[a,b,*], V.V. Satya Prasad[a], Brahma Raju Golla[b], R.G. Baligidad[a], A.A. Gokhale[c]

[a] Defence Metallurgical Research Laboratory, Hyderabad, India
[b] National Institute of Technology, Warangal, India
[c] Indian Institute of Technology, Bombay, India

ARTICLE INFO

Keywords:
Lightweight steel
Low density steel
Fe-Al alloys
Grain refinement
Mechanical properties

ABSTRACT

Microstructural modifications and their effect on tensile properties in an Fe-7 wt.% Al alloy by additions of 0.5% TiB_2, 0.5% ZrB_2 or both has been studied. Alloys are examined in the as-cast as well as in the hot-rolled and annealed conditions. Solidification structure of the Vacuum Arc Remelted pancake ingots was columnar dendritic. Further, boride modified alloys are found to have finer grains in as-cast as well as in hot-rolled and annealed conditions. In the annealed condition, boride containing alloys were found to have superior tensile yield strength, ductility and strain hardening behaviour. These property improvements are attributed to boride aided grain refinement during casting as well as during thermo-mechanical processing of the steels.

1. Introduction

Steels are engineering materials that are produced in very large quantities. They find application in various engineering sectors such as automotive, aerospace, ships, building and construction, heavy equipment, and machinery. Despite the evolution of lightweight materials, such as Al and Mg alloys, and various composites and plastics, steels are used extensively because of their excellent combination of strength, formability, affordability and recyclability [1–4]. However, density of steel is much higher as compared to the light materials mentioned above. Therefore there is an urgent pressure on the steel producers to innovate new grades of steels with lower density.

Considering its strong effect on density reduction and improvement in strength as well as other engineering aspects such as alloy making and workability, Al has emerged as the single most important alloying element in the development of low-density bulk steels. Al, being a ferrite stabilizer, reduces the austenitic loop significantly while expanding the ferritic phase field [5]. This results in a fully ferritic microstructure at room temperature. Although Al can be added in low-density ferritic steels upto 11 wt.% [5–8] it has been suggested that the Al content should be restricted to less than about 6.5 wt.% [3,6] due to the propensity for short-range ordering at higher Al contents, which increases brittleness and adversely affects formability [3,6–12].

The Fe-Al ferritic steels received relatively less attention in early steel literature, probably because of their unattractive combination of strength and ductility [1,3,7,12]. Recently some of the present authors have reported that with about 7 wt.% Al steel could be made by air induction melting with flux cover (AIMFC), and could be hot and cold rolled to thin sheets [13–15]. They exhibited about 18% tensile elongation and 300 MPa yield strength at room temperature in hot rolled condition. However the strength and ductility values are still low as compared to other competitive structural materials [1,11,16]. Hence there is a need to further improve the room temperature tensile properties and formability of these steels. Grain refining plays an important role in this context. In the present work, the effect of TiB_2 and ZrB_2 particle additions on microstructure and properties of Fe-7 wt.% Al steel has been reported.

2. Experimental procedure

High purity Fe, Al, TiB_2 and ZrB_2 were used as starting materials for preparing the steels in pancake form with nominal compositions of Fe-7 Al, Fe-7 Al-0.5 ZrB_2 and Fe-7 Al-0.5 TiB_2 (all the compositions are in wt.% unless otherwise specified). Two sets of pancakes of 100 mm diameter and 10 mm thickness were prepared by non consumable electrode DC arc melting process using a thoriated tungsten electrode under argon atmosphere. Fe and Al pieces of 5 mm in size and ZrB_2 and TiB_2 powders (average diameter of the particles as 3–6 μm and 2–10 μm, respectively) were premixed and directly placed in the water cooled crucible cavity. The melt chamber was evacuated to 1×10^{-4} mbar and refilled with argon gas to about 600 mbar pressures. This evacuation and gas refilling cycle was repeated twice. Argon gas at 600 mbar pressure was maintained throughout the melting process. To prevent contamination of the melt from the electrode, a high frequency

* Corresponding author at: Defence Metallurgical Research Laboratory, Hyderabad, India.

http://dx.doi.org/10.1016/j.msea.2017.05.011
Received 13 January 2017; Received in revised form 2 May 2017; Accepted 3 May 2017
Available online 04 May 2017

Trans Indian Inst Met
https://doi.org/10.1007/s12666-018-1434-5

TECHNICAL PAPER

Microstructural Characterisation of Ti Containing Fe-7Al-0.35C Based Low-Density Steel

Shivkumar Khaple[1,2] · V. V. Satya Prasad[1] · Brahma Raju Golla[2]

Received: 15 July 2018 / Accepted: 12 September 2018

Abstract In this paper, the role of Ti on the in-situ formation of carbides and its effect on the microstructure of Fe-7Al-0.35C alloy have been investigated. Initially, Thermo-Calc software was used to predict the phases present in the alloys which were validated by experimental work. Vacuum arc remelting process was used to make an alloy pancake of 10-mm thickness, which was hot-rolled to 2-mm thickness. The alloys were characterised by X-ray diffraction, optical, scanning electron microscope and electron probe micro-analysis. The results show that all the alloys exhibit two types of TiC precipitates, which are dark cuboidal as primary and dark acicular type as secondary precipitates along with grey-coloured needle-shaped κ-carbide precipitate in α(Fe–Al) matrix. The carbon present in the alloy is partitioned between TiC and κ-carbide precipitates. Addition of Ti has also resulted in grain refinement of all the alloys.

Keywords Low-density steel · Fe-7Al-0.35C alloy · TiC · Thermo-Calc

1 Introduction

Low-density steels, with an excellent combination of mechanical properties and specific weight, are promising for automobile structural applications [1–4]. Recently, these steels have drawn increasing interest as they can bring down the gasoline consumption and reduce the greenhouse effect [1–3]. The main reduction in density of this steel is offered by aluminium. About 7wt% (compositions: wt%) of Al offers 9–10% reduction in density with simultaneously increasing the strength by solid solution strengthening. Addition of carbon leads to the formation of κ-carbide. By controlling the size and distribution of κ-carbide, the strength of this large grain ferritic steel can be further improved [3]. Recently, the effect of carbon on structure and properties of Fe-7Al steel has been reported [5]. The present work is aimed to predict the phase formation by the addition of titanium to Fe-7Al-0.35C steel and validate with the microstructural characterisation of this steel.

2 Experiment

Fe-7Al-0.35C based steel with varying Ti (0.2–1%) content was melted in non-consumable vacuum arc melting furnace. The details of the melting process are illustrated elsewhere [6]. Finally, 100-mm diameter and 10-mm thick pancakes were obtained. The preheated (1100 °C-1 h) pancakes were hot-rolled to sheets of 2-mm thickness using DEMAG rolling mill. The chemical analysis of nitrogen, carbon and hydrogen was done using Leco analyser, and alloying elements (Ti and Al) were determined by wet analysis. The samples from the hot-rolled sheet were cut, mechanically polished and etched with a solution comprising of $33\%CH_3COOH + 33\%HNO_3 + 1\%HF + 33\%H_2O$ by volume for optical and SEM microstructural study. Philips X-ray diffractometer (XRD) was used to identify the phases present in the alloy. EPMA (electron probe micro-analysis) was carried out to find the distribution of the elements in phases of the alloy. The image

✉ Shivkumar Khaple
sikaple@yahoo.com

[1] Defence Metallurgical Research Laboratory, Hyderabad, India

[2] National Institute of Technology, Warangal, India

Published online: 01 October 2018

Bull. Mater. Sci. (2019) 42:234
https://doi.org/10.1007/s12034-019-1930-1

Evolution of microstructure with increasing carbon content and its effect on mechanical properties of disordered iron–aluminium alloy

SHIVKUMAR KHAPLE[1,2,*], D V V SATYANARAYANA[1], V V SATYA PRASAD[1] and BRAHMA RAJU GOLLA[2]
[1]Defence Metallurgical Research Laboratory, Hyderabad 500058, India
[2]National Institute of Technology, Warangal 506004, India
*Author for correspondence (sikaple@yahoo.com)

MS received 17 November 2018; accepted 21 May 2019

Abstract. Correlation of microstructure and mechanical properties of hot-rolled Fe–7 wt.% Al with varying carbon contents has been investigated in detail. The microstructures of the alloys change significantly with an increase in the carbon content. An alloy with 0.012 wt.% carbon shows a single ferrite phase, whereas with increase in carbon up to 0.65 wt.%, the microstructure evolves into a dual phase consisting of ferrite and κ-pearlite. At about 1.5 wt.% carbon, the alloy exhibits only κ-pearlite and with a further increase in carbon to 2.2 wt.%, an additional phase starts precipitating in the form of graphite. The room temperature tensile strength of the alloy increased significantly with an increase in the carbon content, which is in agreement with the microstructure. The yield strength and hardness of the steels with different carbon contents can be correlated well with the inter-barrier spacing in different steels.

Keywords. Low-density steel; iron aluminium alloys; lightweight steels; mechanical properties.

1. Introduction

Disordered iron–aluminium alloys are an emerging class of low-density/lightweight steels containing aluminium in the range of 6–9 wt.% in steel. These Fe–Al alloys with a disordered A2 ferrite structure have raised considerable interest due to their low-density, high ductility, cost-effective and feasibility for bulk production. These low-density and high-strength materials are envisaged in the development of an advanced lightweight ground transportation system, huge structures like bridges, tunnels and also being deemed for certain defence applications like troops carrier, armour, etc. Alternatively, they are also considered as potential candidates for steam turbines in thermal power plants [1–7]. Al being a ferrite stabilizer, reduces the austenitic loop and enhances the ferrite phase field, which results in a complete ferrite microstructure at room temperature [8–10]. This disordered ferritic (A2) phase results in good ductility, but suffers from the loss of strength compared to the other existing structural materials such as heat-resistant stainless steel [3–6]. To overcome the strength issue of these alloys, alloy modifications were attempted with Mn and carbon, which resulted in higher strength than the existing Fe–Al alloys [11–13]. Nevertheless, these alloys had a setback in the form of cracking during the rolling stage.

The effect of carbon on the improvement of strength of ordered Fe_3Al alloys has been reported in detail [8,14–17]. However, very less work has been reported on the effect of carbon on the microstructure evolution effect, and hence, on the properties of disordered ferritic steels [6,7].

Therefore, it is of current interest to explore the potential of carbon as an alloying element to enhance the strength of disordered ferritic Fe–7 wt.% Al-based low-density steel. It is interesting to note that the density advantage of about 10% is still retained in Mn free steels as the density reduction mainly results from the addition of Al. In the present study, the effect of carbon on the evolution of the microstructure and its impact on mechanical properties and fracture behaviour of Fe–Al-based steels containing 7 wt.% Al have been investigated and the results are presented in this paper.

2. Experimental

An air induction melting process was used to make five melts of low-density Fe–Al-based steel with different carbon contents, each weighing about 40 kg. The steels containing 0.012, 0.35, 0.65, 1.5 and 2.2 wt.% carbon were hereafter designated as 'S1', 'S2', 'S3', 'S4' and 'S5' steels, respectively. The details of the charge preparation and melting procedure was discussed elsewhere [6,8]. The melt was top poured into split cast iron moulds with a diameter of 55 mm. The hot working of the steel from ingots to 12 mm thick plate is described

Published online: 19 July 2019

Metallography, Microstructure, and Analysis
https://doi.org/10.1007/s13632-020-00622-9

TECHNICAL ARTICLE

Effect of Niobium Addition on Microstructure and Mechanical Properties of Fe–7Al–0.35C Low-Density Steel

Shivkumar Khaple[1,3] · Ujjwal Prakash[2] · Brahma Raju Golla[3] · V. V. Satya Prasad[1]

Received: 4 March 2019 / Accepted: 5 February 2020

Abstract
The present work reports the effect of niobium addition on a Fe–7wt.%Al–0.35wt.%C-based low-density steel. A hot rolling temperature of 1100 °C was selected to carry out rolling in the intercritical (ferrite + austenite) region. The phases formed on adding Nb were predicted by thermodynamic calculations using ThermoCalc. All the alloys exhibited a significant (20% or more) tensile elongation. Niobium addition also resulted in a significant increase in strength and hardness of the hot-rolled steel. About 80% increase in the yield strength is observed as the Nb content increases from 0.2 to 1.0 wt.%. Nb carbides present at rolling temperature resist grain growth and lead to improved mechanical properties. This study demonstrates the advantages of adding Nb to Fe–Al–C-based low-density steels. Earlier attempts to add Nb to low-density steels resulted in very low ductility. This may be related to their susceptibility to hydrogen embrittlement. Melting of high aluminum low-density steels in a controlled atmosphere may lead to a considerable improvement in mechanical properties. Further, it is also important to maintain a high C/Nb ratio to avoid the formation of Laves phases.

Keywords Low-density steel · Nb addition · NbC · Fe–Al–C–Nb · ThermoCalc · Mechanical properties

Introduction

The density of steel can be reduced by the addition of aluminum [1–4]. Each wt.% addition of Al gives about 40 MPa increase in strength by solid solution strengthening [1–5] and a density reduction of about 1.5% [3–7]. Aluminum addition also leads to an improved corrosion resistance [1, 8]. Because of their low-density, high specific strength, and good corrosion resistance, these steels are considered potential structural materials in thermal power plants and petrochemical industry [1–13]. Reducing the weight of an automobile by 10% can hike the fuel economy by 6–8%, and therefore, these materials have applications in the automotive industry [1–4, 10, 11]. Further, they may also have potential defense applications [12]. We have earlier reported properties of Fe–7wt.%Al alloys with carbon addition [5, 7].

✉ Shivkumar Khaple
sikaple@yahoo.com

[1] Defence Metallurgical Research Laboratory, Hyderabad, Telangana State, India

[2] Indian Institute of Technology Roorkee, Roorkee, India

[3] National Institute of Technology Warangal, Warangal, India

Published online: 18 February 2020

Here, we report the effect of Nb addition on microstructure and mechanical properties of a Fe–7wt.%Al–0.35wt.%C alloy (all compositions are in wt.%). In order to predict the formation of phases on Nb addition, thermodynamic calculations were performed using ThermoCalc software and compared with the experimental results. Earlier attempts to add Nb to low-density steels resulted in very low ductility [13–16]. This may be related to their susceptibility to hydrogen embrittlement. All the alloys studied in the present work exhibited significant (20% or more) tensile elongation. It is suggested that the melting of high aluminum low-density steels in a controlled atmosphere may be necessary to achieve improved mechanical properties.

Experimental Procedure

High-purity raw materials such as iron, aluminum, graphite, and niobium were used for preparing steel pancakes of desired compositions. Non-consumable DC arc melting process with a thoriated tungsten electrode was used for melting the raw materials. The melting chamber was evacuated to 1×10^{-3} mbar and refilled with argon. The process of evacuation and refilling was performed twice.

BIO-DATA

1. Name	:	Shivkumar Khaple
2. Date of Birth	:	01 Nov 1975
3. Educational Qualifications	:	
a) B. Tech	:	National Institute Technology, Karnataka (*formerly Regional Engineering college) KREC, Surathkal,* Karnataka State.
Year of passing	:	1998
b) M. E	:	Indian Institute of Science, Bangalore, Karnataka State
Specialization	:	Metallurgy
Year of passing	:	2001
c) Pursuing Ph.D.	:	National Institute of Technology, Warangal
4. Research topic	:	Effect of alloying additions on the microstructure and mechanical properties of Fe-Al based lightweight steel.
5. Professional Experience	:	1 Year In steel plant as Quailty Engineer in M/s Kalyani Steels Limited, Bellary. 3 years as Software Engineer at Syntel India Limited , Chennai as Programmer. 16 Years as Scientist in Defence Metallurgical Research Laboratory (DMRL), Kanchanbagh, Hyderabad Telangana State
6. Contact details:		
Permanent Address	:	**Ho. No. 17-1-382, Plot 10& 11** Flat 103, Sai Krishna Residency, Apartment Karmanghat, Hyderabad, Telangana State Pin: 500079
E-mail	:	sikaple@yahoo.com
Contact Numbers	:	+91-97386362761, +91-9505733693.